11. SITE 696[1]

Shipboard Scientific Party[2]

HOLE 696A

Date occupied: 23 February 1987, 1300 local time

Date departed: 24 February 1987, 2245 local time

Time on hole: 33 hr, 45 min

Position: 61°50.945′S, 42°55.984′W

Bottom felt (rig floor; m, drill-pipe measurement): 661.0

Distance between rig floor and sea level (m): 11

Water depth (drill-pipe measurement from sea level, m: 650

Penetration (m): 103

Number of cores: 12

Total length of cored section (m): 106

Total core recovered (m): 58.3

Core recovery (%): 55

Oldest sediment cored:
Depth sub-bottom (m): 106
Nature: diatom-bearing clayey mud
Age: lower Pliocene
Measured velocity (km/s): 1.52

HOLE 696B

Date occupied: 24 February 1987, 2245 local time

Date departed: 2 March 1987, 0415 local time

Time on hole: 125 hr, 30 min

Position: 61°50.959′S, 42°55.996′W

Bottom felt (rig floor; m, drill-pipe measurement): 661.0

Water depth (drill-pipe measurement from sea level; m): 650

Penetration (m): 645.6

Number of cores: 62

Total length of cored section (m): 569

Total core recovered (m): 156.69

Core recovery (%): 27.5

Oldest sediment cored:
Depth sub-bottom (m): 645.6
Nature: sandy mudstone
Age: late Eocene-Oligocene
Measured velocity (km/s): 1.90

Principal results: Site 696 lies on the southeast margin of the South Orkney microcontinent (SOM), South Scotia Ridge, in 650 m of water at 61°50.945′S, 42°55.984′W. Site 696 is the shallowest site in the Weddell Sea depth transect for studies of late Mesozoic and Cenozoic water-mass stratification and Antarctic climatic history. Two holes were drilled: Hole 696A includes 10 APC cores to 89 mbsf and 2 XCB cores from 89 to 103 mbsf, (55% recovery); Hole 696B includes a wash core to 76.6 mbsf, 2 interstitial water cores, and 59 rotary cores from 76.6 to 645.6 mbsf (27.5% recovery). The site was abandoned at the maximum penetration allowed by safety restrictions.

The sedimentary sequence, poorly recovered and commonly disturbed, is terrigenous, hemipelagic, and pelagic with ice-rafted detritus (IRD) and a minor volcanogenic component. The sequence ranges from the middle or upper Eocene to the Quaternary. Ice-rafted dropstones of all sizes are common from the middle upper Miocene (366 mbsf; about 8 Ma) to the present. Otherwise, rare coarse-grained IRD was found at two levels between 530 and 570 mbsf in sediments likely to be Oligocene or lower Miocene. Calcareous material is present as planktonic and benthic foraminifers in the uppermost 4 m of the Quaternary, as benthic and planktonic foraminifers and calcareous nannofossils in a short interval in the upper Miocene, and as benthic foraminifers and nannofossils with very few planktonic foraminifers in the basal Eocene sediments. The pelagic component is almost totally biosiliceous, principally diatoms.

The Site 696 sequence consists of three parts: an upper hemipelagic part to 214 mbsf, a middle diatomaceous part to 530 mbsf and a lower terrigenous and authigenic part to the base of the hole. The sequence consists of a condensed Quaternary to upper Pliocene, expanded lower Pliocene and upper to middle Miocene, and condensed Oligocene(?) to Eocene. Preliminary stratigraphy indicates a brief hiatus or condensed sequence during the uppermost Pliocene to lowest Quaternary, and a possible brief hiatus during the middle Pliocene. Another condensed barren interval separates Neogene and Paleogene sequences and hinders understanding of the transition. A magnetic polarity stratigraphy has been identified for the lower Pliocene to the present. Prospects are poor for the Miocene due to poor recovery, but good for Paleogene sediments. Biostratigraphic ages for the Neogene are based almost entirely on diatoms and radiolarians. Paleogene sediments are barren of siliceous microfossils; age assignments have been based upon calcareous nannofossils and palynomorphs. This is the first recovery of pollen and spores in sediments of the deep Weddell Sea. Benthic foraminifers are persistent but rare through most of Site 696, and are almost exclusively low-diversity assemblages of agglutinated forms except for the calcareous Paleogene faunas.

The seven units drilled are: Unit I, seafloor to 64.2 mbsf, Quaternary to lower upper Pliocene diatomaceous muds and oozes; Unit II, 64.2–124.8 mbsf, lower upper to lower Pliocene diatom-bearing silty and clayey mud; Unit III, 124.8–211.8 mbsf, lower Pliocene to upper Miocene silty and clayey mud, with minor diatom-bearing clayey mud; Unit IV, 211.8–260.1 mbsf, upper Miocene diatom ooze and muddy diatom ooze; Unit V, 260.1–269.7 mbsf, upper Miocene coarse turbiditic sand; Unit VI, 269.7–529.8 mbsf, diatom ooze and mud-bearing diatom ooze passing down to diatomite and mud-bearing diatomite; Unit VII, 529.8 m to base of hole at 645.6 mbsf, Miocene(?) to Eocene, dominantly terrigenous sediments divided into four subunits; Subunit VIIA, sandy mudstone (possibly Miocene); Subunit VIIB, claystone, clayey mudstone, and silty mudstone (undifferentiated upper Paleogene to lower Miocene); Subunit VIIC, glauconitic silty mudstone and claystone (undifferentiated upper Paleogene to lower Miocene); and Subunit VIID, sandy mudstone (upper Eocene to lower Oligocene).

The Eocene sandy mudstones reflect the dominant terrigenous regime of the SOM while still contiguous with the West Antarctic continental margin. Benthic foraminiferal assemblages indicate deposition in an inner neritic environment under slightly hyposaline and hypoxic conditions. The sediments contain abundant assemblages of Mollusca and Cnidaria. Diverse calcareous nannofossil assemblages attest to the warmth of the Southern Ocean in the Eocene. The palynoflora indicates the presence of temperate beech forests

[1] Barker, P. F., Kennett, J. P., et al., 1988. *Proc. ODP, Init. Repts.*, 113: College Station, TX (Ocean Drilling Program).

[2] Shipboard Scientific Party is as given in the list of Participants preceding the contents.

with an undergrowth of ferns on West Antarctica. The hypothesis of a warm climate is supported by a clay association dominated by smectite as in the Eocene sediments of Maud Rise and resulting from the predominance of chemical weathering over physical processes.

A condensed neritic sequence of about 77 m of poorly dated terrigenous glauconitic sediments separates Eocene and middle Miocene sediments. Rare, reworked freshwater diatoms indicate the presence of freshwater lakes in West Antarctica. Nearly all of the overlying section contains only agglutinated benthic foraminifers and virtually no calcareous planktonic microfossils, indicating a change to highly undersaturated bottom waters, even at these shallow depths. The paucity of fossils makes it difficult to interpret climatic conditions in this interval, but rare agglutinated benthic foraminifers suggest cool bottom waters from Subunit VIIB upward. IRD is almost totally absent. Clay mineral associations consist of abundant to exclusive smectite and common to abundant illite.

This condensed sequence passes (perhaps disconformably) up into a 300-m sequence of poorly recovered but dominantly biosiliceous (90% diatoms) sediments of middle to uppermost Miocene. Lack of terrigenous sediment deposition in the middle Miocene reflects the isolation of the SOM from West Antarctica due to formation of Powell Basin. As far as we can tell from the very poorly recovered section, sedimentation rates were fairly constant and moderately high from about 14 to 5 Ma, with an average of 35–41 m/m.y. High productivity, excellent preservation, and taxonomic composition of diatoms suggest that the Antarctic Convergence was located just to the north of the SOM during much of the Miocene and that there was little sea-ice in the area. The continued absence of calcareous microfossils through most of the Miocene indicates that the carbonate compensation depth (CCD) was exceedingly shallow, and less than (present-day depth) 650 m. The lack of IRD in the middle and lower upper Miocene sediments suggests that major glaciation had not yet commenced on West Antarctica, in concordance with trends observed in other Leg 113 sites. A major change in the climate of West Antarctica during the middle Miocene is indicated by changes in clay mineral assemblages. At this time, smectite, the dominant clay mineral in the lower middle Miocene, is replaced by illite and chlorite. This indicates a strong decrease in chemical relative to physical weathering. This may have resulted from major cooling of West Antarctica. A similar change in clay associations occurred in the lower Oligocene at sites adjacent to East Antarctica and Maud Rise, indicating that major cooling occurred earlier in East Antarctica than West Antarctica. In the early late Miocene, diatomaceous sediments continued to dominate. An increase in hemipelagic sediments, the appearance of an important ice-rafted component, and the further increase in illite and chlorite, all resulted from the development of a West Antarctic ice-sheet during the late Miocene. At the Miocene/Pliocene boundary, diatomaceous sediments were largely replaced by diatom-bearing silty and clayey muds. This resulted from the development, during the latest Miocene, of a major and probably permanent West Antarctic ice-sheet, the main supplier of fine terrigenous sediments to the West Antarctic continental margin. At the same time, a general regional decrease occurred in biosiliceous productivity. Site 696 also exhibits the characteristic regional decrease in sedimentation rates from the early Pliocene to the late Pliocene and Quaternary. The Quaternary is marked by abundant *Neogloboquadrina pachyderma* and a low-diversity benthic foraminiferal assemblage, as found throughout the Weddell Sea.

BACKGROUND AND OBJECTIVES

Site 696 (W8) is located 50 km northeast of Site 695 on the southeast part of the crest of the SOM, in 650 m of water (Fig. 1). It is the shallowest of three sites (696, 695, and 697) that form a depth transect in the northwest Weddell Sea for studies of sedimentary and climatic history and surface to bottom-water evolution (Antarctic Shelf Water, Circumpolar Deep Water, Antarctic Bottom Water) during the late Paleogene and Neogene. Together with the other sites drilled in the Weddell Sea (Sites 689–694), they form a depth transect over a greater depth range within the circum-Antarctic water-mass structure (650–4664 m) and over an age range of Cretaceous to Quaternary. Site 696 is of special interest because it is one of the five shallowest sites drilled in the open ocean around Antarctica, the others (Sites 270 through 273) being located in the Ross Sea. Site 696 and the previously cored Site 695 were selected to obtain high-quality (APC, XCB), continuously-cored sequences through the upper Paleogene and Neogene on the West Antarctic margin. Site 696 is located in water 660 m shallower than at Site 695. Being so close, both sites lie beneath the same present-day water mass. No major oceanographic boundary lies between them in the present day, nor did probably in the past.

Site 696 is located on multichannel seismic reflection profile AMG845-18 (Figs. 2 and 3), that runs northward from Site 695 along the eastern margin of the SOM. As already described in "Background and Objectives" section, "Site 695" chapter (this volume), the SOM underwent extensional tectonic disruption during the early to middle Oligocene (35–30 Ma: King and Barker, 1988), when it separated from the northern Antarctic Peninsula, forming Powell Basin to the west and Jane Basin to the east (Barker et al., 1984). Jane Basin may have opened initially at about 25–35 Ma ago (late Oligocene; King and Barker, 1988; Lawver et al., 1986). The geographic isolation of the SOM caused by the formation of Powell and Jane Basins and the subsequent subsidence of the SOM would have greatly reduced the supply of terrigenous sediment to Site 696, and a dominantly pelagic biogenic regime during the Neogene was anticipated.

Site 695 had been expected to provide a basic record of late Paleogene and Neogene paleoceanographic and paleoclimatic change for the SOM region. Site 696 was expected to complement this and also provide a more calcareous sediment sequence than the deeper site. An unexpectedly thick sequence of Pliocene pelagic and hemipelagic sediments, however, was encountered at the depth at which the XCB was lost at Site 695 (341 mbsf). It was then estimated that the remaining 200 m of the Site 695 sequence that we planned to drill (above the prominent bottom-simulating reflector, BSR) could be no older than late Miocene. A tracing of prominent, and apparently continuous, seismic reflection horizons indicated a thinning of the sediment sequence from Site 695 to 696, so that an upper Paleogene through Neogene sequence would more likely be accessible at Site 696. Therefore, Site 695 was abandoned to allow more time to be spent at Site 696, instead of using more time at Site 695, obtaining only a late Neogene sequence.

The multichannel seismic reflection profile (Fig. 2) indicates the presence of a relatively thin (~0.6 s two-way traveltime, twt) sequence of acoustically layered sediments overlying a distinct reflector interpreted as a breakup unconformity and expected to coincide with a distinct lithologic change. The sediment sequence overlying the breakup unconformity was expected to represent biogenic ooze and hemipelagic sediments with ice-rafted and glacial-marine components. The breakup unconformity is underlain in turn by a thick (~0.8 s twt) sequence of northward-dipping sediments considered to represent hemipelagic and terrigenous volcanogenic deposition on the West Antarctic continental margin prior to the opening of Jane Basin.

There were several major objectives at Site 696, nearly all related to the paleoclimatic and paleoceanographic development of Antarctica. We had hoped but were unable to meet several of these objectives at Site 695:

1. The especially shallow section at Site 696 was selected during the early planning stages with the hope of providing a carbonate record through much of the upper Paleogene and Neogene. After coring the almost carbonate-free facies at Site 693 (East Antarctic continental margin) and Site 695, nearby on the SOM, it seemed that a carbonate record might be limited to the upper Paleogene to lower Neogene, when the SOM was shallower and Antarctic glacial conditions were less severe. Site 696 was expected to provide valuable data on the history of the CCD in an area close to the West Antarctic margin. Calcareous benthic assemblages were expected to provide information on depth

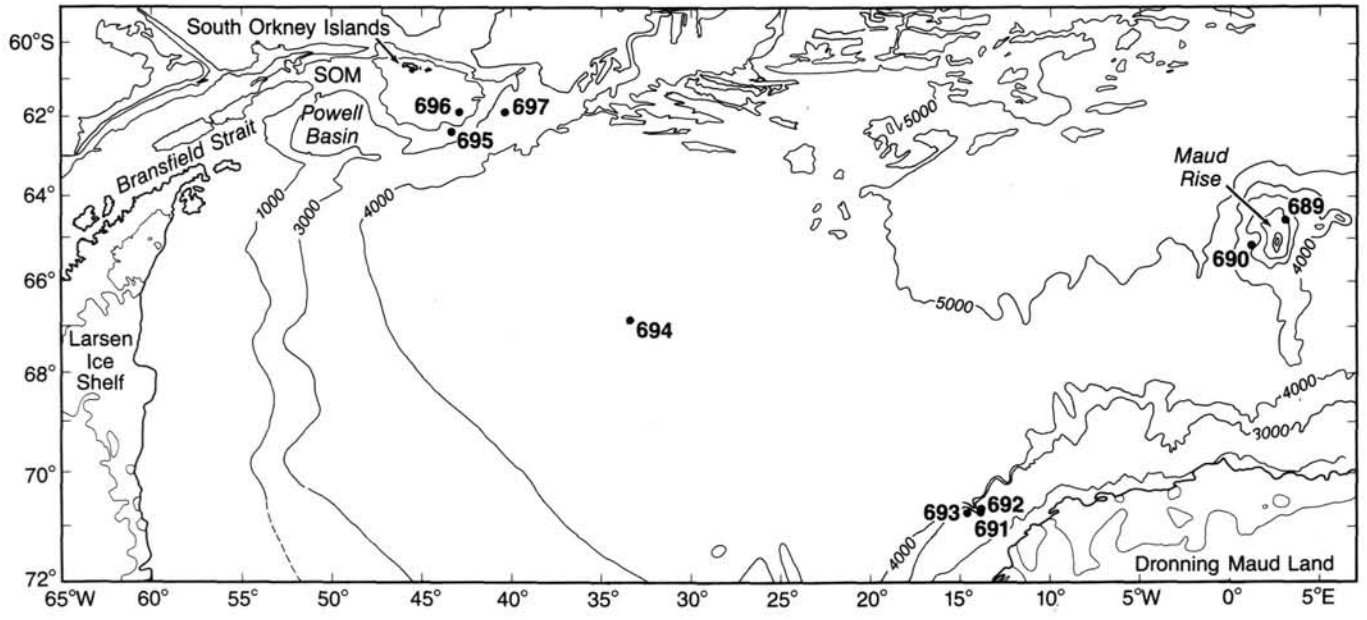

Figure 1. Regional setting of Site 696 on the northeastern margin of the Weddell Sea. SOM = South Orkney microcontinent.

changes, associated perhaps with glacio-eustasy and vertical tectonic movement.

2. Site 696 could provide important information about the paleoclimatic and paleoglacial development of the Antarctic. Changes in the rates of deposition of ice-rafted detritus should lead to insights about the development of glaciation and ice-sheet formation during the late Neogene. It may be possible eventually to differentiate sediment detritus from East and West Antarctic sources and to use this information for comparative studies of glacial evolution. Is there evidence of much ice rafting of detritus to Site 696 from East Antarctica during the early Neogene, prior to the inferred late Neogene formation of major ice-sheets on West Antarctica? The Weddell Gyre may have been weaker during the Paleogene to early Neogene, a time of lower global latitudinal temperature gradients. Furthermore, the probable development of large and extensive ice shelves during the late Neogene leaves open the possibility that extensive shallow seaways previously extended deep into the interior of Antarctica south of the Weddell Sea (in the region presently covered by the Filchner-Ronne ice shelves), perhaps even linking the Weddell and Ross seas. Circulation through such seaways could have modified the Weddell Gyre and, in turn, the delivery of ice-rafted detritus from East Antarctica. After the ice shelves developed, ice-rafting of sediments should have increased in the northwest Weddell Sea and over the SOM.

Changes in clay composition in Site 696 could also assist in evaluating the climatic evolution of West Antarctica including its ice-sheets. Site 696 could contain a record of spores and pollen from terrestrial vegetation on the Antarctic Peninsula during the Paleogene or even earliest Neogene.

3. Drilling at Site 696 was also expected to assist in understanding the development of the Antarctic Convergence, from examination of the Neogene biosiliceous record. The site's location in the northwest Weddell Sea near 62°S (about 3° north of the Maud Rise sites), was considered well-placed to record the Neogene development of the highly productive biosiliceous zone associated with the Antarctic Convergence, similar to Site 278 in the Southwest Pacific sector (Kennett, Houtz, et al., 1975) Previous studies had indicated that the Antarctic Convergence and associated highly biosiliceous zone migrated northward during the Miocene (Tucholke et al., 1976). Prior to this migration, did this zone lie at or near Site 696 and in the southern part of Drake Passage?

4. Did the opening of Drake Passage during the late Oligocene and Neogene (Barker and Burrell, 1976; 1977) affect sediment deposition at Site 696? Site 696 is in such shallow water that it may have been affected by intensified flow through a shallow or highly constricted Drake Passage in its early stages of opening.

OPERATIONS

Hole 696A

Site 696 is located 50 km north-northeast of Site 695. The sea voyage took 3 hr and the site was reached near noon on 23 February. The bit selected was a used RBI C4 serial number S-695. The bottom-hole assembly (BHA) consisted of the bit, long bit sub, seal bore collar, landing saver sub, long top sub, head sub, seven 8 1/4-in. drill collars, cross-over sub (XO), one 7 1/4-in. drill collar, XO, two stands of 5 1/2-in. drill pipe and XO.

The precision depth recorder (PDR) water depth was 659.3 m and the seabed was established by the first core to be at 661 m from the rig floor. At a depth of 12 mbsf, the piston shoe hit a hard object and broke 2 ft from its end. Core recovery was poor for the first 41 m (Table 1) possibly because of the presence of sand. Cores 113-696A-10H and 113-696A-11X had only partial stroke and no recovery.

The XCB system was employed in an attempt to improve recovery. Core 113-696A-12X, the second XCB core hit a hard layer after making 6.6 m, and as a precaution it was retrieved. The cutter was not damaged and a regular saw-tooth cutter was again run. The next core cut 3 m in normal time but the barrel could not be pulled free. It was moved 12 m but unfortunately could not be pulled clear of the BHA. After two wireline attempts to free the barrel the drill pipe was pulled clear of the seafloor. With the drill collars in the rotary table, an attempt was made to jar the barrel free with the wireline. The coring assembly parted inside the spring shaft housing and the lower portion was lost on the seafloor.

The remains of the assembly were dismantled and it was found that a large nut had stripped off the spring shaft. It is

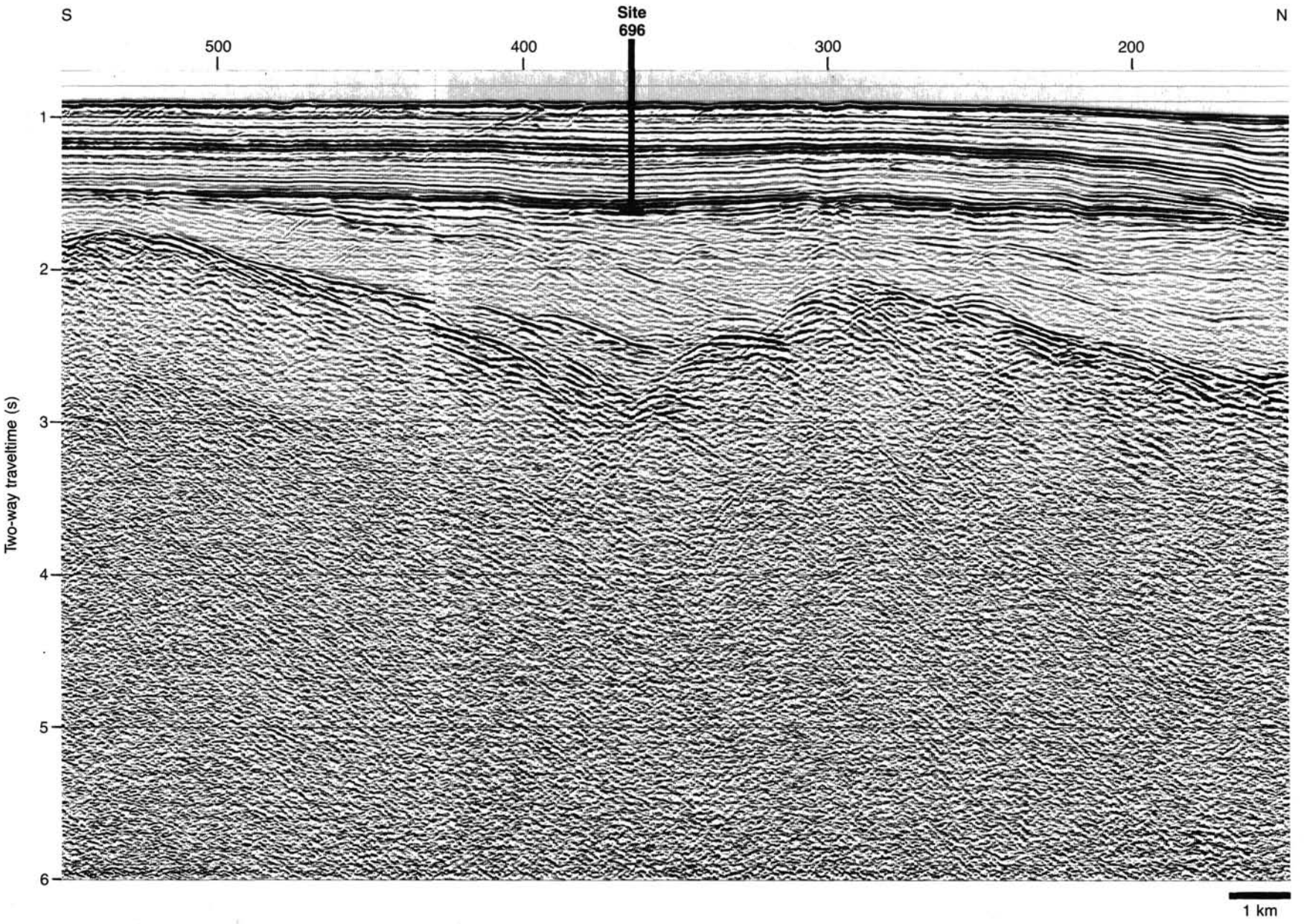

Figure 2. Section of seismic profile AMG845-18, showing location of Site 696.

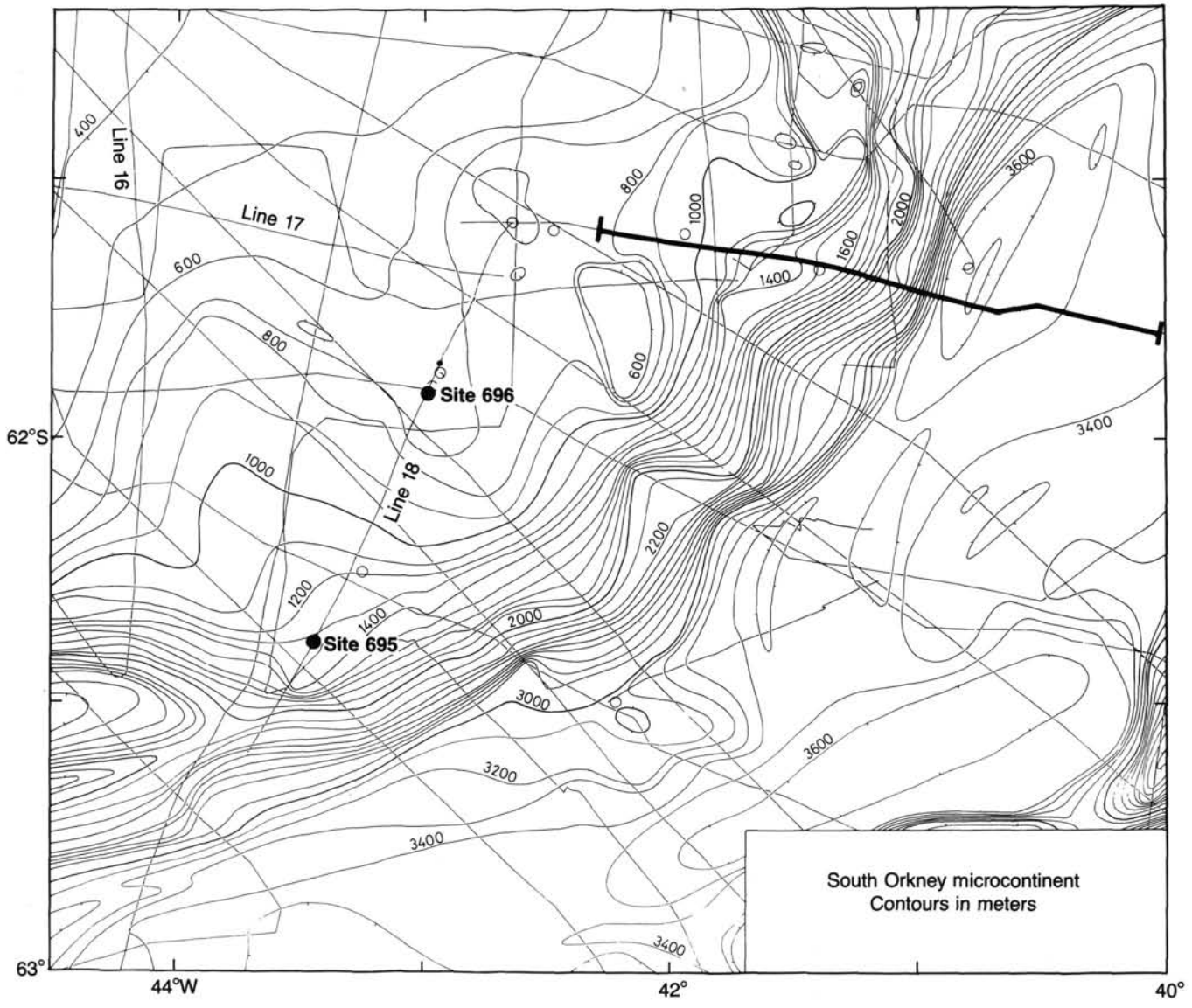

Figure 3. Bathymetry (in meters) of eastern margin of the South Orkney microcontinent (SOM) and Jane Basin. Leg 113 sites, and tracks of British Antarctic Survey/Birmingham University MCS profiles AMG845-16, 17, and 18 also shown.

likely that the stripping took place at the surface and was unrelated to the downhole sticking of the inner barrel. The nut was discovered to be stainless steel rather the design heat-treated 4140. It probably had been made on the ship in an emergency and never discarded when the approved parts arrived.

Heavy losses of the stock of XCB parts available on the ship had created a critical situation. Only two more catastrophic losses could be tolerated before it would be necessary to attempt manufacturing of parts on the ship. It was decided to conserve the remaining XCB stock for W6, and a rotary-coring system was used to continue Site 696.

A positive achievement resulting from the loss of the core barrel was that it locked open the new lockable float valve as it went down the hole, proving the success of the tool. That dark cloud had a silver lining.

Hole 696B

The plan was to log the hole and logging required a releasable bit. A used RBI C4 was run with a hydraulic bit release and profile sub. The remainder of the BHA was the same as that used for the Hole 696A.

The first core was a wash core to 76.6 mbsf (Table 1). Cores 113-696B-2R to 113-696B-47R, 76.6–501.2 mbsf, had virtually no core recovery. Many combinations of surface variables were tried in an effort to increase recovery, but our conclusion is that we cannot core soft, highly sandy sediments (as at Site 694) or diatom oozes (as at this site) with a rotary system. Core 113-696B-9I was the interstitial pore-water test that obtained a temperature of 7.4°C which, based on one measurement, established a thermal gradient of 52°C/km. This gradient required any possible gas hydrate zone to be at 264 mbsf, and there was no geophysical evidence to support one at that depth. Core 113-696B-18I was a second test. The probe broke off in what may have been hard sand or rocks thus ending temperature measurements in the hole.

Core recovery below 501.2 mbsf increased, and the last core recovered from 635.9 to 645.6 contained 9.79 m. The scientific staff desired to continue, but the depth limitation imposed by the Safety Panel had been reached.

Table 1. Coring summary, Site 696

Core no.	Date (Feb. 1987)	Time	Depth (mbsf)	Cored (m)	Recovered (m)	Recovery (%)
113-696A-						
1H	23	1945	0-5.5	5.5	2.12	38.5
2H	23	2015	2.5-12.0	9.5	9.28	97.7
3H	23	2230	12.0-21.6	9.6	0.75	7.8
4H	23	2300	21.6-31.2	9.6	1.14	11.9
5H	23	2345	31.2-40.8	9.6	6.42	66.9
6H	24	0030	40.8-50.4	9.6	9.61	100.0
7H	24	0100	50.4-60.0	9.6	9.89	103.0
8H	24	0300	60.0-69.6	9.6	9.51	99.0
9H	24	0245	69.6-79.3	9.7	8.35	86.1
10H	24	0430	79.3-89.0	9.7	0	0
11X	24	0745	89.0-96.4	7.4	1.17	15.8
12X	24	0930	96.4-103.0	6.6	0.06	0.9
				106.0	58.30	
113-696B-						
1W	24	2245	0-76.6	76.6	0	0
2R	24	2345	76.6-86.2	9.6	0.88	9.2
3R	25	0100	86.2-95.9	9.7	6.61	68.1
4R	25	0230	95.9-105.5	9.6	0	0
5R	25	0430	105.5-115.2	9.7	9.12	94.0
6R	25	0600	115.2-124.8	9.6	5.42	56.4
7R	25	0745	124.8-134.5	9.7	6.17	63.6
8R	25	0915	134.5-144.1	9.6	2.78	28.9
9I	25	1030	144.1-144.8	0.7	0	0
10R	25	1300	144.1-153.8	9.7	2.31	23.8
11R	25	1245	153.8-163.5	9.7	0	0
12R	25	1415	163.5-173.2	9.7	0.98	10.1
13R	25	1545	173.2-182.9	9.7	0.76	7.8
14R	25	1700	182.9-192.5	9.6	0	0
15R	25	1800	192.5-202.2	9.7	0	0
16R	25	1900	202.2-211.8	9.6	0	0
17R	25	2000	211.8-221.5	9.7	2.09	21.5
18I	25	2115	221.5-222.2	0.7	0	0
19R	25	2215	221.5-231.1	9.6	0.27	2.8
20R	25	2315	231.1-240.8	9.7	4.60	47.4
21R	26	0100	240.8-250.4	9.6	3.88	40.4
22R	26	0215	250.4-260.1	9.7	0.38	3.9
23R	26	0515	260.1-269.7	9.6	7.91	82.4
24R	26	0630	269.7-279.4	9.7	2.67	27.5
25R	26	0800	279.4-289.0	9.6	1.50	15.6
26R	26	0915	289.0-298.7	9.7	4.93	50.8
27R	26	1030	298.7-308.3	9.6	2.66	27.7
28R	26	1145	208.3-319.0	9.7	5.80	59.8
29R	26	1245	318.0-327.6	9.6	0	0
30R	26	1400	327.6-337.3	9.7	2.68	27.6
31R	26	1515	337.3-347.0	9.7	0.74	7.6
32R	26	1630	347.0-356.6	9.6	3.26	33.9
33R	26	1745	356.6-366.3	9.7	0.03	0.3
34R	26	1845	366.3-376.0	9.7	4.11	42.4
35R	26	1945	376.0-385.6	9.6	0	0
36R	26	2100	385.6-395.3	9.7	0	0
37R	26	2200	395.3-404.9	9.6	0	0
38R	26	2345	404.9-414.6	9.7	0	0
39R	27	0115	414.6-424.2	9.6	0	0
40R	27	0230	424.2-433.9	9.7	0.36	3.7
41R	27	0400	433.9-443.5	9.6	0	0
42R	27	0515	443.5-453.2	9.7	0	0
43R	27	0700	453.2-462.8	9.6	0	0
44R	27	0800	462.8-472.5	9.7	0.16	1.7
45R	27	0915	472.5-482.0	9.5	1.88	19.8
46R	27	1030	482.0-491.6	9.6	0.67	7.0
47R	27	1200	491.6-501.2	9.6	1.42	14.8
48R	27	1300	501.2-510.7	9.5	3.34	35.1
49R	27	1345	510.7-520.2	9.5	1.28	13.5
50R	27	1515	520.2-529.8	9.6	1.94	20.2
51R	27	1645	529.8-539.4	9.6	2.49	25.9
52R	27	1830	539.4-548.9	9.5	0.46	4.8
53R	27	2030	548.9-558.5	9.6	9.28	96.6
54R	27	2200	558.5-568.2	9.7	5.32	54.8
55R	28	0000	568.2-577.9	9.7	8.02	82.7
56R	28	0145	577.9-587.6	9.7	2.56	26.4
57R	28	0300	587.6-597.2	9.6	1.22	12.7
58R	28	0445	597.2-606.9	9.7	2.23	23.0
59R	28	0600	606.9-616.6	9.7	7.26	74.8
60R	28	0730	616.6-626.2	9.6	8.23	85.7
61R	28	0845	626.2-635.9	9.7	6.24	64.3
62R	28	1045	635.9-645.6	9.7	9.79	101.0
				647.0	156.69	

The hole was to be logged. The first attempt to log the hole was on 28 February. Prior to pulling out of the hole it was circulated and swept with 50 bbl of high-viscosity mud, and the hydraulic bit release functioned successfully. The bit was pulled to 99 mbsf and there was no abnormal pipe drag. Because 6 hr was required to rig the sidewall entry sub (SES) it was decided to attempt to log without it. Unfortuately the logging tools contacted a bridge at only 62 m below the drill pipe, ending any hopes of an easy logging job. The logging tools were lowered and raised for more than an hour before they finally broke through the upper obstruction. The tools were then pulled into the drill pipe and tripped out of the hole. On examining the tool assembly, it was noticed that the caliper arm was slightly bent. Hole conditioning was necessary before any further logging could be attempted. A wiper trip was made with the bitless drill pipe. Many ledges and bridges were encountered and there was about 30 m of fill on the bottom which was washed out with some difficulty. The hole was swept with 100 bbl of 100+ viscosity mud, circulated, and a second 100 bbl of mud was spotted in the hole.

The SES and logging tools were rigged up and started in the hole. The drill pipe was run to 633 mbsf. This trip is testimony that a large amount of high-viscosity mud is helpful in controlling sand or siliceous ooze. An attempt to lower the logging tools below the end of the pipe failed when a bridge was encountered at 475 mbsf or 158 m above the end of (inside) the pipe. Efforts to pump the pipe down were not successful. The pipe was pulled to 555 mbsf and the bridge apparently fell out because circulation was possible. The tools were lowered out the end of the pipe and the hole was logged from 632 mbsf to the end of the pipe.

To continue logging it was necessary to pull additional pipe. Before additional pipe could be pulled, the circulating head and hose which were high in the derrick had to be removed. Because the hole had a history of back-flowing, it was decided to slug the drill pipe with mud before breaking off the circulating head. Rather than risk the logging tools in the open hole they were pulled approximately 30 m inside the drill pipe before circulating to assure the safety of the tools. The mud pump stroked 23 times or 115 gal, and the drill-pipe pressure surged to 800 psi. The weight indicator in the Schlumberger logging unit dropped to the low end of the scale and approximately 1100 lb line weight was noted.

The drill pipe was pulled to the SES. It was found that the weak point in the logging line had failed, leaving the entire string of logging tools in the hole. Sand or other material may have packed around the tools forming a hydraulic seal so that the tools were blown out of the end of the line during circulation.

An effort was made to fish for the tool assembly using a mock core barrel with a 4-in. landing shoulder and Larson slip-type core catcher. It was realized that the chances of success were small, but an attempt was required by the insurance policy on the equipment. The first objective was to attempt to stab the BHA over the logging tools in the open hole. The pipe was run in to 575 mbsf where the top drive was picked up. The pipe was carefully washed and rotated to 596 mbsf where it began to take weight and the torque increased. It was concluded that the top of the tool had been reached.

The overshot was run in the hole on the core line and the core barrel was latched. The barrel could not be pulled with the maximum allowable line tension. This was an encouraging indication that the tool had indeed been caught. Initial attempts to shear the pins in the overshot failed and the Kinley line-cutter was dropped. It did not fire. As a last alternative the overshot was sheared free and the line pulled from the hole. The drill pipe was pulled from to the surface, but the overshot was empty.

There were no indications of the tool having been in the overshot. The core barrel was jammed tightly in the outer barrel which explained the false indication of the tool being caught. Hole 696B was abandoned on 2 March 1987.

LITHOSTRATIGRAPHY

Introduction

The sedimentary sequence drilled at Site 696 is mainly of mixed terrigenous and pelagic origin; volcanic products are present but are of less importance. The sediments recovered have been divided into seven lithologic units (Fig. 4 and Table 2) primarily based on composition as determined from smear-slide analyses (Fig. 5) and diagenetic maturity. Changes in the abundance of biosiliceous components, mainly diatoms with radiolarians, silicoflagellates, and sponges, are the most important distinguishing characteristic. Terrigenous and authigenic components are important at certain intervals, mostly in the lower part of Hole 696B, as is the diagenetic sediment maturity (lithification).

Diatom abundance rapidly increases with depth from low values at the surface to high values (as high as 70%) downcore to 64.2 mbsf (Sample 113-696A-8H-3, 120 cm). From there it drops to less than 10% at 173.95 mbsf (Sample 113-696B-13R-1, 75 cm). Between 211.8 (Core 113-696B-17R) and 529.8 mbsf (Core 113-696B-50R) diatom abundance is high, and oozes containing 90% diatoms are present. Below 529.8 mbsf diatoms comprise less than 10% of the sediment or are absent. Silicoflagellates and radiolarians are present only in minor amounts.

The biogenic calcareous component, which is exclusively planktonic foraminifers, is minor (less than 20%) occurring in isolated patches in the uppermost two Sections 113-696A-1H-1 and 113-696A-1H-2.

Authigenic deposits such as cherts and glauconite occur from 356.6 (Core 113-696B-33R) to 521.7 mbsf (Sample 113-696B-50R-1, 68 cm) and from 569.7 (Section 113-696B-55R-2) to 599.4 mbsf (Section 113-696B-58R-2), respectively. Authigenic dolomite occurs at 502.2 (Sample 113-696B-48R-1, 100–105 cm) and 599.2 mbsf (Sample 113-696B-58R-2, 55–75 cm).

Terrigenous components are dominant from 64.2 (Sample 113-696A-8H-43, 120 cm) to 213.3 mbsf (Section 113-696B-17R-2), from 254.9 (Section 113-696B-22R-1) to 269.7 mbsf (Section 113-696B-23R-6), and from 521.7 (Section 113-696B-50R-2) to the base of Hole 696B at 645.6 mbsf (Section 113-696B-62R, CC). Devitrified volcanic ash and glass are a minor component between 50.4 (Core 113-696A-7H) and 153.8 mbsf (Core 113-696B-10R) and between 510.7 (Core 113-696B-49R) and 597.2 mbsf (Core 113-696B-57R).

Lithostratigraphic Unit I, 64.2 m thick (Table 2), is composed mainly of diatom-rich sediments of Quaternary to late Pliocene age. It is divided into two subunits: Subunit IA is 8.5 m thick and consists of Quaternary diatom-bearing sediments with minor amounts of calcareous foraminifers and silicoflagellates. Subunit IB, 55.7 m thick and of late Pliocene age (middle Upsilon Zone), is composed of diatom clayey mud and muddy diatom ooze.

Lithostratigraphic Unit II, 60.6 m thick, of early to late Pliocene age (middle Upsilon Zone to lower Tau Zone), is characterized by a distinct decrease in biosiliceous components and is composed mainly of diatom-bearing silty and clayey mud.

Lithostratigraphic Unit III, 87.0 m thick, early Pliocene (lower Tau Zone) to late Miocene (upper *Cycladophora spongothorax* Zone) in age, comprises predominantly silty and clayey mud and some diatom-bearing mud.

Lithostratigraphic Unit IV, 48.3 m thick, is characterized by a significant increase in the biosiliceous component. It consists of diatom ooze and muddy diatom ooze and is late Miocene (*C. spongothorax* Zone) in age.

Lithostratigraphic Unit V, 9.6 m thick, is of late Miocene (*C. spongothorax* Zone) age and consists of coarse-grained sand.

Lithostratigraphic Unit VI, 260.1 m thick, is of early late–late middle Miocene to late Miocene age, and consists of diatom-rich sediments. It can be divided into two subunits. Subunit VIA is 202.8 m thick, late Miocene or early late–late middle Miocene in age, and is composed of diatom ooze and mud-bearing diatom ooze. Subunit VIB, 57.3 m thick, is of early late–late middle Miocene age and consists of lithified diatomite and mud-bearing diatomite.

Lithostratigraphic Unit VII, 115.8 m thick, is predominantly terrigenous in origin, middle Miocene(?) to Eocene in age, and is divided into four subunits: Subunit VIIA consists of middle Miocene(?) sandy mudstone, Subunit VIIB is composed of lower Miocene(?) to late Paleogene(?) claystone, clayey mudstone, and silty mudstone, Subunit VIIC is composed of lower Miocene(?) to Oligocene(?) glauconite silty mudstone and claystone, and Subunit VIID consists of sandy mudstone of lower Oligocene-Eocene age.

Drilling disturbance and core recovery at Site 696 are a problem (Table 3). Hole 696A was drilled by APC/XCB to 106.0 mbsf with a total recovery of about 55%. About 29% of the recovered core was very disturbed or showed soupy structures, 33% was moderately to slightly disturbed and only 38% was undisturbed. Hole 696B was rotary drilled from 76.6 to 645.6 mbsf and recovered 156.7 m of sediment, a recovery rate of approximately 27%. About 26% of the core recovered was very disturbed or soupy, 62% was moderately to slightly disturbed and only 12% was undisturbed.

Three long intervals in Hole 696B from 175 to 212, from 370 to 424, and from 425 to 453 mbsf lack any information because there was no recovery. Defining lithostratigraphic boundaries and interpreting the sedimentary sequences was severely hampered in these intervals, especially the boundaries between Units III and IV and between IV and V, and subdivisions of Unit VI.

Bioturbation is generally minor to moderate, and distinct burrows are difficult to recognize even in undisturbed cores. Poor recovery and preservation of the cores recovered from Holes 696A and 696B, however, may produce unrepresentative data on bioturbation. Primary sedimentary structures were also difficult to identify, and the overall description may be strongly biased because of the lack of information.

Unit I (Depth 0–64.2 mbsf; Age Quaternary to late Pliocene)

Core 113-696A-1H through Sample 113-696A-8H-3, 120 cm; thickness 64.2 m; Quaternary to late Pliocene (middle Upsilon Zone) in age.

Lithostratigraphic Unit I is divided into two subunits mainly based on the abundance of diatoms, but also on the presence of silicoflagellates and planktonic foraminifers, as well as the frequency of occurrence of ice-rafted dropstones.

Subunit IA (Depth 0–8.5 mbsf)

Core 113-696A-1H through Section 113-696A-2H-4; thickness 8.5 m; Quaternary in age.

The sediments of Subunit IA consist predominantly of olive (5Y 4/3) to olive gray (5Y 4/2, 5/2) diatom-bearing silty mud and olive (5Y 4/2), greenish gray (5GY 6/1) to gray (N 6/0) diatom-bearing clayey mud. The abundance of diatoms in Subunit IA generally does not exceed 30%. Silicoflagellates are present in very small amounts (less than 2%). Minor amounts of calcareous planktonic foraminifers (generally less than 5%, but as much as 20%) are present in short intervals of Samples 113-696A-1H-1, 0–10 cm, and 89–110 cm; 113-696A-1H-2, 21–26 cm, 30–32 cm, and 38–48 cm, and may locally form foraminifer- and diatom-bearing sandy mud. The very strong drilling

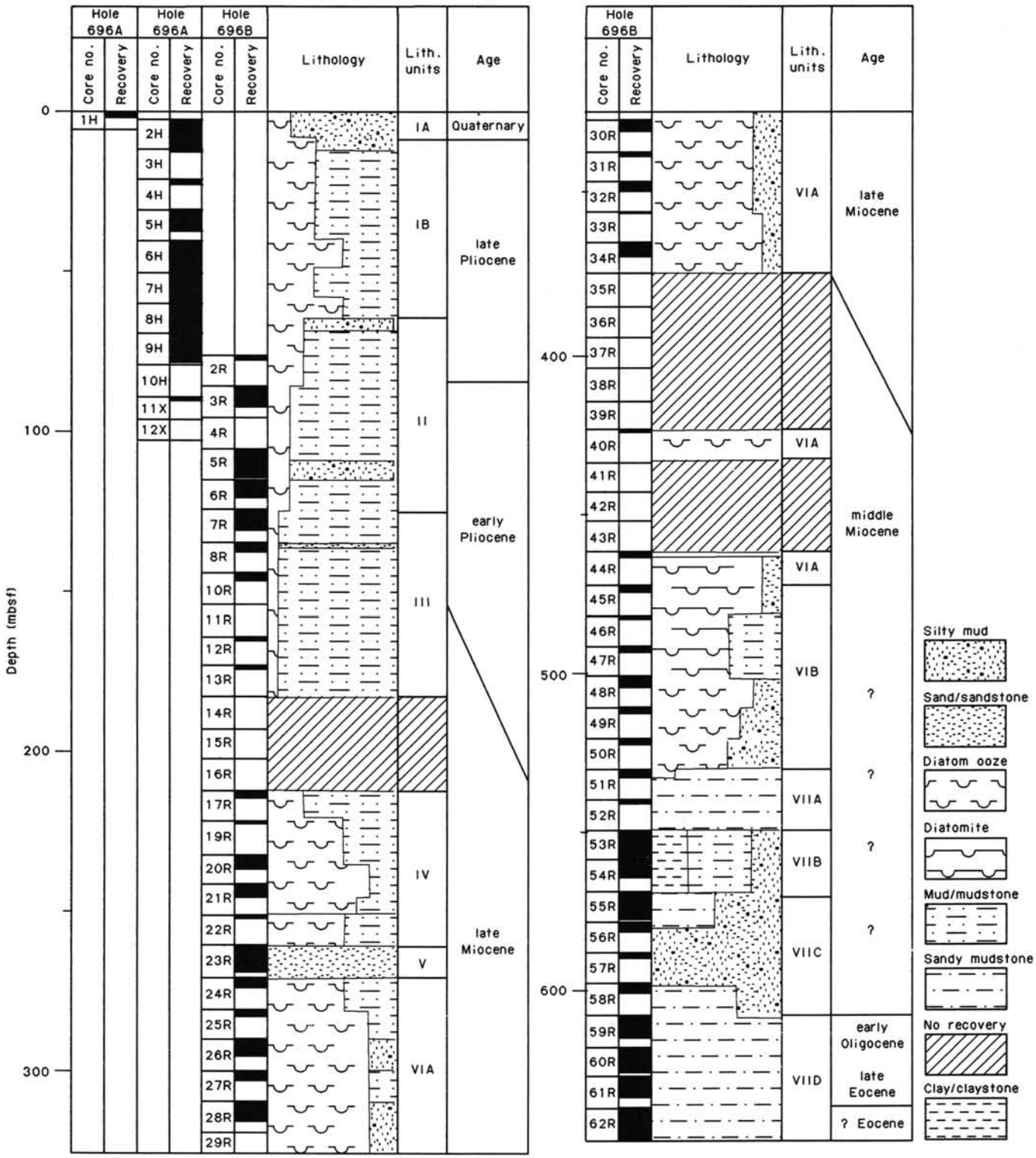

Figure 4. Lithostratigraphic summary, Site 696. Legend is given in Figure 3, Sites 691 and 692 chapter (this volume).

Table 2. Lithostratigraphic units from Site 696.

Unit	Dominant lithology	Interval (mbsf)	Thickness (m)	Age
I				
IA	Diatom-bearing silty mud	0–8.5	8.5	Quaternary
IB	Diatom clayey mud Muddy diatom ooze	8.5–64.2	55.7	late Pliocene (middle Upsilon Zone)
II	Diatom-bearing silty mud Diatom-bearing clayey mud	64.2–124.8	60.6	late Pliocene (middle Upsilon Zone) to early Pliocene (lower Tau Zone)
III	Silty and clayey mud Diatom-bearing clayey mud	124.8–211.8	87.0	early Pliocene (lower Tau Zone) to late Miocene (upper *C. spongothorax* Zone)
IV	Diatom ooze Muddy diatom ooze	211.8–260.1	48.3	late Miocene (*C. spongothorax* Zone)
V	Coarse sand	260.1–269.7	9.7	late Miocene (*C. spongothorax* Zone)
VI				
VIA	Diatom ooze Mud-bearing diatom ooze	269.7–472.5	202.8	late Miocene to early late or late middle Miocene
VIB	Mud-bearing diatomite Diatomite	472.5–529.8	57.3	early late or late middle Miocene to middle Miocene
VII				
VIIA	Sandy mudstone	529.8–548.9	19.1	middle Miocene(?)
VIIB	Claystone Clayey mudstone Silty mudstone	548.9–569.7	20.8	early Miocene(?) to late Paleogene
VIIC	Glauconite silty mudstone Claystone	569.7–606.9	37.2	early Miocene(?) to late Oligocene(?)
VIID	Sandy mudstone	606.9–645.6	38.7	early Oligocene-Eocene

disturbance in Core 113-696A-1H blurs or obscures the details of the lithologic sequence, making many finer-scale sedimentary features difficult to recognize.

Ice-rafted dropstones of 0.5–3 cm in size are abundant in Subunit IA. Well-rounded to subangular igneous and volcanic rocks predominate over sedimentary rocks.

A color cyclicity of alternating greenish gray (5GY 6/1), olive (5Y 4/4), and olive gray (5Y 4/2) beds in the diatom silty muds of Core 113-696A-2H shows sharp and gradational color contacts (Fig. 6). These contacts are not accompanied by any significant change in the sediment composition.

Subunit IB (Depth 8.5–64.2 mbsf)

Section 113-696A-2H-5 through Sample 113-696A-8H-3, 120 cm; thickness 55.7 m; late Pliocene (middle Upsilon Zone) in age.

The sediments of Subunit IB are generally rich in diatoms. The main lithologies are olive gray (5Y 5/2) and dark greenish gray (5GY 4/1, 5G 4/1, 5BG 4/1) to greenish gray (5GY 5/1, 5G 5/1) diatom clayey mud and olive gray (5Y 5/2) to gray (5Y 5/1) muddy diatom ooze commonly showing subtle gradational color changes. Less common olive gray (5Y 5/2) diatom mud and diatom silty mud were also recovered.

As a minor lithology several volcanic ash layers are present. Dark olive gray (5Y 3/2) and dark greenish gray 5GY 4/1) to grayish green (5G 5/2) thin beds (less than 1 cm thick) of devitrified volcanic ash occur beginning in Section 113-696A-7H-2. At about the same level as the devitrified ash, the sediment color changes from olive gray (5Y 5/2) to dark greenish gray (5G 4/1). Two pronounced very dark gray (5Y 3/1) to black (5Y 2.5/1) layers of fresh, angular volcanic glass occur in Samples 113-696A-7H-3, 5–10 cm, and 113-696A-7H-7, 52–55 cm, both showing sharp contacts at their base; the former is normally graded, the latter is slightly bioturbated showing a very distinct pattern of vertical burrowing (Fig. 7).

Silty/sandy normally-graded or laminated beds and patches are observed in Cores 113-696A-7H and 113-696A-8H in the lower part of Subunit IB. Sand-sized ice-rafted detritus and dropstones (ice-rafted detritus coarser than 0.3 cm) are present throughout this subunit. The dropstones are well rounded to subrounded and as large as 3 cm in size.

Less-regular millimeter-sized silty "mud clasts" of pure quartz silt also occur. They may represent biogenic features rather than ice-transported mud clasts. The well-sorted angular grains show some structural features that could perhaps have been formed by agglutinated benthic foraminifers, although diagnostic foraminifer structures have not been observed.

Bioturbation in Subunit IB is generally minor and only halo burrows and Planolites are observed. Connected with the volcanic glass layer is a typical wiggly vertical burrow pattern which is common throughout the glaciomarine sequences drilled (Fig. 7). Because the sediment cores are cut vertically, oval cross-sectional cuts, the only distinct pattern of burrowing recognized in the sediments recovered, predominate.

Unit II (Depth 64.2–124.8 mbsf; Age early to late Pliocene in age)

Sample 113-696A-8H-3, 120 cm, through Core 113-696A-12X; 64.2–103.0 mbsf; thickness 38.8 m; Pliocene (middle Upsilon Zone to lower Tau Zone) in age. Cores 113-696B-2R through 113-696B-6R; 76.6–124.8 mbsf; thickness 48.8 m; Pliocene (middle Upsilon Zone to lower Tau Zone) in age. The total combined thickness for Unit II from Holes 696A and 696B is 60.6 m.

Sediments of Unit II are characterized by a large and abrupt decrease in the biosiliceous component from 70% at 63.9 mbsf

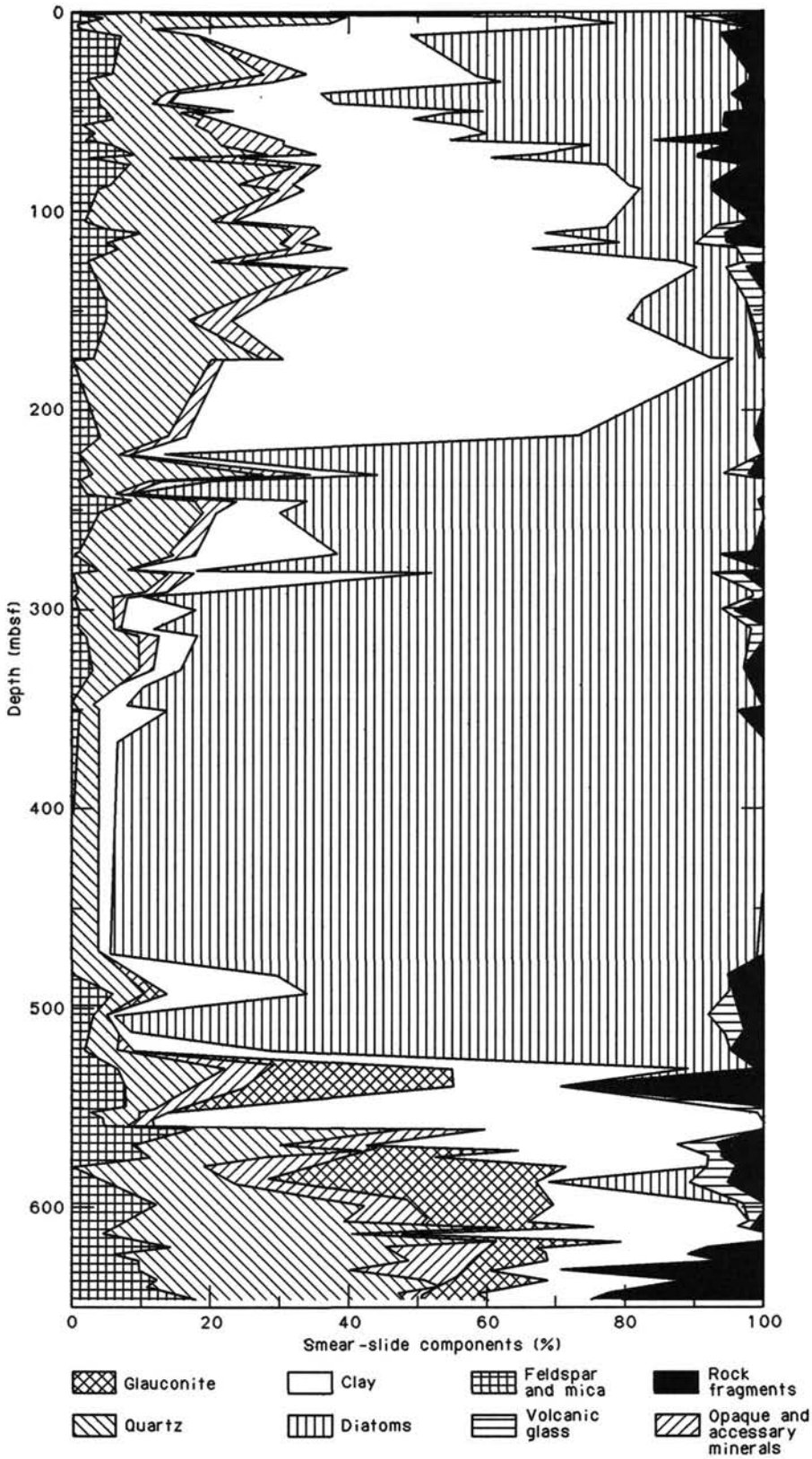

Figure 5. Sediment composition, Holes 696A and 696B, from smear-slide data.

(Sample 113-696A-8H-3, 95 cm) immediately above the top of the unit, to 30% at 64.6 mbsf (Sample 113-696A-8H-4, 10 cm). The predominant lithologies are dark greenish gray (5G 4/1, 5BY 4/1) to greenish gray (5B 5/1, 5BG 5/1, 5 GY 5/1) diatom-bearing clayey mud, dark greenish gray (5G 4/1, 5GY 4/1) to greenish gray (5G 5/1) and gray (5Y 5/1) diatom clayey mud, and less common dark greenish gray (5GY 4/1, 5G 4/1) and gray (5Y 5/1) diatom-bearing silty mud.

Table 3. Recovery and preservation of cores drilled at Site 696.

	Meters cored	Meters recovered
Hole 696A	106.0	58.3 = about 55%
Hole 696B	[a]645.6	156.7 = about 27%

	Disturbance (%)				
	Soupy	Very	Moderately	Slightly	Undisturbed
Hole 696A	7	22	22	11	38
Hole 696B	3	23	34	28	12

[a] Washed to 76.6 m.

As a minor lithology, thin beds (less than 1 cm thick) of grayish green (5G 5/2) devitrified volcanic ash are very common throughout this unit, especially in Cores 113-696B-5R through 113-696B-6R. Dark greenish gray (5BG 4/1) and dark olive gray (5Y 3/2) volcanic-glass-rich beds, well bedded or slightly dispersed through the sediment, occur at many levels (Samples 113-696A-9H-2, 4–6 cm; 113-696B-3R-4, 140–145 cm; 113-696B-5R-6, 135–140 cm).

At 89.2 mbsf (Sample 113-696A-11X-1, 20–30 cm) a dark greenish gray (5G 4/1), very hard silty mudstone was recovered (Fig. 8). Lithic fragments and mud clasts similar in composition to the surrounding sediment were apparently cemented by diagenetic dolomite.

Sand-sized ice-rafted detritus is common throughout this unit and sometimes occurs in layers (e.g., Sample 113-696A-11X-1, 65–70 cm). Well-rounded to subangular dropstones are present but rare in the upper Unit II. Volcanic and metamorphic rock fragments are more abundant than sedimentary dropstones.

Bioturbation is minor to absent throughout Unit II.

Unit III (Depth 124.8–211.8 mbsf; Age early Pliocene to late Miocene)

Cores 113-696B-7R through 113-696B-16R; thickness 87 m; Pliocene (lower Tau Zone) to late Miocene (*C. spongothorax* Zone).

Sediments of lithostratigraphic Unit III are predominantly terrigenous in origin. The biosiliceous component (mainly diatoms) comprises less than 15%. The main lithologies are dark bluish gray (5B 4/1), dark greenish gray (5G 4/1) to dark gray (N 4/0) diatom-bearing clayey mud and dark greenish gray (5G 4/1) to dark gray (N 4/0) silty mud. Dark greenish gray (5G 4/1) clayey mud is a less common major lithology.

Grayish green (5G 5/2), thin, devitrified volcanic ash beds occur as a minor lithology and are especially abundant in Core 113-696B-10R. Volcanic activity during deposition of Unit III is further documented by the occurrence of a small (about 2 cm in diameter) reddish colored pumice pebble (Fig. 9).

Ice-rafted detritus is present throughout this unit. Well rounded to subangular dropstones are common especially in Core 113-696B-7R and reach 5 cm in diameter. Sedimentary, igneous, and metamorphic rocks are equally abundant.

Bioturbation is minor to moderate in Core 113-696B-7R. No specific burrow types are recognized due to strong drilling disturbance and poor recovery.

Unit IV (Depth 211.8–260.1 mbsf; Age late Miocene)

Cores 113-696B-17R through 113-696B-22R; thickness 48.3 m; late Miocene (*C. spongothorax* Zone) in age.

Lithostratigraphic Unit IV is characterized by a strong increase in the biosiliceous component, as high as 90%, enough to form biosiliceous oozes.

Unit IV consists predominantly of olive (5Y 5/3), olive gray (5Y 5/2, 4/2) and gray (5Y 5/1) diatom ooze; olive gray (5Y 5/2) and gray (5Y 5/1) muddy diatom ooze; and dark greenish gray (5G 4/1) diatom-bearing clayey mud and diatom mud. The diatom mud occurs only at the top of this unit in Core 113-696B-17R.

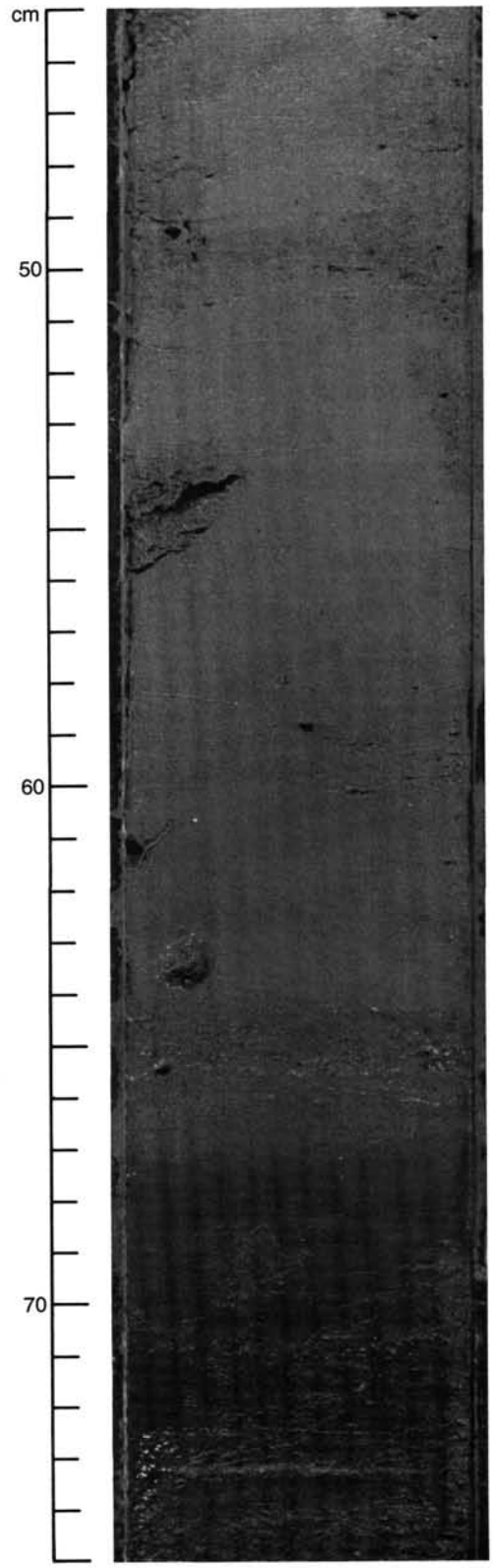

Figure 6. Sharp color contact between olive (5Y 4/4, bottom) and greenish gray (5GY 6/1, top) diatom silty muds (Sample 113-696A-2H-2, 45–75 cm).

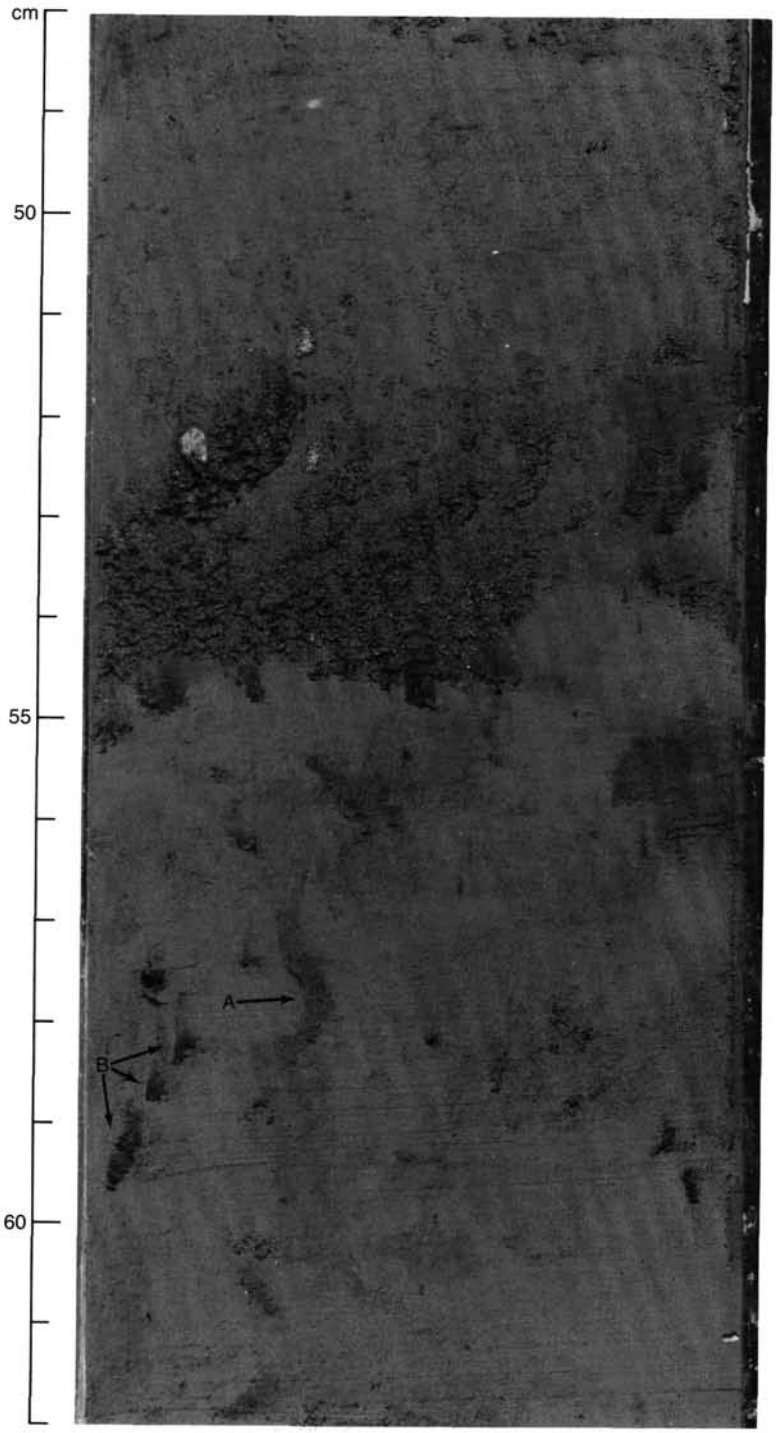

Figure 7. Volcanic ash layer containing a high percentage of angular, fresh volcanic glass. The layer is slightly blurred by burrowing. The vertical, wiggly burrow (A) below the glass layer and its oval-shaped cross-sectional cuts (B) represent a more typical burrow feature seen during Leg 113 (Sample 113-696A-7H-7, 48–62 cm).

Two dark greenish gray (5G 4/1) beds of devitrified volcanic ash occur in Samples 113-696B-17R-2, 16–17 cm, and 28–29 cm.

Ice-rafted detritus and dropstones are present throughout this unit. The latter are very common in Core 113-696B-20R. The dropstones reach 6 and 7 cm in diameter (Section 113-696B-22R-1) and show a clear dominance of sedimentary rocks (mudstone, siltstone, sandstone) over metasediments and igneous rocks.

Bioturbation and other sedimentary structures are impossible to recognize because of strong drilling disturbance and poor recovery.

Unit V (Depth 260.1–269.7 mbsf; Age late Miocene)

Core 113-696B-23R; thickness 9.6 m; late Miocene (*C. spongothorax* Zone) in age.

Lithostratigraphic Unit V consists of a very coarse grained, well sorted sand, probably strongly disturbed by the drilling

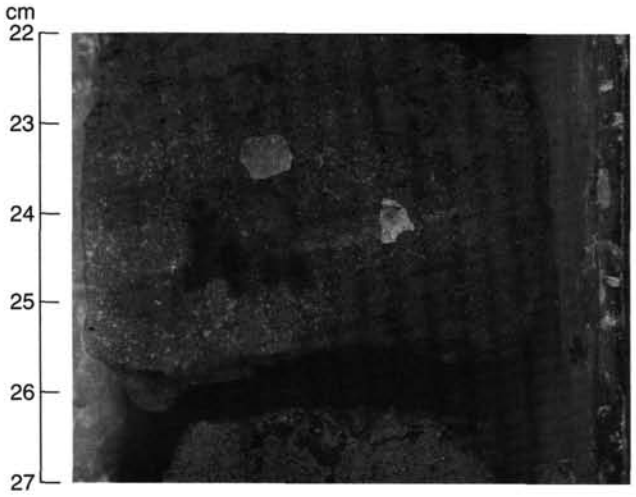

Figure 8. Lithified silty mudstone from Core 113-696A-11X-1, 22-27 cm. Quartz, lithic fragments, and mud clasts are lithified by diagenetic dolomite.

Figure 9. Well-preserved pumice pebble from early Pliocene, diatom-bearing clayey mud, Sample 113-696B-7R-2, 137–139 cm.

process. Clear drill cuttings could not be identified. The sediment sequence recovered in Core 113-696B-23R did not show any obvious grading or sorting, neither small-scale within section, nor large-scale from section to section downcore, although some small and water-rich, deformed mud clasts occur intermixed in Sections 113-696B-23R-4 and 113-696B-23R-5. The sand is very immature and is composed mainly of angular lithic fragments of very diverse rock types. Both angular and very well-rounded and polished quartz grains commonly occur.

Unit V is considered to represent a coarse-grained turbidite sequence. A recovery of approximately 8 m out of a total 9.7-m drilled interval may indicate rather reduced vertical mixing by drilling and it is presumed that the sequence is still largely in place.

Unit VI (Depth 269.7–529.8 mbsf; Age late to middle Miocene)

Cores 113-696B-24R through 113-696B-50R; thickness 260.1 m; late Miocene to middle Miocene in age.

Sediments of Unit VI are characterized by a very high abundance of biosiliceous components, predominantly diatoms. Based on sediment maturity, Unit VI is divided into two subunits: Subunit VIA consists of soft and semilithified sediments, whereas Subunit VIB is composed of indurated sediments.

Subunit VIA (Depth 269.7–472.5 mbsf)

Cores 113-696B-24R through 113-696B-44R; thickness 202.8 m; late to early late or late middle Miocene in age.

The main lithologies of Subunit VIA are olive gray (5Y 5/2, 4/2), light olive (5Y 6/2), dark gray (5Y 4/1) and olive (5Y 4/3) mud-bearing diatom ooze, olive gray (5Y 5/2, 4/2) to dark gray (5Y 4/1) muddy diatom ooze and olive (5Y 4/3) to olive gray (5Y 4/2) diatom ooze. Less common olive (5Y 4/3) mud-bearing diatom ooze and dark greenish gray (5GY 4/1) diatom clayey mud occur. In Cores 113-696B-34R and 113-696B-40R the sediment sequence is, in part, more indurated, forming an olive (5Y 4/4, 4/3) diatomite.

A few grayish green (5G 5/2) devitrified, thin (1–2 cm thick) volcanic ash beds are present in Cores 113-696B-26R and 113-696B-28R. Volcanic glass occurs as a minor component (1%–4%) dispersed in the sediments from Core 113-696B-24R at the top of this subunit down to Core 113-696B-30R at 337.3 mbsf.

Cherts were recovered from different horizons within Subunit VIA. A faintly laminated, dark olive gray (5Y 3/2) chert, 4 cm thick, showing a well-preserved Zoophycos layer, occurs at 356.6 mbsf (Core 113-696B-33R, Fig. 10). Very light, fragmented black (5Y 2.5/1) chert, lacking any sedimentary structures, was recovered from 462.8 mbsf (Core 113-696B-44R).

Ice-rafted detritus and dropstones were only recovered from the top of Subunit VIA down to 376.0 mbsf (Core 113-696B-34R). Sand-sized ice-rafted detritus is common throughout this interval. Dropstones are most abundant in Cores 113-696B-26R through 113-696B-28R and in Core 113-696B-30R and are generally less than 2 cm in diameter. Angular to subangular sedimentary rocks predominate over metamorphic and igneous rocks.

Minor to moderate bioturbation was observed in Cores 113-696B-25R through 113-696B-28R showing only halo burrows and Chondrites as distinct burrow patterns.

Subunit VIB (Depth 472.5–529.8 mbsf)

Cores 113-696B-45R through 113-696B-50R; thickness 57.3 m; early late or late middle Miocene to middle Miocene(?) in age.

Figure 10. Dark olive gray (5Y 3/2) late Miocene chert from Subunit VIA with Zoophycos burrows, 366.3 mbsf (Sample 113-696B-33R, CC).

The sediments of Subunit VIB predominantly consist of olive gray (5Y 4/2, 5/2) to olive (5Y 4/3) mud-bearing diatomite and olive gray (5Y 5/2) to olive (5Y 4/4) diatomite. Less commonly, olive gray (5Y 4/2) to olive (5Y 4/3) muddy diatomite occurs.

As a minor lithology, fragments (as large as 6 cm in diameter) of black (5Y 2.5/1), light brownish gray (2.5Y 6/2) and dark olive gray (5Y 3/2) chert were recovered at 491.6 mbsf (Sample 113-696B-47R-1, 0–16 cm). Chert fragments, 1.5–3 cm in size, from the top of Core 113-696B-49R most probably represent downhole contamination rather than *in-situ* sediments. Very dark olive gray (5Y 3/2) to very dark gray (5Y 3/1) well-laminated chert was recovered from the base of Section 113-696B-49R, CC, and is similar to the laminated black (5Y 2.5/2) and dark gray (5Y 4/1) chert occurring at the top of Sample 113-696B-50R, 0–68 cm.

A light gray (5Y 7/1) layer of very fine grained, pure dolomite (data from shipboard X-ray diffraction) occurs intercalated with a mud-bearing diatomite at 502.2 mbsf (Sample 113-696B-48R-1, 96–106 cm). A carbonate-cemented (dolomitic?) muddy diatomite occurs in Sample 113-696B-46R-1, 30–45 cm.

A very dark gray (5Y 3/1) volcanic ash bed is present in Sample 113-696B-49R-1, 62–63 cm. Volcanic glass (as much as 8%) finely dispersed through the sediment as well as a few pumice grains (as large as 3 mm in size) occur throughout Core 113-696B-49R.

Ice-rafted detritus was not observed in the sediments of Subunit VIB. A gabbro dropstone (5 cm in diameter) at the top of Core 113-696B-49R is probably due to downhole contamination.

Primary sedimentary structures such as parallel lamination and cross lamination are present and are most common in Cores 113-696B-47R through 113-696B-50R.

Bioturbation is moderate to strong throughout this subunit (Fig. 11) and well-preserved burrows of Zoophycos (Fig. 10), Teichichnus (Fig. 12), Chondrites (Fig. 13), Planolites, and halo burrows were observed.

Unit VII (Depth 529.8–645.6 mbsf; Age middle Miocene(?) to Eocene)

Cores 113-696B-51R through 113-696B-62R: thickness 115.8 m; middle Miocene(?) to Eocene in age.

The sediments of Unit VII are almost exclusively terrigenous in origin. On the basis of texture and composition, Unit VII is divided into four subunits.

Subunit VIIA (Depth 529.8–548.9 mbsf)

Cores 113-696B-51R through 113-696B-52R; thickness 19.1 m; middle Miocene(?) in age.

The main lithology of Subunit VIIA is a very dark gray (5Y 3/1) glauconitic to glauconite-bearing sandy mudstone. Glauconite content of the sediment is as high as 30%; weathered lithic fragments are abundant in the sand-sized fraction.

Very dark gray (5Y 3/1) claystone occurs as a minor lithology in patches, clay pockets, and rip-up clasts in Samples 113-696B-51R-1, 53–80 cm, and 113-696B-51B-2, 30–40 cm, and 72–73 cm. Several fragments of finely laminated, black (5Y 2.5/1) chert occur intercalated with olive gray (5Y 5/2) sandy mudstone at the very top of this subunit in Sample 113-696B-51R-1, 4–18 cm. Carbonate-cemented mudstone occurs at the base of Section 113-696B-51R-1.

Sand-sized ice-rafted detritus was not recognized; however, a few millimeter-sized dropstones(?), one of which is a quartzite, are present in Section 113-696B-51R-1.

Some primary sedimentary structures such as lamination occur throughout Section 113-696B-51R-1. Bioturbation is minor to moderate in this subunit showing some Teichichnus burrows in Sample 113-696B-51R-1, 0–10 cm.

Subunit VIIB (Depth 548.9–579.4 mbsf)

Cores 113-696B-53R through 113-696B-55R-1; thickness 20.8 m; early Miocene(?) to late Paleogene(?) in age.

The major lithologies within Subunit VIIB are dark olive gray (5Y 3/2) to uniformly black (5Y 2.5/2) claystone and clayey mudstone. At the base of this subunit very dark gray (5Y 3/1) and dark olive gray (5Y 3/2) silty mudstone occurs; both lithologies contain minor amounts (less than 2%) of glauconite.

Very dark gray (5Y 3/1) glauconitic sandy mudstone occurs as a minor lithology at the top of this subunit in Sample 113-696B-53R-1, 0–30 cm. Small pyrite concretions (as large as 2 cm in diameter) are common throughout the subunit. Silicified benthic foraminifers are present in Core 113-696B-54R.

A few small (0.3–2 cm in diameter) rounded sedimentary dropstones(?) occur in Cores 113-696B-53R and 113-696B-54R. Primary sedimentary structures such as fine lamination are more abundant in the siltstones than in the claystones and mudstones. Bioturbation is minor to strong, generally increasing toward the base of this subunit.

Subunit VIIC (Depth 569.7–606.9 mbsf)

Cores 113-696B-55R-2 through 113-696B-58R; thickness 37.2 m; early Miocene(?) to late Paleogene(?) in age.

Sediments of Subunit VIIC are generally characterized by high amounts of glauconite, as high as 45%. The main lithologies are very dark gray (5Y 3/1) to dark olive gray (5Y 3/2) and olive gray (5Y 4/2) sandy mudstones and silty mudstones in the upper part of this subunit from 569.7 to 579.4 mbsf (Sections 113-696B-55R-2 through 113-696B-56R-1). The most visually striking sediment of Subunit VIIC, however, is black (5Y 2.5/2) to very dark gray (5Y 3/1) glauconite silty mudstone (in Section 113-696B-56R-2).

As a minor lithology, a calcite-cemented, very dark gray (5Y 3/1) sandy mudstone, strongly bioturbated, occurs in Sample 113-696B-58R-2, 35–73 cm (Fig. 14), at the very base of this subunit.

Sediments of Subunit VIIC are moderately to strongly bioturbated; burrows of Zoophycos, Planolites, and Teichichnus types are well preserved.

Subunit VIID (Depth 606.9–645.6 mbsf)

Cores 113-696B-59R through 113-696B-62R; thickness 38.7 m; early Oligocene-Eocene in age.

The main lithology of Subunit VIID is a dark olive gray (5Y 3/2), black (5Y 2.5/2), and dark olive gray (5Y 3/2) sandy mudstone. Less commonly dark olive gray (5Y 3/2) clayey mudstone occurs.

Dark olive gray (5Y 3/2) glauconite-bearing sandy mudstone is present as a minor lithology in Sample 113-696B-59R-1, 0–100 cm. Several horizons of carbonate-cemented sandy mudstone occur near the base of Subunit VIID in Samples 113-696B-62R-2, 52–76 cm, 113-696B-62R-4, 105–125 cm, and 113-696B-62R-5, 55–63 cm.

The sediments of Subunit VIID contain abundant macrofossil shells and shell fragments. Most fragments are thin-shelled bivalves and ribbed gastropods; solitary corals occur as well.

Bioturbation of the sediments of this subunit is minor to moderate but only a few well defined burrows (e.g., Teichichnus) are preserved.

Clay Mineralogy

X-ray diffraction analyses were completed on 41 samples from Holes 696A and 696B (Fig. 15). The objectives of the clay mineral studies at Site 696 are (1) to identify the major paleoenvironmental changes as expressed by clay associations, using a sampling interval of one per core and (2) to compare the clay associations with those observed at other sites in the Weddell Sea and in the adjacent Falkland Plateau area.

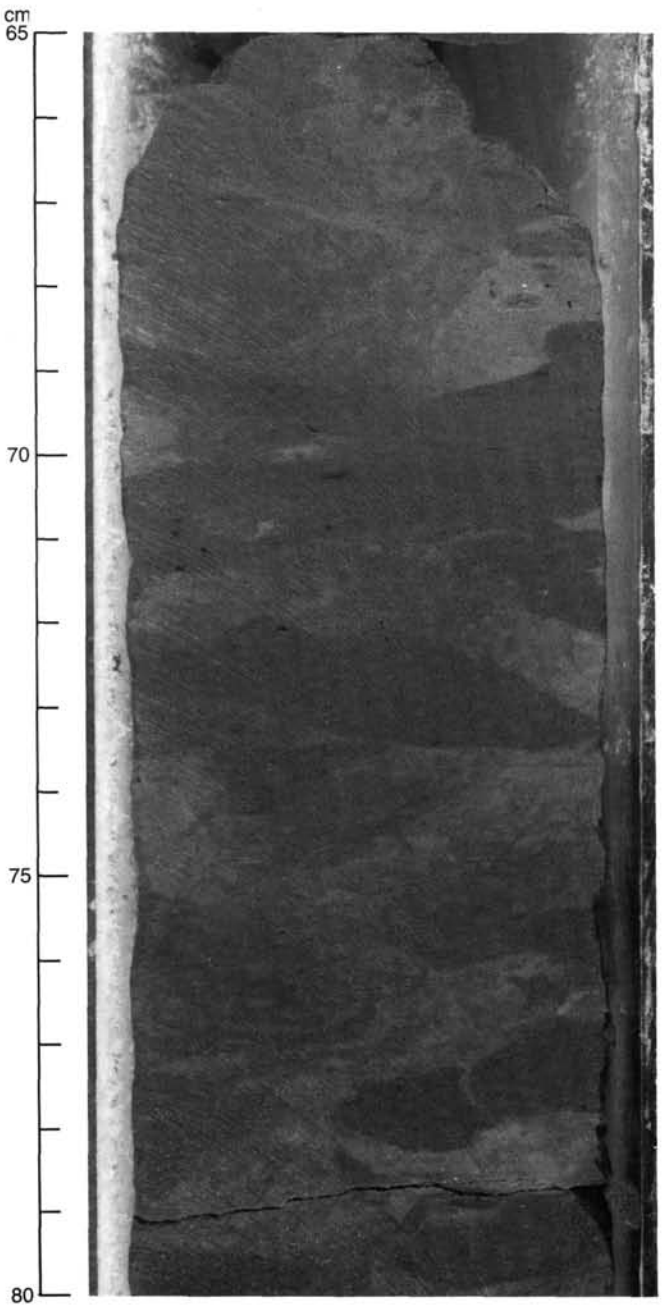

Figure 11. Strongly burrowed (mainly by Planolites and Chondrites) middle Miocene(?) diatomite from Sample 113-696B-45R-1, 65–80 cm.

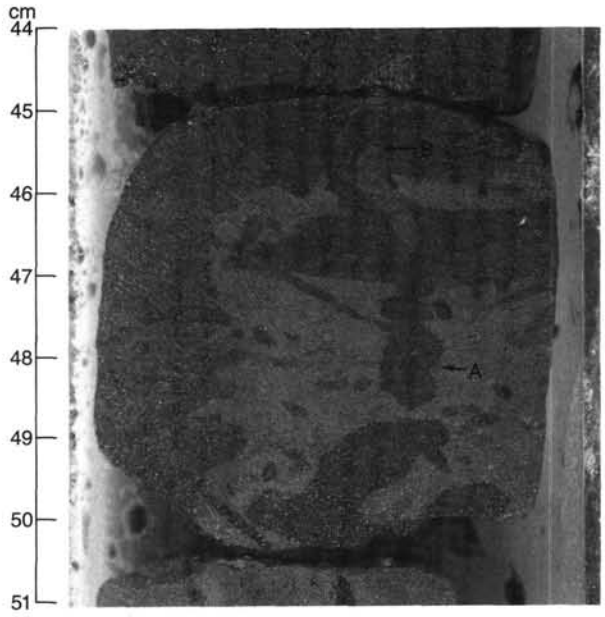

Figure 12. Moderately bioturbated middle Miocene muddy diatomite; burrows of Teichichnus (A) and Planolites (B) contain some glauconite; Sample 113-696B-46R-1, 44–51 cm.

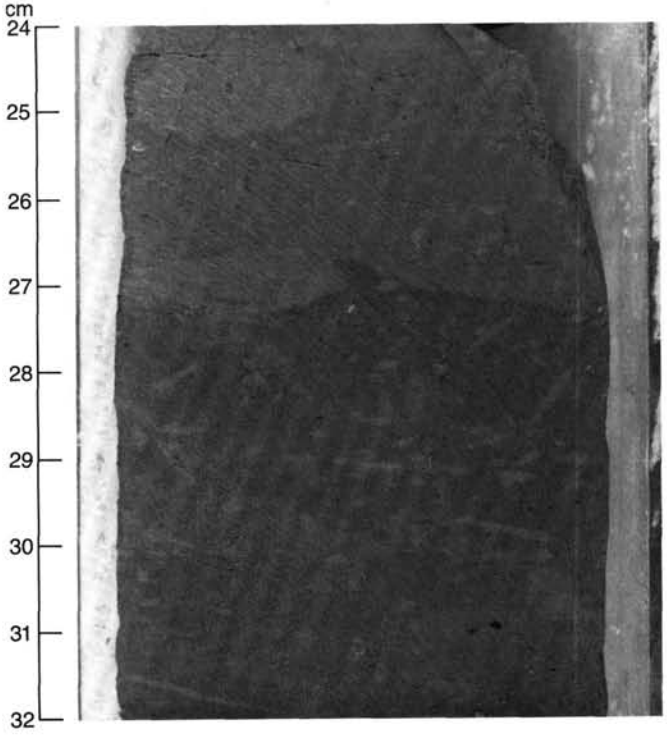

Figure 13. Strongly bioturbated middle Miocene diatomite showing numerous Chondrites burrows; Sample 113-696B-45R-1, 24–32 cm.

Results

The clay minerals identified include chlorite, illite, kaolinite, and smectite (Fig. 15). Based on the relative abundances of the clay species, four clay units (C1–C4) have been recognized for Site 696.

Unit C1, upper Pliocene to Pleistocene, extends from the seafloor to 69 mbsf. It has a clay association of illite and chlorite (common to abundant) associated with smectite and kaolinite (rare to common).

Unit C2 extends from 69 to 250 mbsf and consists of chlorite (abundant to very abundant), illite (abundant), kaolinite (rare to common), and sporadic rare smectite. This unit ranges from upper Miocene to upper Pliocene.

Unit C3 extends from 250 to 500 mbsf and consists of illite (common to very abundant), chlorite (common to abundant), kaolinite (rare to common), and sporadic smectite (rare to abundant). This unit is lower middle to upper lower Miocene to upper Miocene.

Unit C4 extends from 500 mbsf to the bottom of Hole 696B at 645.6 mbsf and has a clay association of smectite (common

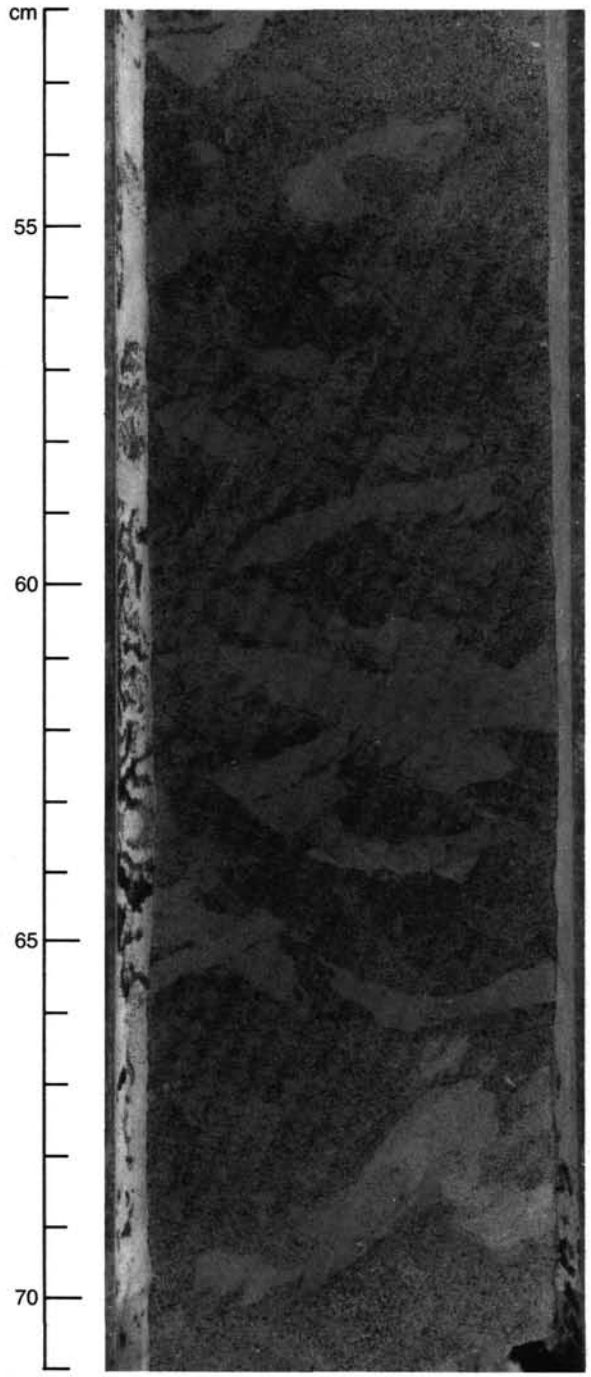

Figure 14. Glauconite containing strongly bioturbated, calcite-cemented sandy mudstone from the base of Subunit VIIC; Sample 113-696B-58R-2, 52–71 cm.

to exclusive) and illite (rare to abundant), associated with sporadic chlorite and kaolinite (rare to common). Below 560 mbsf, low abundance and moderate crystallinity of chlorite and kaolinite make it very difficult to distinguish between the two clay minerals. This unit ranges from Eocene to lower middle or upper lower Miocene.

Paleoenvironmental History from Clay Mineral Analyses

Unit C4 (Eocene to lower middle or upper lower Miocene) is characterized by common to exclusive smectite. High abundances of smectite occur at the same time interval on the Falkland Plateau at DSDP Sites 329, 511, and 513 (Robert and Maillot, 1983). Near Antarctica, at Sites 693 and 694, lower Oligocene to lower Miocene sediments contain rare to common smectite, but abundant to very abundant chlorite and illite. At Site 696, clay associations suggest that during this time interval, the clay minerals were mainly supplied from West Antarctica (as well as from southern South America), then characterized by warmer climatic conditions than East Antarctica, and where smectite genesis was favored.

In the upper part of this unit (Core 113-696B-48R), well-crystallized smectite associated with pumice particles suggests that the smectite could partially result from weathering of volcanic materials. Further detailed analyses should elucidate the importance of this process.

Smectite decreases in Unit C3 (lower middle or upper lower to upper Miocene), while principally illite and chlorite increase significantly. This clay association is similar to those of the middle and upper Miocene at Sites 693 and 694. During the same time interval, in the Falkland Plateau area at DSDP Sites 329 and 513, clay associations are still characterized by dominant smectite (Robert and Maillot, 1983). The change in the clay mineral associations at Site 696 indicates a strong decrease of the intensity of weathering (and dominance of physical erosion), induced by a major climatic cooling in West Antarctica during the middle(?) Miocene. Meanwhile, clay minerals from South America, where climatic conditions remained warm enough to favor smectite genesis, were still supplied to the Falkland Plateau area. This is in keeping with previous models of plate tectonic and climatic evolution. Following the beginning of seafloor spreading between South America and the Antarctic Peninsula during the lower Miocene (Barker and Burrell, 1977), Drake Passage and the Scotia Sea widened progressively. Initiation of the Antarctic Circumpolar Current through Drake Passage isolated the terrigenous detrital supplies of both South America and West Antarctica. By the same time, glaciation had increased on Antarctica (Kennett, 1977; Kennett and Von der Borch, 1986).

Unit C2 (upper Miocene to upper Pliocene) is characterized by the further decrease of smectite, and corresponding increase of chlorite abundance. The clay association reflects an increased influence of the poorly developed soils (extending over deglaciated areas) associated with decreased removal rates of ancient sediments. This unit correlates with Units C4 and C2 at Site 695, but the equivalent of Unit C3 at Site 695 is missing at Site 696. Unit C3 at Site 695 was characterized by an increased smectite content of lower Pliocene age. Lower Pliocene smectite was also recorded at Sites 693 and 694, and was interpreted to indicate increased erosion of ancient sediments in relation to increased circulation of Antarctic waters. It is suggested that the distinctive clay mineralogy at Site 696 may be related to its much shallower water depth. It would appear that the increased smectite content only occurred in the deep and intermediate Antarctic waters, perhaps transported in a nepheloid layer.

Unit C1 (upper Pliocene to Pleistocene) is characterized by increasing smectite (and decreasing chlorite and illite) content, which probably reflects a resumption of erosion of ancient sediments on Antarctic margins. This unit correlates with Unit C1 at Site 695 where the mineralogic change results from cooler climatic conditions, associated with enhanced circulation. Cooling on Antarctica and widespread erosion by both deep and shallow waters of the Southern Ocean have been reported near the Gauss/Matuyama boundary (Mercer, 1978; Ledbetter and Ciesielski, 1986).

Petrography of Ice-Rafted Dropstones from Hole 696B

Four dropstones were collected from Hole 696B for petrographic analysis. They range in size from 1 × 2 to 3 × 3 cm, are

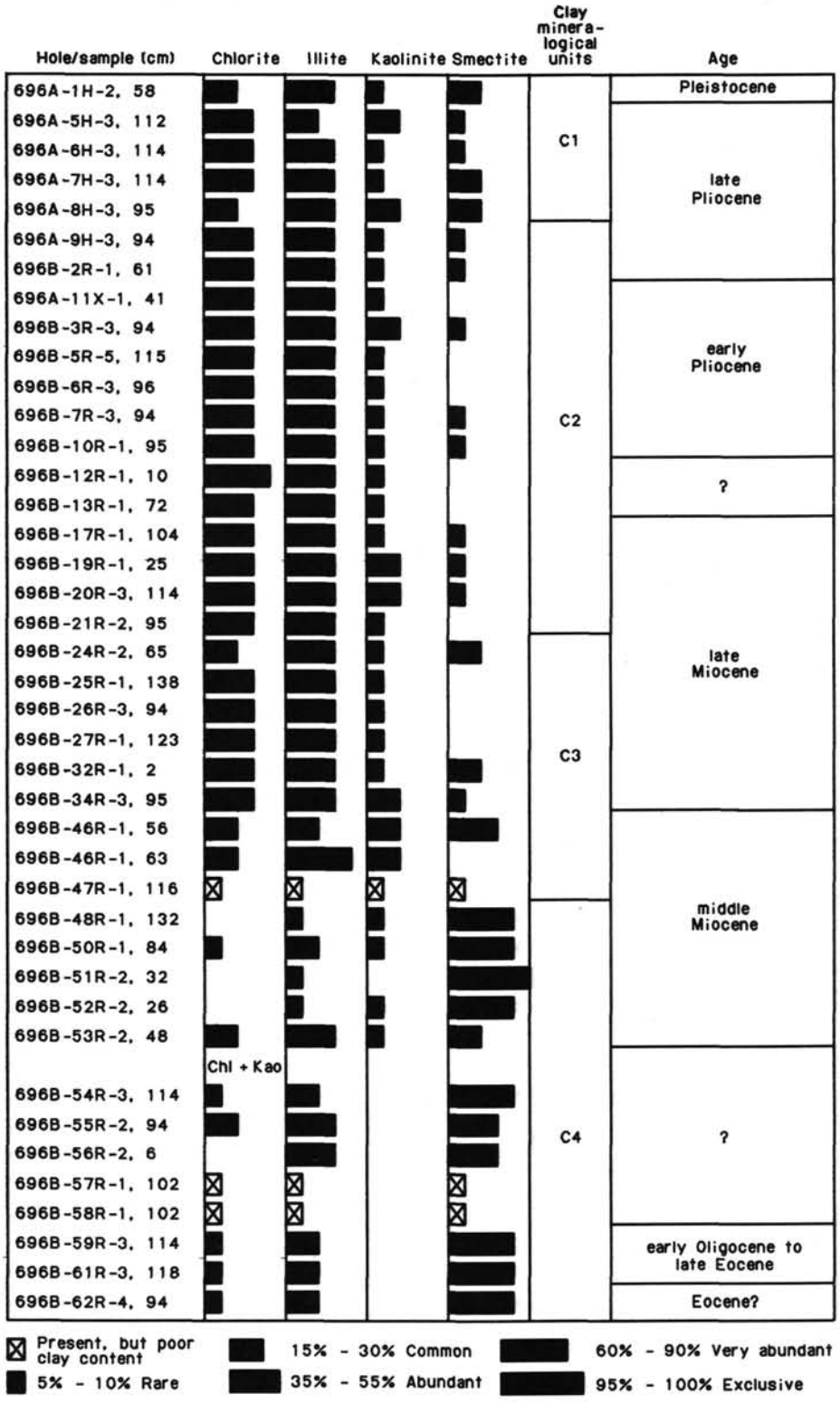

Figure 15. Clay mineralogy distribution, Site 696.

subangular, and do not show signs of weathering. Lithologically, the suite of dropstones is made up of one volcanic and three sedimentary rocks. The volcanic rock is an olivine-bearing basaltic andesite, and the sedimentary rocks are sandstones. A detailed petrographic description of four dropstones is given in Table 4. Lithology of dropstones in Hole 696B indicates the Antarctic Peninsula as the source area.

The olivine-bearing basaltic andesite is a porphyritic rock. Phenocrysts are broken, and some K-feldspars and plagioclase are zoned. Olivine glomeroporphyries have been altered to iddingsite. The matrix is altered to blebby chlorite, and quartz phenocrysts are skeletal.

The sandstones are medium to fine-grained and have irregular grain boundaries. In some sandstones, grains are cemented

Table 4. Petrographic description of ice-rafted dropstones from Site 696.[a]

Rock number: 113-696A-2H-1, 67–72 cm
Name: Sandstone—quartzite
Size: 3 × 3 cm
Depth: 3.2 mbsf
Shape: subangular
Weathering: none

Major minerals	%	Accessory minerals	Comments
Plagioclase	35	Muscovite	Irregular, embayed grain boundaries; only slight sericitization. Some elongation of a number of grains.
Quartz	50	Sericite	
Orthoclase	15		

Rock number: 113-696B-8R-CC, 0–5 cm
Name: olivine andesite
Size: 3 × 2 cm
Depth: 137.2 mbsf
Shape: subangular
Weathering: none

Major minerals	%	Accessory minerals	Comments
Plagioclase	20	Magetite	Highly porphyritic rock. Broken and euhedral phenocrysts show zoning. Olivine is altering to iddingsite. Skeletal quartz.
Quartz	20	Sericite	
Chlorite	45	Zircon	
Orthopypxene	5	K-feldsapr	
		Iddingsite	

Rock number: 113-696B-21R-2, 0–5 cm
Name: Sandstone
Size: 2 × 2 cm
Depth: 247.3 mbsf

Major minerals	%	Accessory minerals	Comments
Quartz	93	Sericite	Equigranular rock with embayed grain boundaries. Mortar texture between grains.
		Muscovite	

Rock number: 113-696B-22R-1, 34–38 cm
Name: Sandstone
Size: 2 × 1 cm
Depth: 250.7 mbsf
Shape: subangular
Weathering: none

Major minerals	%	Accessory minerals	Comments
Quartz	70	Magnetite	Granulated, cemented rock with carbonate matrix. Perthitic plagioclase and strained albite are common.
Plagioclase	10		
Chlorite	10	Carbonate	

[a] When major mineral assemblage does not equal 100%, remaining components are formed by accessory minerals.

with carbonate-rich material and in some others, granulated quartz grains with mortar texture occur interstitially.

PHYSICAL PROPERTIES

Index properties measured on samples selected from the most intact portions of cores are listed in Table 5. Profiles of bulk density, water content (dry basis), and grain density are illustrated in Figure 16. A profile of porosity is illustrated in Figure 17.

Due to the disturbed conditions of the sediments cored and the abundance of coarse-grained material at Site 696 there are insufficient physical property data to characterize the site in detail. There are, however, sufficient data to assign specific geotechnical properties to the seven major lithostratigraphic units.

The lithostratigraphic subdivisions of Site 696 and their geotechnical characteristics consist of the following:

Lithostratigraphic Subunit IA, 0–8.5 mbsf, diatom-bearing silty mud of Quaternary age.

	Range		
	Low	High	Average
Bulk density (g/cm^3)	1.48	1.76	1.62
Water content (%)	53	82	67
Grain density (g/cm^3)	2.30	2.78	2.54
Porosity (%)	60	65	62

Lithostratigraphic Subunit IB, 8.5–64.2 mbsf, diatom clayey mud and muddy diatom ooze of Pliocene (middle Upsilon Zone).

	Range		
	Low	High	Average
Bulk density (g/cm^3)	1.38	1.67	1.52
Water content (%)	62	134	98
Grain density (g/cm^3)	2.36	2.71	2.56
Porosity (%)	62	79	72

Lithostratigraphic Unit II, 64.2–124.8 mbsf, upper Pliocene to lower Pliocene (middle Upsilon to lower Tau Zone) diatom-bearing silty mud and diatom-bearing clayey mud.

	Range		
	Low	High	Average
Bulk density (g/cm^3)	1.65	1.71	1.70
Water content (%)	60	71	63
Grain density (g/cm^3)	2.60	2.79	2.71
Porosity (%)	62	68	64

Lithostratigraphic Unit III, 124.8–211.8 mbsf, lower Pliocene (lower Tau Zone) to upper Miocene silty and clayey mud and diatom-bearing clayey mud.

	Range		
	Low	High	Average
Bulk density (g/cm^3)	1.79	2.03	1.92
Water content (%)	29	37	37
Grain density (g/cm^3)	2.63	2.75	2.67
Porosity (%)	45	55	50

Lithostratigraphic Unit IV, 211.8–260.1 mbsf, upper Miocene diatom ooze and muddy diatom ooze.

	Range		
	Low	High	Average
Bulk density (g/cm^3)	1.90	1.90	1.90
Water content (%)	27	27	27
Grain density (g/cm^3)	2.55	2.55	2.55
Porosity (%)	50	50	50

Lithostratigraphic Unit V, 260.1–269.7 mbsf, upper Miocene coarse sand; no physical properties were measured on this unit.

Lithostratigraphic Subunit VIA, 269.7–472.5 mbsf, upper Miocene to lower upper or lower Middle Miocene diatom ooze and mud-bearing diatom ooze.

	Range		
	Low	High	Average
Bulk density (g/cm^3)	1.29	1.80	1.50
Water content (%)	49	108	107
Grain density (g/cm^3)	2.17	2.81	2.47
Porosity (%)	64	81	72

Lithostratigraphic Subunit VIB, 472.5–529.8 mbsf, upper lower or lower middle Miocene to middle Miocene mud-bearing diatomite and diatomite.

Table 5. Index properties, water content, porosity, bulk density, and grain density, measured on samples from Site 696 (WW = wet weight, DW = dry weight).

Core, section top (cm)	Depth (mbsf)	Water content (%WW)	Water content (%DW)	Porosity (%)	Bulk density (g/cm^3)	Grain density (g/cm^3)
113-696A-						
2H-3, 30	5.8	34.57	52.84	59.47	1.76	2.78
2H-5, 29	8.8	45.05	81.98	65.00	1.48	2.30
3H-1, 43	12.4	43.33	76.47	68.89	1.63	2.65
5H-2, 66	33.4	54.87	121.57	77.13	1.44	2.58
5H-4, 110	36.8	51.81	107.53	73.45	1.45	2.52
6H-2, 110	43.4	57.43	134.93	78.53	1.40	2.57
6H-4, 90	46.2	51.30	105.34	73.17	1.46	2.44
6H-6, 90	49.2	50.34	101.36	71.80	1.46	2.36
6H-7, 40	50.2	38.41	62.35	62.31	1.66	2.59
7H-2, 90	52.8	50.88	103.57	76.49	1.54	2.64
7H-4, 90	55.8	41.26	70.25	67.05	1.66	2.71
7H-6, 90	58.8	56.61	130.47	76.24	1.38	2.46
8H-2, 90	62.4	42.51	73.94	69.47	1.67	2.65
8H-4, 90	65.4	39.60	65.56	65.67	1.70	2.65
8H-6, 90	68.1	42.21	73.03	67.80	1.65	2.63
9H-1, 90	70.5	41.47	70.85	67.97	1.68	2.79
9H-2, 90	72.0	37.43	59.81	62.64	1.71	2.63
9H-4, 90	75.0	38.00	61.28	62.28	1.68	2.60
11X-1, 22	89.2				2.71	
113-696B-						
2R-1, 69	77.3	35.65	55.41	62.08	1.78	2.92
3R-4, 33	91.0	36.67	57.90	61.73	1.72	2.69
3R-4, 131	92.0	32.67	48.53	59.01	1.85	2.93
5R-2, 127	108.3	44.16	79.08	68.30	1.58	2.61
5R-4, 107	111.1	35.61	55.30	60.10	1.73	2.68
5R-6, 76	113.8	41.56	71.11	66.53	1.64	2.76
7R-1, 44	125.4	31.42	45.82	54.91	1.79	2.64
10R-2, 68	146.3	26.72	36.47	50.62	1.94	2.63
13R-1, 63	173.8	22.60	29.19	44.83	2.03	2.75
17R-2, 14	213.4	26.85	36.70	49.91	1.90	2.55
24R-1, 137	271.1	33.38	50.09	58.31	1.79	2.77
24R-2, 0	271.2	33.06	49.38	58.00	1.80	2.68
25R-1, 19	279.6	56.40	129.37	77.05	1.40	2.57
25R-1, 147	280.9	38.63	62.95	63.68	1.69	2.81
26R-1, 11	289.1	47.63	90.94	72.29	1.56	2.52
26R-2, 105	291.6	55.27	123.55	75.18	1.39	2.30
27R-1, 110	299.8	49.83	99.31	71.69	1.47	2.61
27R-2, 71	300.9	53.19	113.63	72.48	1.40	2.31
28R-1, 36	308.7	43.80	77.93	68.44	1.60	2.43
28R-2, 99	310.8	45.67	84.06	67.11	1.51	2.28
32R-2, 86	349.4	64.28	179.97	80.90	1.29	2.19
34R-2, 113	349.6	57.86	137.29	77.69	1.38	2.56
40R-1, 15	424.4	55.58	125.11	74.00	1.36	2.32
45R-1, 37	472.9	55.53	124.85	84.68	1.56	2.78
45R-1, 105	473.6	59.52	147.05	79.22	1.36	2.24
45R-CC, 20	474.2	53.01	112.80	72.62	1.40	2.17
46R-1, 23	482.2	47.70	91.21	65.27	1.40	2.58
46R-1, 63	482.6	39.65	65.71	62.55	1.62	2.56
47R-1, 34	491.9	45.52	83.55	72.32	1.63	2.77
47R-1, 137	493.0	49.98	99.93	72.60	1.49	3.10
48R-1, 50	501.7	54.04	117.60	74.88	1.42	2.66
48R-2, 146	504.2	55.02	122.30	75.77	1.41	2.49
49R-1, 115	511.9	51.81	107.53	75.78	1.50	2.73
50R-1, 29	520.5				2.29	
50R-2, 18	521.9	44.72	80.91	68.85	1.58	2.47
51R-1, 18	530.0	8.42	9.19	18.63	2.27	2.50
53R-1, 1	548.9	24.17	31.87	46.98	1.99	2.65
53R-3, 3	551.9	25.05	33.43	48.55	1.99	2.78
53R-3, 42	552.3	45.03	81.92	83.73	1.90	2.54
53R-5, 74	555.6	24.11	31.77	44.37	1.89	2.50
53R-CC, 3	558.0	25.91	34.97	47.31	1.87	2.58
54R-2, 80	560.8	25.15	33.60	47.09	1.92	2.69
54R-4, 28	563.3	24.67	32.75	46.96	1.95	2.69
54R-CC, 12	563.7	18.42	22.58	36.56	2.03	2.49
55R-1, 110	569.3	25.63	34.46	49.57	1.98	2.85
55R-2, 41	571.1	20.87	26.38	44.06	2.16	2.93
55R-4, 0	572.7	24.82	33.01	47.18	1.95	2.73
55R-6, 30	576.0	11.61	13.14	26.36	2.33	2.71
55R-CC, 0	576.1	12.82	14.70	29.95	2.39	2.67
56R-1, 12	578.0	20.87	26.37	44.79	2.20	2.89
56R-1, 84	578.7	21.20	26.90	43.54	2.10	2.88
56R-2, 51	579.9	13.99	16.27	32.03	2.35	2.81
57R-1, 52	588.1	19.86	24.78	43.69	2.25	2.96
58R-1, 105	598.3	19.80	24.69	41.35	2.14	2.76
59R-1, 56	607.5	22.41	28.88	44.54	2.04	2.66

Table 5 (continued).

Core, section top (cm)	Depth (mbsf)	Water content (%WW)	Water content (%DW)	Porosity (%)	Bulk density (g/cm^3)	Grain density (g/cm^3)
113-696B- (Cont.)						
59R-3, 62	610.5	23.99	31.57	46.43	1.98	2.72
59R-5, 1	612.9	22.06	28.30	43.31	2.01	2.71
60R-2, 29	618.4	22.33	28.76	44.73	2.05	2.74
60R-3, 145	621.1	21.62	27.59	43.76	2.07	2.78
60R-6, 68	624.8	22.89	29.69	44.67	2.00	2.66
61R-1, 53	626.7	21.15	26.83	42.60	2.06	2.76
61R-5, 2	632.2	22.92	29.74	45.52	2.03	2.73
62R-2, 146	637.8	21.71	27.74	41.33	1.95	2.53
62R-CC, 1	645.5	17.79	21.64	34.54	1.99	2.76

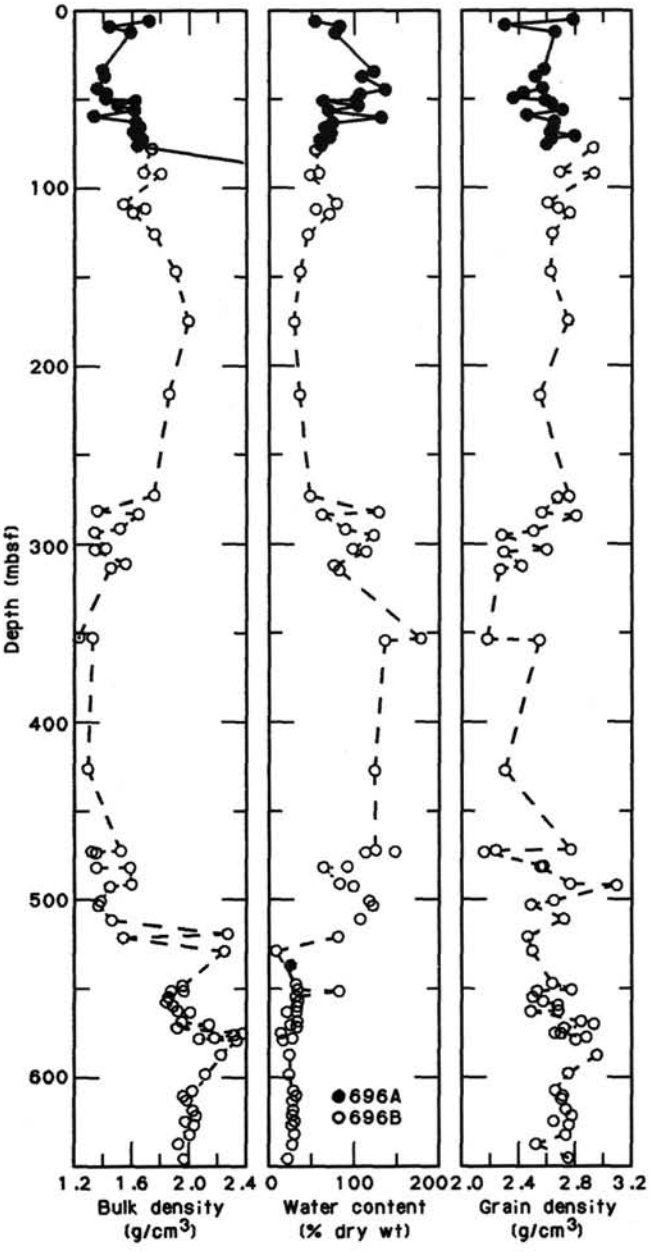

Figure 16. Profile of bulk density, water content, and grain density, Site 696. Data given in Table 5.

	Range		
	Low	High	Average
Bulk density (g/cm³)	1.40	1.63	1.50
Water content (%)	66	122	96
Grain density (g/cm³)	2.47	3.10	2.65
Porosity (%)	63	76	71

Lithostratigraphic Subunit VIIA, 529.8–548.9 mbsf, middle Miocene(?) sandy mudstone.

	Range		
	Low	High	Average
Bulk density (g/cm³)	1.99	2.27	1.50
Water content (%)	9	32	21
Grain density (g/cm³)	2.50	2.65	2.57
Porosity (%)	19	47	33

Lithostratigraphic Subunit VIIB, 548.9–569.7 mbsf, lower Miocene to upper Paleogene claystone, clayey mudstone, and silty mudstone.

	Range		
	Low	High	Average
Bulk density (g/cm³)	1.87	2.39	2.05
Water content (%)	13	35	35
Grain density (g/cm³)	2.49	2.93	2.70
Porosity (%)	26	49	46

Lithostratigraphic Subunit VIIC, 569.7–606.9 mbsf, lower Miocene to Oligocene(?) glauconite silty mudstone and claystone.

	Range		
	Low	High	Average
Bulk density (g/cm³)	2.14	2.35	2.25
Water content (%)	16	25	22
Grain density (g/cm³)	2.76	2.96	2.84
Porosity (%)	32	44	39

Lithostratigraphic Subunit VIID, 606.9–645.6 mbsf, lower Oligocene to Eocene sandy mudstone.

	Range		
	Low	High	Average
Bulk density (g/cm³)	1.95	2.06	2.04
Water content (%)	21	32	28
Grain density (g/cm³)	2.53	2.76	2.70
Porosity (%)	41	45	43

The diatom oozes of Subunits IB, VIA, and VIB have the highest porosities and water content and the lowest bulk and grain densities. The sandy mudstones and glauconite silty mudstones of Subunits VIIA and VIIC have the lowest porosities and water content and the highest grain and bulk densities of the sediments at Site 696. The geotechnical properties measured at Site 696 indicate that the sediments are normally consolidated (i.e., the degree of compaction is normal for the present-day overburden stresses).

Shear Strength

The undrained shear strength of the sediment was determined using the ODP Motorized Vane Shear Device with standard 1.2-cm equidimensional miniature vanes. Its operation and calculations follows procedures outlined in the *Physical Properties Handbook* (used on the ship). Strength measurements were made on the least disturbed sections of the cores.

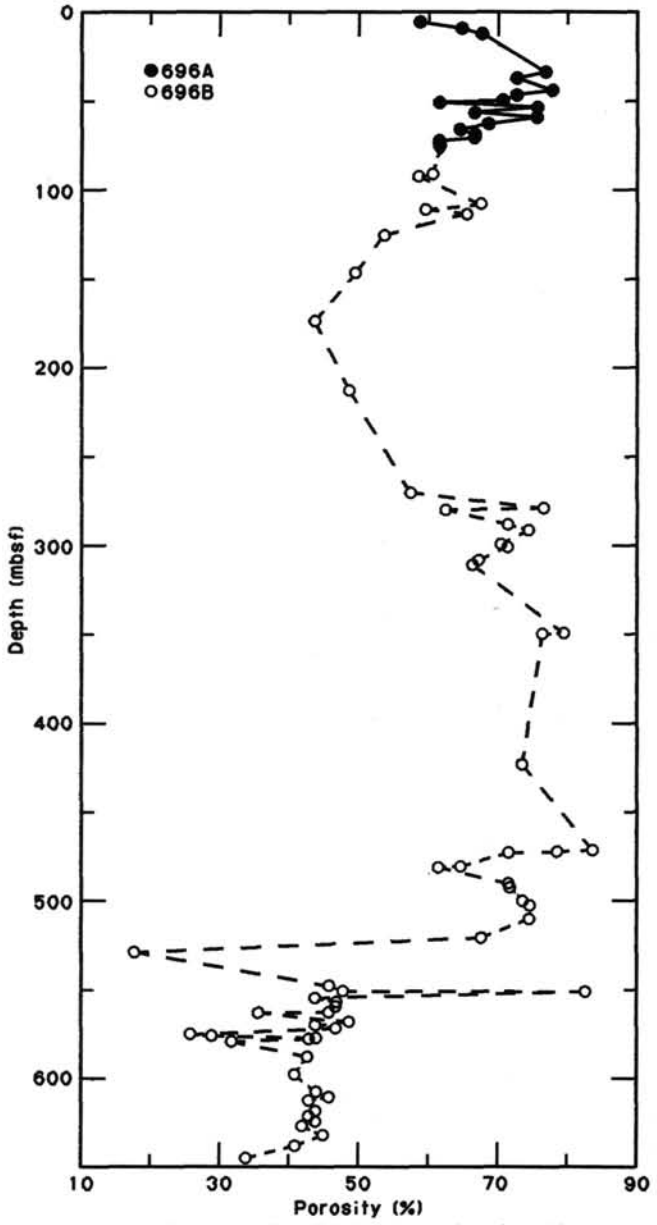

Figure 17. Profile of porosity, Site 696. Data given in Table 5.

The shear strengths determined for Site 696 are listed in Table 6 and illustrated in Figure 18. Few shear strength measurements were made due to the disturbed conditions of the core and the large amount of sandy sediment present. The line of best fit through the strength data translates into a shear strength gradient of 0.8 kPa/m.

Compressional Wave Velocity

The results of velocity measurements made on the Hamilton Frame are listed in Table 7 and illustrated in Figure 19. A continuous compressional wave velocity profile for sediments from Holes 696A and 696B as determined by the P-wave logger is illustrated in Figure 20. The average velocity of the sediments in the various lithostratigraphic units are listed in Table 8. Table 8 also lists the assumed average *in-situ* velocities. The average *in-situ* velocities were determined by using the difference between laboratory measured (Hamilton Frame) velocities and those measured by downhole logging at Site 693. Table 8 also lists the in-

Table 6. Undrained shear strength determined on samples from Site 696.

Core, section top (cm)	Depth (mbsf)	Shear strength (kPa)
113-696A-		
2H-3, 47	6.0	5.5
2H-5, 20	8.7	48.9
3H-1, 50	12.5	4.0
5H-2, 63	33.3	1.6
5H-4, 90	36.6	1.4
6H-2, 90	43.2	53.5
6H-4, 84	46.1	41.9
6H-6, 84	49.1	60.5
6H-7, 40	50.2	8.4
6H-7, 49	50.3	9.3
7H-2, 84	52.7	44.2
7H-4, 84	55.7	57.0
7H-6, 84	58.7	62.8
8H-2, 84	62.3	55.9
8H-4, 84	65.3	61.7
8H-6, 84	68.3	76.8
8H-6, 100	68.5	76.8
9H-1, 84	70.4	53.5
9H-2, 114	72.2	18.6
9H-4, 84	74.9	11.6
113-696B-		
3R-5, 22	93.9	104.7
5R-CC, 8	114.5	53.5
5R-6, 111	114.1	176.9
7R-4, 60	129.9	121.0
10R-2, 72	146.3	58.2
17R-2, 10	213.4	93.1

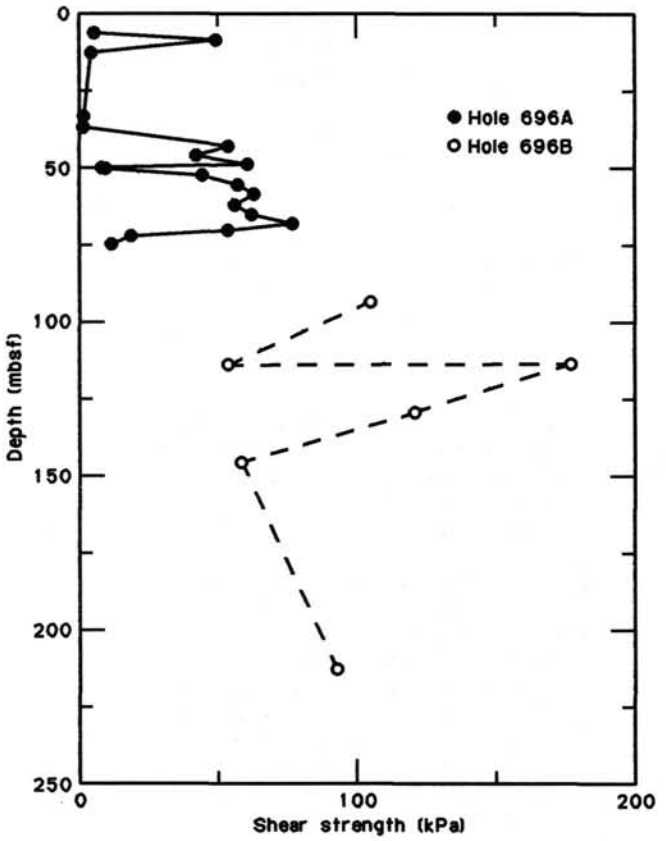

Figure 18. Undrained shear strength profile, Site 696. Data given in Table 6.

Table 7. Compressional wave velocities (Hamilton Frame) measured on samples from Site 696.

Core, section top (cm)	Depth (mbsf)	Velocity (m/s)	Remarks
113-696A-			
2H-3, 30	5.8	1554	
2H-5, 29	8.8	1538	
3H-1, 43	12.4	1548	
5H-2, 66	33.4	1797	
5H-4, 110	36.8	1498	
6H-2, 110	43.4	1504	
6H-4, 90	46.2	1494	
6H-6, 90	49.2	1497	
7H-2, 90	52.8	1500	
7H-4, 90	55.8	1525	
7H-6, 90	58.8	1481	
8H-2, 90	62.4	1475	
8H-4, 90	65.4	1543	
8H-6, 90	68.1	1524	
9H-1, 90	70.5	1516	
9H-2, 90	72.0	1525	
9H-4, 90	75.0	1527	
11X-1, 22	89.2	3196	
113-696B-			
2R-1, 69	77.3	1487	
3R-4, 131	92.0	1535	
5R-2, 127	108.3	1494	
5R-4, 107	111.1	1529	
7R-1, 44	125.4	1521	
10R,-2 68	146.3	1571	
17R-2, 14	213.4	1580	
24R-1, 137	271.1	1608	
24R-2, 0	271.2	1617	
25R-1, 19	279.6	1561	
25R-1, 147	280.9	1576	
26R-2, 105	291.6	1581	
28R-1, 36	308.7	1551	
28R-2, 99	310.8	1544	
45R-1, 37	472.9	1550	
45R-CC, 20	474.2	1562	
46R-1, 63	482.6	1783	Very good
47R-1, 34	491.9	1627	Very good
47R-1, 137	493.0	1602	
48R-1, 50	501.7	1729	
48R-2, 146	504.2	1623	
49R-1, 115	511.9	1584	
50R-1, 29	520.5	3926	Chert
50R-2, 18	521.9	1722	
51R-1, 18	530.0	3748	Chert
51R-2, 88	532.2	2195	A Same Sample
51R-2, 95	532.3	2302	C
53R-1, 1	548.9	1802	True section
53R-3, 3	551.9	1768	True section
53R-3, 42	552.3	2105	True section
53R-5, 74	555.6	2121	True section
54R-4, 28	563.3	1777	
54R-CC, 12	563.6	2302	Very hard siltstone
55R-1, 110	563.7	1874	
55R-2, 41	571.1	1777	
55R-4, 0	572.7	1795	
55R-6. 30	576.0	2670	Very hard siltstone
55R-CC, 0	576.1	2931	Very hard siltstone
56R-1, 12	578.0	1802	
56R-1, 84	578.7	1803	
56R-2, 55	580.0	2791	Very hard siltstone
57R-1, 52	588.1	1855	
58R-1, 105	598.3	1798	Sandy
59R-1, 56	607.5	1921	Sandy
59R-3, 62	610.5	1841	Sandy
59R-5, 1	612.9	1989	Sandy
60R-2, 29	618.4	1813	Sandy
60R-3, 145	621.1	1919	Sandy
60R-6, 68	624.8	1867	Sandy
61R-1, 53	626.7	1880	Sandy
61R-5, 53	626.7	1830	Sandy
62R-2, 146	637.8	1982	Sandy
62R-4, 110	640.4	4246	Very hard siltstone
62R-CC, 1	645.5	1847	Sandy

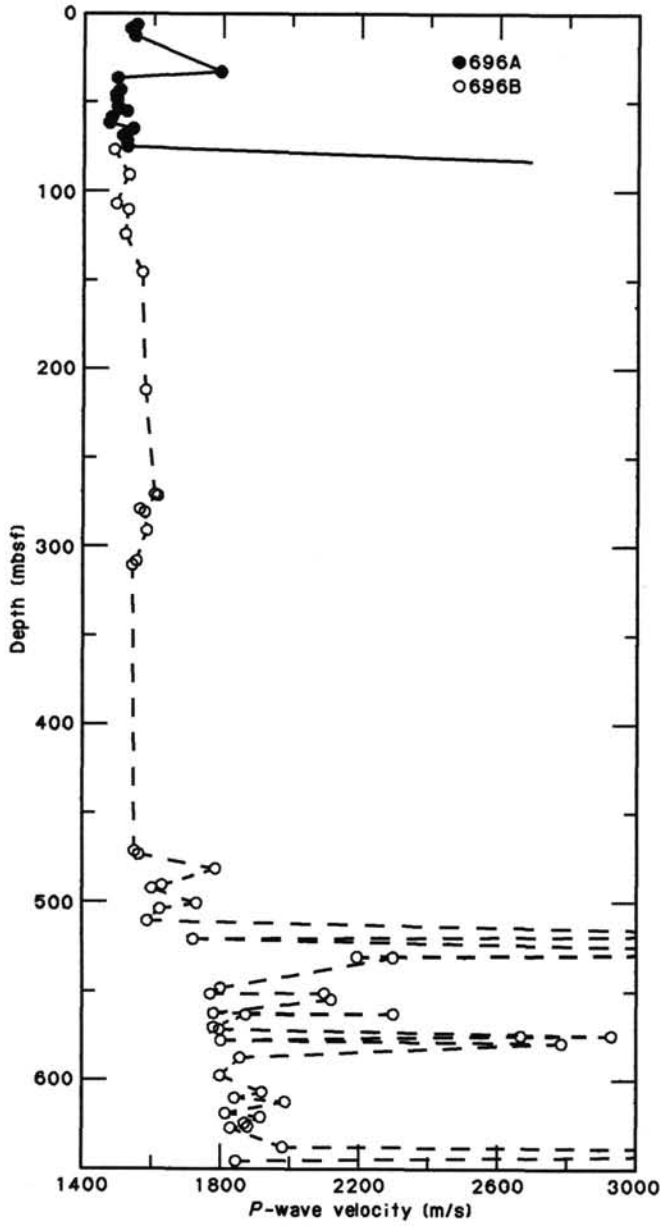

Figure 19. Compressional wave velocities (Hamilton Frame) for Site 696. Data given in Table 7.

terval transit time, the two-way traveltime (twt) to the base of each lithostratigraphic unit and the time (twt) to the major seismic horizons. Figure 21 illustrates the positions of the lithostratigraphic units on the seismic profile of Site 696. The base of the lithostratigraphic units matched most of the major seismic horizons on the seismic profile. In general the laboratory measured velocity data agree with the P-wave logger measurements. Table 7 lists the velocities of the chert and very hard siltstones recovered in the deeper cores.

Thermal Conductivity

At this site, "normal" and "oblique" methods were used to measure the thermal conductivity (see "Physical Properties" section, "Site 694" chapter, this volume). The measured thermal conductivity values are listed in Table 9 and illustrated in Figure 22. Thermal conductivity ranges from 0.959 W/m-K at 46.3 mbsf to 1.472 W/m-K at 72 mbsf. The average value of thermal conductivity for Subunit IA is 1.324 W/m-K, Subunit IB is 1.195 W/m-K, and Subunit IC is 1.380 W/m-K.

Summary

The characteristics of the physical properties at Site 696 are rather poorly defined due to the disturbed nature of the cores, unrecovered intervals, and the abundance of sandy sediment. There are, however, sufficient physical property data to discuss a characteristic geotechnical profile for the lithostratigraphic units of Site 696.

Subunit IA, relative to other near-seafloor material, contains a low-porosity and low-water-content sediment. The acoustic velocity in this unit is unusually high, 1554 m/s. Subunit IB is a high-water-content, high-porosity sediment with a low acoustic velocity (1482 m/s). Unit II consists of a diatom-bearing mud with an average porosity of 64% and an average velocity of 1528 m/s. Unit III contains clayey muds, silty muds, and diatom-bearing muds with an average porosity of 50% and an average velocity of 1549 m/s. Unit IV is a diatom ooze with a porosity of 50% and an average velocity of 1580 m/s. Unit V is a sandy unit that was not tested for its physical properties. Subunit VIA is a diatom ooze with a average porosity of 72% and an average acoustic velocity of 1560 m/s. Subunit VIB is a mud-bearing diatomite with an average porosity of 71% and an average acoustic velocity of 1668 m/s. It is interesting that Unit V has a velocity on the average 6% higher than Subunit VIA and yet Subunit VIA has a porosity the same as Subunit VIB. Subunit VIIA, a sandy mudstone, has the lowest porosity and water content of all the sediments cored at Site 696. The average acoustic velocity of this unit is 1802 m/s. Subunit VIIB, a clayey and silty mudstone, has an average porosity of 46% and an average acoustic velocity of 1799 m/s. Subunit VIIC, a glauconite silty mudstone and claystone, has an average porosity of 39% and an average acoustic velocity of 1826 m/s. Subunit VIID is a sandy mudstone with an average porosity of 39% and an average acoustic velocity of 1888 m/s. Thermal conductivity ranged from 0.959 (46.3 mbsf) to 1.472 (72 mbsf) W/m-K.

SEISMIC STRATIGRAPHY

Site 696 is located at SP 365 on British Antarctic Survey/Birmingham University multichannel seismic profile AMG845-18, about 70 km north-northeast of Site 695 (Figs. 2 and 3).

Core recovery was low overall (27.5% in Hole 696B) and uneven, including gaps of 30 and 85 m. The majority of the rotary-drilled cores were disturbed. This meant that P-wave logger velocities could not be relied upon to reflect *in-situ* values, and few samples were available for Hamilton Frame or index property measurements (see "Physical Properties" section, this chapter). Only a short section of Hole 698B, between 618 and 559 mbsf, was logged before the logging tool was lost (see "Operations" and "Downhole Measurements" sections, this chapter). Thus, correlation of the drilled sequence with the seismic reflection profile is uncertain. Nevertheless, the attempt is worthwhile, since the reflection profile is the only evidence available to supplement the recovered sediment in trying to decide what lithologies might be present in the sections with zero recovery.

Reference should be made to the "Physical Properties" section (this chapter) where the physical properties and lithostratigraphy have been compared with the reflection profile. For this exercise, the Hamilton Frame-measured values of velocity were first corrected for the change from *in-situ* conditions using the relation between shipboard data and the sonic log from Site 693. The corrections all *increased* the measured velocities, by as much as 120 m/s. Mean velocities were then assumed for each lithologic unit and subunit. These mean velocity levels are plotted in Figure 23 as a series of crosses with a connecting solid line. In the same figure, the unmodified P-wave logger values

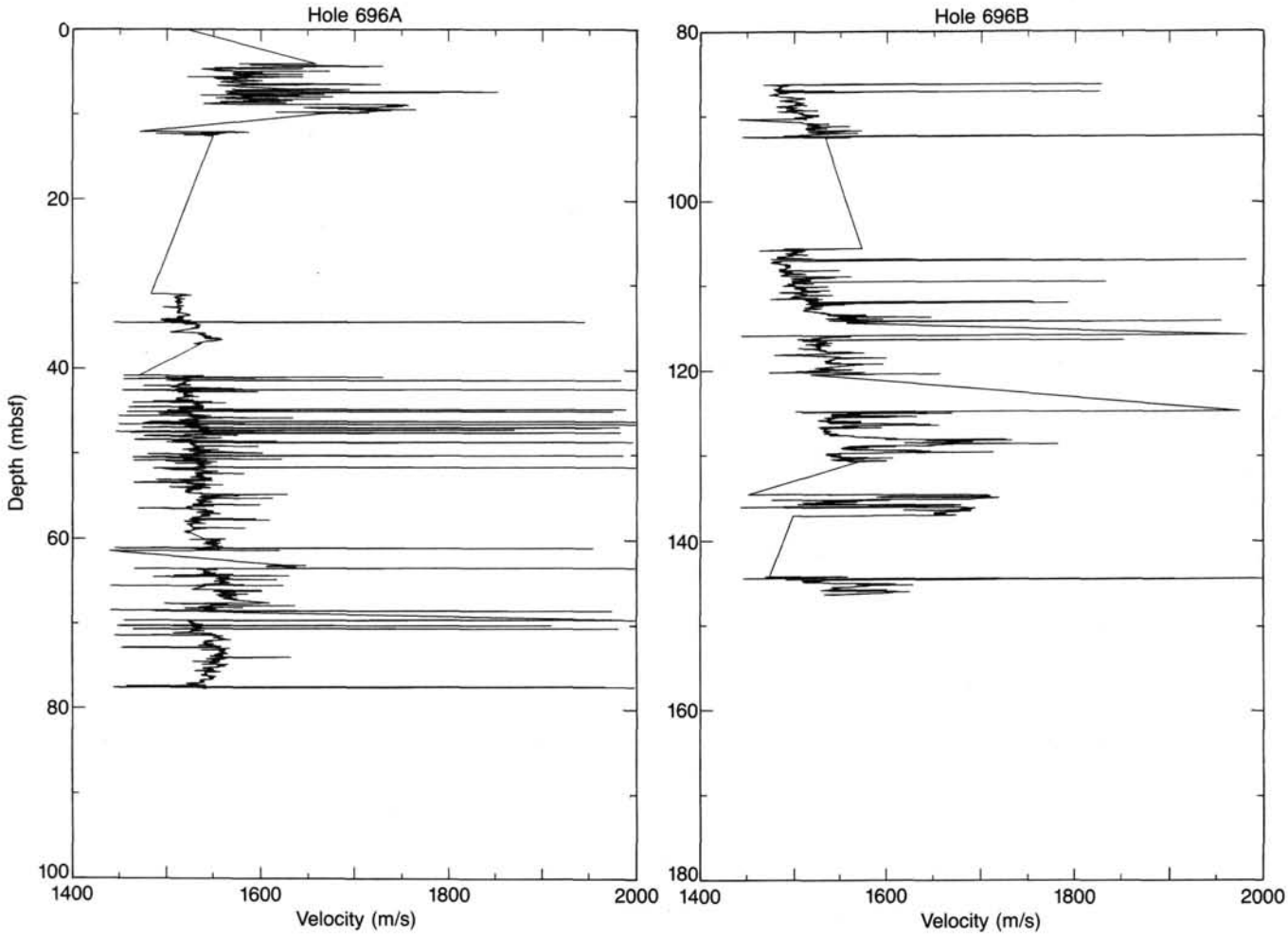

Figure 20. Continuous compressional wave velocity profile as determined by P-wave logger for Hole 696A and the upper part of Hole 696B.

Table 8. Lithostratigraphic unit velocities and depth to seismic horizons.

Litho-stratigraphic Unit	Depth (mbsf)	Average laboratory velocity (m/s)	Assumed *in-situ* velocity (m/s)	Interval thickness (m)	Interval transit time (s)	Depth to base of unit (twt) (s)	Depth of seismic horizon (twt) (s)
IA	0–8.5	1554	1560	8.5	0.010	0.010	—
IB	8.5–64.2	1482	1520	55.7	0.074	0.084	0.08
II	64.2–124.8	1528	1568	60.6	0.077	0.161	0.19
							0.25
III	124.8–211.8	1549	1600	87.0	0.109	0.270	0.28
IV	211.8–260.1	1580	1680	48.3	0.057	0.327	0.32
V	260.1–269.7	1612	1720	9.6	0.011	0.338	0.35
							0.41
							0.48
							0.56
VIA	269.7–472.5	1560	1680	202.8	0.241	0.579	0.60
VIB	472.5–529.8	1668	1788	57.3	0.064	0.643	0.65
VIIA	529.8–548.9	1802	1920	19.1	0.020	0.663	0.67
VIIB	548.9–569.7	1799	1920	20.8	0.022	0.685	0.69
VIIC	569.7–606.9	1826	1926	37.2	0.038	0.723	0.73
VIID	606.9–645.6	1888	1988	38.7	0.037	0.759	—

are plotted as a simple solid line and the Carlson et al. (1986) empirical relationship as a dashed line.

Several features of this figure are significant. First, the great majority of the P-wave logger values are lower than both the Carlson et al. (1986) and the physical properties models, a natural consequence of the core disturbance. Second, for most of the cored depth, the physical properties model is also significantly slower than the Carlson et al. (1986) model. This could mean that some of the Hamilton Frame measurements were made on disturbed sediments, despite efforts to avoid them, or that the Site 693-based corrections were not always appropriate. However, the greatest departures from the Carlson curve occur

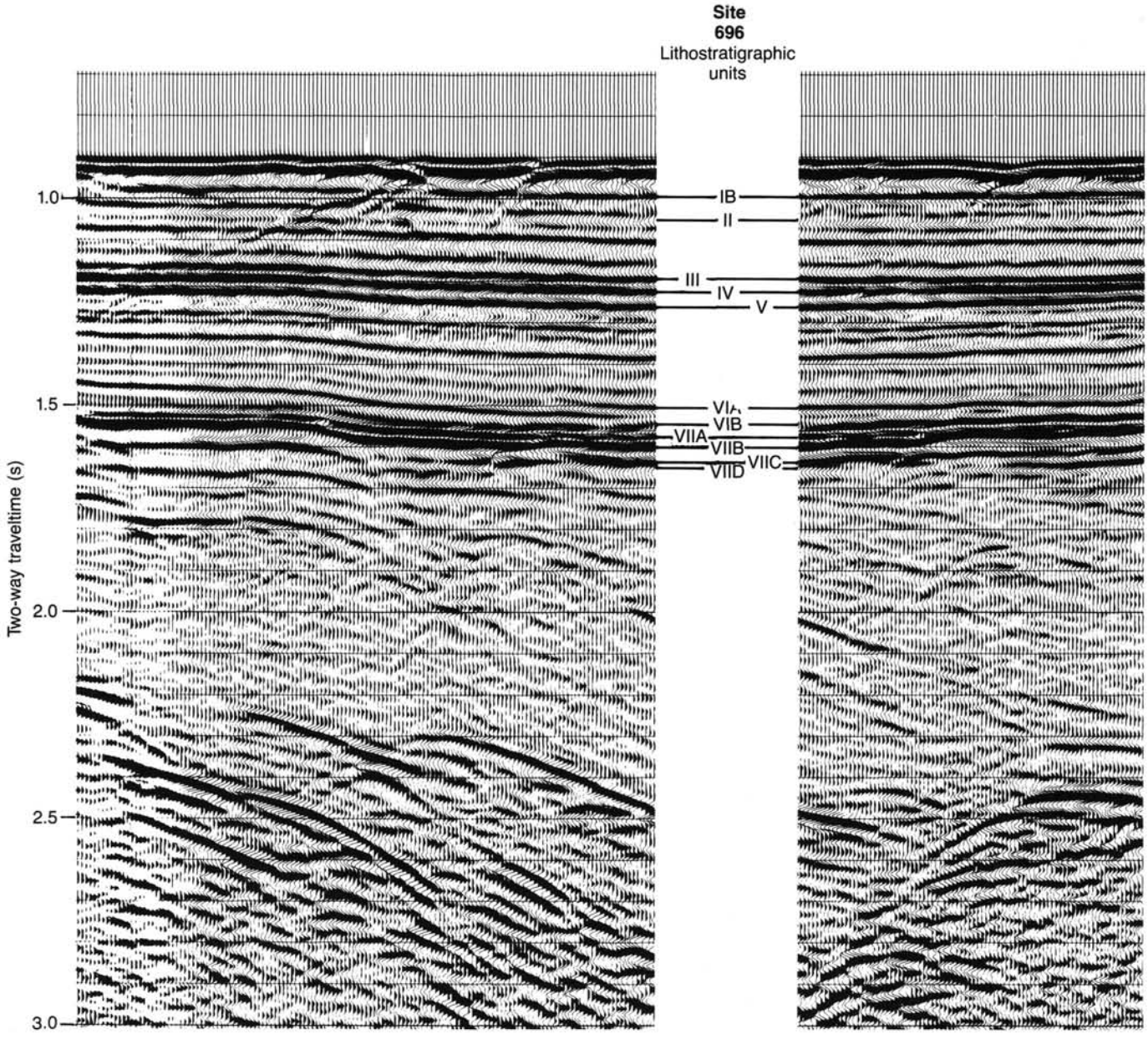

Figure 21. Seismic profile showing the location of the base of the lithostratigraphic units. Data used to correlate lithologies and seismic units given in Table 8.

Table 9. Thermal conductivities of sediments from Site 696.

Core, section top (cm)	Depth (mbsf)	K (W/m-K)	Remarks
113-696A-			
2H-4, 111	8.1	1.324	Oblique
3H-1, 44	12.4	1.183	Oblique
5H-3, 88	35.1	1.101	Oblique
6H-4, 96	46.3	0.959	Oblique
7H-2, 65	52.6	1.212	Oblique
7H-4, 65	55.6	1.420	Oblique
8H-2, 60	62.1	1.087	
8H-4, 60	65.1	1.408	
9H-2, 90	72.0	1.472	
9H-4, 90	75.0	1.289	

at depths where the recovered sediments have a high diatom content, known from drilling at other Leg 113 sites to produce low velocities. Thus, the physical properties model could be a reasonable approximation. Third, there are depth intervals where the unmodified P-wave logger values are higher than even the upward-corrected physical properties model. These are near the seabed, (Subunit IA), at the top of Unit III between 125 and 150 mbsf, and in Unit V near 260 mbsf. These are all thin sand layers with high velocities: they will affect the time-depth model only very slightly, and their existence in no way invalidates the physical properties model.

In summary, either the physical properties or the Carlson time-depth correlations could be the closer approximation. The only additional data available are from the sonic log of the base of Hole 696B, which does not help to resolve between them since at those depths the two velocity-depth models coincide.

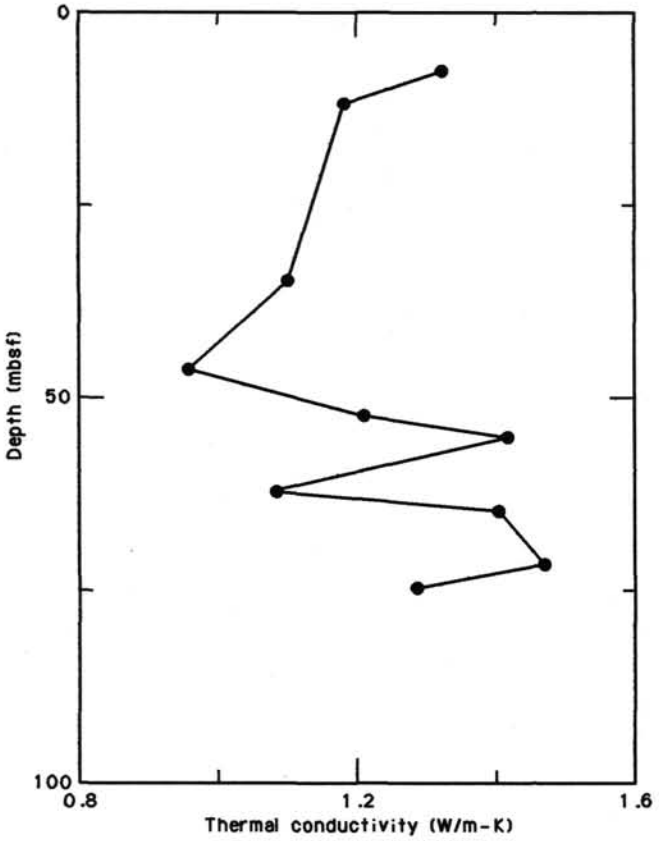

Figure 22. Profile of thermal conductivity, Site 696. Data given in Table 9.

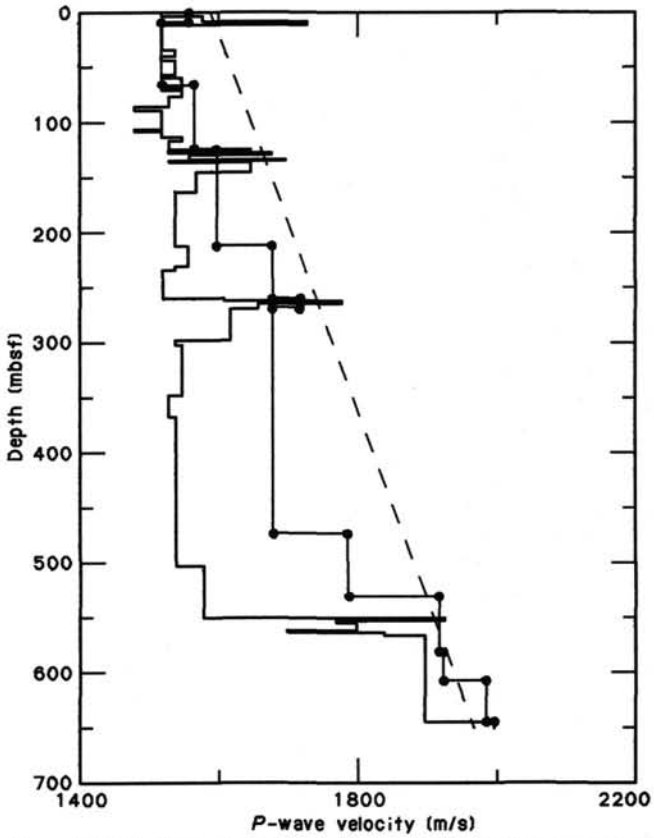

Figure 23. Velocity-depth data from *P*-wave logger (solid line) compared with Carlson et al. (1986) empirical velocity-depth relation (dashed line) and velocity-depth model extracted from Hamilton Frame mean velocity measurements (line connecting dots)(see "Physical Properties" section, this chapter).

For the present, the two alternatives may best be used together, to show the limits of the uncertainty surrounding time-depth correlation at Site 696. Figure 21 and Table 8 of the "Physical Properties" section (this chapter) show the physical properties interpretation. The Carlson velocity-depth and time-depth curves give depths to a given reflector which are about 7% deeper.

Sites 695 and 696 lie on the same reflection profile. At Site 695, drilling ended in uppermost Miocene sediments at 341 mbsf, corresponding to a strong reflector at 435 ms. The same reflector can be traced to 195 ms at Site 696, equivalent to a depth of about 150 m. This fits very well the position of the base of the radiolarian Tau zone which coincides approximately with the Miocene/Pliocene boundary, although core recovery around that depth is very poor. The main middle section reflector sequence at 285–350 ms at Site 696 seems to coincide with the top of the diatomaceous Unit IV and the thin sand of Unit V. This reflector sequence, of probable late Miocene age, can be traced back to Site 695 where, had drilling continued in an additional hole, it would have been as deep as Pollution Prevention Safety Panel considerations would have permitted us to drill.

The basal sequence of strong reflectors at 640–720 ms at Site 696 corresponds to impedance changes within the basal Unit VII, possibly but not certainly including the top of Unit VII at 530 m. Other reflectors occur within the drilled sequence but none as strong as those already discussed. This provides comment of a sort on the intervals where recovery was essentially zero, between 175 and 205 mbsf, and between 375 and 460 mbsf. Approximately, these depths correspond to 220–260 ms and 460–560 ms, respectively. Seismic reflectors within these ranges are of low or moderate amplitude, and do not support the notion of major lithologic units (such as a massive sand) occurring undetected within the coring gaps. It seems most probable that the unsampled intervals are diatom ooze and diatomite.

The BSR discussed in the "Site 695" chapter (this volume) coincides at Site 696 with the complex of strong reflections between 0.65 and 0.75 s twt. Mineralogic studies and related investigations are continuing into the possibility that it results from a silica diagenetic reaction rather than being the base of a gas hydrate zone as originally considered at the area around Site 695.

BIOSTRATIGRAPHY

Site 696 was drilled on the eastern South Orkney Platform in 650 m of water. The site is the shallowest of all sites drilled during Leg 113 and the uppermost of a three-site transect (Sites 697, 695, and 696) from Jane Basin to the crest of the South Orkney microcontinent. Site 696 was drilled to recover a carbonate record, especially for the Oligocene through middle Neogene, and to study the history of circumpolar deep water and the glacial history of the Antarctic Peninsula.

Site 696 sampled a 645.6-m-thick Quaternary to Paleogene (?Eocene) sediment sequence rich in biosiliceous components (mainly diatoms), especially in the middle to upper Miocene. In the lower part of Site 696, assigned to the Paleogene, siliceous microfossils occur only in traces and are mostly pyritized. Calcareous microfossils were only found in a strongly condensed Quaternary to uppermost Pliocene sequence, in an upper Miocene interval, and in the Paleogene. Agglutinated foraminifers were rare throughout the Neogene. Palynomorphs were only found in the lowermost two cores (Paleogene). Thus biostratigraphic age assignments of the Quaternary and Neogene sequence are mainly based on siliceous microfossils (diatoms, radiolarians, silicoflagellates), whereas Paleogene age assignments were provided by calcareous nannofossils and foraminifers.

Recovery of the sediment sequence which was cored by APC/XCB in the upper part (Hole 696A, 0–103.0 mbsf) and rotary drilled in the middle and lower part (Hole 696B, 76.6–645.6 mbsf) is in general low (averaging 27% at Hole 696B). In some intervals, however, recovery is moderate to good, such as in the uppermost 150 m (72%), and from 549 to 643.9 mbsf (63%).

Because of the poor recovery it was not possible to determine exact biostratigraphic and chronostratigraphic boundaries and to identify possible hiatuses, especially in the lowermost Pliocene and in the Miocene.

All depths referred to are sub-bottom depths in meters (mbsf) and, unless otherwise stated, samples are from the core catcher. On the summary biostratigraphic chart (Fig. 24), the age or biostratigraphic zone assigned to a given core catcher is extrapolated to the midpoint of the overlying and underlying core. The section is always described from the top down.

Planktonic Foraminifers

Neogloboquadrina pachyderma is abundant in the Quaternary of Core 113-696A-1H and rare in uppermost Pliocene, Sections 113-696A-2H, CC, 113-696A-3H, CC, and 113-696B-2H, CC. The remainder of the Neogene, although poorly recovered at Site 696, appears to be essentially barren of planktonic foraminifers except for a short interval in the upper Miocene (Section 113-696B-22R, CC) where rare *Globigerina woodi* and *Globigerina bulloides* occur together with moderately diverse assemblages of calcareous benthic foraminifers (see "Benthic Foraminifers," discussion below).

The occurrence of calcareous-rich sediment in the Quaternary and its absence in much of the Neogene at this and other Leg 113 sites may suggest that carbonate productivity in the Weddell Sea has increased significantly at some time during the past 2 m.y. This could account for a depressed CCD and the deposition of carbonate-rich sediments throughout the Weddell Sea. If this is true, it raises several questions. For example, is the increased *N. pachyderma* productivity in the Quaternary a result of a biological adaptation which has enhanced the species' tolerance to polar conditions? Additionally, has that increased productivity and/or biological adaptation been induced by changing paleoceanographic/paleoclimatic conditions in the Weddell Sea?

It is also possible that the abundance of carbonate in the Quaternary is independent of carbonate productivity changes in the Weddell Sea. Paleoceanographic changes alone may account for a depressed CCD and thus, enhanced carbonate preservation.

The Eocene(?) is also essentially barren of planktonic foraminifers despite the presence of diverse calcareous benthic assemblages in Cores 113-696B-59R through 113-696B-62R. Only several poorly preserved specimens of *Catapsydrax* sp. were observed in Section 113-696B-60R, CC. In contrast to the Neogene, however, the absence of more abundant and diverse Oligocene planktonic assemblages may be due to this site's shallow location as suggested by the abundance of neritic benthic foraminifers in that interval. If eurysaline or hypersaline conditions existed during this interval, they may have inhibited planktonic foraminiferal productivity.

Benthic Foraminifers

Benthic foraminifers were studied in all core catcher samples from Holes 696A, 696B, and a mud-line sample (Sample 696A-1H-1, 0–2 cm). Most samples contain low-diversity assemblages of agglutinated foraminifers; specimens are rare. Interpretation of these scarce faunas is difficult; comparison with Recent faunas from the Scotia Sea (Echols, 1971) and data from Site 695 suggest that depth ranges of species in the Pliocene were different from Recent depth ranges. Changes in faunal composition of the agglutinated faunas might be related to fluctuations in the location of the CCD through the middle Miocene to Quaternary. Mixed calcareous-agglutinated faunas in samples from depths between 250 and 330 mbsf (upper Miocene?; see Table 10) probably do not reflect living assemblages, but are mixtures of assemblages brought together by drilling disturbance, downhole contamination, or sediment transport (or a combination of these factors). Moderately preserved and moderately diverse calcareous faunas in Sections 113-696B-59R, CC, through 113-696B-62R, CC, suggest deposition in an inner neritic (20–100-m water depth), slightly hyposaline, hypoxic environment. The age of these sediments can not easily be inferred from the benthic faunas, but is probably late to middle Eocene.

The mud-line sample is dominated by agglutinated species with *Miliammina arenacea* and *M. lata* (together 55.9%) as the most common species. Other species (*Marsipella elongata*, *Textularia wiesneri*, *Cribrostomoides contortus*, *Reophax* sp. A [Earland], *Portatrochammina eltaninae*, *Jaculella obtusa*, and "*Reophax*" *difflugiformis*) are rare. The most common calcareous species are *Angulogerina earlandi* (17.3%) and *Bulimina aculeata* (5.0%). All calcareous species together are 27% of the assemblage, whereas at Site 695 (water depth 1310 m) only agglutinated species are present in the mud-line sample. This suggests that Site 695 is close to the present CCD.

The calcareous fauna in Section 113-696A-1H, CC (the shallowest of the Leg 113 sites at 650 mbsf) differs from that in sediments with *Neogloboquadrina pachyderma* at the other sites by being less diverse (14 species per 200 specimens) and strongly dominated by *A. earlandi* (87.6%). Other species are *Cassidulina crassa* (1.6%), *Globocassidulina subglobosa* (0.8%), and *Uvigerina asperula* (2.4%). The differences between the calcareous benthic foraminiferal faunas in sediments with *N. pachyderma* at other Leg 113 sites cannot be evaluated presently because the precise ages of the different samples are not known.

Milliammina arenacea and *M. lata* or *Martinotiella antarctica* are dominant in most lower samples. These three species have been reported to use siliceous cement and to occur predominantly in diatomaceous sediments (Echols, 1971). *Karreriella bradyi*, *Sigmoilina tenuis*, *Eggerella bradyi*, and *Cystammina pauciloculata* are present in some samples. In Core 113-696A-2H and the top of Core 113-696A-3H, *M. arenacea* and *M. lata* are dominant (*Miliammina* assemblage) and *M. antarctica* is absent (Fig. 24). In Sections 113-696A-3H, CC, through 113-696A-11X, CC (higher interval of mixed *Milliammina-Martinotiella* assemblage), and 113-696B-21R, CC, through 113-696B-30R, CC (lower interval), these species occur together at varying absolute and relative abundances (Fig. 25). In Sections 113-696B-3R, CC, through 113-696B-5R, CC (higher interval of *Martinotiella* assemblage), and 113-696B-17R, CC, through 113-696B-19R, CC (lower interval), *M. antarctica* is dominant. Sections 113-696B-6R, CC, through 113-696B-16R, CC, and 113-696B-31R, CC, through Sample 113-696B-51R-1, 48–50 cm, contain rare *M. antarctica*. The boundaries between the benthic foraminiferal assemblages cannot be located precisely because of the extremely poor core recovery at Site 696 (Fig. 25).

The environmental interpretation of the poor assemblages at Site 696 is questionable because depth zonations of benthic faunas in the Antarctic region are not usable from one region to another: faunas at the mud line at the Leg 113 sites are not similar to faunas at equivalent depths in other Antarctic areas (Bandy and Echols, 1964; Theyer, 1971; Milam and Anderson, 1981). Recent faunas dominated by *M. arenacea* occur in the Scotia Sea at depths of less than 1300 m, whereas faunas dominated by *M. antarctica* occur in waters deeper than 2000 m. It seems improbable that Site 696 (present water depth 640 m) was at depths of more than 2000 m in the Pliocene: Pliocene depth ranges of *M. antarctica* and *M. arenacea* were probably different from the

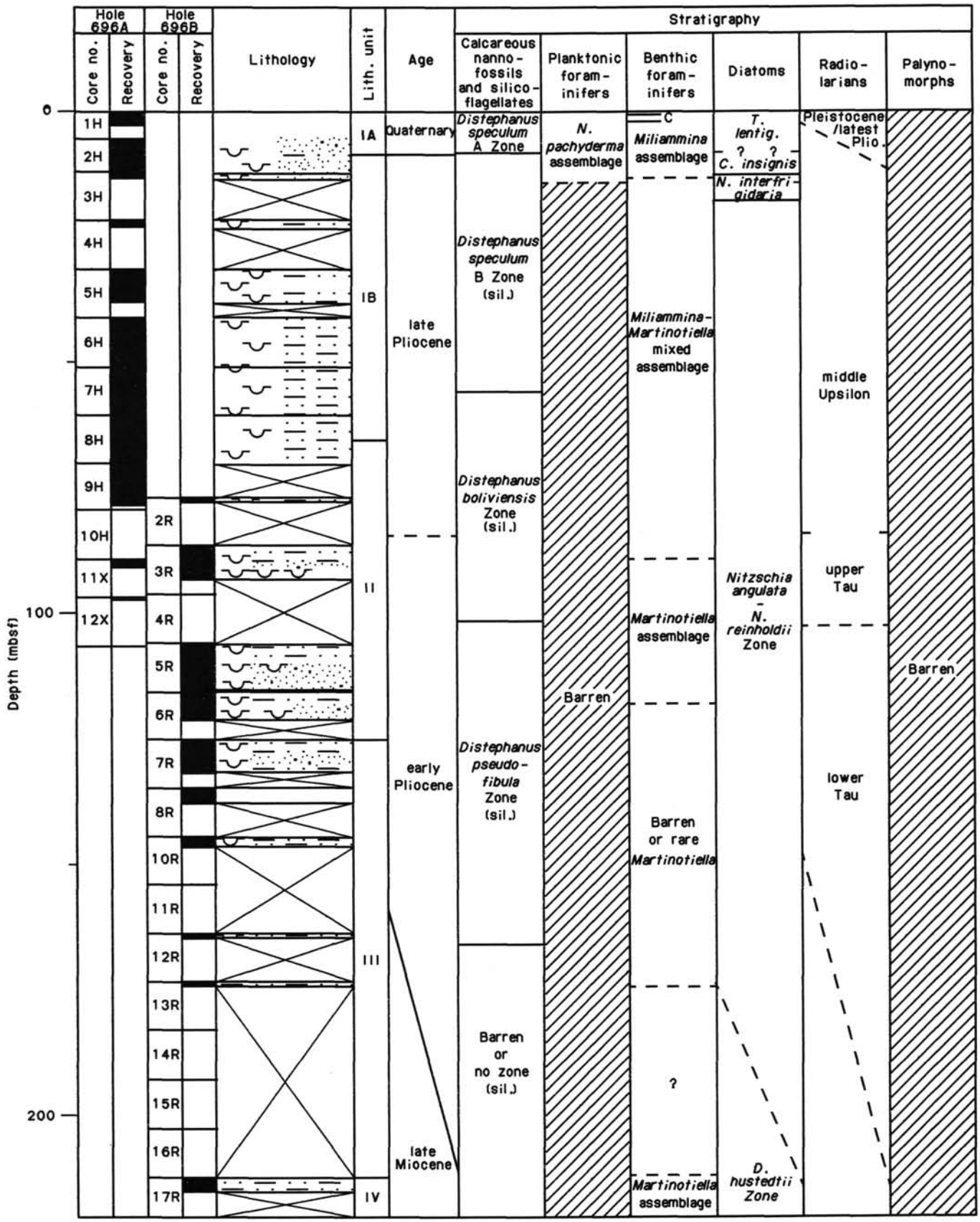

Figure 24. Biostratigraphic summary chart, Site 696.

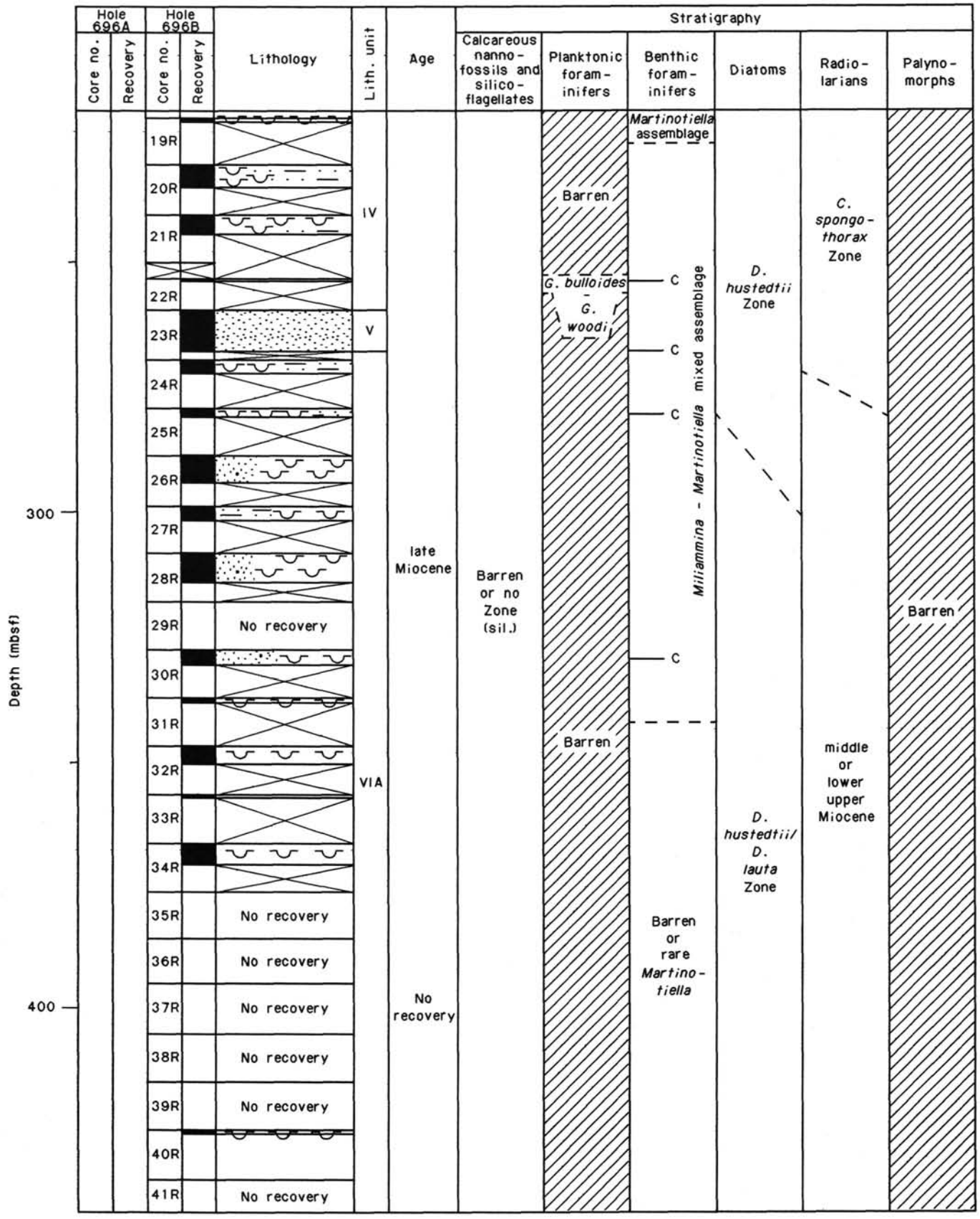

Figure 24 (continued).

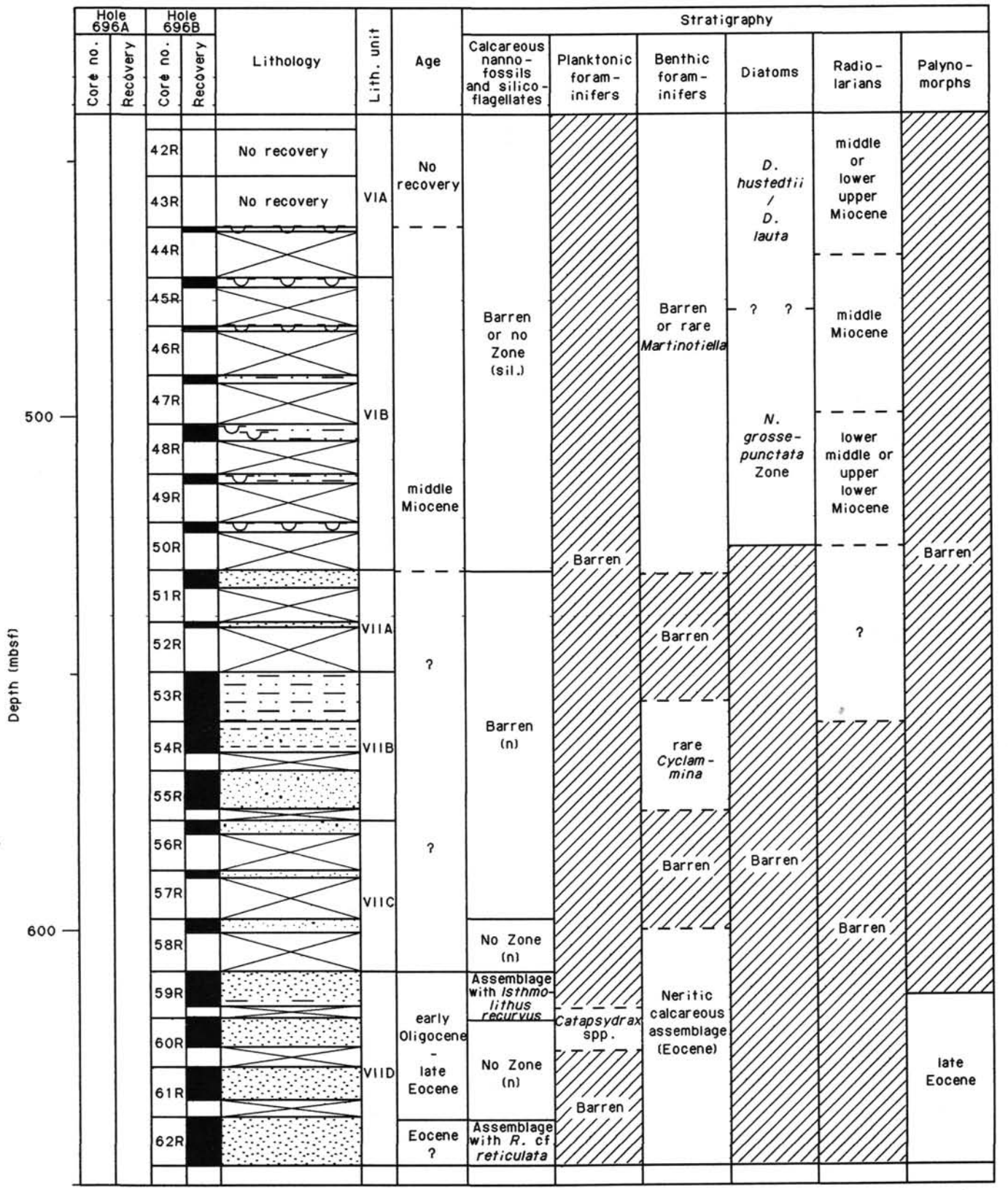

Figure 24 (continued).

Recent ranges. Faunas at Site 695 (at about 1300 m water depth) show a similar variation in species composition as faunas in the upper part of Site 696 (Fig. 26). Possibly the change from *Milliammina* assemblage through mixed *Miliammina-Martinotiella* assemblage through *Martinotiella* assemblage represents a change from faunas living closer to the CCD to faunas living further below the CCD. This suggests that the CCD in the region of Sites 695 and 696 was greater in the middle Miocene than it is

Table 10. Abundance and diversity of faunas in samples with calcareous specimens, Site 696.

Sample or Section	Depth (mbsf)	Number of species	Number of specimens	Dominant form
113-696A-1H-1, 0–2	0.0	20	202	*M. arenacea* (56%) (27% calcareous, 73% agglutinated)
113-696A-1H, CC	2.1	14	251	*A. earlandi* (88%) (99% calcareous, 1% agglutinated)
113-696B-22R, CC	253.8	26	231	*Cibicidoides* spp. (23%) (89% calcareous, 11% agglutinated)
113-696B-23R, CC	268.0	30	231	*Cibicidoides* spp. (29%) (78% calcareous, 22% agglutinated)
113-696B-25R, CC	280.9	7	207	*M. arenacea* (76%) (7% calcareous, 93% agglutinated)
113-696B-30R, CC	330.3	12	43	*E. exigua* (33%) (14% calcareous, 86% agglutinated)
113-696B-59R, CC	614.2	32	150	*Anomalinoides* spp. (25%) *Cibicidoides* spp. (18%)
113-696B-60R, CC	624.8	26	179	*Anomalinoides* spp. (15%) *P. ovata* (12%) *A. carinata* (12%)
113-696B-61R, CC	632.4	32	255	*P. ovata* (12%) *G. subglobosa* (11%) *F. commune* (10%)
113-696B-62R, CC	645.6	27	155	*Turrilina* sp. (18%) *Brizalina* spp. (18%) *G. subglobosa* (15%)

today, became shallower to about its present depth for a period in the late Miocene (see below), and deeper in the latest Miocene and early Pliocene. The CCD gradually became less during the early Pliocene to Quaternary to reach its present depth just below 650 mbsl.

The mixed calcareous-agglutinated assemblages in samples between 253 and 331 mbsf (upper Miocene?; see Table 10) are difficult to interpret: the faunas appear to be mixed assemblages, and the core recovery in this interval is extremely poor. The agglutinated specimens in these samples are *M. arenacea*, *M. antarctica*, *K. bradyi*, and *E. bradyi*, species present in the Site 696 samples with agglutinated species only. Their preservation appears to be moderate to good, and not different from that in other samples. The calcareous forms show great variation in preservation, from broken and abraded thick-walled specimens to well-preserved, delicate, thin-walled specimens. The most common thick-walled species are *Cibicidoides* spp., *Pullenia* spp., *Sphaeroidina bulloides*, *Lenticulina* spp., *Nodosaria radicula*, and *Globocassidulina subglobosa*. Thin-walled species are less common and include *Angulogerina earlandi*, *Anomalinoides macroglabra*, *Astrononion echolsi*, *Epistominella exigua*, and *Discorbis williamsoni*. The thin-walled species appear to be similar to faunas close to the top of the section; they may represent downhole contamination at this rotary-drilled site, or are *in-situ* faunas. The thick-walled species probably lived at depths considerably shallower than the CCD, and may have been transported downslope. The faunas may have occurred at different layers in the sediments, and been mixed by the extreme drilling disturbance in the few centimeters of sediment recovered in the cores.

Sample 113-696B-51R-1, 48–50 cm, is the lowest sample with *M. antarctica*; no samples lower in Cores 113-696B-51R or 113-696B-52R were studied. In Sections 113-696B-53R, CC, through 113-696B-55R, CC (Lithologic Subunit VIIB), only rare specimens of *Cyclammina* sp. are present; the species can not be determined because all specimens are deformed (flattened). *Cyclammina pusilla* occurs in the Scotia Sea area recently at the

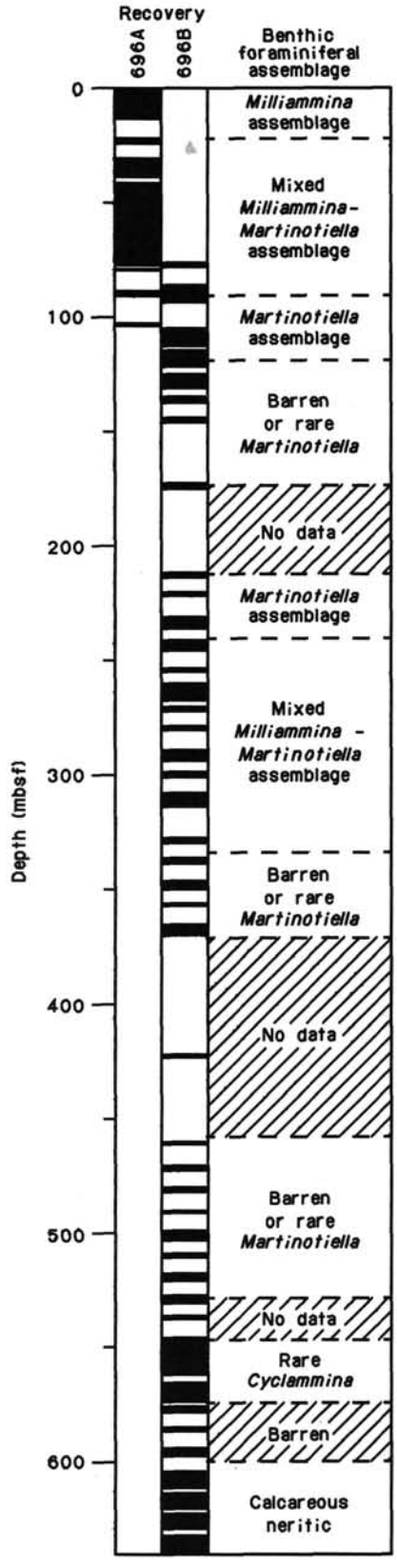

Figure 25. Core recovery and benthic foraminiferal assemblages at Site 696. Note that the boundaries of assemblages cannot be precisely located because of poor recovery.

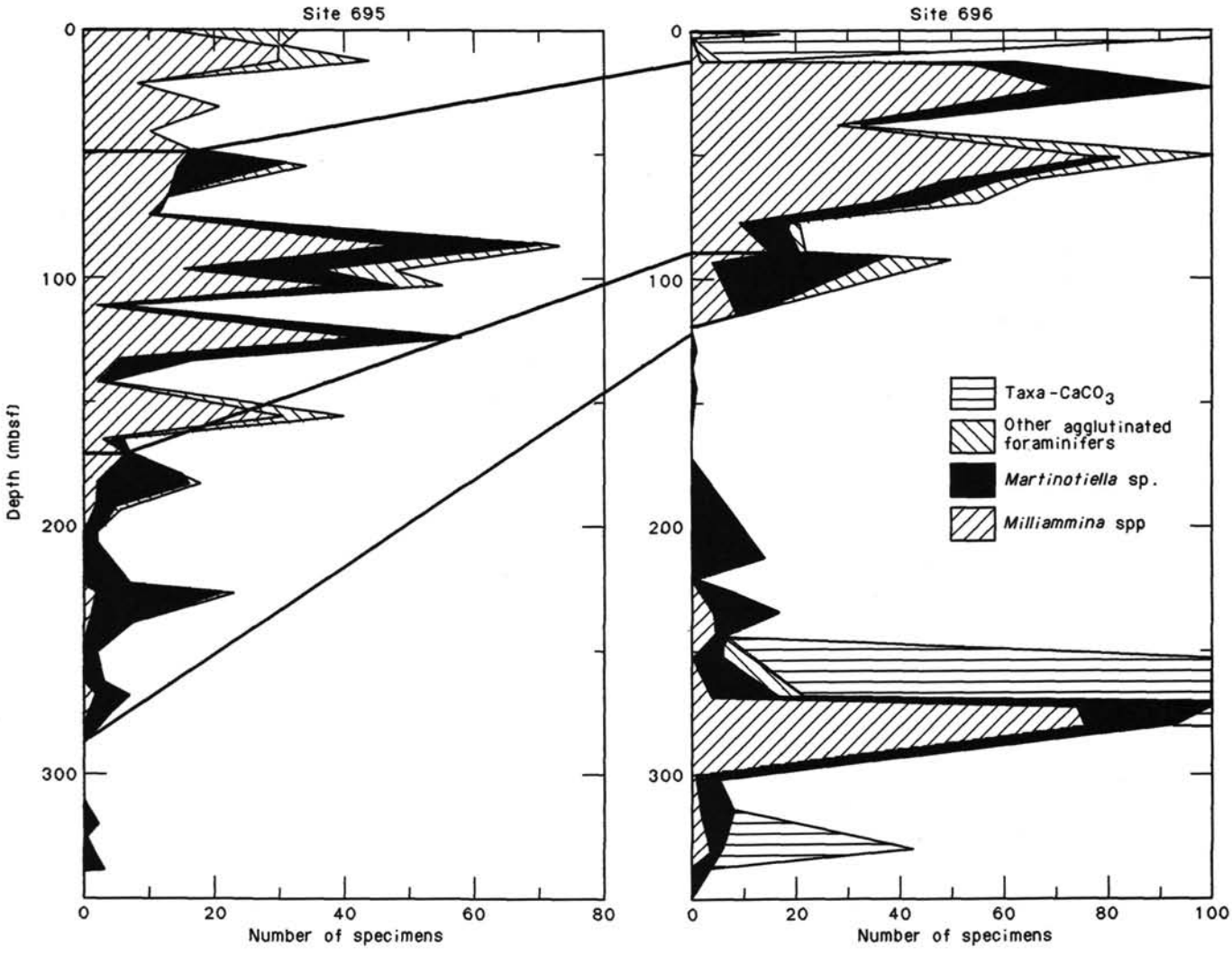

Figure 26. Abundance of species of benthic foraminifers in core catcher samples from the upper 350 m at Site 696 (Holes 696A and 696B) and Hole 695A; the sample size is not constant. Correlation lines are drawn at boundaries between assemblages (see Fig. 24).

same depths as *M. antarctica*, but in areas of nondiatomaceous sediments (Echols, 1971). Thus the change in benthic fauna between lithologic Units VI and VIIB may represent a change in availability of biogenic silica in the sediments. Section 113-696B-56R, CC, through Sample 113-696B-58R-2, 60–62 cm (lithologic Subunit VIIC), are barren. During the deposition of this barren interval the largest change in benthic foraminiferal faunas at Site 696 took place: fully calcareous faunas below, predominantly agglutinated faunas above.

Faunas in Sections 113-696B-59R, CC, through 113-696B-62R, CC (lithologic Unit VIID), are calcareous, moderately diverse (see Table 10), and moderately preserved; preservation becomes better downhole. The samples are very sandy, and benthic foraminifers are rare in the larger than 63-μm size fraction. The dominant species in the upper three cores are *Cibicidoides* spp. (including epiphytic species), *Anomalinoides* spp., and *Asterigerina carinata* (an epiphytic species). Other common species are *Praeglobobulimina ovata*, *Florilus commune*, *Elphidium* spp., *Gyroidinoides* spp., and *Turrilina* spp. In the lowermost core *Turrilina* spp. and *Brizalina* spp. become dominant, together with *Globocassidulina subglobosa* and *Alabamina obtusa*. In all samples there are specimens of *Buccella* sp., a possibly undescribed species that appears to be related to *Trochoelphidiella* sp., observed at Site 693. On the generic level, the assemblage with *Cibicidoides*, *Anomalinoides*, *Gyroidinoides*, and *Praeglobobulimina* is similar to assemblages described from Eocene-Oligocene deposits in the Hampshire Basin (England; Murray and Wright, 1974) and the Austral Basin (Argentina; Bertels, 1977), but many of the species probably have not been described. The environment of deposition was probably inner neritic (less than 100 m), with slightly hyposaline and slightly hypoxic conditions. The greater abundance of epiphytic species higher in the section suggests that water depths may have decreased upsection; unfortunately the recovered section is too short to determine this with certainty. The age of the sediments is probably middle to late Eocene, but cannot be determined precisely because many of the species have not been described earlier.

Calcareous Nannofossils

Neogene

Neogene calcareous nannofossils were found only in Section 113-696B-22R, CC (260.1 mbsf), which contains a monospecific assemblage of *Reticulofenestra perplexa*. Few in number, these nannofossils are dated as late Miocene by diatoms (*Denticulop-*

sis dimorpha portion of the *D. hustedtii* Zone, about 7.5–8.5 Ma; (see "Diatom," discussion below). Nannofossils were otherwise absent throughout the Miocene-Quaternary section, a reflection of an exceedingly shallow CCD at this rather shallow site (water depth = 650 m).

The same nannofossil assemblage was seen in larger numbers on the Dronning Maud Land margin in Section 113-689A-27R, CC, just above sediments dated within the *Denticulopsis dimorpha* acme. Taking both sites together, the incursion of nannofossils over the continental margins and promontories around the perimeter of the Weddell Sea at this time during the late Miocene could signal a slight amelioration in climate. This may have enhanced nannoplankton productivity throughout the basin, thereby temporarily depressing the CCD sufficiently to allow deposition of coccoliths. Otherwise, Site 696 as well as Site 693 were clearly inhospitable to nannofossil productivity and the preservation of their skeletons, a situation in strong contrast to conditions on Maud Rise where nannofossils accumulated at a high rate during most of the Miocene.

As discussed previously (see "Biostratigraphy" section, Site 693 chapter), Maud Rise was apparently bathed from the northeast or east by somewhat warmer return currents of the Weddell Gyre. On the other hand, Weddell Gyre currents moving westward along the margin were cooled by marginal sea-ice and ice shelves. We can speculate that the effect of the marginal ice was twofold: (1) to cool surface waters below the life-tolerance limits of the calcareous nannoplankton, thus inhibiting productivity, and (2) to form corrosive bottom waters capable of dissolving most of the skeletal carbonate produced. The overall effect was to raise the CCD, thereby leaving more of the Neogene sediments drilled at Sites 693 and 696 devoid of calcareous nannofossils.

Paleogene

Calcareous nannofossils were next encountered in Core 113-696B-58R (597.2–606.9 mbsf), which contained elements of an assemblage that is better developed in Core 113-696B-59R. The core catcher of Core 113-696B-59R yielded well-preserved and common *Isthmolithus recurvus*, *Reticulofenestra oamaruensis*, few *R. bisecta*, *R. davisii*, *Chiasmolithus altus*, *Coccolithus pelagicus*, and rare *Braarudosphaera bigelowii*. *Isthmolithus recurvus* ranges from the earliest Oligocene to the latest Eocene (about 35–38 Ma). An assemblage from Sample 113-696B-59R-4, 41 cm, is dominated by the holococcolith, *Zyghrablithus bijugatus*; the remainder of the assemblage in poorly preserved.

Cores 113-696B-60R and 113-696B-61R contain assemblages similar to the above, but *Isthmolithus recurvus* was not detected, thus these samples are presumably older than 38 Ma. The lowermost core in the hole, 113-696B-62R, contained *Reticulofenestra reticulata*, which ranges from middle middle to upper Eocene (about 45–37 Ma).

Silicoflagellates

Silicoflagellates were sufficiently numerous for zonation within the upper 150 m of Site 696. Core 113-696A-1H contained *Distephanus speculum speculum* and *D. septenarius*, and is assigned to the *D. speculum* A Zone of Ciesielski (1975). Short-spined *D. speculum* dominate Cores 113-696A-2H to 113-696A-6H, and these are assigned to the *D. speculum* B Zone.

The *Distephanus boliviensis* Zone extends from 55 to 101 mbsf, with an acme in the numbers of silicoflagellates in Cores 113-696A-11X and 113-696A-12X as well as in Core 113-696B-3R. The *Distephanus pseudofibula* Zone encompasses Cores 113-696B-5R to 113-696B-12R, below which silicoflagellates are absent or of no zonal value.

Diatoms

Hole 696A

In Hole 696A we recovered a 106-m-thick Quaternary to (?)lower Pliocene sequence. Section 113-696A-1H, CC, is placed in the upper Quaternary "*Coscinodiscus*" (*Thalassiosira*) *lentiginosus* Zone. Other species include *Eucampia balaustium, Nitzschia kerguelensis, N. curta, Stellarima microrias, Thalassiosira gracilis*, and *Rouxia antarctica*. Part of the upper Pliocene and lower Pleistocene are likely missing from this site because Section 113-696A-2H, CC, is in the middle upper Pliocene *Cosmiodiscus insignis* Zone. In addition to the nominate taxon, *Nitzschia linearis, E. balaustium, Schimperiella antarctica, Coscinodiscus vulnificus, N. curta, T. gracilis* and *R. antarctica* are present.

The diatoms in Section 113-696A-3H, CC, are largely fragmented, and thus we are uncertain about the stratigraphic placement of this interval. It very likely belongs to the lower upper Pliocene *Nitzschia interfrigidaria* Zone, based on the occurrence of the nominate taxon and the absence of *C. insignis* and *C. vulnificus*. We also note *Nitzschia curta, N. angulata, R. antarctica, S. microrias*, and *Stephanopyxis turris*. A possible *Nitzschia praeinterfrigidaria* was also observed. The zonal designation of Section 113-696A-4H, CC, is also doubtful. We tentatively place it in the lower upper Pliocene interval which represents the transition from *Nitzschia praeinterfrigidaria* to *N. interfrigidaria* (see Diatoms discussion in "Biostratigraphy" section, "Site 695" chapter, this volume). Associated species are *Rouxia naviculoides, S. turris*, E. *balaustium, Cosmiodiscus intersectus*, and *N. curta*.

The interval from Sections 113-696A-5H, CC, through 113-696A-12X, CC, belongs to the combined *Nitzschia angulata/N. reinholdii* Zone and is assigned to the lowermost upper to lower Pliocene. Unlike the lower Pliocene sections in other holes drilled during Leg 113, diatoms are few to common and preservation is generally poor to moderate. Among species present are *C. intersectus, R. naviculoides, Thalassiosira oestrupii, T. torokina, N. praeinterfrigidaria* (only present in Section 113-696A-5H, CC), and sporadic *Nitzschia angulata*. We also record rare occurrences of forms such as *Nitzschia* cf. *N. januaria, N. porteri* sensu Schrader (1976), *Nitzschia* sp. 14 (Schrader, 1976), *Cestodiscus* sp. 1 (Schrader, 1976), and *D. hustedtii*. These may have been reworked from the underlying upper Miocene.

Hole 696B

Sections 113-696B-2R, CC, to 113-696B-13R, CC, are assigned to the combined *N. angulata/N. reinholdii* Zone. We are less sure of our zonal designation in the lower part of this interval because of the absence of definite zonal markers. Diatoms are few and the preservation is poor to moderate. We find species such as *Rouxia antarctica, R. naviculoides, D. hustedtii, A. ingens, T. excavata, T. pileolus, T. torokina*, and such forms described from Miocene sediments as *N. januaria, N. porteri*, and *Nitzschia* sp. 14 (Schrader, 1976). Cores 113-696B-14R to 113-696B-16R were empty.

The top of the *D. hustedtii* Zone occurs in Section 113-696B-17R, CC, and is defined by an upsection abundance decrease in this species. The base of the zone (which ranges from the lower upper Miocene to the lowermost Pliocene) is poorly defined but probably occurs between Cores 113-696B-25R and 113-696B-27R. We note an increase in abundance of *D. dimorpha* in one section (113-696B-22R, CC). At other sites, this abundance increase usually occurs in an interval in the lower part of the *D. hustedtii* Zone. Interestingly, this is the only level (Section 113-696B-22R, CC) where we see calcareous nannofossils and fora-

minifers in the Miocene section of this site. Besides the two species mentioned above, the *D. hustedtii* Zone contains *S. turris, Nitzschia januaria, N. porteri* sensu Schrader (1976), *N. claviceps, A. ingens, Coscinodiscus deformans*, and *E. balaustium*.

The top of the upper middle to lower upper Miocene *Denticulopsis hustedtii–D. lauta* and *Nitzschia denticuloides* Zones is tentatively placed between Sections 113-696B-25R, CC, and 113-696B-27R, CC. The stratigraphic position of this sample interval is defined by the last occurrence of *Nitzschia denticuloides, N. efferans*, and *D. lauta*. The top of this zone however, is not well defined by Weaver and Gombos (1981) and should be redefined. The base of the interval related to the *D. hustedtii–D. lauta* and *N. denticuloides* Zones is placed in Section 113-696-45R, CC. The diatom assemblage in this interval also includes *Nitzschia claviceps*, rare *E. balaustium, Rouxia* spp., *N. porteri, Rhizosolenia praebarboi, D. hustedtii*, and *A. ingens*. The latter two species are common to abundant in some intervals.

The top of the lower middle Miocene *N. grossepunctata* Zone occurs in Section 113-696B-46R, CC. In this sample we also note the first occurrence of *D. hustedtii*, which has been placed in the upper part of the *N. grossepunctata* Zone above the last appearance datum (LAD) of *Denticulopsis maccollumii* by Weaver and Gombos (1981). The latter LAD falls within Section 113-696B-47R, CC. In addition to these species we also found *Denticulopsis punctata, A. ingens* (few to common), *Coscinodiscus marginatus, Trinacria* spp., and *Chaetoceros* resting spores (common in Section 113-696B-47R, CC). The *N. grossepunctata* Zone ranges down to Section 113-696B-50R, CC. Below that interval diatoms are sporadic, rare, and poorly preserved, so that a biostratigraphic age assignment is not feasible. We note that diatoms found in the interval from Section 113-696B-56R, CC, to Section 113-696B-62R, CC, are pyritized. In Section 113-696B-58R, CC, several specimens of fresh-water diatoms (*Melosira* cf. *granulata*) are present.

In contrast to the Quaternary and Pliocene, all samples from the *D. hustedtii, D. hustedtii–D. lauta-N. denticuloides* and the *N. grossepunctata* Zones (Cores 113-696B-17R through 113-696B-50R) contain common to abundant, moderate to well-preserved diatoms.

Summary

Site 696 can be seen as the western Weddell Sea counterpart to Sites 689, 690, and 693 in the eastern Weddell Sea; it records the late Neogene, and earlier, history of the Weddell Gyre. Although recovery is not ideal, this site should help us to reconstruct the late Neogene paleoclimatic and paleoceanographic history of the Atlantic sector of the Southern Ocean.

Site 696 contains a condensed Quaternary to upper Pliocene sequence which may contain hiatuses as did Site 695. In contrast, the lower upper to lower Pliocene part (combined *N. angulata/N. reinholdii* Zone) is less expanded. A large part of the section at Site 696 (Cores 113-696B-17R through 113-696B-50R) is assigned to the upper to middle Miocene and contains abundant diatoms which are well-preserved.

Because of rare occurrence of diatoms in the lowermost part of Site 696, a biostratigraphic age assignment was not feasible for Cores 113-696B-51R through 113-696B-62R.

We point out two major differences between this site and all previous Leg 113 Sites:

1. The diatom assemblages recovered in the lower Pliocene sediments of Site 696 are poor to moderately preserved.

2. The Miocene diatom associations (*D. hustedtii–D. lauta-N. denticuloides* and *N. grossepunctata* Zone) at Site 696 contain few to abundant specimens of *Denticulopsis lauta* which suggests that the biogeographic province of this species may be more appropriately linked to the Subantarctic and northern Antarctic region of the Southern Ocean. Additional comments on taxonomy and biostratigraphy can be found in the diatoms discussion of the "Biostratigraphy" sections, "Site 689" and "Site 697" chapters (this volume).

Radiolarians

Hole 696A

Radiolarians are common to abundant and well preserved in all samples examined from Hole 696A. In many slides prepared from the > 63-μm fraction, radiolarian abundances are reduced due to dilution by large centric diatoms, although not enough to prevent stratigraphic analysis of the fauna. Of the 12 cores taken in this hole, two (Cores 113-696A-10H and 113-696A-12X) recovered insufficient amounts of sediment for radiolarian analysis.

Section 113-696A-1H, CC, is tentatively assigned to the Phi Zone, based on the co-occurrence of *Cycladophora davisiana* and *Clathrocyclas bicornis*, and the absence of common *Helotholus vema* and *Desmospyris spongiosa*. Rare *D. spongiosa* were seen in this sample, suggesting the presence of some reworked Pliocene material. If *C. bicornis* is reworked as well, this sample could be of later Pleistocene age.

Cores 113-696A-2H through 113-696A-9H are assigned to the middle part of the Upsilon Zone, based on the presence of *H. vema* and *D. spongiosa* and the absence of upper and lower Upsilon indicators *C. davisiana* and *Prunopyle titan*. Other species found in these samples include *C. bicornis, Antarctissa strelkovi, Antarctissa denticulata, Antarctissa ewingi*, and *Eucyrtidium calvertense*. Many of the specimens assigned to *H. vema* are morphologically atypical, and resemble the latest Miocene to basal Pliocene form of the unnamed species ancestral to *H. vema*. The first appearance datum (FAD) of *H. vema* (and by definition the base of the Upsilon Zone) is therefore difficult to define at this Site (see "Biostratigraphy" section, "Site 695" chapter, this volume, for description and stratigraphic discussion). The presence of *D. spongiosa*, however, indicates that these samples are indeed within the Upsilon Zone.

Core 113-696A-11X contains *H. vema* (atypical morphs) but no *D. spongiosa*, and no earlier Pliocene indicators, such as *Prunopyle titan* or *Lychnocanium grande*. It is tentatively assigned to the upper Tau Zone, based on the absence of *D. spongiosa*. If the absence of this species is due to ecologic restriction, however, this sample may be middle Upsilon.

Hole 696B

Core 113-696B-1W, a wash core, was not examined for radiolarians. Sections 113-696B-2R, CC, and 113-696B-3R, CC, are stratigraphically equivalent to Core 113-696A-11X, containing *H. vema*(?) but no other zonal indicators, and are thus tentatively assigned to the upper Tau Zone. Core 113-696B-4R recovered no sediment.

Sections 113-696B-5R, CC, through 113-696B-10R, CC, contain common *L. grande, A. strelkovi, A. denticulata*, and *C. bicornis*, but no Miocene forms, and are assigned to the lower Tau Zone. Preservation of radiolarians in this interval is generally poor, and abundances low (few to rare). Radiolarians are also few and poorly preserved in Sections 113-696B-12R, CC, and 113-696B-13R, CC. No zonal assignment is possible for these two samples, although the presence of rare to few *Lithomelissa stigi* in Section 113-696B-12R, CC, suggests that the Miocene/Pliocene boundary lies within Section 113-696B-11R. Radiolarians from this core will need to be prepared using special techniques. No sediment was recovered in the next three cores (113-696B-14R through 113-696B-16R). Cores 113-696B-17R through 113-696B-24R are assigned to the *Cycladophora spongothorax*

Zone, based on the presence of the nominate species, *Dendrospyris haysi* and *Antarctissa conradae*.

Cores 113-696B-25R through 113-696B-44R contain very high abundances of large (>63 μm) centric diatom valves, which so dilute the radiolarians that too few specimens can be found on a strewn slide to permit zonal assignments to be made. *Helotholus sp., Cycladophora humerus* (= *Clathrocyclas humerus* of Petrushevskaya, 1975), *D. haysi*, and *A. conradae* are present in these cores however, and imply a Miocene age. Cores 113-696B-45R through 113-696B-47R contain middle to early Miocene indicator species such as *Amphistylus angelinus* and *Cyrtocapsella isopera*. Cores 113-696B-48R through 113-696B-50R contain common *Cycladophora golli golli*, and are thus assignable to the lower middle to upper lower Miocene, based on the range of this species reported by Chen (1975). Sections 113-696B-51R, CC, and 113-696B-52R, CC, contain common, very poorly preserved radiolarians. No species could be identified in these two sections. All remaining cores from Hole 696B (113-696B-53R through 113-696B-62R) are barren of radiolarians.

Discussion

The Pliocene and Pleistocene section recovered at Site 696 appears to be very similar to that recovered by Site 695, with a condensed Pleistocene through upper Pliocene, and a highly expanded lower Pliocene section. A hiatus may be present in Site 696 between about 78 and 90 m (Cores 113-696A-9H and 113-696A-11X), which has removed sediments of lower Upsilon age (basal Gauss through C3N1). This inference is based on the absence of *Prunopyle titan* in all samples assigned to the Upsilon Zone, and the presence of upper Tau(?) radiolarian assemblages in Sections 113-696A-11X, CC, 113-696B-2R, CC, and 113-696B-3R, CC. Inferring the presence of a hiatus on the absence of a single species is risky, but *Prunopyle titan* does not appear to be absent from this section due to ecologic restriction, as it is common in lower Upsilon sediments at nearby Site 695, and is also present in basal Pliocene through upper Miocene sediments in Site 696. The depth at which this possible hiatus occurs corresponds (at least approximately) to the level where unusually hard formation conditions resulted in the loss of the Hole 696A and poor core recovery in both Holes 696A and 696B. Because recovery was poor in this interval, the more precise biostratigraphic definition of this hiatus, if it exists, will be difficult.

The basal Pliocene interval of poorly preserved radiolarian assemblages with Subantarctic faunal elements seen at Site 695 is also seen at Site 696. This interval appears to extend into the uppermost Miocene (Cores 113-696B-12R and 113-696B-13R), although this only a tentative conclusion, based as it is on poor biostratigraphic control and low core recovery in this interval.

Palynology

All core catcher samples from the seafloor down to 616.6 mbsf at Site 696 (113-696A-1H, CC, through 113-696A-12X, CC, and 113-696B-2R, CC, through 113-696B-59R, CC) are barren of palynomorphs. A few samples from Cores 113-696B-60R and 113-696B-62R (Section 113-696B-60R, CC, Sample 113-696B-60R-3, 75–79 cm, Section 113-696B-62R, CC, and Sample 113-696B-62R-4, 72–75 cm) were processed with hydrofluoric acid (HF). They yielded a lower Tertiary palynomorph flora of variable preservation.

Several species of the pollen genus *Nothofagidites*, such as *N. asperus, N. lachlanae*, and *N.* sp. 1 (Truswell, 1983) are most common. One pollen grain of the family Proteaceae (*Proteacites parvus*) was found. Spores of Pteridophyta were also encountered, including some specimens of the genera *Leiotriletes* and *Osmundacidites*. The fern family Polypodiaceae is represented by the spore genera *Laevigatosporites* and *Polypodiaceoisporites*. The dinoflagellate cysts *Lejeunecysta hyalina* (lower Eocene-lowermost Miocene) and *Deflandrea* were also found.

The floral composition of this palynoflora is similiar to that of a lower Oligocene/upper Eocene flora from the Petrified Forest Member of Ezcurra Inlet Group, Admiralty Bay, King George Island, South Shetland Islands (Stuchlik, 1981). This author considered recent *Nothofagus* forests of New Zealand (Auckland Province) to represent a vegetation model of the Antarctic early Tertiary forest communities. The New Zealand forests between 550 and 1100 m altitude are mainly composed of red and silver beeches (*Nothofagus fusca* and *N. menziesii*) with an undergrowth of fern genera such as *Cyathea, Hymenophyllum*, and *Blechnum*.

Summary

At Site 696 we sampled a 645.6-m thick, but poorly recovered, sediment sequence consisting of a condensed Quaternary to upper Pliocene, an expanded lower Pliocene and upper to middle Miocene, with some Oligocene(?) to Eocene material at the base. An interval barren of biostratigraphically useful fossils separates the sequences assigned to the Neogene and Paleogene, which hinders the understanding of the Paleogene/Neogene transition.

The Quaternary and uppermost Pliocene contain calcareous microfossils (foraminifers) and rare to common siliceous microfossils. The remainder of the Neogene is barren of calcareous microfossils, except in one short interval in the upper Miocene, but is rich in silicoflagellates, radiolarians, and diatoms. The latter are especially dominant in Miocene sediments. The Paleogene sediments are barren of biostratigraphically useful siliceous microfossils, but the occurrence of calcareous microfossils (nannofossils, foraminifers) provides age control. The Paleogene sediments also bear palynomorphs, the first *in-situ* Paleogene pollen and spores recovered during Leg 113.

The Quaternary, which corresponds to lithostratigraphic Unit IA, has an estimated thickness of 2–7 m. It contains abundant *Neogloboquadrina pachyderma* and a low-diversity calcareous benthic foraminiferal assemblage. The benthic foraminifers from the mud line indicate that Site 696 (water depth 650 m) is located at or below the present CCD. At Site 695, drilled in a water depth of 1300 m, Quaternary samples were also rich in planktonic foraminifers, but the mud-line sample contains only agglutinated benthic foraminifers (compare with "Biostratigraphy" section, "Site 695" chapter, this volume). Carbonate-rich sediments are widespread in the Quaternary sequences recovered from the Weddell Sea embayment and from Maud Rise. The occurrence of calcareous foraminifers in Pliocene sediments at Site 695 and 696 (absent at Site 695; rare and restricted to the uppermost Pliocene at Site 696), suggests that the CCD underwent at least one fluctuation cycle since the late Neogene. The increase in CCD commenced in the latest Pliocene to reach a maximum (below the position of Site 695) sometime during the Quaternary and rose again in the latest Quaternary to its present-day depth (about depth of Site 696). Whether the fluctuation of the CCD was caused by enhanced carbonate productivity during the past 2 m.y. or whether it was solely induced by changes in oceanographic patterns (e.g., influx of cold bottom water) or both, should be the aim of further investigations.

Radiolarians and diatoms assign Section 113-696A-2H, CC (12 mbsf), to the upper Pliocene (*Cosmiodiscus insignis* diatom Zone; middle Upsilon radiolarian Zone). This indicates a strongly condensed Pliocene/Pleistocene transition or a hiatus corresponding to the early Pleistocene to latest Pliocene. A hiatus close to the Pliocene/Pleistocene boundary is also suggested at Site 690 (Maud Rise) and at Site 695. Pliocene sediments were recovered down to an interval between Sections 113-696B-10R, CC, and 113-696B-13R, CC (153.8–182.9 mbsf). Radiolarians suggest that the Miocene/Pliocene boundary lies within Core 113-696B-11R, whereas diatoms assign Core 113-696B-13R to the Pliocene combined *N. angulata/N. reinholdii* Zone. Because of the poor recovery between 150 and 212 mbsf (Cores 113-

696B-11R to 113-696B-16R) it will be nearly impossible to precisely define the Miocene/Pliocene boundary at Site 696. The lower/upper Pliocene boundary is placed at about 78 mbsf. Radiolarians suggest a hiatus between 78 and 96.4 mbsf (Cores 113-696A-9H and 113-696A-11X), which has removed sediments of lower Upsilon radiolarian Zone age (basal Gauss through C3N1), whereas diatoms and silicoflagellates show no evidence for such a hiatus. Unfortunately the interval in question is poorly recovered.

The Pliocene includes lithostratigraphic Units I, II, and III. The sediments contain biosiliceous components which decrease in abundance and preservation downward. Compared to other Leg 113 Sites (689, 690, 693, and 695), diatoms recovered in the Pliocene are less abundant and preservation is inferior. However, the decrease in abundance and preservation of biosiliceous components close to the Pliocene/Miocene boundary seems to be a consistent pattern at all sites, which may indicate restricted biosiliceous productivity during this interval. Depth estimates based on the occurrence of agglutinated foraminifers (*Milliammina* and *Martinotiella* assemblages) recovered throughout the Pliocene are not feasible because the assemblages are poor, and published depth assignments for these species are not applicable at Site 696.

The youngest sediments assigned to the Miocene by both radiolarians and diatoms are in Core 113-696B-17R (211.8–221.4 mbsf) and were placed in the upper Miocene *C. spongothorax* and the *D. hustedtii* Zone, respectively. The upper Miocene contains the only occurrence of Neogene planktonic foraminifers, calcareous benthic foraminifers, and calcareous nannofossils, the latter consisting of a monospecific *Reticulofenestra perplexa* assemblage (Section 113-696B-22R, CC; 260.1 mbsf). The calcareous interval can be dated using the occurrence of the diatom *Denticulopsis dimorpha* acme, which occurs in the lower part of the *D. hustedtii* Zone. A similiar nannofossil assemblage also occurs at Site 693 (off Dronning Maud Land) near the *D. dimorpha* acme, representing the only Neogene occurrence of calcareous nannofossils at this site. Possibly the incursion of calcareous nannofossils over the continental margins of the Weddell Sea during the short late Miocene time interval signals a slight amelioriation in climate, enhancing nannoplankton productivity and thereby depressing the CCD.

Most of the interval from Cores 113-696B-35R through 113-696B-43R (376.0–462.8 mbsf) was not recovered. Radiolarians suggest that the interval is lowermost upper or middle Miocene, whereas diatoms indicate that it is lower upper Miocene to upper middle Miocene (*D. hustedti/D. lauta–N. denticuloides* Zone).

Based on the occurrence of definite middle Miocene radiolarians in Core 113-696B-45R and middle middle Miocene diatoms (*N. grossepunctata* Zone) in Core 113-696B-46R, the upper/middle Miocene boundary is tentatively placed within Cores 113-696B-44R and 113-696B-45R (462.8–482.0 mbsf). The middle middle Miocene *N. grossepunctata* diatom Zone extends through Core 113-696B-50R (529.8 mbsf).

All sediments assigned to the Miocene (Cores 113-696B-17R through 113-696B-50R, 211.8–529.8 mbsf) are especially rich in diatoms and indicate high biosiliceous productivity. These sediments coincide with lithostratigraphic Units IV through VI. The few to abundant *Denticulopsis lauta* (diatom) in the lower upper to middle Miocene (*D. hustedti/D. lauta-N. denticuloides* and *N. grossepunctata* diatom Zones) suggests that Miocene surface water at Site 696 had closer affinities to the Subantarctic compared to Sites 689, 690, and 693, where *D. lauta* was found only rarely.

Below Core 113-696-50R there is a prominent change in facies from biosiliceous to the more sandy and muddy sediments of lithostratigraphic Unit VII. This unit contains glauconite in two intervals (Subunits VIIA and VIIC). The upper part of Unit VII (Cores 113-696B-51R through 113-696B-58R, 529.8–606.9 mbsf) is barren of biostratigraphically useful microfossils. Radiolarians are common but highly abraded and corroded in Cores 113-696B-51R and 113-696B-52R and absent below this level. Diatoms are rare to barren, strongly fragmented, and pyritized. Poorly preserved (flattened) agglutinated benthic foraminifers (*Cyclammina* sp.) found in Unit VIIB (Sections 113-696B-53R, CC, through 113-696B-55R, CC) may represent a change in availability of biogenic silica in the depositional environment, because in the present day the species is restricted to areas of nondiatomaceous sediments in the Scotia Sea. They suggest an age of Oligocene or younger.

Only the lowermost interval of Site 696, represented by the lowermost Subunit VIID (Cores 113-696B-58R through 113-696B-62R), bears biostratigraphically useful species, calcareous nannofossils and foraminifers. Nannofossils from Section 113-696B-59R, CC, indicate an age ranging from earliest Oligocene to the latest Eocene (about 35–38 Ma, *Isthmolithus recurvus* range). The nannofossil assemblage from the lowermost core (113-696B-62R) contains *Reticulofenestra reticulata*, which probably indicates a late Eocene age for the base of the hole. A late Eocene age for the base is confirmed by the palynoflora found in Cores 113-696B-60R through 113-696B-62R. Benthic foraminifers cannot be used for precise dating because several species have not been previously described, but suggest a middle to late Eocene age. Possibly the well-preserved invertebrate macrofossils (*Gastropoda, Bivalvia, Cnidaria*, and *?Echinodermata*) observed in Cores 113-696B-58R through 113-696B-62R are in place and may provide additional age and paleoenvironmental information. The moderate to well-preserved calcareous benthic foraminifers indicate deposition in an inner neritic (less than 100 m water depth) environment, under slightly hyposaline and slightly hypoxic conditions. This interpretation is tentatively supported by high chlorinity in the pore waters (see "Inorganic Geochemistry" section, this chapter). The increase in relative abundance of epiphytic species suggest that water depth may have decreased upsection (Cores 113-696B-62R through 113-696B-59R). This would be in agreement with the occurrence of glauconitic sands and muds (Subunit VIIB) recovered above this interval.

PALEOMAGNETISM

Site 696, situated in a water depth of about 650 m on the South Orkney Platform, is the shallowest site in the depth transect for high-resolution studies of Neogene-Paleogene sediments. Although 404 samples were measured for paleomagnetic study, only the depth intervals from 0 to 150 mbsf and from 550 to 650 mbsf with a recovery of more than 50% could be interpreted magnetostratigraphically. The interval with very low average recovery of 16% could not be used for definition of magnetozones.

In contrast to Site 695, the histogram of distribution of natural remanent magnetization (NRM) inclination values (Fig. 27) is strongly biased towards steep negative inclinations suggesting normal polarity overprinting. However, from an initial assessment of downhole inclination variation (Fig. 28), a clear polarity assignment was derived for Hole 696A down to 80 mbsf. For the uppermost 70 m of Hole 696B the definition of polarity boundaries is less precise due to a recovery of only 50% and a larger scatter in NRM inclinations. Such assignments are subject to further interpretation after shore-based magnetic cleaning.

A considerable increase in recovery occurs below 550 mbsf of Hole 696B. The indurated sandy sediments in this interval show higher intensities of 1–4 mA/m and a scatter of inclination values between -90° and +20°. Due to a good control of relative

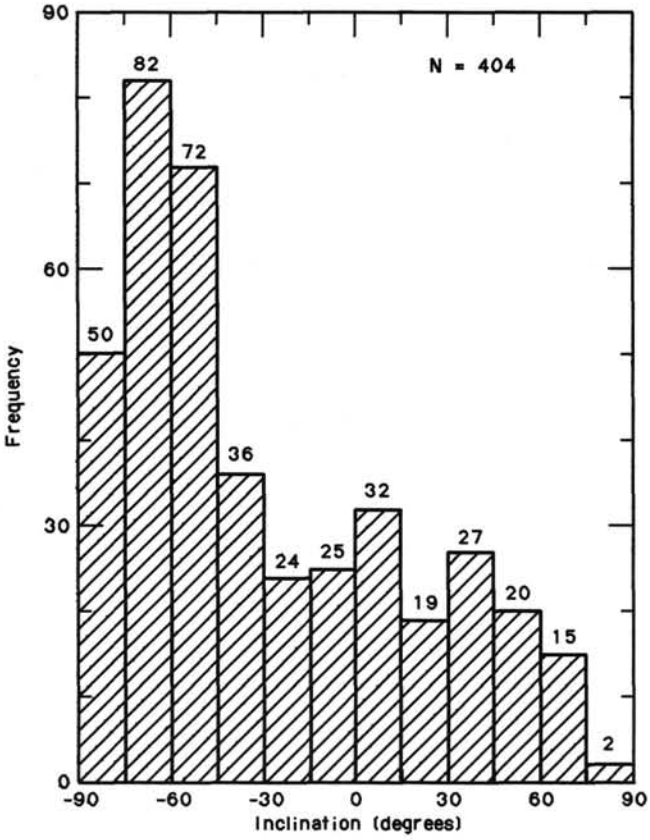

Figure 27. Histogram of distribution of NRM inclination values for Site 696.

azimuthal orientation in continuous core sections, often at least 50 cm in length, the declination values could also be used occasionally for verification of polarity changes. It was also possible to use short polarity intervals, based upon only one sample, in this preliminary polarity assignment.

Figure 29 shows the inferred age-depth relationship for both paleomagnetic ages and biostratigraphic data (see "Biostratigraphy" section, this chapter). A Pliocene-Quaternary age can be assumed for the uppermost 150 m of Site 696. The poorly recovered interval from 150 to 550 mbsf is of middle/late Miocene age and is separated by a major hiatus in the interval between 550 and 600 m from underlying upper to possibly middle Eocene sediments. Magnetostratigraphic interpretation of the Pliocene sequence is mainly based on paleomagnetic data obtained from Cores 113-696A-6H through 113-696A-9H and 113-696B-5R through 113-696B-7R. Due to a large number of reversals, this interpretation (Fig. 30) implies continuous sedimentation in the early Pliocene, although this is not entirely confirmed by the biostratigraphic evidence. Due to the ambiguity of the paleomagnetic age determinations, further studies are required to affect an improvement in the magnetostratigraphy, but the inherent gaps in recovery in the uppermost 100 m will probably make a final interpretation very difficult.

The lowermost 50 m of the sediments comprising mainly coarse grained glauconite-bearing shallow water sediments, was assigned biostratigraphic ages of Oligocene-Eocene (Fig. 31). The sediments are predominantly normally magnetized, although a limited number of reversed samples defines a clear polarity pattern. This sequence can readily be assigned to the late and middle Eocene part of the geomagnetic polarity time scale (Chrons C16–C18) with an estimated overall sedimentation rate of 6 m/m.y. A fit of the same interval to the Oligocene reversal sequence is unlikely as the polarity record cannot be matched to the very long reversed Oligocene polarity Chrons C12R and C13R.

SEDIMENTATION RATES

The sedimentation-rate curve for Site 696 is constructed from two data sources. Biostratigraphic ages derived from diatoms, radiolarians, and silicoflagellates provide the primary source of age information for Cores 113-696A-1H through 113-696B-50R, and calcareous nannofossils for Cores 113-696B-59R through 113-696B-62R. No biostratigraphic age information is available for Cores 113-696B-51R through 113-696B-58R, because these cores are barren of all stratigraphically useful microfossils. Biostratigraphic data used to construct the age-depth relationship consist of selected datum levels and zonal assignments which are correlated to the chronostratigraphic scale. Accuracy of the calibration between biostratigraphy and chronostratigraphy varies considerably for different fossil groups and different time intervals. The figure was constructed as follows: the dashed age-depth curve is based on biostratigraphic data. The curve is based on biostratigraphic data (data points plotted with identifying number as listed in Table 11). Magnetostratigraphic data are shown as line segments with unlabeled datum points (solid boxes). Error boxes for paleomagnetic data represent the distance (in depth) between two samples of different polarities assigned to different magnetozones. From the preceding and the following magnetozone boundaries a sedimentation rate was estimated and from this rate a corresponding error in age determination is calculated. This age error is represented by the horizontal box line.

Biostratigraphic data are of three types. First and last occurrences of species which are known to occur only within a finite depth interval are plotted as vertical lines; the age of the datum is generally reported without an associated error estimate. Age ranges for individual samples, by contrast, have a finite age range but do not have a depth uncertainty and are plotted as horizontal lines. Finally, a few FAD's and LAD's for which uncertainty estimates are available are plotted as boxes. Many samples have more than one age range estimate from different fossil groups. To make the overlap between multiple data clear, small solid circles are used to mark the end of each datum which plots as a line. FAD's and LAD's represent, respectively, the oldest and youngest possible ages for a depth interval. Arrows indicate datums of this type, with the direction indicating the time direction during which the species occurs. At Site 696 we used 17 datum levels or zones listed in Table 11. The sedimentation rate curve for Site 696 is poorly constrained because core recovery at this site was extremely poor between 12 and 32 mbsf and 150 and 470 mbsf. The estimated age for the LAD of *Distephanus boliviensis* (datum number 7 in Table 11) may have to be recalibrated but has been included in Table 11 and Figure 32 as given by Shaw and Ciesielski (1983).

Magnetic polarity data were correlated by comparison of the inferred downhole polarity pattern to the geomagnetic polarity time scale by Berggren et al. (1985). This correlation was constructed using biostratigraphic data as tiepoints for the interpretation of separate polarity sequences because of the extreme difficulties in interpretation due to some major gaps even in intervals with better recovery.

Our preliminary interpretation is based on a relatively small number of polarity reversals in the intervals between 0 and 150 mbsf and 550 and 645 mbsf under the assumption of fairly constant sedimentation rates and a minimum number of hiatuses. Overprinting on about 30% of the samples makes the interpretation more difficult and open for later reinterpretation. Shore-based study, including magnetic cleaning by stepwise demagnetization, is required to obtain a more complete polarity record.

The sedimentation rate at Site 696 shows the pattern of dramatic decrease from the lower Pliocene into the upper Pliocene and Pleistocene that was seen at previously drilled sites of Leg 113, but the timing of the change is less precise at this site. According to the biostratigraphic data, the sedimentation rates were moderately low in the Pleistocene and upper Pliocene averaging between 3 and 5 m/m.y. for the last 2.5 m.y. Poor core recovery in the interval between 13 and 40 mbsf precludes good estimates of the sedimentation rate lower in the hole. A preliminary estimate in best agreement with all biostratigraphic data is about 20 m/m.y. between 2.5 and 3.1 Ma, increasing to 220 m/m.y. between 3.1 and 3.4 Ma (dashed line in Fig. 32). This interpretation of the interval between 40 and 78 mbsf, however, does not agree with the preliminary paleomagnetic age interpretation (Fig. 32).

Below the interval of poor recovery (Section 113-696A-4H, CC), a diatom transition zone (Datum 5) at the base of the Gauss Chron is used as a tiepoint for magnetostratigraphic interpretation. The number of inferred magnetozones from Cores 113-696A-5H through 113-696A-9H is higher than expected from the biostratigraphically-constrained assignment to the Gilbert Chron reversal sequence, which suggests that the sedimentary sequence is probably continuous. We might expect to detect short polarity events in high-latitude, high-resolution magnetostratigraphies, but comparable studies did not show as many reversals within the Gilbert Chron. A greater age for this interval (into the Miocene) is more likely from the paleomagnetic evidence of NRM measurements.

Radiolarian data indicate the presence of a short (about 0.5 m.y.) hiatus between about 80 and 90 mbsf. Note that the lower boundary of the radiolarian upper Tau Zone (Datum 8 in Table 11) is plotted at the bottom of the interval recovered in Core 113-696B-3R (93 mbsf) and the top of the radiolarian lower Tau Zone (Datum 10 in Table 11) at the top of the interval recovered in Core 113-696B-5R; the boundary between these two zones is not extrapolated into the unrecovered interval of Core 113-696B-4R. The location of the lower boundaries of the radiolarian Tau Zone and the diatom combined *Nitzschia reinholdii–N. angulata* Zone is imprecise and the sedimentation rate for the lower part of the Pliocene section is difficult to estimate because of poor core recovery. The sedimentation rate may have been on the order of 77 m/m.y. (dashed line in Fig. 32).

As far as we can tell from the limited data for the Miocene, the sedimentation rate may have been fairly constant overall from about 14 to 5 Ma, with an average of about 35 to 41 m/m.y. This estimate, however, requires that the ages of the LAD of *Lophocyrtis golli* and of the lower boundary of the *Nitzschia grossepunctata* diatom Zone are as listed in Table 11 (Numbers 14 and 15), but these ages may be greater and may have to be recalibrated (see "Biostratigraphy" section, "Site 690" chapter, this volume). The lower boundary of the radiolarian *Cycladophora spongothorax* Zone cannot be located precisely because in samples below 279 mbsf, radiolarians are far outnumbered by diatoms. The estimate of the sedimentation rate for this interval must be seen as an overall approximation, and relatively short hiatuses or periods of increased sedimentation rate may be undetected.

No estimate of sedimentation rates can be made for the interval between 530 and 610 m/m.y. because no biostratigraphic data are available. Biostratigraphic data for the lower part of the section are not sufficient for a sedimentation rate estimate. Paleomagnetic interpretation of this interval results in a mainly normal polarity sequence with short reversed magnetozones. Although the polarity record is based on fairly reliable NRM inclination, and occasionally declination measurements, a demagnetization study may provide a different polarity pattern. The interval from 610 to 645 mbsf is assigned to the middle late Eocene polarity Chrons C16–C18, using two nannofossil datums and assuming an overall low sedimentation rate of 5–6 m/m.y. A higher sedimentation rate is possible if the polarity record contains a number of undetected short polarity intervals, if the interpretation is partly based on disturbed intervals, or if the preservation of the magnetostratigraphic signal is less reliable in the coarse-grained sediment.

INORGANIC GEOCHEMISTRY

Introduction and Operation

Data on the chemical composition of interstitial water are presented for Holes 696A and 696B. Due to adverse hole conditions, Hole 696A was abandoned after APC-coring to 79.3 mbsf and XCB-coring from 79.3 to 103.0 mbsf. Overall recovery from this hole was 55%, and three whole-round samples for squeezing were obtained. Hole 696B was rotary-drilled to 645.6 mbsf after washing to 76.6 mbsf. Overall recovery for the rotary-cored interval was 27.5% which allowed 11 whole-rounds to be sampled. In connection with downhole temperature measurements, an *in-situ* pore water sample was extracted at 144.80 mbsf in Hole 696B. Fourteen whole-round sediment samples (10 of 5-cm and 4 of 10-cm thickness) were squeezed and analysed. The chemical data are summarized in Table 12 which also contains data on drilling-mud filtrate analysed at Site 693 (see "Inorganic Geochemistry," section, "Site 693" chapter, this volume). For details on sampling and analytical procedures see "Explanatory Notes" chapter (this volume).

Evaluation of Data

Data from Whole-Round Samples

At the previous sites of Leg 113, a charge balance based on the assumption of constant Na/Cl ratio equal to that of present-day seawater has been calculated. At each site it was found that to maintain electroneutrality, the Na/Cl ratio would have to decrease with increasing depth. At Site 696, to maintain charge balance the Na/Cl ratio of the pore water would have to decrease from that of present-day seawater (0.858) in the upper section (Section 113-696A-2H-3) to 0.794 at 642 mbsf (Section 113-696B-62R-5). This change involves the removal of 35 mmol sodium per liter of interstitial solution, a more extensive removal than observed at other Leg 113 sites. Error analyses (see "Inorganic Chemistry" section, "Site 693" chapter, this volume) show that the charge imbalance is not an experimental artifact. On the contrary, the systematic variations indicate high-quality data. For further discussion of the mechanisms of removal of alkali metals, see potassium discussion below.

Data From In-Situ Pore Water Extractor

There are some indications (see below) that the *in-situ* pore water sample extracted at 144.8 mbsf is contaminated by seawater used for circulation.

Chlorinity and Salinity

Chloride data are presented in Figure 33A and Table 12. There is a slight increase in chloride concentration from 560.0 mmol/L in the upper section (Section 113-696A-2H-3) to 583.9 mmol/L in the deepest sample at 642 mbsf (Section 113-696B-62R-5). Assuming the same salinity/chloride relationship as seawater (as provided by Stumm and Morgan, 1981), these chloride concentrations correspond to seawater salinities of 34.6 and 36.1 g/kg, respectively. Of these, the lower value equals (within analytical accuracy) the salinity of present-day seawater at this depth (650 m) and latitude as provided by Sverdrup et al. (1942). Manheim and Sayles (1974) suggested that chloride concentrations of comparable magnitude to those observed in the deepest

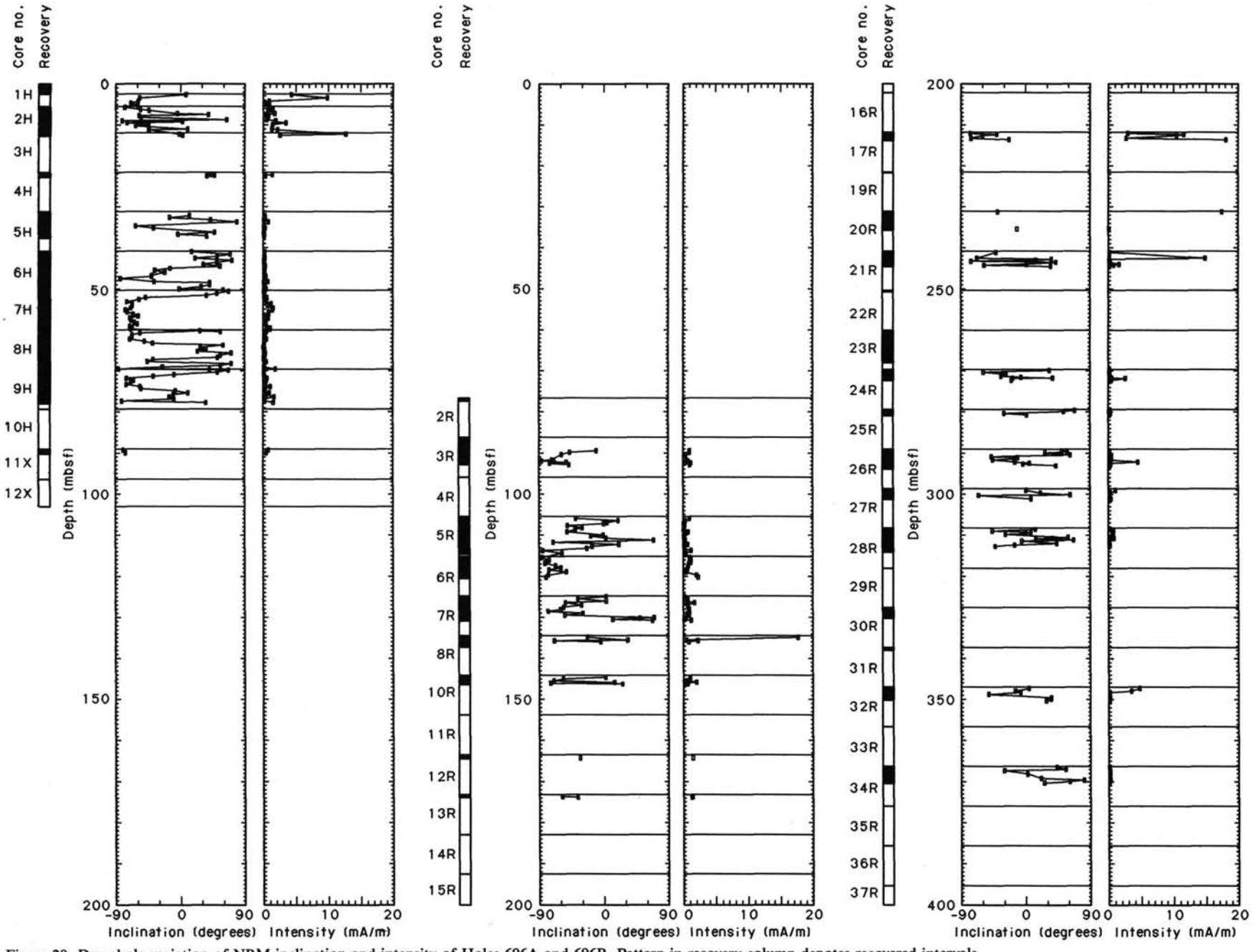

Figure 28. Downhole variation of NRM inclination and intensity of Holes 696A and 696B. Pattern in recovery column denotes recovered intervals.

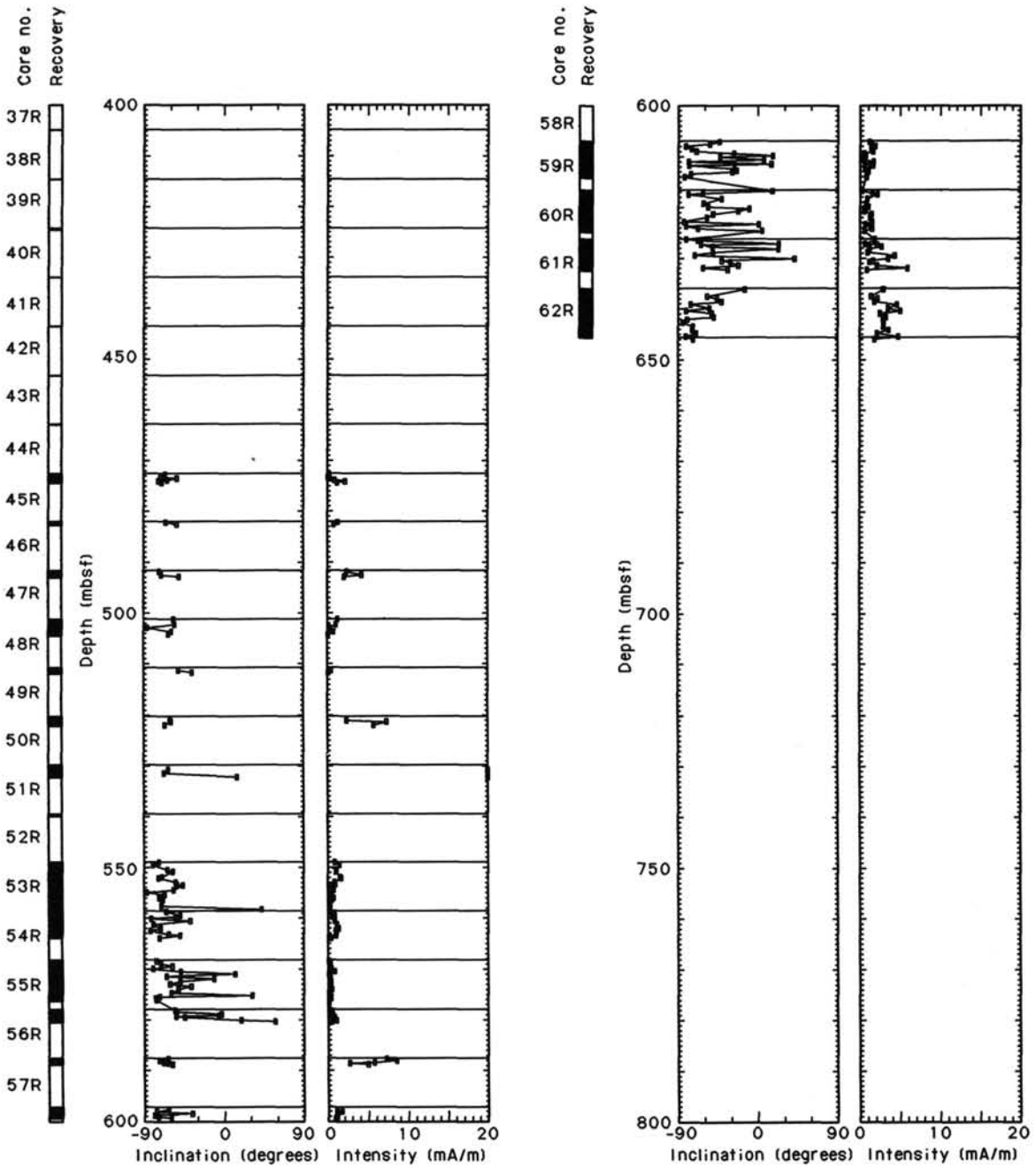

Figure 28 (continued).

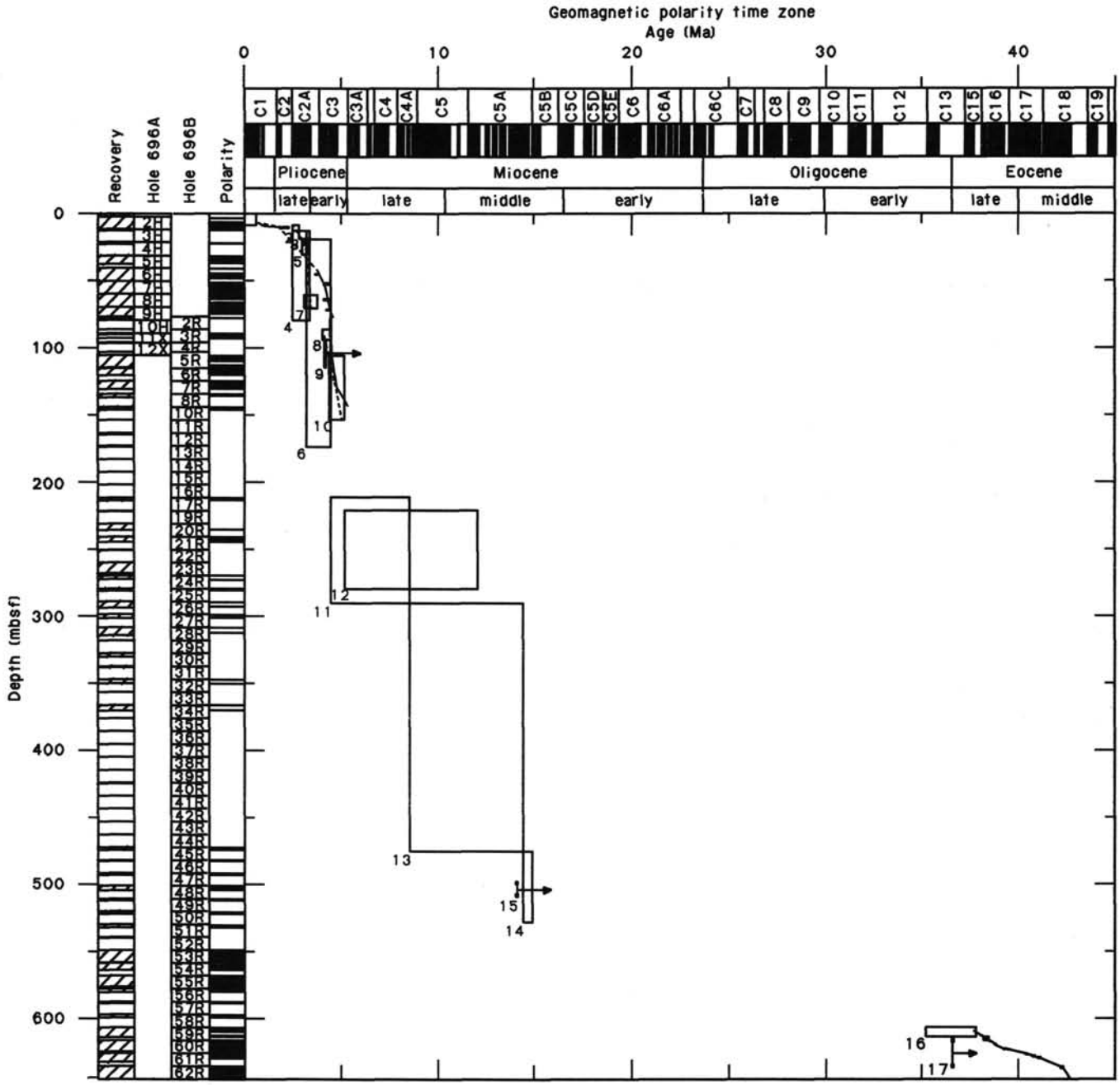

Figure 29. Age-depth relationship for both paleomagnetic and biostratigraphic data (see "Sedimentation Rates" section, this chapter) for Site 696.

samples represent pore waters deposited during more saline conditions. In this part of the hole epiphytic foraminifers indicative of hyposaline conditions were identified (see "Biostratigraphy" section, this chapter).

The concentration of chloride in the seawater used for circulation is about 540 mmol/L, thus it is plausible that the slightly lower chloride concentrations in the *in-situ* pore water sample at 144 mbsf (Core 113-696B-9I) and the sample from 90 mbsf (Core 113-696-3R-3) are caused by some mixing of waters. Due to melting of ice, the halocline in the Weddell Sea is steep at this time of year. The vertical movement of the ship will cause the salinity of the water used for circulation to vary considerably, thus no correction of the data on these samples has been attempted.

According to the drilling log, drilling mud was used between cutting each core below Core 113-696B-48R. The low chloride concentration in the sample from Section 113-696B-53R-4 is caused by dilution by drilling-mud filtrate. Using the composition of drilling-mud filtrate given in Table 12 (see "Inorganic Chemistry" section, "Site 693" chapter, this volume) and interpolating between bracketing samples (Sections 113-696B-34R-1 and 113-696B-59R-3) gives an amount of drilling-mud filtrate of 14%. The data from Section 113-696B-53R-4 are corrected for this dilution (see Table 12 and Figs. 33A–K).

The salinity measurements using the optical refractometer differ from those calculated from the chloride data by about 2 g/kg. No correlation exists between the two.

pH

The pH (Fig. 33B and Table 12) varies between 7.90 and 8.65 generally increasing downhole but exhibiting a lower level about 400 mbsf. The average pH of 8.1 is similar (within uncertainties

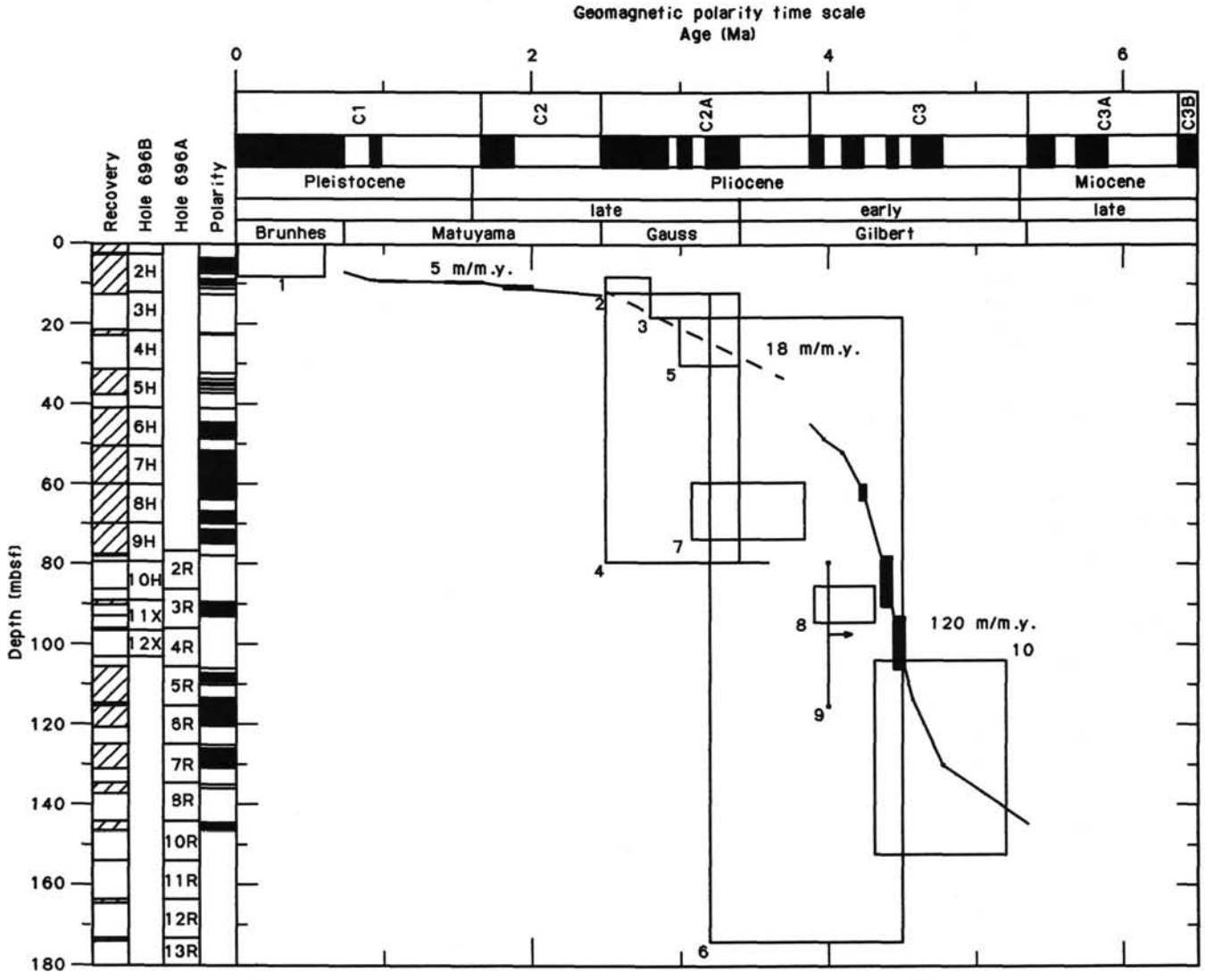

Figure 30. Age-depth relationship inferred from paleomagnetic polarity record in comparison with biostratigraphic data for the uppermost 150 m of Site 696.

introduced by sampling) to the pH observed at Sites 695 (8.1), 694 (8.1), and 693 (8.0), but the high pH below 500 mbsf is higher than observed at previous Leg 113 sites. Studies by Sayles et al., (1973) indicate that ion exchange equilibria may shift during squeezing. The long squeezing time (2–3 hr) of these dry sediments may have affected the pH.

Alkalinity, Sulfate

The alkalinity data are presented in Figure 33C. Despite extensive reduction of sulfate (see below), hydrogen sulfide was not detected (by smell) and the concentration of orthophosphate is low (Table 12), thus the carbonate alkalinity equals the titration alkalinity (within experimental accuracy). The alkalinity decreases erratically from about 4 meq/L in the upper 100 mbsf to less than 2 meq/L below 500 mbsf. Assuming stoichiometric oxidation of organic matter, the alkalinity is much lower than that calculated from the sulfate data, and lower than at Site 695. These differences are related to the different distribution of sulfate-reducing activity (see below) and to the chemistry of the alkaline earths.

The sulfate profile is presented in Figure 33D. The concentration of sulfate decreases exponentially from close to seawater value (26.6 mmol/L) at 6.70 mbsf (Section 113-696A-2H-3) to 2.4 mmol/L at 642 mbsf (Section 113-696B-62R-5). Most of the change takes place in the upper 120 mbsf. At Site 695, almost linear distribution of sulfate was observed down to zero at 370 mbsf. These differences are related to differences in rates of deposition, water depths, and input of organic matter. The interaction between the controlling variables, their effect on the sulfate profile, and the fractionation of stable isotopes of sulfur will be subjected to modeling in future studies. The shape of the sulfate profile below 120 mbsf indicates that the rate of reduction of sulfate is very low allowing sulfate to be observed throughout.

Phosphate and Ammonia

The concentration profile for phosphate is presented in Figure 33E and Table 12. The profile exhibits a subsurface maximum of 7.9 μmol/L at 35.4 mbsf (Section 113-696A-5H-3), and concentrations decrease to less than 1 μmol/L at depth. A similar profile was observed at Site 695. At Site 696 the subsurface maximum is located closer to the seafloor. This is consistent with the higher sulfate-reducing activity and the consequent shallower position of the redox boundary (phosphate is released from iron hydroxides/oxyhydroxides as these are reduced upon

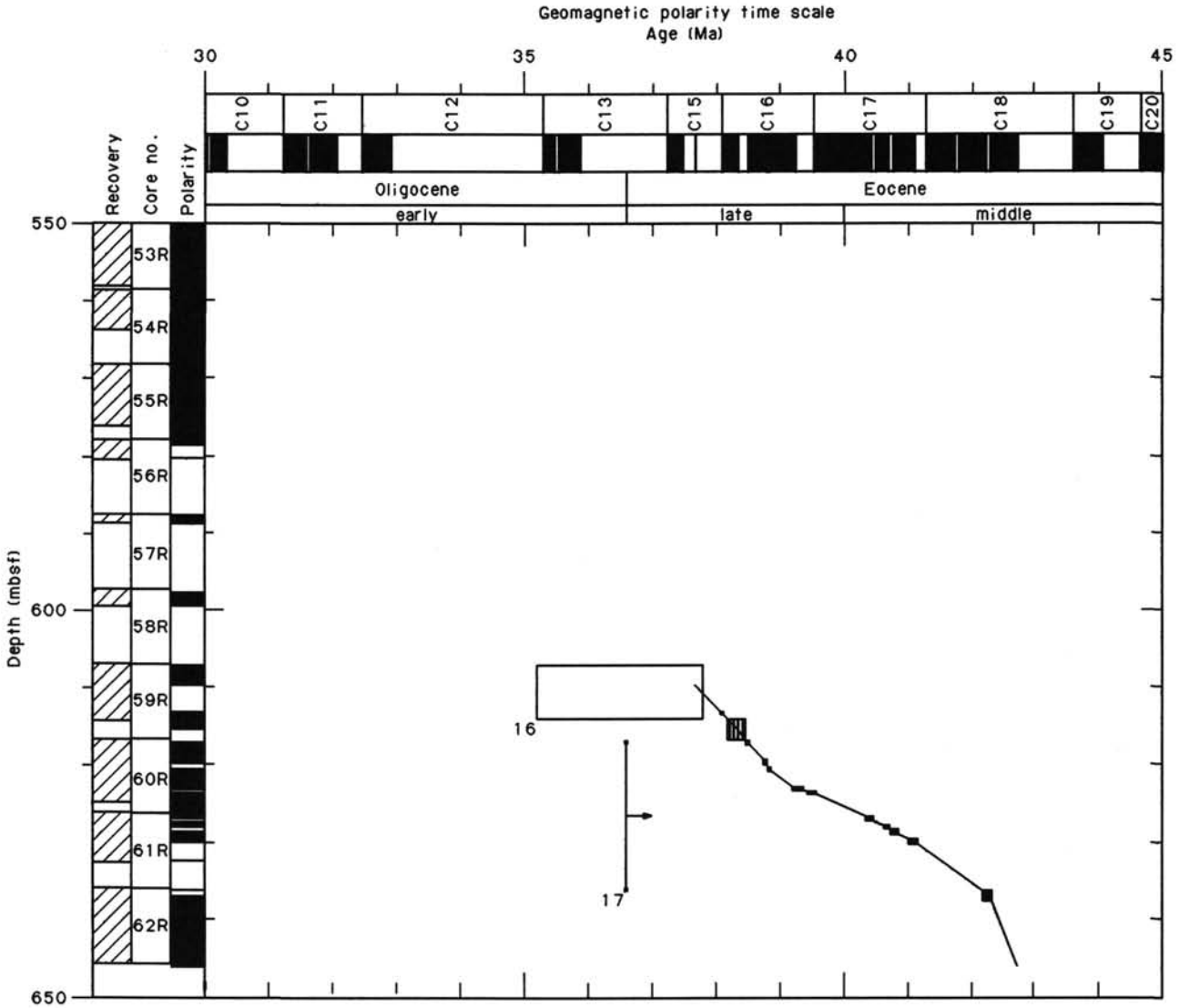

Figure 31. Preliminary magnetostratigraphic interpretation of the lowermost 50 m of Site 696.

Table 11. Biostratigraphic data used to construct the sedimentation rate curves in Figure 32.

Datum	Age (Ma)	Depth (mbsf)
1. *C. lentiginosus* Zone—D	0.01-0.6	0.01-8.0
2. *C. insignis* Zone—D	2.5-2.8	8.0-12.0
3. *N. interfrigidaria* Zone—D	2.8-3.2	12.0-18.0
4. middle Upsilon Zone—R	2.5-3.4	12.0-79.3
5. transition *N. praeinterfrigidaria-N. interfrigidaria*—D	3.0-3.4	18.0-30.0
6. *N. angulata-N. reinholdii* Zone—D	3.2-4.5	18.0-174.0
7. LAD *D. boliviensis*—S	3.1-3.8	60.0-70.0
8. upper Tau Zone—R	4.0-4.4	85.0-93.0
9. LAD *D. pseudofibula*—S	4.1-4.2	93.0-115.0
10. lower Tau Zone—R	4.4-5.2	105.5-153.8
11. *D. hustedtii* Zone—D	4.5-8.5	212.0-291.0
12. *C. spongothorax* Zone—R	5.2-12.0	221.4-279.4
13. *D. hustedtii-N. denticuloides-D. lauta* Zone—D	8.5-14.3	291.0-478.0
14. *N. grossepunctata* Zone—D	14.3-14.8	478.0-530.0
15. LAD *L. golli*—R	14.0	501.2-510.7
16. *I. recurvus* occurrence—N	35.2-37.8	607.0-614.0
17. LAD *R. reticulata*—N	36.6	617.0-636.0

Key to table: Depth range given for First and Last Appearance Datums (FAD's and LAD's). Age range given for zones, and in some instances for uncertainty in age calibration of a FAD or LAD. Letters following each datum name refer to the fossil group: D = diatoms; R = radiolarians; S = silicoflagellates; N = nannofossils.

burial beneath the redox boundary, Stumm and Leckie, 1970). The phosphate levels in the interstitial water are higher than observed at other Leg 113 sites with the exception of Site 695.

The concentration of ammonia is shown in Figure 33F. The concentration of ammonia increases from 0.12 mmol/L in the shallower sample (Section 113-696A-2H-3) to 1.74 mmol/L at 554.6 mbsf (Section 113-696B-53R-4). A slight decrease toward the bottom is observed. Decreasing ammonia concentrations with increasing depth are usually attributed to absorption and ion exchange processes (Berner, 1974). It is possible, however, that organisms capable of fermenting organic matter to methane (such as *Methanobacillus omelianskii*, Goldhaber and Kaplan, 1974) utilize dissolved ammonia as a nitrogen source. At both Sites 695 and 696, the concentration of ammonia decreases at the first appearance of presumably biogenic methane (see "Organic Geochemistry" section, this chapter, and "Site 695" chapter, this volume). We are not aware of any studies on this subject.

Calcium and Magnesium

Calcium and magnesium data are presented in Figure 33G and 33H, respectively. The concentration of calcium increases

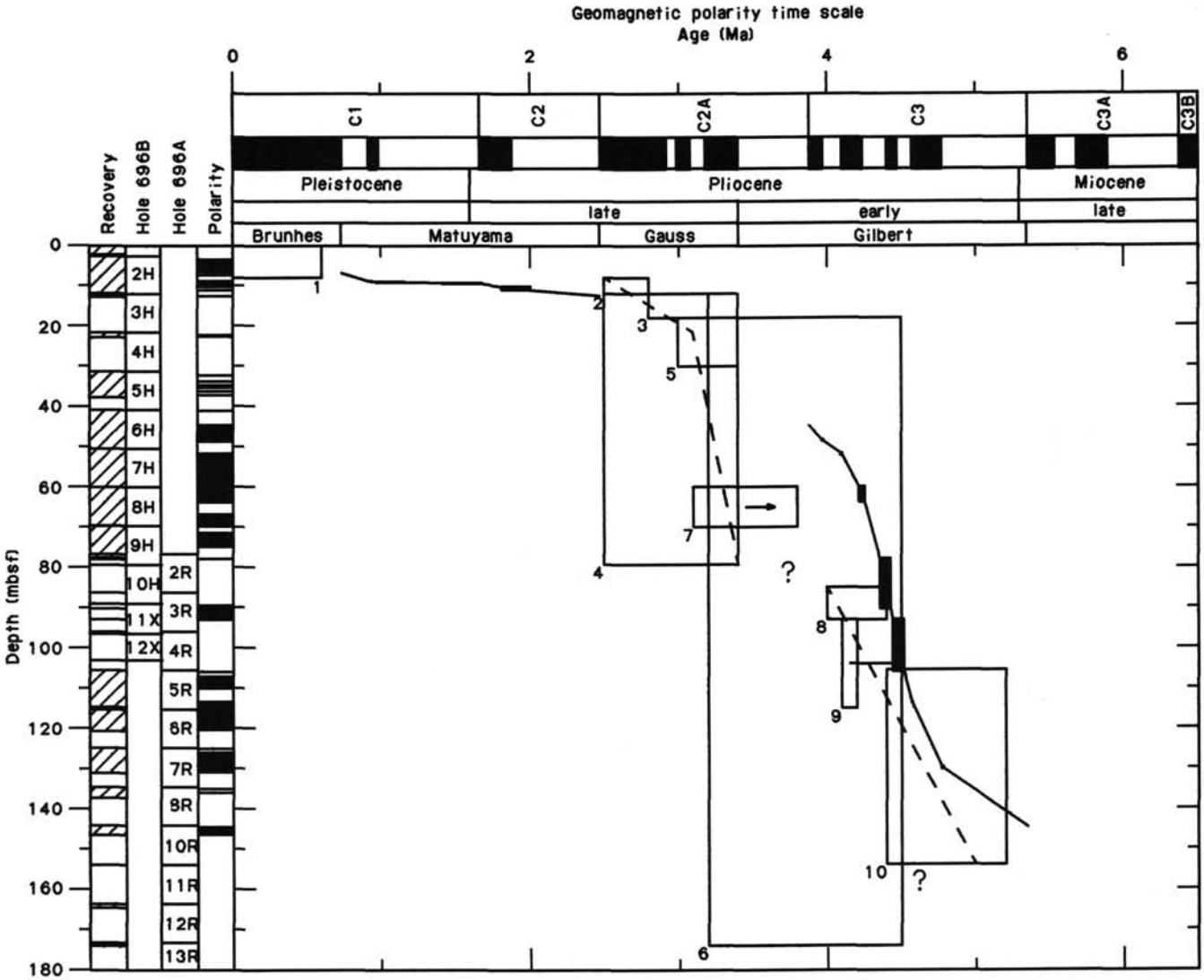

Figure 32. Age-depth interpretation of Site 696. See text for details about how the figure was constructed.

from a slightly higher than seawater value (11.81 mmol/L) at 6.70 mbsf (Section 113-696A-2H-3) to 40.14 mmol/L at 642 mbsf (Section 113-696B-62R-5). This is the largest enrichment of calcium measured at any site of Leg 113 and, conceivably, the high calcium level depresses the alkalinity (see above) by precipitation of carbonate.

The concentration of magnesium decreases from slightly less than seawater value in the upper section (Section 113-696A-2H-3) to 20.43 mmol/L at 642 mbsf (Section 113-696B-62R-5). At this site the relation between the increase in calcium and the decrease in magnesium is 1.01 (n = 13, r = 0.95) (Fig. 33I). The observation of several dolomite-cemented horizons (as determined by shipboard X-ray diffraction analyses) make it plausible that formation of dolomite controls the alkaline earth chemistry.

Potassium

The concentration profile for potassium is shown in Figure 33J. The concentration of potassium decreases erratically from 12.2 mmol/L at 6.7 mbsf (Section 113-696A-2H-3) to 2.1 mmol/L at 642 mbsf (Section 113-696B-62R-5). The view is generally held (Mackenzie and Garrels, 1966; Manheim and Sayles, 1974) that potassium (and sodium) are removed from interstitial water by authigenic formation or alteration of clay minerals. At Site 696 the largest (of all Leg 113 sites) decreases in concentration of potassium and sodium are observed. Also, the greatest discrepancy between the alkalinity expected from the extent of sulfate reduction and the observed alkalinity is found at this site. As the reversed weathering mechanism consumes alkalinity, these observations are mutually consistent.

Dissolved Silica

The concentration of dissolved silica (Fig. 33K) varies between 228 μmol/L (Section 113-696B-59R-3) and 1449 μmol/L in Section 113-696B-34R-1. The large scatter in the silica data was suspected to indicate analytical noise, thus the analysis was repeated 24 hr later by a second analyst. The results of the two runs are compared on Figure 34. Evidently the scatter is not caused by analytical errors. After filtering the scatter, a general increase toward a high of about 1400 μmol/L between 250 and 400 mbsf followed by a rapid decline to 308 μmol/L is observed. The high levels occur in the diatom-rich Units IV and VI (see "Lithostratigraphy" section, this chapter). Based on thermodynamic data provided by Stumm and Morgan, 1981, the concentrations of dissolved silica fall between quartz saturation and saturation with respect to amorphous silica. The lower part of the profile constitutes a steep concentration gradient along which

Table 12. Summary of shipboard interstitial water data.

Core, section interval (cm)	Depth (mbsf)	Vol (mL)	pH	Alk. (meq/L)	Sal. (g/kg)	Mg (mmol/L)	Ca (mmol/L)	Cl (mmol/L)	SO_4 (mmol/L)	PO_4 (μmol/L)	K (mmol/L)	NH_4 (mmol/L)	SiO_2 (μmol/L)	Mg/Ca
113-696A-														
2H-3, 120–125	6.7	25	7.90	3.94	34.1	49.70	11.81	560.0	26.6	6.6	12.2	0.12	726	4.21
5H-3, 120–125	35.4	40	7.94	3.84	33.9	41.11	16.53	567.0	17.3	7.9	9.3	0.46	1245	2.48
8H-4, 120–125	65.7	40	8.21	4.40	33.8	36.13	19.28	571.0	12.0	5.8	12.4	0.80	826	1.87
113-696B-														
3R-3, 120–125	90.4	25	8.23	3.73	33.4	37.54	18.32	560.5	15.3	3.4	10.4	0.86	892	2.01
6R-3, 120–125	119.4	45	8.14	4.14	33.6	30.68	23.23	572.0	6.4	2.8	8.9	1.13	1020	1.32
9I	144.8	22				32.54	24.91	564.0	8.1	3.6	8.1	1.02	783	1.31
20R-2, 120–125	233.8	55	7.84	2.64	33.8	28.66	29.11	578.9	5.3	2.0	6.8	1.46	1417	0.98
26R-2, 120–125	291.7	25	7.84	2.64	33.5	29.76	28.38	577.9	7.9	2.6	6.6	1.40	1154	1.05
34R-1, 120–125	367.5	25	7.67	3.07	33.2	28.64	24.83	579.9	5.5	4.6	6.6	1.69	1449	1.15
53R-4, 115–125	554.6	20	8.34	2.65	33.8	17.94	32.52	517.1	1.7	1.3	5.5	1.59	438	0.55
59R-3, 115–125	611.1	20	8.65	1.24	33.9	20.53	37.00	576.4	3.0	0.5	2.2	1.51	228	0.55
62R-5, 115–125	640.0	30	8.57	1.79	34.2	20.43	40.14	583.9	2.4	0.5	2.1	1.42	308	0.51
[a]53R-4, 115–125	554.6	20				20.46	37.17	577.1	0.1	0.5	6.1	1.74	423	0.55
Drilling-mud filtrate						2.14	3.37	141.2	13.1	8.9	1.6	0.52	529	0.64

[a] Corrected for the presence of drilling-mud filtrate.

the diffusive flux of ammonia is considerable. To maintain this feature, silica would have to be removed at depth.

ORGANIC GEOCHEMISTRY

Light Hydrocarbon Analyses

Data are presented in Table 13 and plotted vs. depth in Figure 35. As at Site 695, levels of methane are consistently low until an inflection in the concentration curve is reached. At this site, concentrations rose substantially at and below 611.04 mbsf, while at Site 695 the increase occurred at and below 259.8 mbsf. Neither trend could be followed to its maximum because drilling was terminated.

Methane/ethane ratios are low in all samples (Table 13), increasing significantly below 611.0 mbsf. As at Site 695, sulfate reduction appears to have proceeded to a sufficient degree at this depth to have facilitated methanogenesis. There is an exponential decrease in sulfate concentration in pore waters, reaching near-zero values at 550 mbsf (Fig. 33D). No gas partings were observed in the cores.

All analyses were carried out on the Natural Gas Analyzer (NGA) system incorporated in the Hewlett Packard 5890 gas chromatograph. As this system is nonlinear for methane at levels above approximately 800 ppm, the thermal conductivity detector was operated in series with the ionization detector. These means were adopted because of the high expected levels of gas at Sites 695 and 696. The process resulted in certain gains and several offsetting shortcomings. The NGA has a substantial background of hexane-plus compounds (minimally 17 ppm) which might, in fact, be derived from the air sealed in the sample vial. Data in Table 13 are not corrected for C_{6+} background. The concentration of methane in the laboratory air was observed at 1.7 ppm, a normal level, for which no correction is made in Table 13. The source of the earlier high levels of methane in the laboratory is perhaps the argon-methane counter gas used for the X-ray fluorescence unit. This gas sometimes flows continuously. Ethene is evident in the samples with the higher resolution of the NGA. This might derive from acetylene in the air (used as a torch fuel in sealing water samples). On the positive side, carbon dioxide is detected, and is reported here for Sites 695 and 696. It is possibly due to bacterial fermentation in the sediments, a process which will be further investigated by carbon isotope ratio mass spectrometry.

Rock-Eval Analyses

Data are given in Table 14 and plotted in Figures 36 and 37. The observations are noteworthy for their scatter. Standards were therefore interspersed every fifth analysis in a reexamination of the samples. The standards yielded satisfactorily precise and accurate results (Fig. 38). Scatter is therefore attributable to a remarkable diversity of kerogen types and conditions. As at Site 695, kerogens of all levels of maturity are present here. Figure 37 plots hydrogen index vs. maximum pyrolysis temperature (T_{max}). Both variables are functions of thermal history. Interpretations are made in terms of the standard measure of maturity, equivalent vitrinite reflectance, employing the standard reference curves incorporated into Figure 37, from Herbin et al. (1984), the developers of the Rock-Eval process. It is probable that mixing and oxidation of kerogens complicates the interpretation at Site 696, but evidently planktonic kerogens (Type II) of a wide range of maturities are present: from immature, therefore first cycle, to extremely mature, therefore recycled. Similar features were seen at Site 695.

It is interesting to note that first-cycle, low-maturity terrestrial kerogen, lignitic plant debris of Type III, is absent from the deeper part of the section of Eocene age. This is indicated by the absence of data points along the Type III trend line in Figure 35. Furthermore, no Type III kerogen was present in the Cretaceous section encountered at Sites 692 and 693. In summary, no substantial evidence of terrestrial vegetation contemporary with the drilled sediments has been observed.

DOWNHOLE MEASUREMENTS

Heat Flow Measurements

Temperature Measurements

At Holes 696A and 696B, the Von Herzen APC (advanced piston corer) temperature recording device (VH-probe #1) and the temperature recording instruments for the pore-water sampler (Uyeda/Kinoshita probe, T-probe #14) were used three times (Cores 113-696A-8H, 113-696B-9I, and 113-696B-18I).

Core 113-696A-8H (69.6 mbsf)

Figure 39 shows the temperature record at Core 113-696A-8H using VH-probe #1. The temperature reached 7.57°C just after penetration due to frictional heat production, and just before pull out, the temperature was 4.82°C. The temperature data were gradually approaching the true formation temperature. The temperature data can be extrapolated to equilibrium following Horai and Von Herzen (1985). Using "DECAY3" and "FITTING3" computer programs (see "Explanatory Notes" chapter, this volume), the estimated true formation temperature is

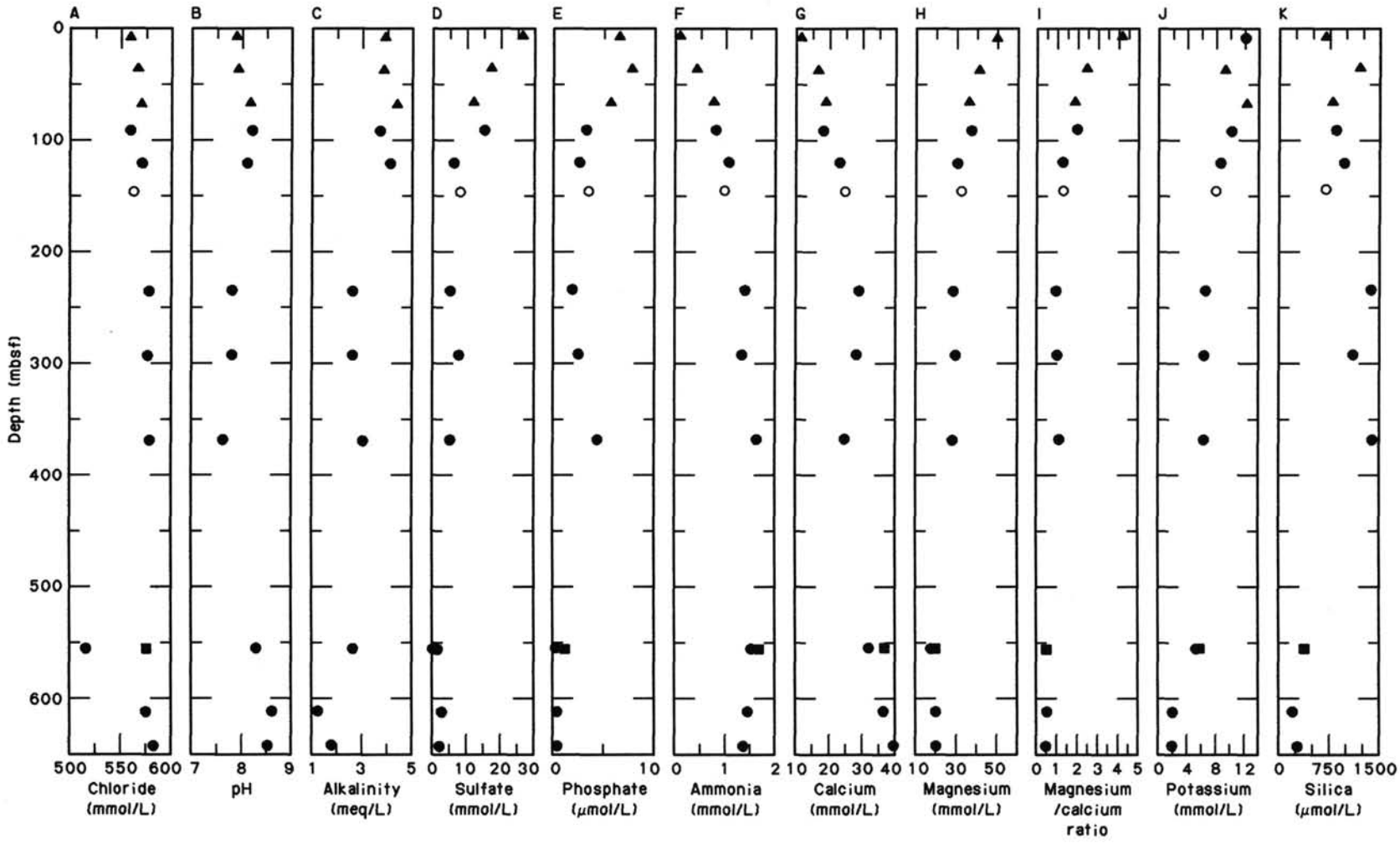

Figure 33. Concentrations vs. depth for Holes 696A and 696B. Data given in Table 12. A. Chloride. B. pH. C. Alkalinity. D. Sulfate. E. Phosphate. F. Ammonia. G. Calcium. H. Magnesium. I. Magnesium/calcium ratio. J. Potassium. K. Silica. Triangles = Hole 696A; dots = Hole 696B; circles = *in-situ* pore water sample; square = sample corrected for drilling-mud filtrate.

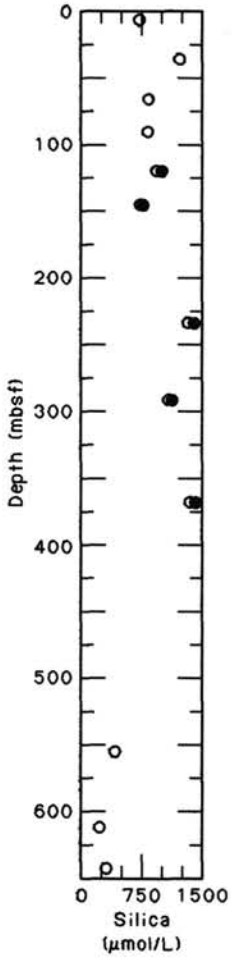

Figure 34. Comparison of two replicate silica analyses for Site 696.

3.4°–3.6°C at 69.6 mbsf (see "Downhole Measurements" section, "Site 689" chapter, this volume). This is a high-quality temperature estimate.

Core 113-696B-9I (144.1 mbsf)

This core was taken to obtain a pore-water sample. T-probe #14 was used. Figure 40 shows the temperature record for Core 113-696B-9I. Just before pull out, the T-probe showed an almost constant, possibly slightly increasing, temperature of 8.20°C. The true formation temperature was at least 8.20°C.

Core 113-696B-18I (222.1 mbsf)

This core was also taken to obtain a pore-water sample and T-probe #14 was used again. A sensor part of the temperature probe was lost and the electronics circuits damaged in stiff sediments. As a result, no temperature data were recovered.

Discussion and Conclusion

At this site, two kinds of temperature recording devices were used (VH-probe and T-probe). Therefore, calibration of the temperature sensors is very important. However, since a cryostat was not available on board the ship, the data obtained by the different tools could not be exactly compared. The T-probe #14 always gave higher temperature measurements than the VH-probe #1 of 0.7°–0.9°C at Site 695 (see "Downhole Measurements" section, "Site 695" chapter, this volume). Unfortunately, the two devices cannot be compared because the T-probe was lost. In this section, we assume that T-probe #14 had a temperature value 0.8°C higher than the VH-probe #1. Thus, 0.8°C has been subtracted from observed T-probe values.

Figure 41 shows the results of the temperature measurements. Circles give the observed temperatures just before pull out, and the arrow shows the direction of the temperature change occurring at that time. The dot shows the estimated true formation temperature for Core 113-696A-8H (69.6 mbsf). A dashed line

Table 13. Headspace analyses of light hydrocarbons, Holes 696A and 696B.

Core, section interval (cm)	Depth (mbsf)	Methane	Ethane	Propane	n-C_4	n-C_5	n-C_6	CO_2	C_1/C_2
		Microliters(gas)/liter(sediment)							
113-696A-									
2H-3, 120–125	6.70	6.4	1.1	0	0	0	44.3	2.0	5.8
113-696B-									
3R-3, 120–125	90.40	5.0	1.5	0	0	0	32.9	1.1	3.2
5R-4, 145–150	111.45	28.4	0	0	0	0	60.1	3.5	—
6R-3, 120–125	119.40	18.5	1.0	0	0	0	26.0	1.6	17.6
8R-1, 147–150	135.97	14.6	5.4	0	0	0	85.5	1.8	2.7
10R-1, 145–150	145.55	19.1	0	0	0.5	0	14.0	1.0	—
20R-2, 120–125	233.80	18.2	1.6	1.4	1.9	0	31.0	4.4	11.4
23R-2, 120–125	262.80	23.6	1.6	tr	0	0.4	37.6	1.5	14.8
26R-2, 120–125	291.70	7.2	2.0	0	1.7	0	52.4	3.1	3.6
28R-2, 147–150	311.27	5.3	0.5	0.2	0	0	17.4	1.5	10.8
32R-1, 149–150	348.49	8.2	0.6	0.4	0	0	19.9	2.3	13.3
34R-1, 120–125	367.50	9.2	0.9	1.6	1.1	0	22.5	2.8	10.6
45R-1, 149–150	473.99	9.2	0.5	0	0	0	30.7	2.8	17.4
47R-1, 141–142	493.01	15.1	1.8	0	0.5	0.4	68.1	1.6	8.6
51R-1, 149–150	531.29	4.2	0	0	0.4	0	21.3	—	—
53R-4, 115–120	554.55	8.1	1.1	0	0	0	22.4	0.2	17.6
54R-2, 148–150	561.48	7.4	1.1	0	0	0.4	23.8	1.1	7.1
55R-3, 149–150	572.69	7.6	0	0	0	0	75.3	0.9	—
56R-1, 149–150	579.39	6.6	0.9	0	0	0	33.3	0.8	6.9
57R-1, 121–122	588.81	6.2	1.4	0	0	0	32.4	0.3	4.3
58R-1, 149–150	598.69	18.9	0	0	0	0	33.2	0.3	—
59R-3, 114–115	611.04	79.9	1.2	0	0	0	30.9	1.7	66.4
60R-4, 149–150	622.59	224.6	0.6	0	0	0	36.0	0.3	381.9
61R-3, 149–150	630.69	205.8	0	0	0	0	30.7	0.2	—
62R-5, 114–115	643.04	380.8	0.6	0	0	0	28.4	2.3	663.4

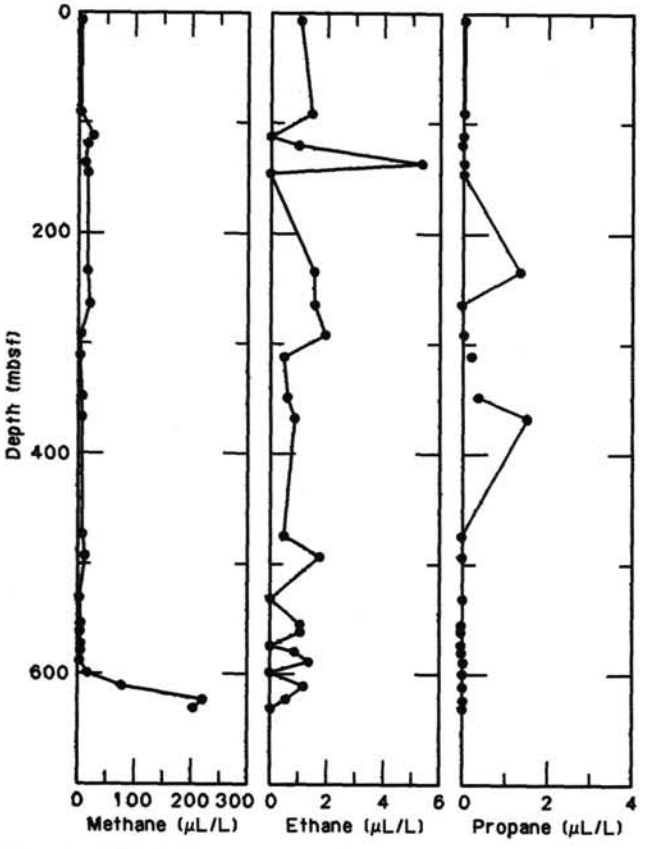

Figure 35. Light hydrocarbon data, Site 696. Data given in Table 13.

shows the estimated temperature-depth relation at Site 696. For this site, a temperature gradient was tentatively calculated as 52 mK/m by using the two values of 3.5°C (69.6 mbsf) and of 7.4°C (144.1 mbsf).

Ten thermal conductivity measurements were made from Hole 696A samples as a part of the physical properties measurements (see "Physical Properties" section, this chapter). The measurements were made to 75 mbsf, and the average value is 1.21 W/m-K.

Heat flow is defined by the product of temperature gradient and thermal conductivity. An estimated heat flow value at Site 696 is 63 mW/m^2; thus Sites 695 and 696 have essentially the same geothermal structure.

Downhole Logging

Introduction

Initially, two logging runs with the following tools were planned: (1) seismic stratigraphic (LSS-DIL-GR-MCD), and (2) lithodensity combinations (LDT-CNTG-NGT-GPIT). After 5 hr of trying unsuccessfully to log past sediment bridges, it was decided that because of poor hole conditions extra time was needed to rig up the sidewall entry sub and condition the hole.

On the second logging attempt, the logging tools were lost during circulation, while the tools were still in pipe at 1184 mbsl. Fifty-five meters of usable logs were recorded from 550 to 605 mbsf. The caliper log showed that the hole diameter varied markedly, making the sonic log unreliable, and the gamma ray and resistivity logs only marginally reliable.

Interpretation

At Hole 696B, 55 m of usable open-hole logs were obtained, spanning the interval from 550 to 605 mbsf (Fig. 42). The hole quality was poor with hole diameter ranging from 8.5 to 13.5 in. The sonic log shows that both the short (DT) and long spacing (DTL) sonic readings are affected by hole quality, making the measurements unreliable. The gamma ray curve (GR), which can also be affected by hole conditions, appears to be less influenced by hole size than the sonic log. The resistivity logs (ILD, ILM, and SFLU), which respond primarily to formation porosity, are less affected by hole quality because they measure three different depths of penetration: flushed (<50 cm into the formation), invaded (1–2 m penetration), and virgin (2 m into the formation). The short interval logged and the variable data quality preclude valid log interpretation at Hole 696B.

SUMMARY AND CONCLUSIONS

Site 696 lies on the southeastern margin of the South Orkney microcontinent (SOM) at 61°50.945'S, 42°55.984'W and in a water depth of 650 m. Site 696 is the shallowest of all sites drilled in the Leg 113 Weddell Sea depth transect, for studies of vertical water-mass stratification and sediment and climatic history during the late Mesozoic and Cenozoic. The site was selected to provide a continuously cored, shallow-water sedimentary record of late Paleogene to Neogene paleoceanography and paleoclimate on the SOM, which has remained close to West Antarctica. The multichannel seismic reflection profile exhibits a relatively thin (about 0.6 s two-way traveltime) sequence of acoustically layered sediments expected to be upper Paleogene-Neogene biogenic oozes and hemipelagics, overlying a distinct reflector packet interpreted as a regional breakup unconformity. This, in turn, is underlain by a thick (about 1.0 s twt) sequence of inferred terrigenous and volcaniclastic sediments of Paleogene and possibly greater age.

Site 696 consists of two holes: Hole 696A includes 10 APC cores to 89 mbsf and 2 XCB cores from 89 to 103 mbsf, providing 55% recovery; Hole 696B includes wash core from 0 to 76.6 mbsf, 2 interstitial water cores, and 59 rotary cores, from 76.6 to 645.6 mbsf with 27.5% recovery. The site was abandoned at the maximum penetration allowed because of safety restrictions.

The sedimentary sequence, poorly recovered and commonly strongly disturbed, is terrigenous, hemipelagic, and pelagic in origin, with an ice-rafted and a minor volcanogenic component. Ice-rafted detritus of a wide size range occurs as a distinct component above about 330 mbsf, from the middle upper Miocene (about 8 Ma) to the mud line (Recent). Only very rare coarse-grained ice-rafted detritus and dropstones were found between 550 and 570 mbsf (Cores 113-696B-51R, 113-696B-53R, and 113-696B-54R) in sediments of unknown age, but likely to be Oligocene or lower Miocene. Calcareous material is absent through almost all of the sequence except as an important planktonic foraminiferal component in the uppermost few meters of the Quaternary section and as calcareous benthic foraminifers and calcareous nannofossils in the basal Eocene section. There is also a thin section containing calcareous microfossils in the upper Miocene. The pelagic biogenic component is dominated by biosiliceous material, particularly diatoms.

In general, the Site 696 sedimentary sequence consists of three parts: an upper, mainly hemipelagic part from the seafloor to about 214 mbsf, a middle diatomaceous part from about 214 to 530 mbsf, and a lower terrigenous to authigenic part from 530 mbsf to the base of the hole. The sequence contains significant amounts of devitrified volcanic ash and glass in the lowermost Pliocene to the lower upper Pliocene (153–50 mbsf) and in the middle Miocene to a lower interval of unknown age (510–597 mbsf). Several chert layers are associated with the middle and lower upper Miocene diatomaceous sediments. Eocene to lower middle Miocene sediments contain a clay mineral association dominated by smectite with occasional common to abundant illite. Above the middle middle Miocene,

Table 14. Rock-Eval data, Site 696.

Core, section interval (cm)	Depth (mbsf)	S_1 mg(HC)/ g(rock)	S_2 mg(HC)/ g(rock)	S_3 mg(CO_2)/ g(rock)	TOC (%)	HI mg(HC)/ g(C)	OI mg(CO_2)/ g(C)	T_{max} (°C)
113-696A-								
2H-3, 120–125	6.70	0.05	0.48	0.06	0.29	165	20	430
5H-3, 120–125	35.45	0.23	1.37	0.31	0.48	285	64	443
8H-4, 120–125	65.70	0.06	0.66	0.14	0.46	143	30	396
113-696B-								
3R-3, 120–125	90.40	0.06	1.37	0.10	0.450	342	25	443
5R-4, 145–150	111.45	0.20	1.65	0.13	0.47	351	27	456
6R-3, 120–125	119.40	0.06	0.99	0.08	0.25	396	32	540
8R-1, 147–150	135.97	0.02	0.50	0.03	0.15	333	20	501
10R-1, 145–150	145.55	0.03	0.80	0.11	0.32	250	34	513
20R-2, 120–125	233.80	0.38	2.24	0.14	0.23	973	60	463
23R-3, 120–125	262.80	0.00	0.15	0.00	0.70	21	0	531
26R-2, 120–125	291.70	0.61	3.02	0.03	0.42	719	7	451
28R-2, 147–150	311.27	0.42	2.41	0.01	0.45	535	2	509
32R-1, 149–150	348.49	0.64	3.78	0.03	0.55	687	5	427
45R-1, 149–150	473.99	0.24	2.10	0.07	0.34	617	20	464
47R-1, 141–142	493.01	0.26	1.39	0.10	0.35	397	28	406
51R-1, 149–150	531.29	0.01	0.07	1.18	0.37	18	318	449
53R-4, 115–120	554.55	0.08	1.36	0.43	0.94	144	45	416
54R-2, 148–150	561.48	0.08	1.61	0.43	0.86	187	50	419
55R-3, 149–150	572.69	0.03	0.82	0.14	0.57	143	24	449
56R-1, 149–150	579.39	0.01	0.48	0.19	0.34	141	55	462
57R-1, 121–122	588.81	0.01	0.50	1.28	0.32	156	400	468
58R-1, 149–150	598.69	0.00	0.35	0.09	0.23	152	39	514
59R-1, 114–115	611.04	0.01	0.18	0.23	0.37	48	62	435
60R-4, 149–150	622.59	0.00	0.00	0.26	0.33	0	78	[a]281
61R-3, 149–150	630.69	0.01	0.48	0.30	0.22	218	136	487
62R-3, 115–120	643.04	0.04	0.51	0.49	0.39	130	123	445
Standard, analysis 1:		0.13	8.51	1.30	2.86	297	45	422
Standard, analysis 2:		0.13	8.25	1.27	2.86	288	44	424
Standard, analysis 3:		0.15	8.60	1.26	2.86	300	44	423
Standard, analysis 4:		0.13	8.05	1.10	2.86	281	38	426
Standard, analysis 5:		0.14	8.73	1.19	2.86	305	41	426
Standard, analysis 6:		0.14	8.61	1.23	2.86	301	43	422
Standard, analysis 7:		0.16	8.96	1.23	2.86	313	43	417
Standard (known values)		0.10	8.62	1.00	2.86	340	33	419

[a] Apparently spurious value.

smectite is much reduced and the clay associations are dominated by illite and chlorite.

The sequence ranges from Eocene (probably middle? or upper Eocene) to the Quaternary. The section of Site 696 consists of a condensed Quaternary to upper Pliocene, an expanded lower Pliocene and upper to middle Miocene, and a condensed Oligocene(?) to Eocene section at the base. The APC part of the section extends from the middle Pliocene (about 80 mbsf) to the Quaternary. As a result of poor core recovery, stratigraphic resolution is often inadequate for the recognition of hiatuses that may exist in the sequence. The preliminary biostratigraphy and magnetostratigraphy indicate the presence of a brief sedimentary hiatus or highly condensed sequence in the uppermost Pliocene to lowest Quaternary, and a possible brief hiatus in the middle Pliocene. Another condensed interval, barren of stratigraphically useful microfossils, separates the sequences assigned to the Neogene and Paleogene and hinders understanding the Paleogene/Neogene transition.

A paleomagnetic polarity stratigraphy has been identified for the lower Pliocene to Recent, but prospects are poor for the Miocene due to the poor core recovery. Good opportunities for a paleomagnetic polarity stratigraphy exist for the Paleogene sediments. The preliminary work has allowed possible identification of Chrons C16 through C18 (Cores 113-696B-59R to 113-696B-62R, middle to upper Eocene).

Biostratigraphic age assignments for the Neogene are based on diatoms, radiolarians, and silicoflagellates. Paleogene sediments are essentially barren of siliceous microfossils, and biostratigraphic age assignments are based upon calcareous nannofossils and palynomorphs. This represents the first recovery of pollen and spores in deep sea sediments of the Weddell Sea. Diatoms occur in variable abundance and preservation in the Neogene sequence. Pliocene and Quaternary diatoms are less abundant and more poorly preserved than at other sites in the Weddell Sea. Diatom preservation is poor and abundance particularly low near the Miocene/Pliocene transition, as at the other sites. Miocene diatoms are both abundant and well preserved. Radiolarians are common to abundant and well preserved in most of the Pliocene, poorly preserved in the basal Pliocene and uppermost Miocene, and are often rare in the lower Miocene. They are absent in the Paleogene. A single species of calcareous nannofossils was found in one upper Miocene sample and apparently at an equivalent interval in Site 693 on the East Antarctic continental margin. Calcareous nannofossil assemblages of moderate abundance, preservation, and diversity occur at at some levels in the Paleogene. Planktonic foraminifers are almost absent except as abundant forms in the Quaternary and rarely in a single upper Miocene and Paleogene sample. Benthic foraminifers are persistent but rare through most of Site 696 and consist almost exclusively of low-diversity assem-

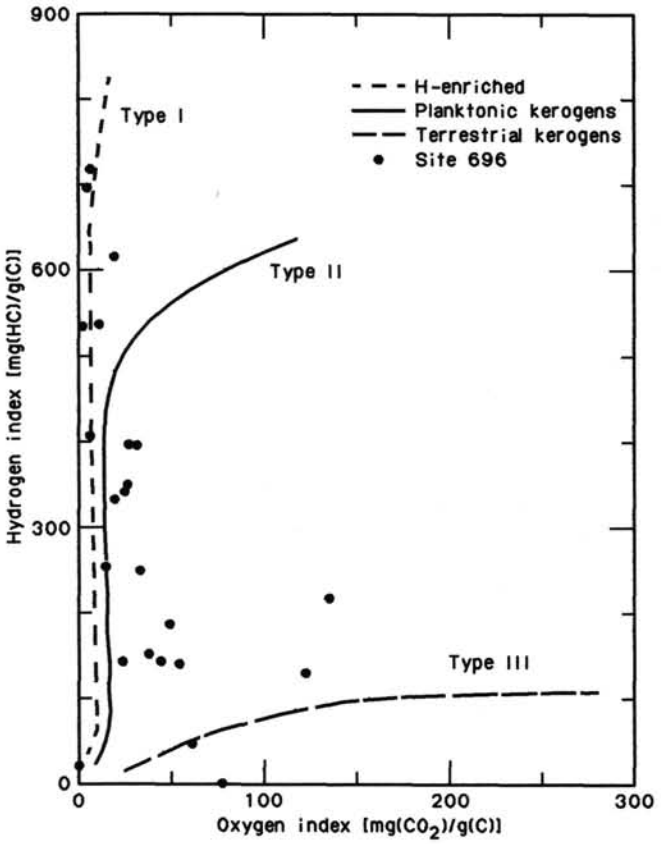

Figure 36. Rock-Eval data, Site 696: hydrogen index vs. oxygen index. Data given in Table 14.

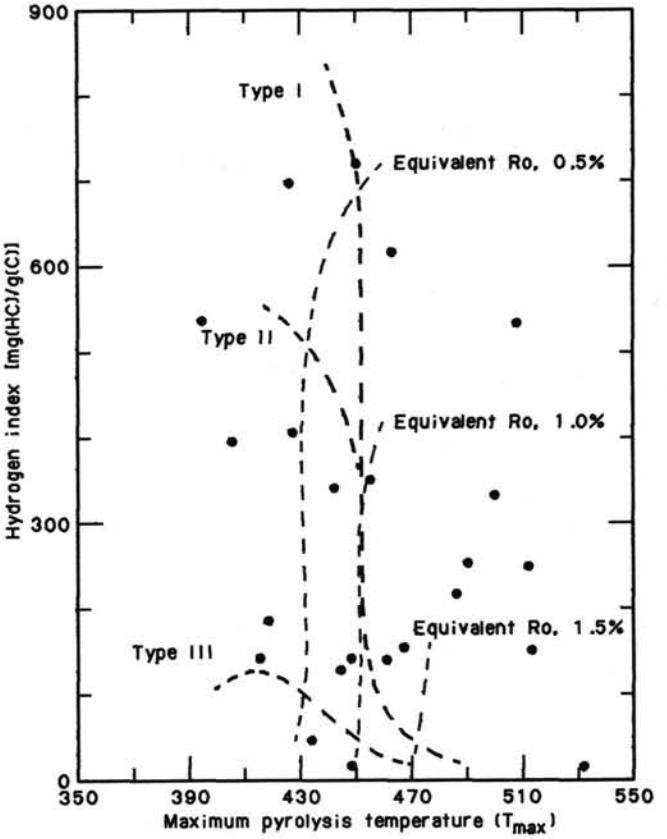

Figure 37. Hydrogen index vs. maximum pyrolysis temperature, T_{max}, for kerogens from Site 696. Ro = vitrinite reflectance (isoreflectance curve).

blages of agglutinated forms. Calcareous benthic assemblages were found only in the Quaternary, in a few upper Miocene samples and in the Paleogene.

The sequence at Site 696 has been divided into seven lithostratigraphic units (see Fig. 4), based upon compositional differences and diagenetic maturity. The Neogene units are largely differentiated on the relative abundance of biosiliceous and terrigenous components. The Paleogene units are subdivided on changes in terrigenous and authigenic components and the degree of diagenetic maturity.

Unit I (Quaternary to lower upper Pliocene) extends from the seafloor to 64.2 mbsf. The sediment is composed primarily of diatomaceous muds and oozes. The upper part of Unit I (Subunit IA, Quaternary) is diatom-bearing silty mud. The lower part of Unit I (Subunit IB, upper Pliocene) is diatom clayey mud and muddy diatom ooze.

Unit II (lower upper Pliocene to lower Pliocene) extends from 64.2 to 124.8 mbsf. This unit is marked by a distinct decrease in biosiliceous material and is composed mainly of diatom-bearing silty and clayey mud.

Unit III (lower Pliocene to upper Miocene) extends from 124.8 to 211.8 mbsf. This unit is dominated by silty and clayey mud, with less important diatom-bearing clayey mud.

Unit IV (upper Miocene) extends from 211.8 to 260.1 mbsf. This unit is marked by a significant increase in biosiliceous material and consists of diatom ooze and muddy diatom ooze.

Unit V (upper Miocene) extends from 260.1 to 269.7 mbsf. This unit consists of coarse-grained sand and is probably a turbidite.

Unit VI (upper to middle Miocene) extends from 269.7 to 529.8 mbsf. The unit consists of diatomaceous sediments and has been divided into two subunits. Subunit VIA is composed of diatom ooze and mud-bearing diatom ooze. Subunit VIB consists of lithified diatomite and mud-bearing diatomite.

Unit VII extends from 529.8 m to the base of the hole at 645.6 mbsf and is possibly Miocene to Eocene. This unit is dominantly terrigenous in origin and has been divided into four subunits as follows: Subunit VIIA is sandy mudstone, possibly Miocene; Subunit VIIB is claystone, clayey mudstone, and silty mudstone, undifferentiated upper Paleogene to lower Miocene; Subunit VIIC is glauconitic silty mudstone and claystone, undifferentiated upper Paleogene to lower Miocene; and Subunit VIID is sandy mudstone, Eocene. The harder layers within the lower part of Unit VII form the strong seismic reflection horizons associated with the breakup unconformity.

Paleoenvironmental History of Site 696

Although sediment recovery at Site 696 was not ideal, the sequence has provided important information about the paleoclimatic, paleoglacial, and paleoceanographic history of the Antarctic region.

During the late Eocene, sandy mudstones (Subunit VIID) were deposited, reflecting the dominantly terrigenous sedimentary regime of the South Orkney microcontinent (SOM) while it was still contiguous with the West Antarctic continental margin (Barker et al., 1984; King and Barker, 1988). Benthic foraminiferal assemblages indicate deposition in an inner neritic environment (less than 100 m water depth), under slightly hyposaline and slightly hypoxic conditions. Abnormally high chlorinity of interstitial waters tentatively supports an interpretation of hyposalinity at the time of sediment deposition. The shallow waters supported an abundant assemblage of invertebrates including Mollusca and Cnidaria. Planktonic assemblages were largely ex-

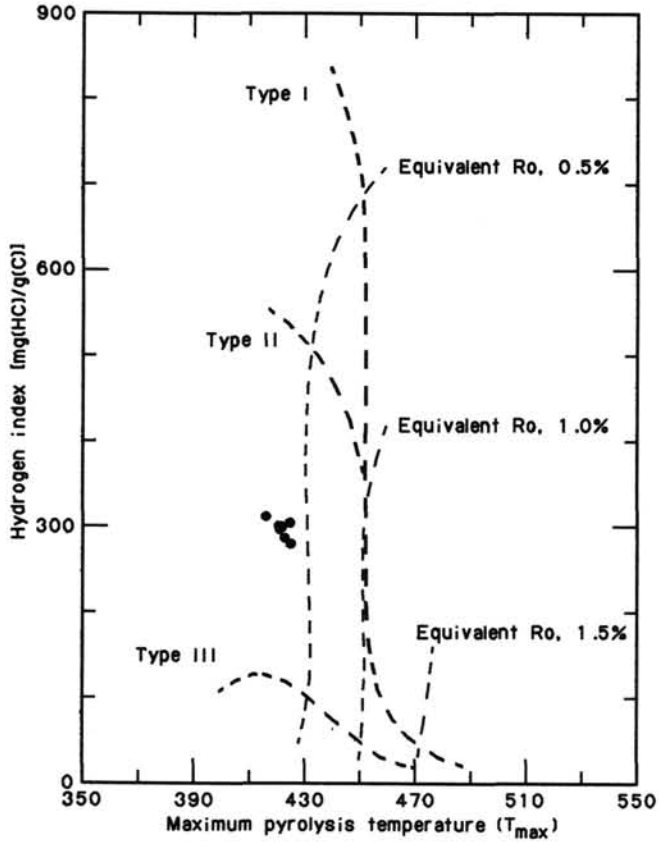

Figure 38. Hydrogen index vs. maximum pyrolysis temperature for analyses of standard sediment. Ro = vitrinite reflectance (isoreflectance curve).

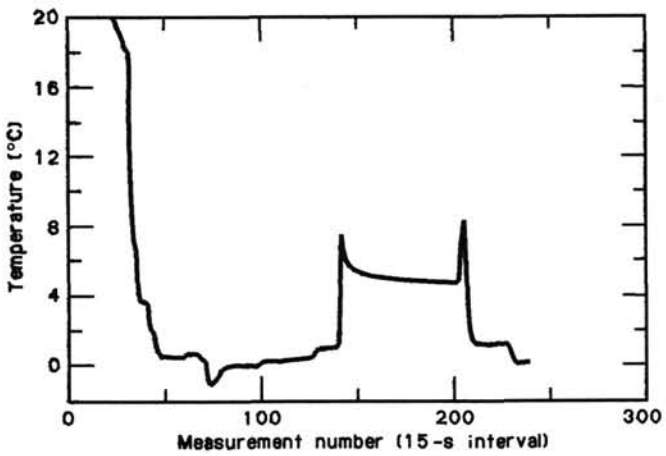

Figure 39. Temperatures measured with the Von Herzen APC tool #1 (VH-probe #1) during Core 113-696A-8H at 69.6 mbsf.

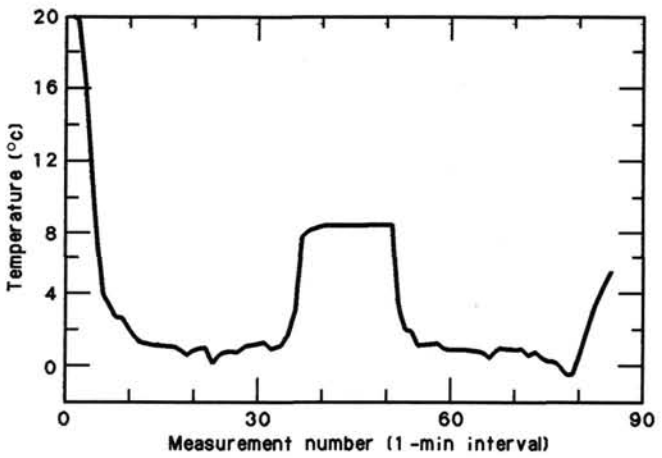

Figure 40. Temperatures measured with the temperature recording instruments for the pore-water sampler (Uyeda/Kinoshita probe, T-probe) #14 during Core 113-696B-9I at 144.1 mbsf.

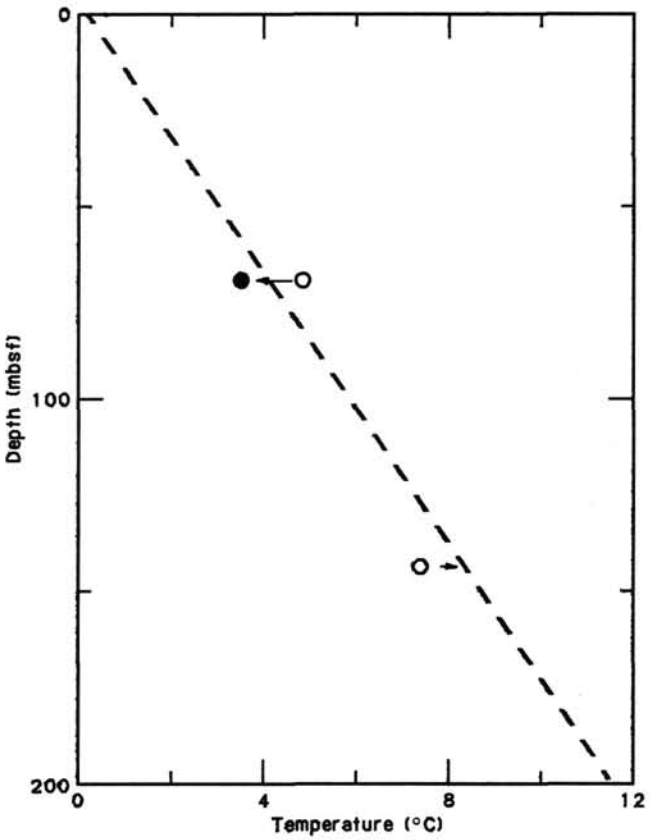

Figure 41. Observed temperature measurements just before pull out (circles) and an estimated true formation temperature (dot). Dashed line shows an estimated temperature gradient at Site 696 of 52 mK/m.

cluded from this sedimentary environment due to shallowness and hyposalinity. Diverse calcareous nannofossil assemblages were preserved occasionally and attest to the warmth of the Southern Ocean in the Eocene. Planktonic foraminifers are very rare. The presence of a palynoflora containing *Nothofagus* pollen and fern spores (Pteridophyta) indicates that temperate beech forests with an undergrowth of ferns living in frost-free conditions occurred on West Antarctica during the ?late Eocene. This supports the observations of Stuchlik (1981), who found a similar flora on the South Shetland Islands. Reworked *Nothofagus* assemblages have been documented in sediments adjacent to East Antarctica (Kemp, 1975), indicating that such forests were widespread and that the Antarctic was relatively warm during the Eocene. The interpretation that the climate was warm is supported by the presence of a clay association dominated by smectite, as in the Eocene sediments of Maud Rise. Clay assemblages dominated by smectite indicate a predominance of chem-

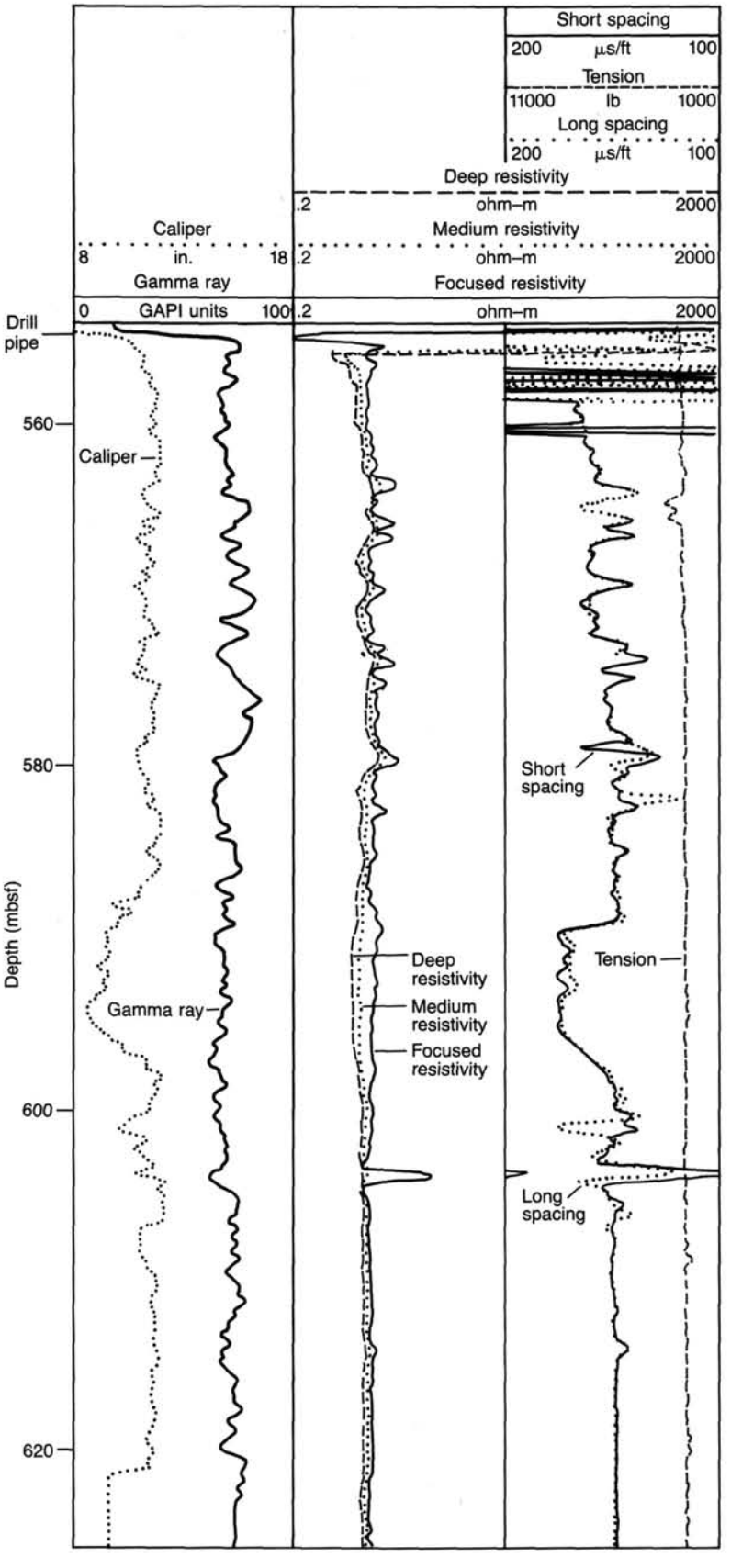

Figure 42. Gamma ray (GR, in GAPI units), caliper (in inches), resistivity (ILD, ILM, and SFLU, in ohm-m) and sonic (DT and DTL, in µs/ft) logs for the open-hole interval at Hole 696.

ical over physical weathering. With Drake Passage yet to open and the Antarctic Circumpolar Current still to form, warm waters in the South Atlantic extended southward into the Weddell Sea, transferring heat and warming the continent and surrounding oceans. Increasing relative abundances of epiphytic benthic foraminifers upsection suggest that waters became shallower during the Eocene.

Following deposition of the Eocene sediments a highly condensed sequence of about 77 m of unfossiliferous or poorly fossiliferous terrigenous sediments (represented by Subunits VIIC through VIIA) was deposited. This sequence is difficult to date and separates Eocene and middle Miocene sediments. The absence of adequate stratigraphic information hinders an understanding of the Paleogene/Neogene transition. These sediments were probably deposited slowly, and major, as yet not precisely located, hiatuses may be present. No evidence has been found of subaerial exposure. Deposition of this sequence began with almost unfossiliferous glauconitic muds and clays (Subunit VIIC). The deposition of glauconites is generally considered to occur in nonoxidizing, shallow marine environments where the rate of deposition is slow (Odin and Matter, 1981) or post-oxic, nonsulfide marine environments containing low abundances of organic material. The glauconitic sediments exhibit no cross bedding or other sedimentary structures indicative of deposition under active bottom currents. Deposition was thus probably at neritic depths flushed by well-oxygenated, relatively low-velocity bottom currents. The presence of rare, reworked freshwater diatoms in this interval (Subunit VIIC) indicates that freshwater lakes occurred in the West Antarctic region at this time.

Nearly all of the section at Site 696 (from Subunit VIIB up) contains only agglutinated benthic foraminiferal assemblages and virtually no calcareous planktonic microfossils, indicating that a change to highly undersaturated bottom waters, even at these shallow water depths, occurred during the time represented by Cores 113-696B-56R through 113-696B-58R. This suggests that a fundamental change occurred in the nature of bottom water around Antarctica. Previous studies have shown that one of the most important oxygen isotopic changes during the Cenozoic occurred just above the Eocene/Oligocene boundary (Shackleton and Kennett, 1975; Savin et al., 1975) when bottom waters cooled as a result of inferred initial East Antarctic glaciation and associated sea-ice formation around Antarctica. The terrigenous sediments represented by Subunit VIIB most likely postdate this event, and could have been deposited at any time during the Oligocene or early Miocene, a time marked by considerable sea-level change (Vail and Hardenbol, 1979), inferred major regional current activity associated with the opening of Drake Passage (Barker and Burrell, 1977; Wise et al., 1985) and increased bottom-water activity associated with expansion of the East Antarctic ice-sheet during the early middle Miocene (Kennett and Von der Borch, 1986). The apparent absence of biostratigraphically useful fossils in these sediments makes it difficult to interpret the climatic conditions at this time but the rare agglutinated benthic foraminifers in Subunit VIIB suggest cool bottom waters. Little evidence exists for glacial activity. Ice-rafted detritus is absent except for a single *in-situ* dropstone observed in Core 113-696B-54R and a few small dropstones in Cores 113-696B-51R and 113-696B-53R. The clay mineral associations of abundant to exclusive smectite and common to abundant illite, indicate that climate was warm enough for the formation of smectite. The abundance of illite in comparison with the Eocene sediments, however, suggests that climatic conditions had become cool enough for the formation of clays by physical weathering.

The dominantly terrigenous and authigenic sediments of Eocene to possible Oligocene age pass (perhaps disconformably at about 530 mbsf) into a 300-m middle to uppermost Miocene sequence of dominantly biosiliceous sediments. The middle and lower upper Miocene sediments are assumed to be almost pure siliceous biogenic oozes although poor recovery has made interpretation difficult. The likely lack of terrigenous sedimentation in the middle Miocene almost certainly reflects the isolation of the South Orkney microcontinent from West Antarctica as a result of the formation of Powell Basin (King and Barker, 1988). These sediments are dominated by diatoms which form as much as 90% of the sediment. Sedimentation rates may have been fairly constant and moderately high from about 14 to 5 Ma, with an average of about 35–41 m/m.y. The high productivity, excellent preservation, and taxonomic composition of the diatoms suggest that the water passing over the South Orkney microcontinent was warmer during much of the Miocene and that there was no major production of sea-ice in the area.

A continued absence of calcareous microfossils through almost all of the Miocene indicates that the CCD was exceedingly shallow, remaining above the present-day depth of 650 m for Site 696. A very shallow CCD is typical of the present-day Antarctic continental margin, as in the southern Scotia Sea (Echols, 1971) and the Ross Sea, where its present-day depth is about 500 mbsf (Kennett, 1966). Drilling in that region also showed that the CCD remained shallow throughout the Neogene (Hayes, Frakes, et al., 1975). The shallowness of the CCD during the Neogene at Site 696 and elsewhere on the Antarctic continental margin probably resulted from the presence of highly corrosive bottom waters and low productivity of calcareous nannofossils. The CCD was considerably deeper on Maud Rise during the Neogene than on the SOM, leading to the deposition there of calcareous sediments. Changes in the agglutinated benthic foraminiferal assemblages at Site 696 seem to reflect changes in the depth of the CCD during the Neogene. The CCD may have risen to close to its present depth (above 650 m) during the early Miocene.

There is no evidence of deposition of ice-rafted detritus during the middle and early late Miocene (at sub-bottom depths below 330 m). This suggests that major glacial activity had not yet commenced on West Antarctica, in concordance with trends observed in several other Leg 113 sites. However, a distinct change in the climate of West Antarctica seems to have occurred during the middle Miocene, as reflected by marked changes in the clay mineral assemblages between about 480 and 505 mbsf at Site 696. At this time, smectite, the dominant clay mineral in the earlier part of the middle Miocene, was replaced by assemblages dominated by illite and chlorite. This change indicates a strong decrease in the intensity of chemical weathering and an increase in physical weathering. We interpret this to have resulted from cooling of West Antarctica during the middle Miocene. A similar change in the clay associations occurred earlier, at the beginning of the Oligocene, in the sites adjacent to East Antarctica and Maud Rise, indicating that major cooling occurred earlier in East Antarctica than West Antarctica. Further to the north in the Falkland Plateau area, smectite remained dominant throughout the Miocene, indicating a continuation of warm conditions.

Beginning in the early part of the late Miocene (corresponding to about 340 mbsf), the terrigenous component increased with deposition of mud-bearing diatom ooze. At the same time, a distinct record of ice-rafted detritus began and continues to the present day. From this time also, chlorite and illite became dominant in the clay mineral assemblages and smectite became rare, reflecting the dominance of physical weathering processes. Diatomaceous sediments continue to dominate. The increase in hemipelagic sediment, the appearance of an important ice-rafted component and the change to dominant illite and chlorite, all occurred as a result of the development of the West Antarctic ice-sheet during the late Miocene. The fine-grained terrigeous material may have been first deposited on the West Antarctic

continental margin from an extensive and unstable ice-sheet, and redistributed to the South Orkney microcontinent by currents flowing northward along the margin.

A very brief amelioration of climate occurred at about 8 Ma, within the late Miocene, as shown by the only occurrence of Neogene calcareous nannofossils at Site 696, essentially coeval with the occurrence of a similar assemblage at Site 693 to the east. These are found together with a rare, low-diversity planktonic foraminiferal fauna and calcareous benthic foraminifers. A productivity increase in calcareous nannofossil assemblages at this time seems to have temporarily depressed the CCD, leading to the preservation of the calcareous assemblages.

A major change in sediment facies occurred during the Miocene/Pliocene transition, when the diatomaceous sediments of the Miocene were largely replaced by diatom-bearing silty and clayey muds of Pliocene and Quaternary age. The addition of a large terrigenous component to the diatomaceous sediments seems to have resulted from the development, during the latest Miocene, of a major and probably permanent West Antarctic ice-sheet, the major supplier of fine-grained terrigenous sediments to the West Antarctic continental margin. Sedimentation rates are not yet tightly constrained, but may have been as high as 200 m/m.y. during part of the early or middle Pliocene. Rates decreased to about 20 m/m.y. during the late Pliocene. This marked decrease in sedimentation to rates of only 3–5 m/m.y. continued into the latest Pliocene and Quaternary (during the last 2.5 m.y.). A hiatus may have formed during the latest Pliocene and earliest Quaternary. Site 696 therefore exhibits the characteristic regional decrease in sedimentation rates from the early Pliocene to the late Pliocene and Quaternary. This decrease may have resulted from a reduction in the supply of terrigenous sediments due to the development of an even more stable West Antarctic ice-sheet, marked by extensive grounded ice shelves.

During the Pliocene and Quaternary, the CCD seems to have increased to more than 1300 m (depth of Site 695) and then shallowed again during the latest Quaternary to its present depth of about 650 mbsf, the depth of Site 696. The Quaternary is marked by an abundant planktonic foraminiferal assemblage of *Neogloquadrina pachyderma* and a low-diversity benthic foraminiferal assemblage. This assemblage was found throughout the Weddell Sea in almost all of the Leg 113 sites. It is not yet clear what created this temporary depression in the CCD, but it may have resulted from an amelioration of climate some time during the Quaternary, or perhaps the development of greater tolerance of *N. pachyderma* for Antarctic conditions.

REFERENCES

Bandy, O. L., and Echols, R. J., 1964. Antarctic foraminiferal zonation. *Antarct. Res. Ser.*, Am. Geophys. Union, 1:73–91.

Barker, P. F., and Burrell, J., 1976. The opening of Drake Passage. *In Proc. J. Oceanogr. Assem.*, 103, FAO (Rome).

_____, 1977. The opening of Drake Passage. *Mar. Geol.*, 25:15–34.

Barker, P. F., Barber, P. L., and King, E. C., 1984. An early Miocene ridge crest-trench collision on the South Scotia Ridge near 36°W. *Tectonophysics*, 102:315–322.

Berggren, W. A., Kent, D. V., Flynn, J. J., and Van Couvering, J. A., 1985. Cenozoic Geochronology. *Geol. Soc. Am. Bull.*, 96:1407–1418.

Berner, R. A., 1974. Kinetic models for the early diagenesis of nitrogen, sulfur, phosphorus, and silicon in anoxic marine sediments. *In* Goldberg, E. D. (Ed.), *The Sea* (Vol. 5): New York (Wiley), 427–450.

Bertels, A., 1977. Paleogene Foraminifera-South Atlantic. *In* Swain, F. M. (Ed.), *Stratigraphic Micropaleontology of Atlantic Basin and Borderlands*: Amsterdam (Elsevier), 411–440.

Brindley, G. W., 1980. Order-disorder in clay mineral structures. *In* Brindley, G. W., and Brown, G. (Eds.), *Crystal Structures of Clay Minerals and Their X-ray Identification*. Mineral. Soc. Monogr. 5.

Carlson, R. L., Gangi, A. F., and Snow, K.R., 1986. Empirical reflection travel time versus depth and velocity versus depth functions for the deep sea sediment column. *J. Geophys Res.*, 91:8249–8266.

Chen, P.H. 1975. Antarctic radiolaria. *In* Hayes, D. E., Frakes, L. A., et al., *Init. Repts. DSDP*, 28: Washington (U.S. Govt. Printing Office), 407–474.

Ciesielski, P. F., 1975. Biostratigraphy and paleoecology of Neogene and Oligocene silicoflagellates from cores recovered during Antarctic Leg 28, Deep Sea Drilling Project. *In* Hayes, D. E., Frakes, L. A., et al., *Init. Repts. DSDP*, 28: Washington (U.S. Govt. Printing Office), 625–691.

Echols, R. J., 1971. Distribution of Foraminifera in sediments of the Scotia Sea area, Antarctic waters. *Antarct. Res. Ser.*, Am. Geophys. Union, 15:93–168.

Goldhaber, M. B., and Kaplan, I. R., 1974. The sulfur cycle. *In* Goldberg, E. D.(Ed.), *The Sea* (Vol. 5): New York (Wiley) 569–655.

Hayes, D. E., Frakes, L. A., et al., 1975. *Init. Repts. DSDP*, 28: Washington (U.S. Govt. Printing Office).

Herbin, J. P., Deroo, G., and Roucaché, J., 1984. Organic geochemistry of Lower Cretaceous sediments from Site 535, Leg 77, Florida Straits. *In* Buffler, R. T., Schlager, W., et al., *Init. Repts. DSDP*, 77: Washington (U.S. Govt. Printing Office), 459–475.

Horai, K., and Von Herzen, R. P., 1985. Measurement of heat flow on Leg 86 of the Deep Sea Drilling Project. *In* Heath, G. R., Burckle, L. H., et al., *Init. Repts. DSDP*, 86: Washington (U.S. Govt. Printing Office), 759–777.

Kemp, E. M., 1975. Palynology of Leg 28 drill sites, Deep Sea Drilling Project. *In* Hayes, D. E., Frakes, L. A., et al., *Init. Repts. DSDP*, 28: Washington (U.S. Govt. Printing Office), 599–624.

Kennett, J. P., 1966. Foraminiferal evidence of a shallow calcium carbonate solution boundary, Ross Sea, Antarctica. *Science*, 153:191–193.

_____, 1977. Cenozoic evolution of Antarctic glaciation, the circum-Antarctic Ocean, and their impact on global paleoceanography. *J. Geophys. Res.*, 82:3843–3860.

Kennett, J. P., Houtz, R. E., et al., 1975. *Init. Repts. DSDP*, 29: Washington (U.S. Govt. Printing Office).

Kennett, J. P., and Von der Borch, C., 1986. Southwest Pacific Cenozoic paleoceanography. *In* Kennett, J. P., Von der Borch, C., et al, *Init. Repts. DSDP*, 90:1493-1517.

King, E. C., and Barker, P. F., 1988. The margins of the South Orkney Microcontinent. *J. Geol. Soc.* (*London*), 145:317–331.

Lawver, L. A., Della Vedova, B., and Von Herzen, R. P., 1986. Heat flow in Jane Basin, a small back-arc basin, Northern Weddell Sea. *Antarct. J. U.S.*, 19:87–88.

Ledbetter, M. T., and Ciesielski, P. F., 1986. Post-Miocene disconformities and paleoceanography in the Atlantic sector of the Southern Ocean. *Palaeogeogr. Palaeoclimatol. Palaeoecol.*, 52:185–214.

MacKenzie, F. T., and Garrels, R. M., 1966. Chemical mass balance between rivers and oceans. *Am. J. Sci.*, 264:507–525.

Manheim, F. T., and Sayles, F. L., 1974. Composition and origin of interstitial waters of marine sediments. *In* Goldberg, E. D. (Ed.), The Sea (Vol. 5): New York (Wiley), 527–568.

Mercer, J. H., 1978. Glacial development and temperature trends in the Antarctic and in South America. *In* Van Zinderen Bakker, E. M., (Ed.), *Antarctic Glacial History and World Paleoenvironments*: Rotterdam (A.A. Balkema), 73–93.

Milam, R. W., and Anderson, J. B., 1981. Distribution and ecology of Recent benthic Foraminifera of the Adelie-George V continental shelf and slope, Antarctica. *Mar. Micropaleontol.*, 6:297–325.

Murray, J. W., and Wright, C. A., 1974. Palaeogene Foraminiferida and paleoecology, Hampshire and Paris Basins and the English Channel. *Spec. Pap. Palaeontol.*, 14:1–171.

Odin, G. S., and Matter, A., 1981. De glauconarium origine. *Sedimentology*, 28:611–643.

Petrushevskaya, M. G., 1975. Cenozoic radiolarians of the Antarctic, Leg 29, DSDP. *In* Kennett, J. P., Houtz, R. E., et al., *Init. Repts. DSDP*, 29: Washington (U.S. Govt. Printing Office), 541–675.

Robert, C., and Maillot, H., 1983. Paleoenvironmental significance of clay mineralogical and geochemical data, Southwest Atlantic, DSDP Legs 36 and 71. *In* Ludwig, W. J., Krasheninnikov, V., et al., *Init. Repts. DSDP*, 71: Washington (U.S. Govt. Printing Office), 317–343.

Savin, S. M., Douglas, R. G., and Stehli, F. G., 1975. Tertiary marine paleotemperatures. *Geol. Soc. Am. Bull.*, 86:1499–1510.

Sayles, F. L., Manheim, F. T., and Waterman, L. S., 1973. Interstitial water studies on small core samples, Leg 13. *In* Ryan, W. B. F., Hsü, K. J., et al., *Init. Repts. DSDP*, 15: Washington (U.S. Govt. Printing Office), 801–809.

Schrader, H. J., 1976. Cenozoic planktonic diatom biostratigraphy of the Southern Pacific Ocean. *In* Hollister, C. D., Craddock, C., et al., *Init. Repts. DSDP*, 35: Washington (U.S. Govt. Printing Office), 605–672.

Shackleton, N. J., and Kennett, J. P., 1975. Paleotemperature history of the Cenozoic and the initiation of Antarctic glaciation: oxygen and carbon isotope analyses in DSDP, Sites 277, 279, and 281. *In* Kennett, J. P., Houtz, R. E., et al., *Init. Repts. DSDP*, 29: Washington (U.S. Govt. Printing Office), 743–755.

Shaw, C. A., and Ciesielski, P. F., 1983. Silicoflagellate biostratigraphy of middle Eocene to Holocene subantarctic sediments recovered by Deep Sea Drilling Project Leg 71. *In* Ludwig, W. J., Krashninnikov, V. A., et al., *Init. Rpts. DSDP*, 71: Washington (U.S. Government Printing Office), 687–737.

Stuchlik, L., 1981. Tertiary pollen spectra from the Ezcurra Inlet Group of Admiralty Bay, King George Island (South Shetland Islands, Antarctica). *Stud. Geol. Pol.*, 72:109–132.

Stumm, W., and Morgan, J. J. (Eds.), 1981. *Aquatic Chemistry* (2nd Ed.): New York (Wiley).

Stumm, W., and Leckie, Z. O., 1970. Phosphate exchange with sediments, its role in the productivity of surface waters. *Advances In Water Pollution Research* (Vol. 2): New York (Pergamon), III:26/1–26/16.

Sverdrup, H. U., Johnson, M., and Fleming, R. (Eds.), 1942. *The Oceans*: Englewood Cliffs, N.J. (Prentice-Hall).

Theyer, F., 1971. Benthic foraminiferal trends, Pacific-Antarctic Basin. *Deep-Sea Res.*, 18:723–738.

Truswell, E. M., 1983. Recycled Cretaceous and Tertiary pollen and spores in Antarctic sediments: a catalogue. *Palaeontographica B*, 186:83–174.

Tucholke, B. E., Hollister, C. D., Weaver, F. M., and Vennum, W. R., 1976. Continental rise and abyssal plain sedimentation in the southeast Pacific Basin. *In* Hollister, C. D., Craddock, C., et al, *Init. Repts. DSDP*, 35: Washington (U.S. Govt. Printing Office), 359.

Vail, P. R., and Hardenbol, J., 1979. Sea level changes during the Tertiary. *Oceanus*, 22:71–79.

Weaver, F. M., and Gombos, A. M., 1981. Southern high-latitude diatom biostratigraphy. *Soc. Econ. Paleontol. Mineral Spec. Publ.*, 32: 445–470.

Wise, S. W., Gombos, A. M., and Muza, J. P., 1985. Cenozoic evolution of polar water masses, southwest Atlantic Ocean. *In* Hsü, K. J., Weissert, M. J. (Eds.), *South Atlantic Paleoceanography*: Cambridge (Cambridge Univ. Press), 283–324.

Ms 113A-112

Summary log for Hole 696B

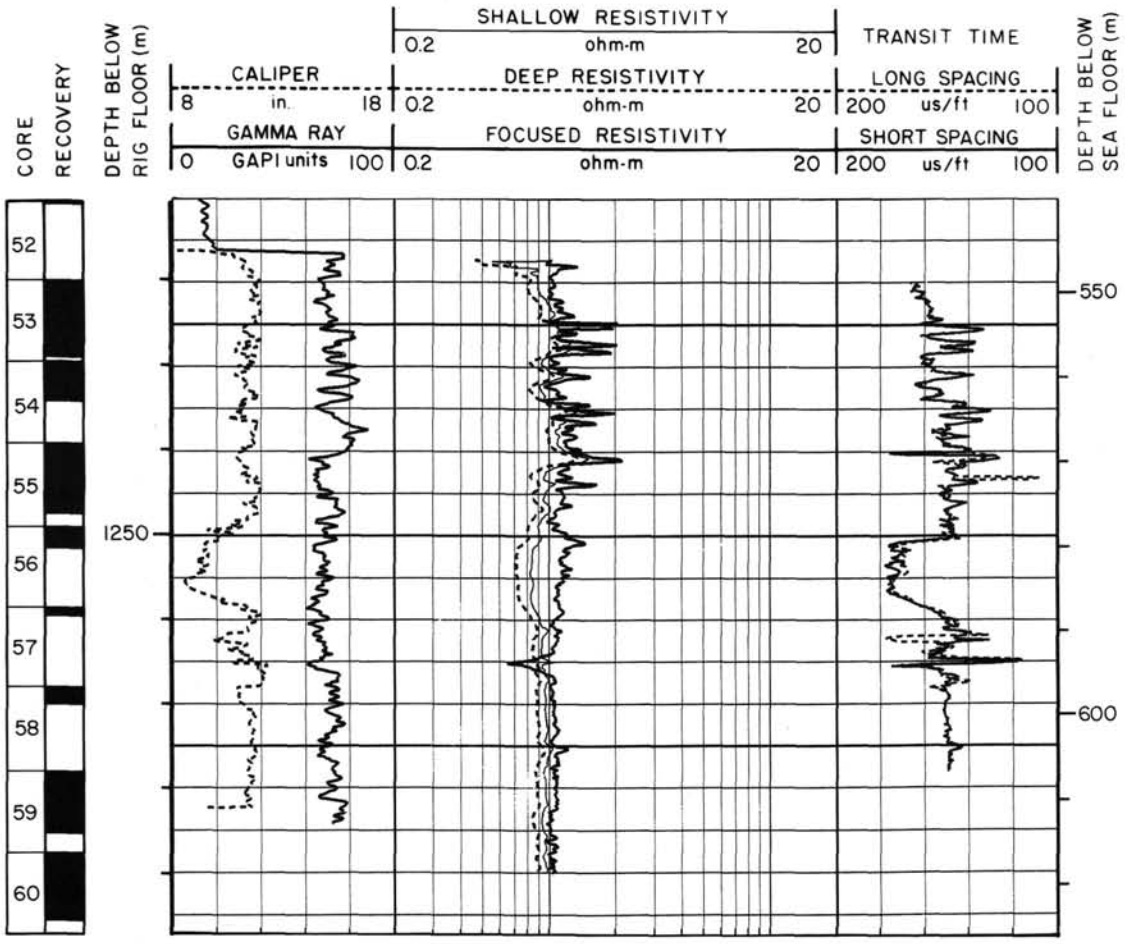

SITE 696 HOLE A CORE 1H CORED INTERVAL 649.9-655.4 mbsl: 0.0-5.5 mbsf

TIME-ROCK UNIT	BIOSTRAT. ZONE/FOSSIL CHARACTER: FORAMINIFERS	NANNOFOSSILS	RADIOLARIANS	DIATOMS	PALYNOMORPHS	PALEOMAGNETICS	PHYS. PROPERTIES	CHEMISTRY	SECTION	METERS	GRAPHIC LITHOLOGY	DRILLING DISTURB.	SED. STRUCTURES	SAMPLES
QUATERNARY	C, G	B	C, G	C, M	B				1	0.5, 1.0	VOID	0000000		* * *
			Phi (?)	*T. lentiginosa*					2					* *

LITHOLOGIC DESCRIPTION

DIATOM-BEARING SILTY MUD and MUDDY DIATOM OOZE

Major lithologies: Diatom-bearing silty mud, olive gray (5Y 4/2) to olive (5Y 4/3 grading to 5Y 4/2). Muddy diatom ooze, greenish gray (5GY 5/1) and light olive gray (5Y 6/2).

Minor lithologies: Diatom silty mud in Section 1, 87-112 cm, dark gray (N 4/0). Diatom and foraminifer-bearing sandy mud in Section 2, 37-47 and 66-83 cm, gray (5Y 5/1). Sand in Section 1, 0-12 cm, dark gray (5Y 4/1).

Lithified dropstone, 3 cm in size (granodiorite), Section 1, 83 cm. Shell fragments in Section 2, 67 cm. Faint laminae in Section 2, 58-64 cm.

SMEAR SLIDE SUMMARY (%):

	1, 1 M	1, 48 D	1, 105 D	2, 3 M	2, 23 D	2, 42 M
TEXTURE:						
Sand	87	15	2	—	—	63
Silt	10	75	68	—	—	30
Clay	10	75	68	—	—	30
COMPOSITION:						
Quartz	3	10	30	—	—	7
Feldspar	65	58	30	18	10	48
Rock fragments	3	3	5	2	1	3
Mica	—	—	1	—	—	—
Clay	1	1	—	—	—	1
Volcanic glass	3	10	30	20	15	7
Accessory minerals:						
Amphibole	3	3	—	1	1	2
Glauconite	1	1	—	—	—	Tr
Garnet	2	—	—	Tr	—	2
Heavy minerals	5	3	2	—	—	—
Opaque minerals	3	2	1	Tr	Tr	1
Micronodules	Tr	Tr	—	—	—	—
Foraminifers	5	2	1	Tr	—	20
Diatoms	5	15	30	58	73	10
Radiolarians	—	—	—	—	—	1
Sponge spicules	3	2	Tr	1	—	3
Silicoflagellates	—	—	—	—	Tr	—

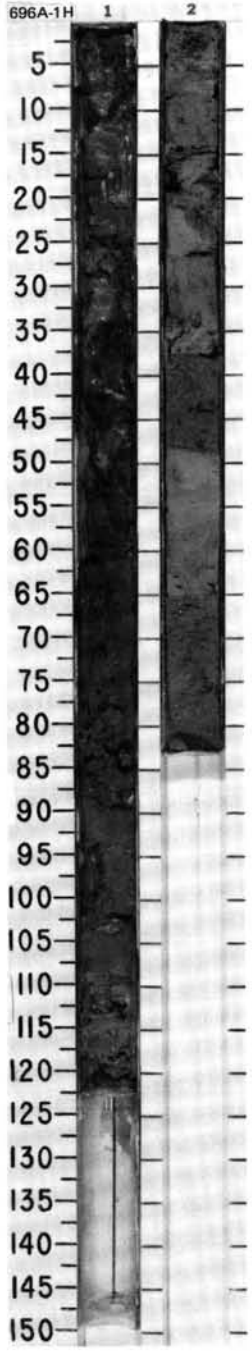

SITE 696 HOLE A CORE 2H CORED INTERVAL 652.4-661.9 mbsl; 2.5-12.0 mbsf

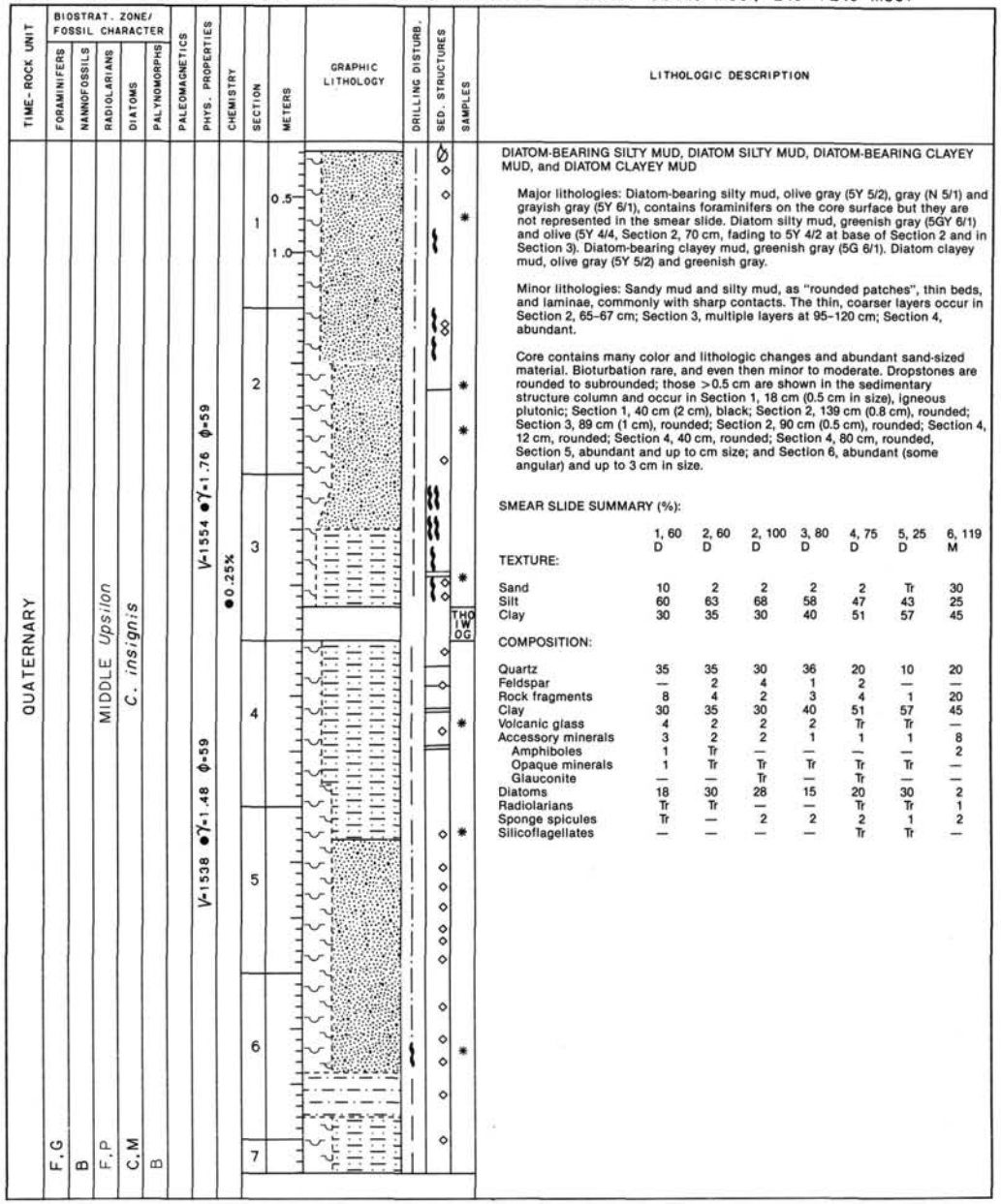

LITHOLOGIC DESCRIPTION

DIATOM-BEARING SILTY MUD, DIATOM SILTY MUD, DIATOM-BEARING CLAYEY MUD, and DIATOM CLAYEY MUD

Major lithologies: Diatom-bearing silty mud, olive gray (5Y 5/2), gray (N 5/1) and grayish gray (5Y 6/1), contains foraminifers on the core surface but they are not represented in the smear slide. Diatom silty mud, greenish gray (5GY 6/1) and olive (5Y 4/4, Section 2, 70 cm, fading to 5Y 4/2 at base of Section 2 and in Section 3). Diatom-bearing clayey mud, greenish gray (5G 6/1). Diatom clayey mud, olive gray (5Y 5/2) and greenish gray.

Minor lithologies: Sandy mud and silty mud, as "rounded patches", thin beds, and laminae, commonly with sharp contacts. The thin, coarser layers occur in Section 2, 65–67 cm; Section 3, multiple layers at 95–120 cm; Section 4, abundant.

Core contains many color and lithologic changes and abundant sand-sized material. Bioturbation rare, and even then minor to moderate. Dropstones are rounded to subrounded; those >0.5 cm are shown in the sedimentary structure column and occur in Section 1, 18 cm (0.5 cm in size), igneous plutonic; Section 1, 40 cm (2 cm), black; Section 2, 139 cm (0.8 cm), rounded; Section 3, 89 cm (1 cm), rounded; Section 2, 90 cm (0.5 cm), rounded; Section 4, 12 cm, rounded; Section 4, 40 cm, rounded; Section 4, 80 cm, rounded, Section 5, abundant and up to cm size; and Section 6, abundant (some angular) and up to 3 cm in size.

SMEAR SLIDE SUMMARY (%):

	1, 60 D	2, 60 D	2, 100 D	3, 80 D	4, 75 D	5, 25 D	6, 119 M
TEXTURE:							
Sand	10	2	2	2	2	Tr	30
Silt	60	63	68	58	47	43	25
Clay	30	35	30	40	51	57	45
COMPOSITION:							
Quartz	35	35	30	36	20	10	20
Feldspar	—	2	4	1	2	—	—
Rock fragments	8	4	2	3	4	1	20
Clay	30	35	30	40	51	57	45
Volcanic glass	4	2	2	2	Tr	Tr	—
Accessory minerals	3	2	2	1	1	1	8
Amphiboles	1	Tr	—	—	—	—	2
Opaque minerals	1	Tr	Tr	Tr	Tr	Tr	—
Glauconite	—	—	Tr	—	Tr	—	—
Diatoms	18	30	28	15	20	30	2
Radiolarians	Tr	Tr	—	—	Tr	Tr	1
Sponge spicules	Tr	—	2	2	2	1	2
Silicoflagellates	—	—	—	—	Tr	Tr	—

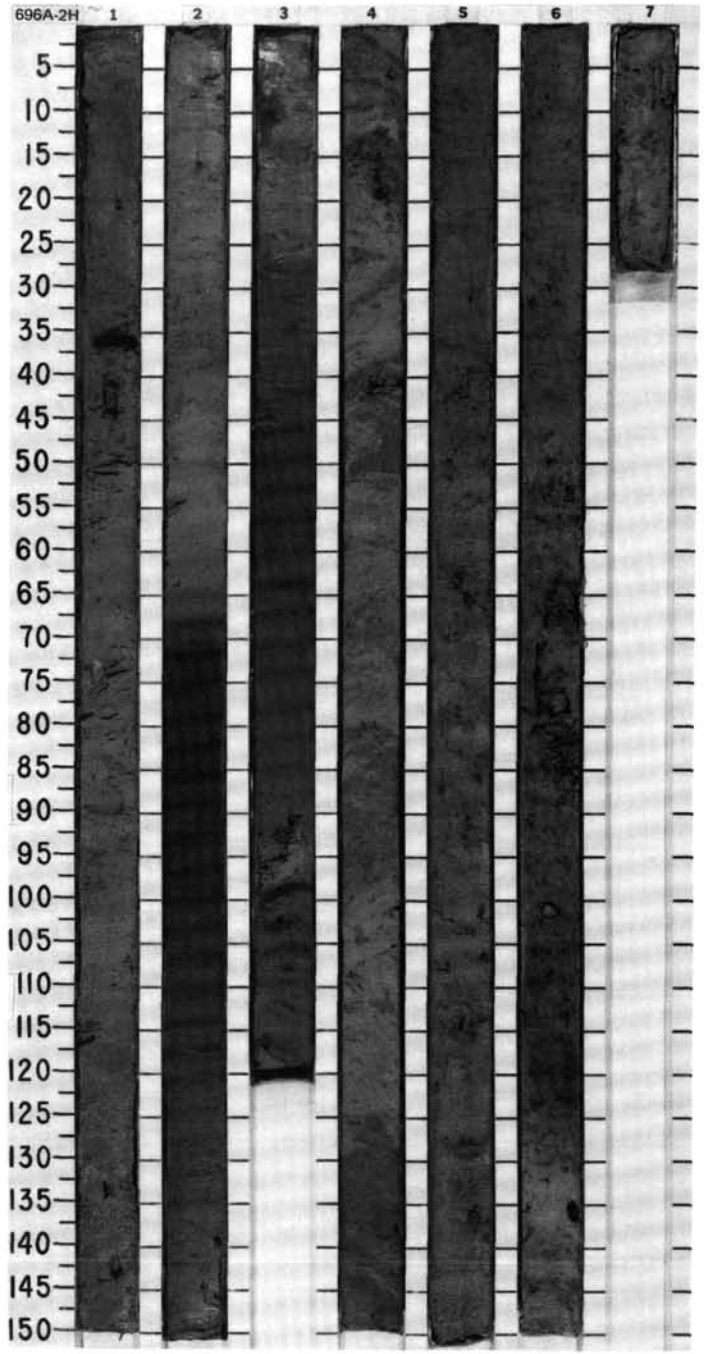

SITE 696 HOLE A CORE 3H CORED INTERVAL 661.9-671.5 mbsl; 12.0-21.6 mbsf

TIME-ROCK UNIT	BIOSTRAT. ZONE/ FOSSIL CHARACTER: FORAMINIFERS	NANNOFOSSILS	RADIOLARIANS	DIATOMS	PALYNOMORPHS	PALEOMAGNETICS	PHYS. PROPERTIES	CHEMISTRY	SECTION	METERS	GRAPHIC LITHOLOGY	DRILLING DISTURB.	SED. STRUCTURES	SAMPLES	LITHOLOGIC DESCRIPTION
UPPER PLIOCENE / MIDDLE *Upsilon*	B	B	A, G		B		γ1548 ϕ=69 γ=1548 ●		1, CC	0.5		○○○		*	DIATOM CLAYEY MUD

Major lithology: Diatom clayey mud, olive gray (5Y 5/2), strongly to moderately disturbed, partly soupy sediment.

SMEAR SLIDE SUMMARY (%):

	1, 40 D
TEXTURE:	
Sand	5
Silt	65
Clay	30
COMPOSITION:	
Quartz	11
Rock fragments	3
Clay	30
Volcanic glass	3
Accessory minerals	4
Opaque minerals	2
Amphibole	1
Diatoms	45
Sponge spicules	1

SITE 696 HOLE A CORE 4H CORED INTERVAL 671.5-681.1 mbsl; 21.6-31.2 mbsf

TIME-ROCK UNIT	BIOSTRAT. ZONE/ FOSSIL CHARACTER: FORAMINIFERS	NANNOFOSSILS	RADIOLARIANS	DIATOMS	PALYNOMORPHS	PALEOMAGNETICS	PHYS. PROPERTIES	CHEMISTRY	SECTION	METERS	GRAPHIC LITHOLOGY	DRILLING DISTURB.	SED. STRUCTURES	SAMPLES	LITHOLOGIC DESCRIPTION
UPPER PLIOCENE / MIDDLE *Upsilon*	B	B	A, G	C,M	B				1, CC	0.5, 1.0		○○○○○○○			DIATOM CLAYEY MUD

Major lithology: Diatom clayey mud, olive gray (5Y 5/2), very disturbed soupy sediment (determined from smear slide from Core 113-696A-3H).

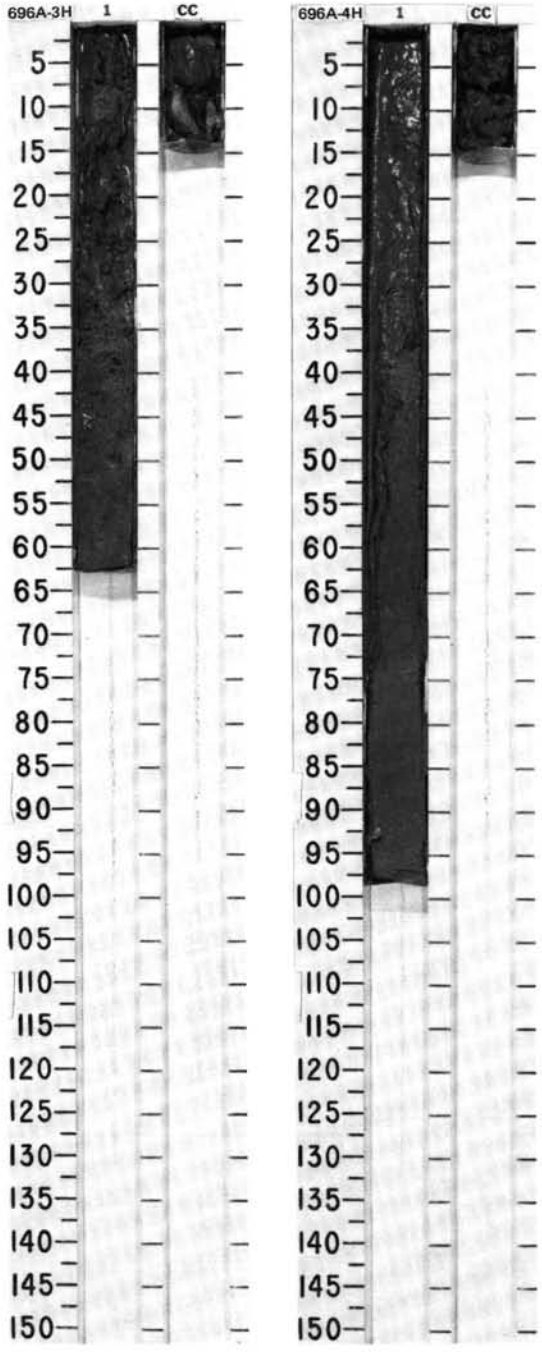

SITE 696 HOLE A CORE 5H CORED INTERVAL 681.1-690.7 mbsl; 31.2-40.8 mbsf

LITHOLOGIC DESCRIPTION

DIATOM SILTY MUD and DIATOM CLAYEY MUD

Major lithologies: Diatom silty mud and diatom clayey mud, olive gray (5Y 5/2), totally disturbed to soupy.

A few dropstones, but they are difficult to see in the disturbed core. Largest dropstone occurs in Section 2, 50 cm, and is subangular, black, and 0.6 cm wide.

SMEAR SLIDE SUMMARY (%):

	1, 90 D	2, 90 D	3, 90 D	4, 90 D
TEXTURE:				
Sand	2	1	6	4
Silt	74	64	62	60
Clay	24	35	32	36
COMPOSITION:				
Quartz	22	25	22	14
Feldspar	4	3	2	2
Rock fragments	—	1	—	Tr
Mica	2	—	4	4
Clay	24	35	32	36
Volcanic glass	2	1	2	—
Accessory minerals	2	2	—	2
Opaque minerals	4	Tr	2	4
Diatoms	40	30	36	38
Radiolarians	—	Tr	—	—
Sponge spicules	Tr	3	Tr	Tr

SITE 696 HOLE A CORE 6H CORED INTERVAL 690.7-700.3 mbsl; 40.8-50.4 mbsf

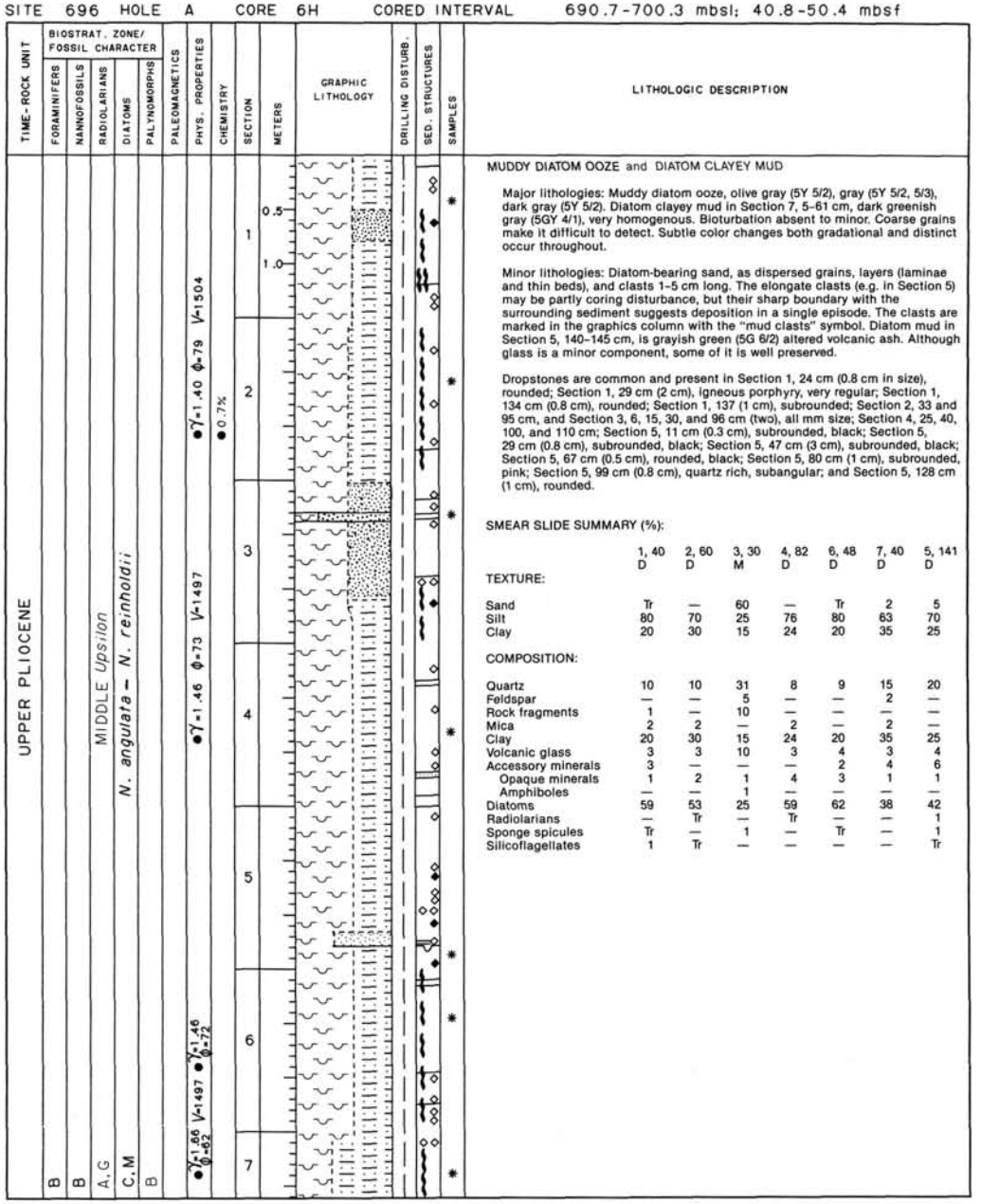

LITHOLOGIC DESCRIPTION

MUDDY DIATOM OOZE and **DIATOM CLAYEY MUD**

Major lithologies: Muddy diatom ooze, olive gray (5Y 5/2), gray (5Y 5/2, 5/3), dark gray (5Y 5/2). Diatom clayey mud in Section 7, 5–61 cm, dark greenish gray (5GY 4/1), very homogenous. Bioturbation absent to minor. Coarse grains make it difficult to detect. Subtle color changes both gradational and distinct occur throughout.

Minor lithologies: Diatom-bearing sand, as dispersed grains, layers (laminae and thin beds), and clasts 1–5 cm long. The elongate clasts (e.g. in Section 5) may be partly coring disturbance, but their sharp boundary with the surrounding sediment suggests deposition in a single episode. The clasts are marked in the graphics column with the "mud clasts" symbol. Diatom mud in Section 5, 140–145 cm, is grayish green (5G 6/2) altered volcanic ash. Although glass is a minor component, some of it is well preserved.

Dropstones are common and present in Section 1, 24 cm (0.8 cm in size), rounded; Section 1, 29 cm (2 cm), igneous porphyry, very regular; Section 1, 134 cm (0.8 cm), rounded; Section 1, 137 (1 cm), subrounded; Section 2, 33 and 95 cm, and Section 3, 6, 15, 30, and 96 cm (two), all mm size; Section 4, 25, 40, 100, and 110 cm; Section 5, 11 cm (0.3 cm), subrounded, black; Section 5, 29 cm (0.8 cm), subrounded, black; Section 5, 47 cm (3 cm), subrounded, black; Section 5, 67 cm (0.5 cm), rounded, black; Section 5, 80 cm (1 cm), subrounded, pink; Section 5, 99 cm (0.8 cm), quartz rich, subangular; and Section 5, 128 cm (1 cm), rounded.

SMEAR SLIDE SUMMARY (%):

	1, 40 D	2, 60 D	3, 30 M	4, 82 D	6, 48 D	7, 40 D	5, 141 D
TEXTURE:							
Sand	Tr	—	60	—	Tr	2	5
Silt	80	70	25	76	80	63	70
Clay	20	30	15	24	20	35	25
COMPOSITION:							
Quartz	10	10	31	8	9	15	20
Feldspar	—	—	5	—	—	2	—
Rock fragments	1	—	10	—	—	—	—
Mica	2	2	—	2	—	2	—
Clay	20	30	15	24	20	35	25
Volcanic glass	3	3	10	3	4	3	4
Accessory minerals	3	—	—	—	2	4	6
Opaque minerals	1	2	1	4	3	1	1
Amphiboles	—	—	1	—	—	—	—
Diatoms	59	53	25	59	62	38	42
Radiolarians	—	Tr	—	Tr	—	—	1
Sponge spicules	Tr	—	1	—	Tr	—	1
Silicoflagellates	1	Tr	—	—	—	—	Tr

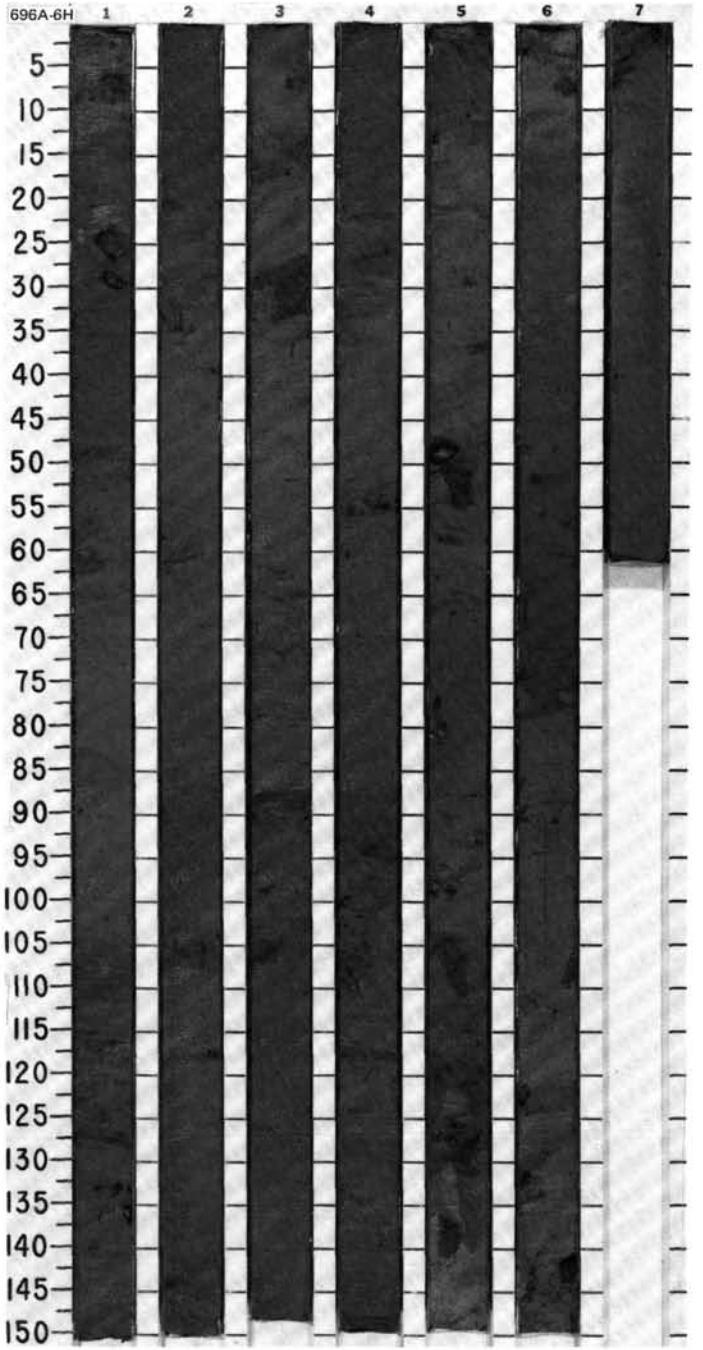

SITE 696 HOLE A CORE 7H CORED INTERVAL 700.3-709.9 mbsl; 50.4-60.0 mbsf

TIME-ROCK UNIT: UPPER PLIOCENE

BIOSTRAT. ZONE/FOSSIL CHARACTER: FORAMINIFERS: B; NANNOFOSSILS: B; RADIOLARIANS: C,G; DIATOMS: MIDDLE *Upsilon*; F,P; *N. angulata – N. reinholdii*; PALYNOMORPHS: B

PALEOMAGNETICS: ●7-1.66 Φ-67 V-1525

PHYS. PROPERTIES: ●7-1.66 Φ-67 V-1525; ●7-1.54 Φ-76 V-1500

CHEMISTRY: ● 0.6%

SECTION: 1, 2, 3, 4, 5, 6, 7, CC

METERS: 0.5, 1.0

GRAPHIC LITHOLOGY

DRILLING DISTURB.

SED. STRUCTURES

SAMPLES: PP

LITHOLOGIC DESCRIPTION

DIATOM CLAYEY MUD and MUDDY DIATOM OOZE

Major lithologies: Diatom clayey mud, dark greenish gray (5G 4/1) and greenish gray (5G 5/1), alternating on a scale of 50–80 cm. Overall core darkens from Section 1 to 5. Muddy diatom ooze, olive gray (5Y 5/2), containing dropstones and mud clasts.

Minor lithologies: Dark olive gray (5Y 3/2) and dark greenish gray (5GY 4/1) layers represent volcanic glass. Altered volcanic ash, grayish green (5G 5/2) layers are abundant in Section 5 and are observed but less common in Sections 2 and 4. Silty/sandy normally graded beds and patches are observed. Layers in Section 1, 60, 85, and 114 cm; Section 3, 14 cm(?); Section 4, 37, 54, and 112 cm; Section 5, 145–148 cm; and Section 6, 0–4 cm.

Dropstones and mud clasts occur throughout: Section 1, 74 and 148 cm (< 1 cm in size), rounded; Section 2, a few, rounded; Section 4, 126 cm (0.8 cm), rounded; Section 5, 18 and 140 cm; and Section 6, 15, 16, and 30 cm. Bioturbation is minor throughout except across volcanic layers. *Planolites* and halo burrows are present.

SMEAR SLIDE SUMMARY (%):

	1, 75 D	2, 75 D	3, 75 D	4, 75 D	5, 75 D	6, 75 D
TEXTURE:						
Sand	4	2	4	6	4	—
Silt	60	76	68	62	64	—
Clay	36	32	28	32	32	—
COMPOSITION:						
Quartz	12	10	13	18	16	10
Feldspar	2	2	2	2	2	2
Rock fragments	4	—	2	4	3	—
Mica	—	2	Tr	4	4	—
Clay	36	32	28	32	32	18
Volcanic glass	—	2	4	Tr	3	—
Accessory minerals	2	2	5	2	2	1
Glauconite	Tr	—	—	—	Tr	—
Opaque minerals	2	—	1	2	—	2
Amphibole	—	—	Tr	—	—	—
Diatoms	40	50	45	36	38	65
Radiolarians	—	—	—	Tr	—	Tr
Sponge spicules	—	—	—	Tr	—	Tr
Silicoflagellates	—	—	—	Tr	—	Tr

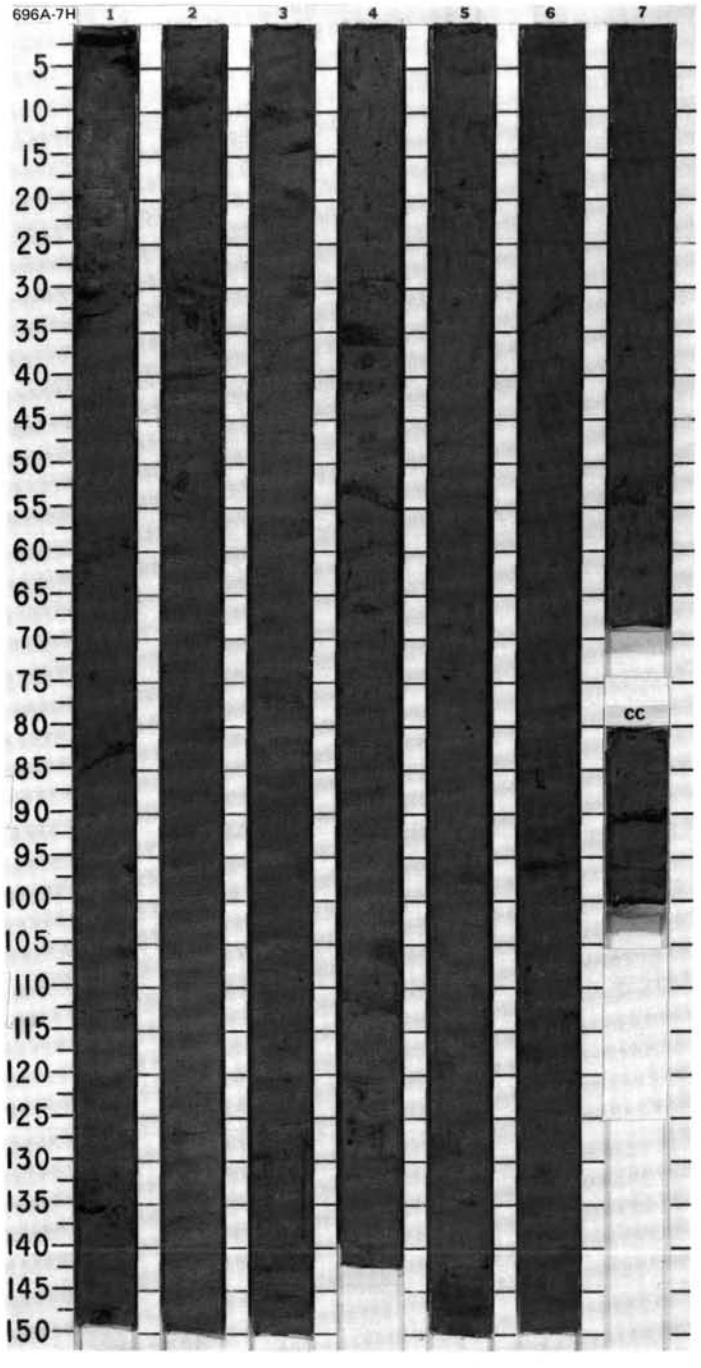

SITE 696 HOLE A CORE 8H CORED INTERVAL 709.9-719.5 mbsl; 60.0-69.6 mbsf

DIATOM CLAYEY MUD, MUDDY DIATOM OOZE, DIATOM-BEARING SILTY MUD, and DIATOM-BEARING CLAYEY MUD

Major lithologies: Diatom clayey mud in Section 1, 0–140 cm, and Section 2, 75 cm, to Section 3, 60 cm; greenish gray (5G 5/1). Muddy diatom ooze in Section 1, 150 cm, to Section 2, 75 cm, and Section 3, 60–125 cm, gray (5Y 5/1) and olive gray (5Y 5/2). Diatom-bearing silty mud in Section 3, 125 cm, to Section 5, 45 cm, dark greenish gray (5G 4/1). Diatom-bearing clayey mud in Section 5, 45 cm, through CC, dark greenish gray (5G 4/1), homogeneous sediment containing some dark gray (N 4/0) mottles. Cyclic color changes from olive gray (5Y 5/2) to greenish gray (5G 5/1) and dark greenish gray (5GY 4/1, 5G 4/1) are observed on a scale of 60–300 cm, with the light (lower) to dark (upper) transition sharp.

Minor lithologies: Altered volcanic ash layers, grayish green (5G 5/2), in thin beds as follows: Section 2, 98, 102, 107, and 115 cm; Section 4, 60–61 cm; Section 5, 100–101 and 125 cm; and Section 6, 94 cm. Silty/sandy layers and patches in Section 1, 110–150 cm, patches; Section 3, 135 cm, graded bed; Section 4, 75, 90, and 118 cm; Section 5, 10, 14, 21, and 54 cm; and Section 6, 16 cm.

Small dropstones are present throughout. Larger metamorphic dropstones occur in Section 3, at 5, 10, and 135 cm, and are 3, 5, and 2.5 cm in size, respectively. Minor bioturbation is present throughout the core.

SMEAR SLIDE SUMMARY (%):

	1, 90 D	2, 40 D	3, 95 D	4, 10 D	5, 95 D
TEXTURE:					
Sand	6	—	—	15	10
Silt	62	—	—	62	46
Clay	32	—	—	23	44
COMPOSITION:					
Quartz	16	10	8	19	16
Feldspar	2	2	—	4	3
Rock fragments	Tr	—	—	12	1
Mica	6	6	2	6	6
Clay	32	20	16	23	44
Volcanic glass	4	—	2	4	4
Accessory minerals	2	—	—	—	4
Zeolites	Tr	2	—	—	—
Opaque minerals	2	—	—	2	2
Glauconite	—	—	—	Tr	—
Diatoms	36	60	72	30	20
Radiolarians	Tr	Tr	—	—	—
Sponge spicules	Tr	—	—	—	—
Silicoflagellates	—	—	—	—	Tr

SITE 696 HOLE A CORE 9H CORED INTERVAL 719.5-729.2 mbsl; 69.6-79.3 mbsf

TIME-ROCK UNIT: UPPER PLIOCENE

BIOSTRAT. ZONE/FOSSIL CHARACTER: FORAMINIFERS: B; NANNOFOSSILS: B; RADIOLARIANS: C,G; DIATOMS: MIDDLE *Upsilon*; PALYNOMORPHS: F,P; PALEOMAGNETICS: B

PHYS. PROPERTIES: V-1525 ●γ-1.68 ϕ-62; V-1525 ●γ-1.71 ϕ-63; V-1516 ●γ-1.68 ϕ-68

CHEMISTRY: ● 0.3%

SECTION: 1, 2, 3, 4, 5, 6, CC

METERS: 0.5, 1.0

GRAPHIC LITHOLOGY

DRILLING DISTURB.

SED. STRUCTURES

SAMPLES: PP

LITHOLOGIC DESCRIPTION

DIATOM-BEARING CLAYEY MUD and DIATOM CLAYEY MUD

Major lithologies: Diatom-bearing clayey mud, dark greenish gray (5G 4/1) and greenish gray (5G 5/1). Diatom clayey mud, greenish gray (5G 5/1), darkening to dark greenish gray (5GY 4/1) in Section 6.

Minor lithologies: Altered volcanic ash, grayish green (5G 5/2), in thin beds in Section 1, 70, 105, 110–111, and 118 cm; and Section 2, 2, 8–9, and 135–136 cm. Silty/sandy mud, as clasts, patches, and layers. Layers occur in Section 1, 30 and 115 cm; Section 3, top and base; and Section 4, deformed layer at 112 cm. Volcanic glass-rich layer, Section 2, 4–6 cm.

Dropstones, rare, are present in Section 1, 1 cm (5 cm in size), subrounded; Section 5, 115 cm (1.5 cm), rounded, volcanic; Section 6, 5 cm, angular, metamorphic; and Section 6, 37 cm (3 cm), subangular, metamorphic. Bioturbation is minor to absent.

SMEAR SLIDE SUMMARY (%):

	1, 106 M	2, 60 D	3, 60 D	4, 112 M
TEXTURE:				
Sand	4	18	6	43
Silt	36	50	58	33
Clay	60	32	36	24
COMPOSITION:				
Quartz	16	20	12	44
Feldspar	—	4	6	6
Rock fragments	—	8	8	4
Mica	4	3	4	2
Clay	60	32	36	32
Volcanic glass	6	2	2	—
Accessory minerals	3	6	—	—
Zeolites	3	1	Tr	—
Opaque minerals	2	2	—	Tr
Amphiboles	—	—	—	Tr
Diatoms	12	22	30	12
Radiolarians	Tr	Tr	Tr	—
Sponge spicules	Tr	—	—	—
Silicoflagellates	—	Tr	Tr	—

CORE 113-696A-10H NO RECOVERY

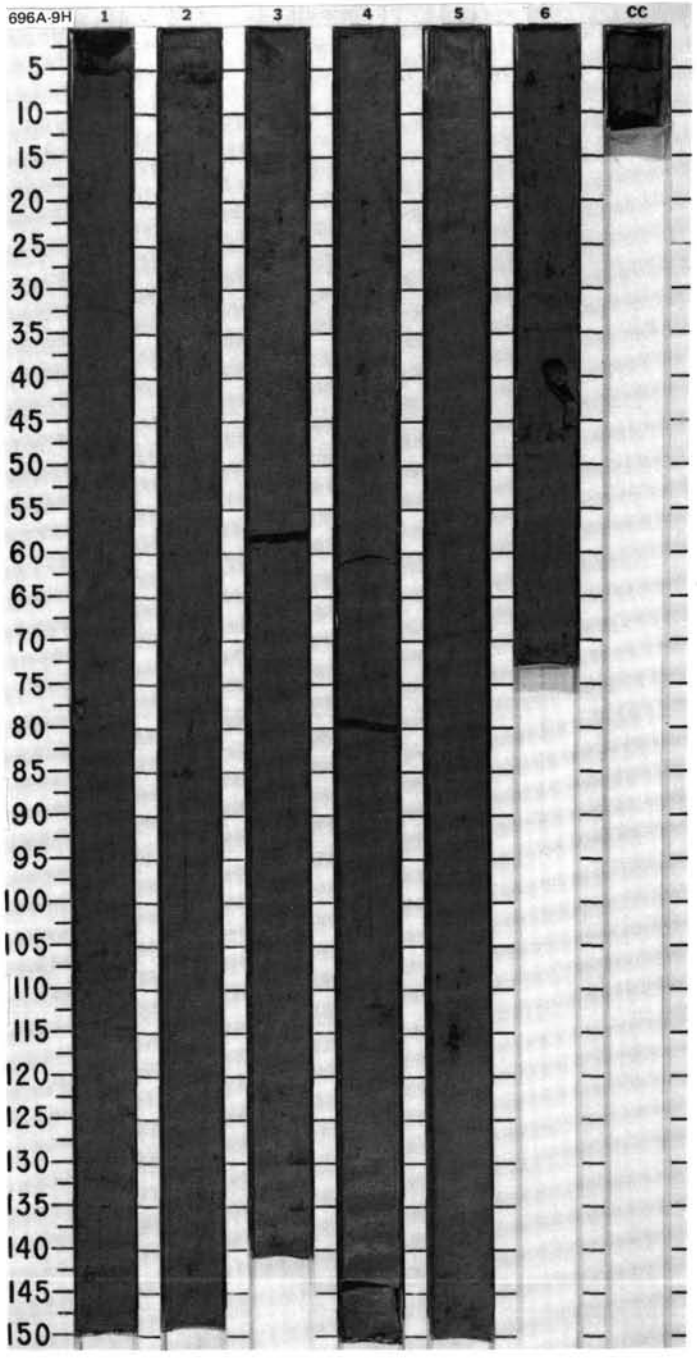

SITE 696 HOLE A CORE 11X CORED INTERVAL 738.9-746.3 mbsl; 89.0-96.4 mbsf

TIME-ROCK UNIT	BIOSTRAT. ZONE/ FOSSIL CHARACTER: FORAMINIFERS	NANNOFOSSILS	RADIOLARIANS	DIATOMS	PALYNOMORPHS	PALEOMAGNETICS	PHYS. PROPERTIES	CHEMISTRY	SECTION	METERS	GRAPHIC LITHOLOGY	DRILLING DISTURB.	SED. STRUCTURES	SAMPLES
LOWER PLIOCENE ?	B	B	UPPER *Tau* ? C,G	*N. angulata*- *N. reinholdii* C,G	B		V=3196 ?=2.71	31.2%	1	0.5 1.0				* **

LITHOLOGIC DESCRIPTION

DIATOM-BEARING SILTY MUD

Major lithology: Diatom-bearing silty mud, color grading from dark greenish gray (5GY 4/1) at 27 cm, to dark greenish gray (5BG 4/1) at 30 cm, to dark greenish gray (5G 4/1) in remainder of the core; lenslike dark greenish gray (5G 4/1) features, amid coarser silty clay (5BG 4/1), in Section 1, 40–60 and 70–110 cm; drilling-induced structures.

Minor lithology: Silty mudstone, dark greenish gray (5G 4/1), Section 1, 20–22 and 25–30 cm; mud clasts within mudstone slightly higher carbonate content than surrounding lithified sediment, diatom abundance greater in mud clasts, quartz content almost comparable.

Minor bioturbation throughout the core. Ice-rafted detritus and mm-sized dropstones occur throughout the core; cm-sized dropstones are less common and occur in a layer, Section 1, 65–70 cm; dropstones are mainly lithic fragments, subangular to rounded.

SMEAR SLIDE SUMMARY (%):

	1, 22 M	1, 22 M	1, 80 D
TEXTURE:			
Sand	2	4	5
Silt	55	66	55
Clay	43	30	40
COMPOSITION:			
Quartz	8	10	20
Feldspar	—	—	2
Mica/chlorite	—	—	2
Clay	43	30	40
Volcanic glass	—	—	1
Carbonate	40	45	—
Accessory minerals	4	5	—
Amphibole	—	—	2
Glauconite	—	—	Tr
Garnet	—	—	1
Heavy minerals	—	—	2
Opaque minerals	—	—	1
Micronodules	—	—	1
Diatoms	5	10	25
Radiolarians	—	—	2
Sponge spicules	—	—	1
Silicoflagellates	—	—	Tr

SITE 696 HOLE A CORE 12X CORED INTERVAL 746.3-752.9 mbsl; 96.4-103.0 mbsf

TIME-ROCK UNIT	FORAMINIFERS	NANNOFOSSILS	RADIOLARIANS	DIATOMS	PALYNOMORPHS	PALEOMAGNETICS	PHYS. PROPERTIES	CHEMISTRY	SECTION	METERS	GRAPHIC LITHOLOGY	DRILLING DISTURB.	SED. STRUCTURES	SAMPLES
LOWER PLIOCENE	B	B		*N. angulata*-*N. reinholdii* F,P	B				CC				*	

LITHOLOGIC DESCRIPTION

DIATOM-BEARING CLAYEY MUD

Major lithology: Diatom-bearing clayey-mud, dark greenish gray (5GY 4/1). Badly disturbed by drilling.

SMEAR SLIDE SUMMARY (%):

	CC, 2 D
TEXTURE:	
Sand	3
Silt	32
Clay	65
COMPOSITION:	
Quartz	12
Feldspar	2
Mica	Tr
Clay	65
Volcanic glass	Tr
Accessory minerals	7
Diatoms	14
Radiolarians	Tr
Sponge spicules	Tr
Silicoflagellates	Tr

CORE 113-696B-1W NO RECOVERY

SITE 696 HOLE B CORE 2R CORED INTERVAL 726.5-736.1 mbsl; 76.6-86.2 mbsf

TIME-ROCK UNIT	FORAMINIFERS	NANNOFOSSILS	RADIOLARIANS	DIATOMS	PALYNOMORPHS	PALEOMAGNETICS	PHYS. PROPERTIES	CHEMISTRY	SECTION	METERS	GRAPHIC LITHOLOGY	DRILLING DISTURB.	SED. STRUCTURES	SAMPLES
LOWER PLIOCENE	R,G	B	A,G MIDDLE *Upsilon ?*	F,P ?	B		γ=1.78 Φ=62 ● V=1487		1 CC	0.5			◆	*

LITHOLOGIC DESCRIPTION

DIATOM-BEARING CLAYEY MUD

Major lithology: Diatom-bearing clayey mud, greenish gray (5BG 5/1).

Minor lithologies: Altered volcanic ash(?), greenish gray (5BG 5/1), in three thin beds. Sandy mud (silt/sand) clast, at Section 1, 62 cm.

Drilling disturbance varies from moderate to strong (soupy sediment). No bioturbation.

SMEAR SLIDE SUMMARY (%):

	1, 70 D
TEXTURE:	
Silt	59
Clay	41
COMPOSITION:	
Quartz	24
Feldspar	2
Mica	1
Clay	41
Volcanic glass	3
Accessory minerals	7
Opaque minerals	2
Diatoms	20
Radiolarians	Tr

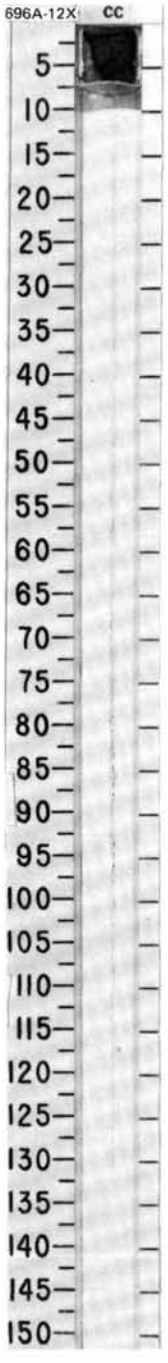

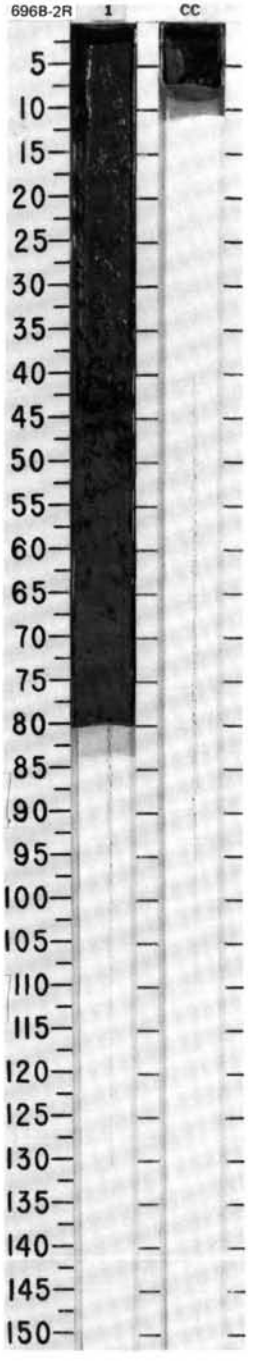

SITE 696 HOLE B CORE 3R CORED INTERVAL 736.1-745.8 mbsl; 86.2-95.9 mbsf

TIME-ROCK UNIT	BIOSTRAT. ZONE/FOSSIL CHARACTER: FORAMINIFERS	NANNOFOSSILS	RADIOLARIANS	DIATOMS	PALYNOMORPHS	PALEOMAGNETICS	PHYS. PROPERTIES	CHEMISTRY	SECTION	METERS	GRAPHIC LITHOLOGY	DRILLING DISTURB.	SED. STRUCTURES	SAMPLES
LOWER PLIOCENE	B	B	UPPER *Tau?* A,G	*N. angulata - N. reinholdii* F,P	B		γ=1.85 Φ=59 ● V=1535 ● γ=1.72 Φ=62		1, 2, 3, 4, 5, CC	0.5, 1.0				TWTHOG

LITHOLOGIC DESCRIPTION

DIATOM-BEARING CLAYEY MUD and MUDDY DIATOM OOZE

Major lithologies: Diatom-bearing clayey mud, dark greenish gray (5G 4/1). Muddy ooze in Section 4, 145 cm, through CC, dark greenish gray (5G4/1).

Minor lithologies: Diatom-bearing silty mud in Section 4, 110-142, dark greenish gray (5G 4/1). Increased coarse component occurs as laminae and dispersed grains. Sandy mud (sand/silt), as a graded layer in Section 4,142-144 and as clasts throughout the core. Clasts are rare and range in size from 1-3 cm. Their location is shown in the graphic column.

Relatively homogeneous sediment. No altered ash layers observed. Minor bioturbation. Dropstones occur in Section 2, 70 cm (0.4 cm in size), subrounded, metamorphic(?); Section 4, 130 cm (3 cm), angular, metamorphic (quartzite?); Section 5, 7 cm (0.3 cm), subrounded, black; and Section 5, 30 cm (1 cm), subrounded, shale(?), black and flat.

SMEAR SLIDE SUMMARY (%):

	1, 60 D	2, 60 D	3, 60 D	4, 142 M	5, 12 D
TEXTURE:					
Sand	Tr	Tr	Tr	60	—
Silt	52	56	52	30	—
Clay	48	44	48	10	—
COMPOSITION:					
Quartz	18	24	26	50	10
Feldspar	—	Tr	Tr	12	2
Rock fragments	6	2	6	16	—
Mica	8	7	4	—	6
Clay	48	44	48	10	15
Volcanic glass	2	6	2	6	2
Accessory minerals	4	—	2	—	3
Opaque minerals	2	2	2	—	2
Glauconite	—	Tr	—	—	—
Amphibole	—	—	—	Tr	—
Diatoms	12	15	10	6	60
Radiolarians	—	Tr	—	—	—
Sponge spicules	—	Tr	Tr	—	Tr
Silicoflagellates	—	—	—	Tr	4

CORE 113-696B-4R NO RECOVERY

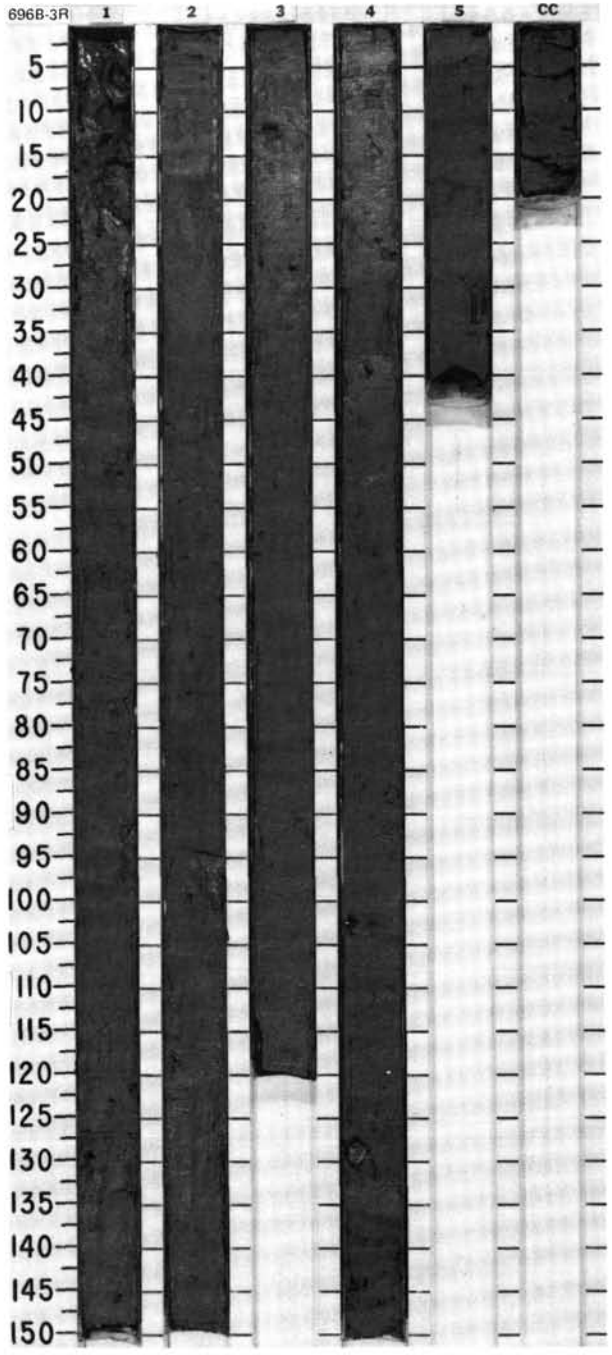

SITE 696 HOLE B CORE 5R CORED INTERVAL 755.4-765.1 mbsl; 106.5-115.2 mbsf

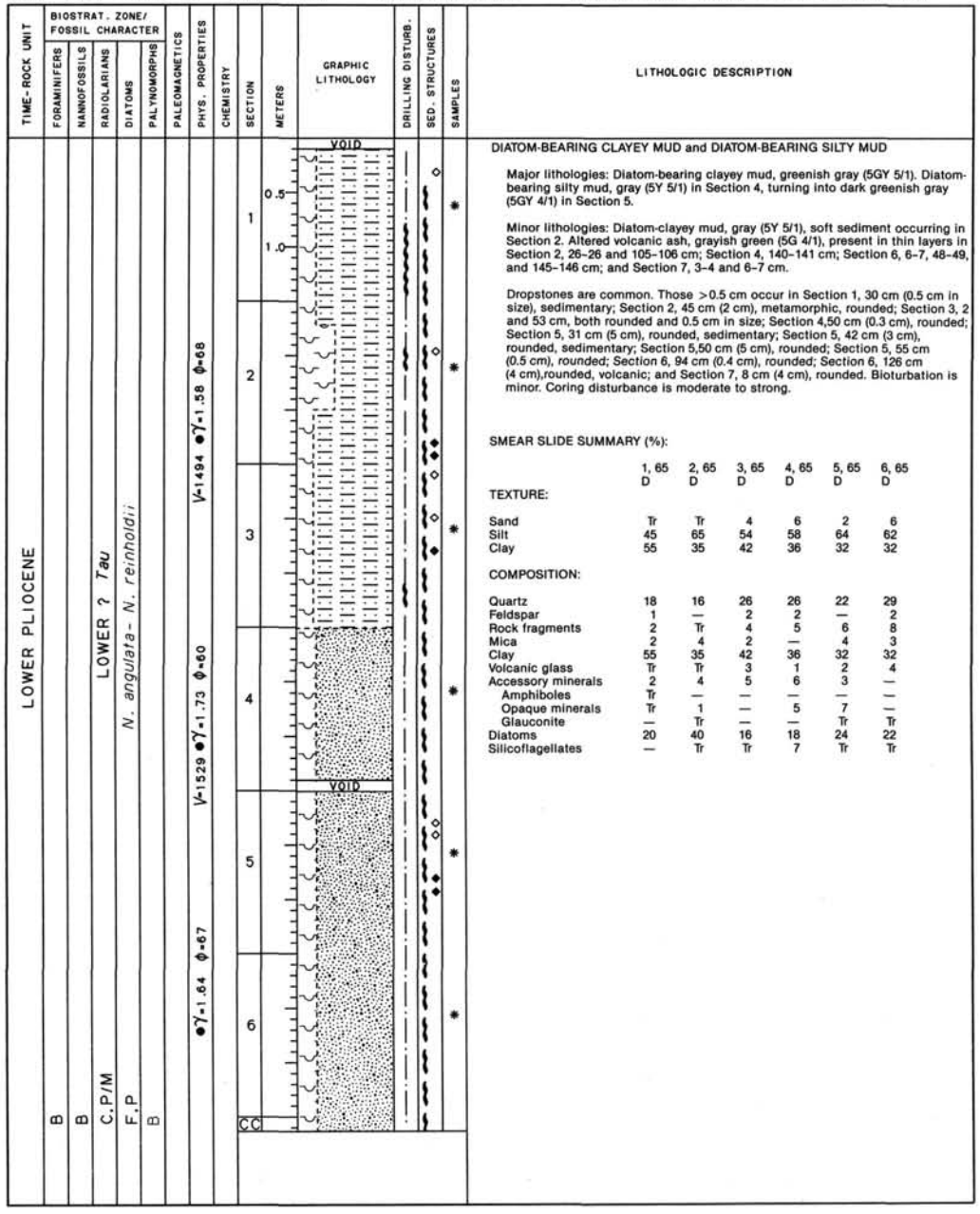

DIATOM-BEARING CLAYEY MUD and DIATOM-BEARING SILTY MUD

Major lithologies: Diatom-bearing clayey mud, greenish gray (5GY 5/1). Diatom-bearing silty mud, gray (5Y 5/1) in Section 4, turning into dark greenish gray (5GY 4/1) in Section 5.

Minor lithologies: Diatom-clayey mud, gray (5Y 5/1), soft sediment occurring in Section 2. Altered volcanic ash, grayish green (5G 4/1), present in thin layers in Section 2, 26–26 and 105–106 cm; Section 4, 140–141 cm; Section 6, 6–7, 48–49, and 145–146 cm; and Section 7, 3–4 and 6–7 cm.

Dropstones are common. Those >0.5 cm occur in Section 1, 30 cm (0.5 cm in size), sedimentary; Section 2, 45 cm (2 cm), metamorphic, rounded; Section 3, 2 and 53 cm, both rounded and 0.5 cm in size; Section 4,50 cm (0.3 cm), rounded; Section 5, 31 cm (5 cm), rounded, sedimentary; Section 5, 42 cm (3 cm), rounded, sedimentary; Section 5,50 cm (5 cm), rounded; Section 5, 55 cm (0.5 cm), rounded; Section 6, 94 cm (0.4 cm), rounded; Section 6, 126 cm (4 cm),rounded, volcanic; and Section 7, 8 cm (4 cm), rounded. Bioturbation is minor. Coring disturbance is moderate to strong.

SMEAR SLIDE SUMMARY (%):

	1, 65 D	2, 65 D	3, 65 D	4, 65 D	5, 65 D	6, 65 D
TEXTURE:						
Sand	Tr	Tr	4	6	2	6
Silt	45	65	54	58	64	62
Clay	55	35	42	36	32	32
COMPOSITION:						
Quartz	18	16	26	26	22	29
Feldspar	1	—	2	2	—	2
Rock fragments	2	Tr	4	5	6	8
Mica	2	4	2	—	4	3
Clay	55	35	42	36	32	32
Volcanic glass	Tr	Tr	3	1	2	4
Accessory minerals	2	4	5	6	3	—
Amphiboles	Tr	—	—	—	—	—
Opaque minerals	Tr	1	—	5	7	—
Glauconite	—	Tr	—	—	Tr	Tr
Diatoms	20	40	16	18	24	22
Silicoflagellates	—	Tr	Tr	7	Tr	Tr

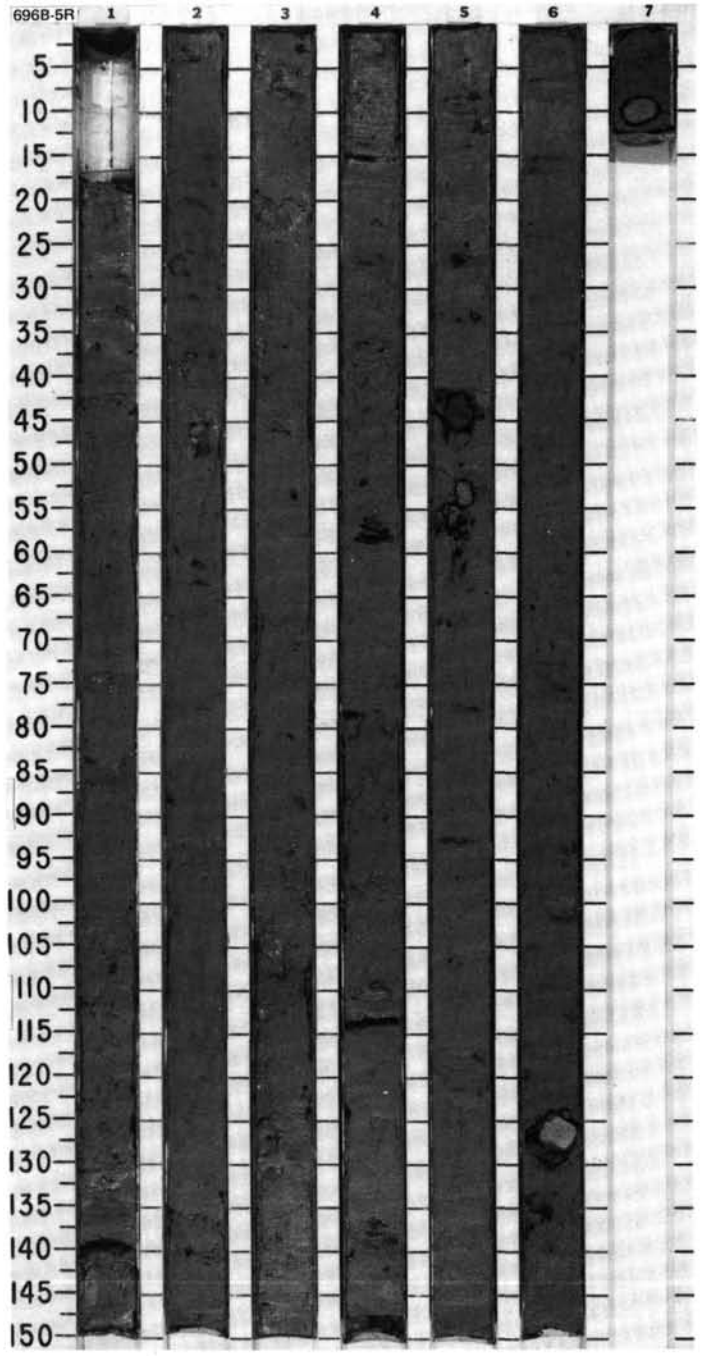

SITE 696 HOLE B CORE 6R CORED INTERVAL 765.1-774.7 mbsl; 115.2-124.8 mbsf

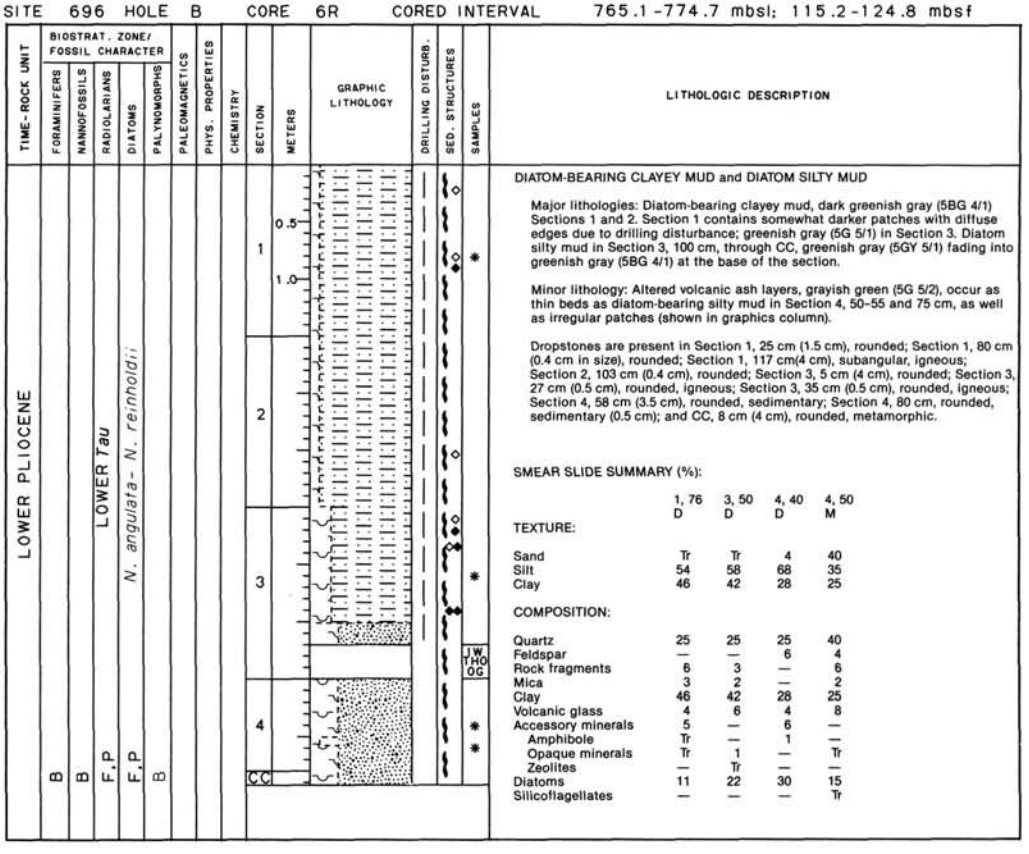

LITHOLOGIC DESCRIPTION

DIATOM-BEARING CLAYEY MUD and DIATOM SILTY MUD

Major lithologies: Diatom-bearing clayey mud, dark greenish gray (5BG 4/1) Sections 1 and 2. Section 1 contains somewhat darker patches with diffuse edges due to drilling disturbance; greenish gray (5G 5/1) in Section 3. Diatom silty mud in Section 3, 100 cm, through CC, greenish gray (5GY 5/1) fading into greenish gray (5BG 4/1) at the base of the section.

Minor lithology: Altered volcanic ash layers, grayish green (5G 5/2), occur as thin beds as diatom-bearing silty mud in Section 4, 50-55 and 75 cm, as well as irregular patches (shown in graphics column).

Dropstones are present in Section 1, 25 cm (1.5 cm), rounded; Section 1, 80 cm (0.4 cm in size), rounded; Section 1, 117 cm(4 cm), subangular, igneous; Section 2, 103 cm (0.4 cm), rounded; Section 3, 5 cm (4 cm), rounded; Section 3, 27 cm (0.5 cm), rounded, igneous; Section 3, 35 cm (0.5 cm), rounded, igneous; Section 4, 58 cm (3.5 cm), rounded, sedimentary; Section 4, 80 cm, rounded, sedimentary (0.5 cm); and CC, 8 cm (4 cm), rounded, metamorphic.

SMEAR SLIDE SUMMARY (%):

	1, 76 D	3, 50 D	4, 40 D	4, 50 M
TEXTURE:				
Sand	Tr	Tr	4	40
Silt	54	58	68	35
Clay	46	42	28	25
COMPOSITION:				
Quartz	25	25	25	40
Feldspar	—	—	6	4
Rock fragments	6	3	—	6
Mica	3	2	—	2
Clay	46	42	28	25
Volcanic glass	4	6	4	8
Accessory minerals	5	—	6	—
Amphibole	Tr	—	1	—
Opaque minerals	Tr	1	—	Tr
Zeolites	—	Tr	—	—
Diatoms	11	22	30	15
Silicoflagellates	—	—	—	Tr

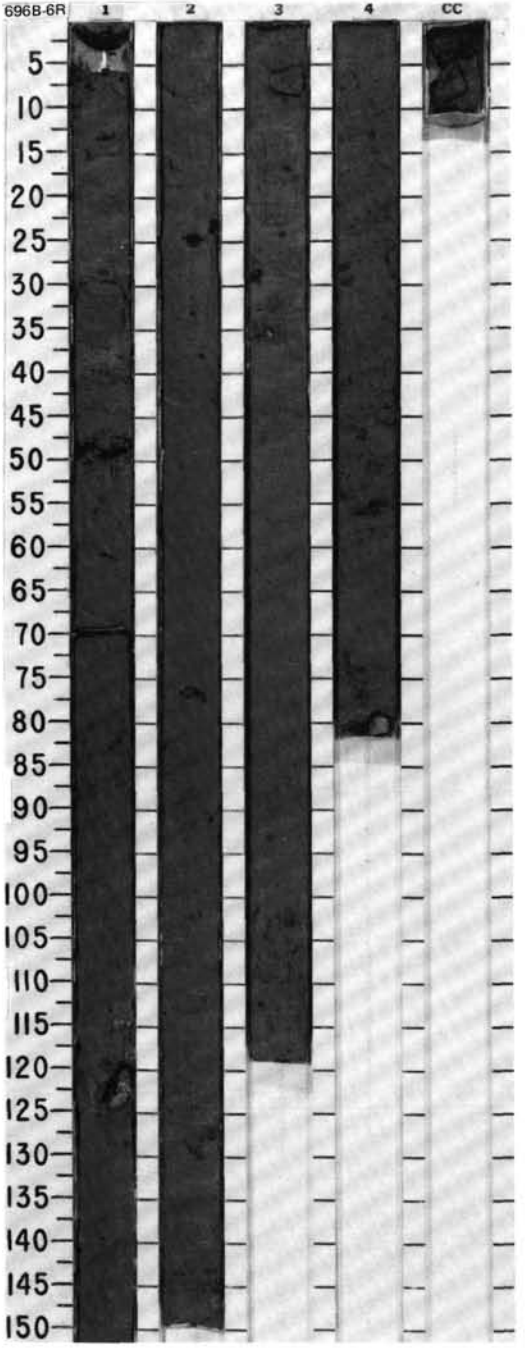

SITE 696 HOLE B CORE 7R CORED INTERVAL 774.7-784.4 mbsl; 124.8-134.5 mbsf

TIME-ROCK UNIT	FORAMINIFERS	NANNOFOSSILS	RADIOLARIANS	DIATOMS	PALYNOMORPHS	PALEOMAGNETICS	PHYS. PROPERTIES	CHEMISTRY	SECTION	METERS	GRAPHIC LITHOLOGY	DRILLING DISTURB.	SED. STRUCTURES	SAMPLES
LOWER PLIOCENE	B	B	LOWER? *Tau*	*N. angulata* - *N. reinholdii*	F,P	F,P	γ=1.79 ϕ=55 V=1521 ●		1 2 3 4 CC	0.5 1.0				* * * *

LITHOLOGIC DESCRIPTION

DIATOM-BEARING CLAYEY MUD and SILTY MUD

Major lithologies: Diatom-bearing clayey mud, dark bluish gray (5B 4/1), dark gray (N 4/0), and dark greenish gray (5BG 4/1). Silty mud, dark gray (N 4/0).

Minor lithologies: Sandy mud (silt/sand) clasts (shown in graphic column) and patches in Section 4, 10, and 95 cm. Altered volcanic ash(?), greenish gray (5G 5/2), thin layer in Section 3, 6–7 cm.

Dropstones larger than a few mm are present in Section 1, 1 cm (4 cm in size), subangular, metamorphic; Section 1, 82 cm (1 cm), rounded, igneous; *Section 1, 89 cm (0.5 cm), rounded; Section 1, 97 cm (0.5 cm), rounded;* Section 1, 147 cm, rounded, quartz; Section 2,4 cm (0.3 cm), angular, igneous; Section 2, 34 cm (0.5 cm), rounded, sedimentary; Section 2, 71 cm (0.5 cm), rounded, sedimentary; Section 2, 118 cm, subangular, metamorphic; Section 2, 135 cm (2.5 cm), red pumice; Section 3, 50 cm (2.5 cm), rounded, sedimentary; Section 3, 90 cm (2 cm), subangular, igneous; Section 4, 30 cm (2.5 cm), rounded, sedimentary; and Section 4, 88 cm (2 cm), rounded, sedimentary.

SMEAR SLIDE SUMMARY (%):

	1, 50 D	2, 105 D	3, 66 D	4, 100 M
TEXTURE:				
Sand	Tr	2	10	70
Silt	37	41	40	20
Clay	63	57	50	10
COMPOSITION:				
Quartz	18	25	32	58
Feldspar	2	2	2	10
Rock fragments	—	1	3	8
Mica	2	—	3	—
Clay	63	57	50	10
Volcanic glass	3	2	3	3
Accessory minerals	1	1	2	4
Opaque minerals	1	2	1	1
Glauconite	—	Tr	Tr	—
Hornblende	—	—	Tr	2
Diatoms	10	10	4	4
Radiolarians	Tr	—	—	—
Silicoflagellates	Tr	—	—	—

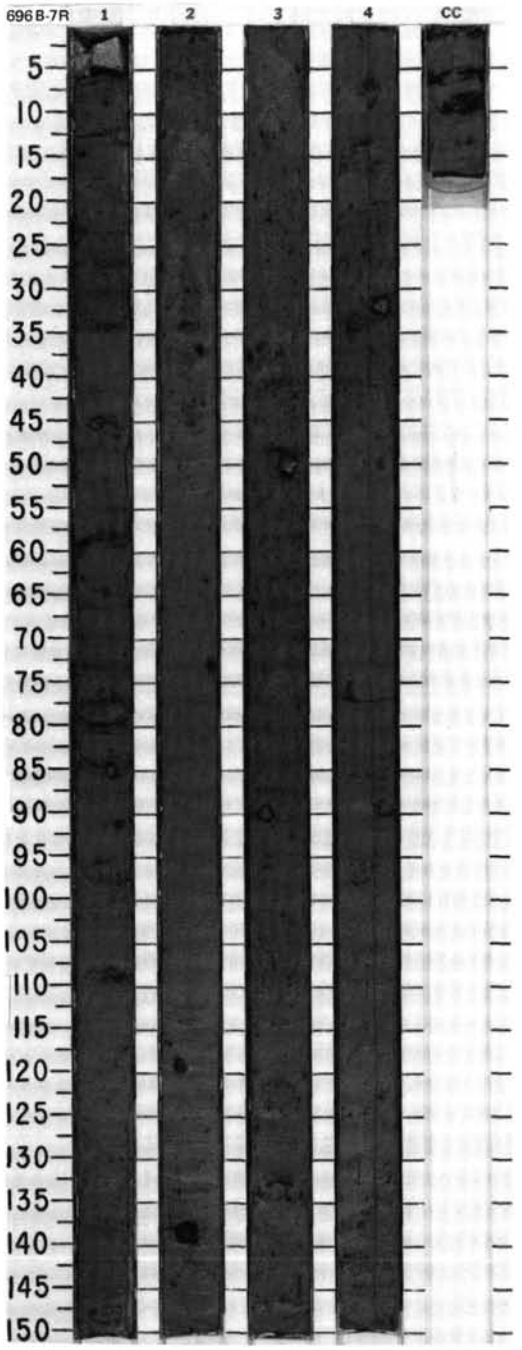

SITE 696 HOLE B CORE 8R CORED INTERVAL 784.4-794.0 mbsl; 134.5-144.1 mbsf

TIME-ROCK UNIT	BIOSTRAT. ZONE/ FOSSIL CHARACTER: FORAMINIFERS	NANNOFOSSILS	RADIOLARIANS	DIATOMS	PALYNOMORPHS	PALEOMAGNETICS	PHYS. PROPERTIES	CHEMISTRY	SECTION	METERS	GRAPHIC LITHOLOGY	DRILLING DISTURB.	SED. STRUCTURES	SAMPLES
LOWER PLIOCENE	B	B	F,P LOWER *Tau*	F,P *N. angulata - N. reinholdii*	B				1 2 CC	0.5 1.0			◇ ◇	*

LITHOLOGIC DESCRIPTION

DRILLING-INDUCED SAND

Major lithology: Coarse sand, dark bluish gray (5B 4/1), well sorted, mainly lithic fragments (75%) of which most are fine-grained sedimentary rocks; subangular. Quartz and feldspar total about 20% and some of the larger quartz grains are rounded and polished. No Fe/Mn coated grains. There is a small, fine tail-sized fraction which is mainly quartz with about 10% lithics and 5% garnet, rare hornblende, and epidote. Sand is coarse tail-graded in Section 2, 60–110 cm; lithic fragments up to 3 mm are angular slate and siltstone.

Minor lithologies: Diatom-bearing clayey mud, dark bluish gray (5B 4/1), forms *large pods, Section 1, 70–127 cm, and small pods, Section 2, 47, 51, and 73 cm.* Gravel at base of core.

Dropstones in CC, 0–5 cm (5 cm diameter), rounded diorite; and CC, 6–11 cm (5 cm), subrounded, pinkish feldspathic sandstone.

SMEAR SLIDE SUMMARY (%):

	1, 72 D
TEXTURE:	
Sand	Tr
Silt	31
Clay	69
COMPOSITION:	
Quartz	8
Feldspar	1
Mica	7
Clay	69
Accessory minerals:	
Amphibole	1
Glauconite	Tr
Heavy minerals	1
Opaque minerals	1
Diatoms	12
Sponge spicules	Tr
Silicoflagellates	Tr

CORE 113-696B-9 NO RECOVERY

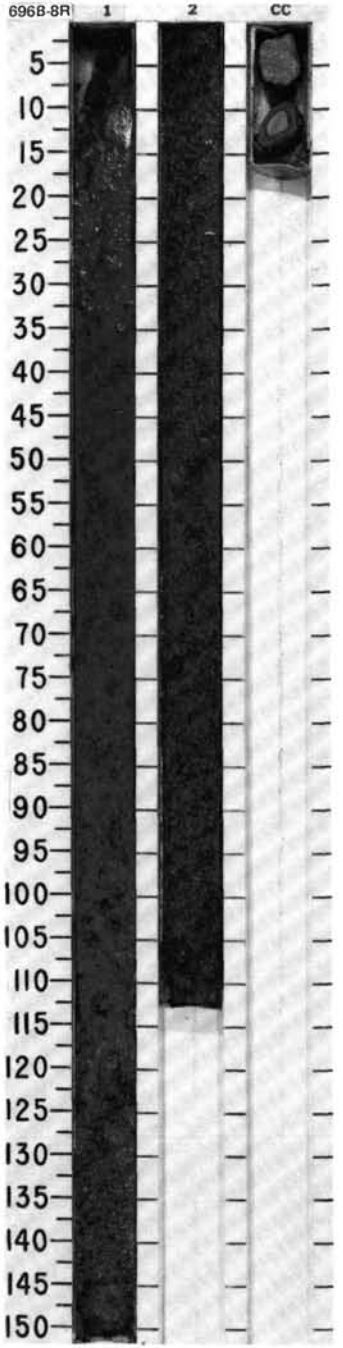

SITE 696 HOLE B CORE 10R CORED INTERVAL 794.0-803.7 mbsl; 144.1-153.8 mbsf

TIME-ROCK UNIT	BIOSTRAT. ZONE/ FOSSIL CHARACTER: FORAMINIFERS	NANNOFOSSILS	RADIOLARIANS	DIATOMS	PALYNOMORPHS	PALEOMAGNETICS	PHYS. PROPERTIES	CHEMISTRY	SECTION	METERS	GRAPHIC LITHOLOGY	DRILLING DISTURB.	SED. STRUCTURES	SAMPLES
LOWER PLIOCENE	B	B	C,P LOWER *Tau*	C,M *N. angulata — N. reinholdii*	B		•γ-1.94 φ-51 V-1571		1, 2	0.5, 1.0	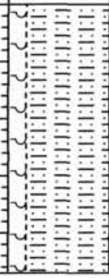			* * *

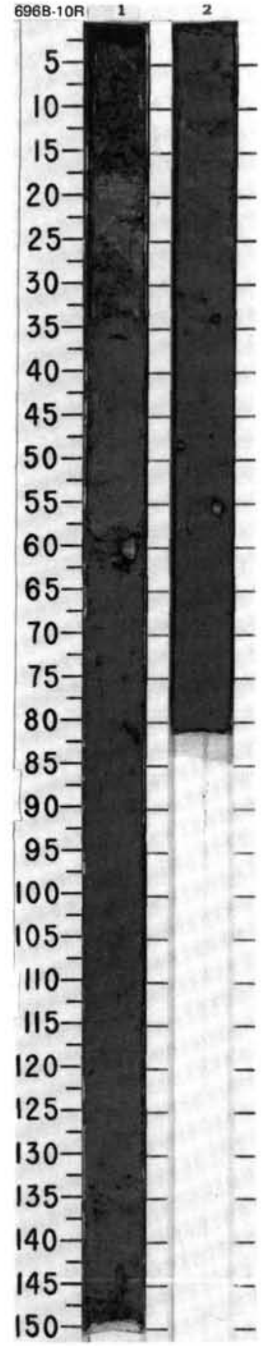

LITHOLOGIC DESCRIPTION

DIATOM-BEARING CLAYEY MUD

Major lithology: Diatom-bearing clayey mud, dark gray (N 4/0) to dark greenish gray (5G 4/1, 5BG 4/1). Color changes are subtle and gradational. Faint minor bioturbation.

Minor lithologies: Diatom-bearing clayey mud, dark greenish gray (5G 4/1), more clay than above (possibly altered volcanic ash) in Section 1, 43-44, 82-83, 89-91, and 135-136 cm; and Section 2, 5-6, 17-18, 22-23, 32-34, and 75-76 cm. Silty mud, gray 5Y 6/1 (appears white by comparison to dark mud), poorly sorted, mainly quartz. Small (1-2 mm) clasts in Section 2, 32, 56, and 58 cm.

SMEAR SLIDE SUMMARY (%):

	1, 50 D	2, 33 M	2, 58 M
TEXTURE:			
Sand	3	1	5
Silt	43	33	75
Clay	54	66	20
COMPOSITION:			
Quartz	18	8	69
Feldspar	1	Tr	7
Mica	4	5	1
Clay	54	66	20
Volcanic glass	3	2	—
Accessory minerals:			
Heavy minerals	1	1	—
Opaque minerals	2	2	—
Glauconite	2	1	—
Diatoms	15	15	3
Radiolarians	—	Tr	—
Sponge spicules	Tr	—	Tr
Silicoflagellates	Tr	Tr	—

CORE 113-696B-11R NO RECOVERY

SITE 696 HOLE B CORE 12R CORED INTERVAL 813.4-823.1 mbsl; 163.5-173.2 mbsf

TIME-ROCK UNIT	FORAMINIFERS	NANNOFOSSILS	RADIOLARIANS	DIATOMS	PALYNOMORPHS	PALEOMAGNETICS	PHYS. PROPERTIES	CHEMISTRY	SECTION	METERS	GRAPHIC LITHOLOGY	DRILLING DISTURB.	SED. STRUCTURES	SAMPLES
LOWER PLIOCENE / UPPER MIOCENE ?	B	B	MIOCENE ? F,P	? *D. hustedtii* F,P	B				1	0.5	VOID			*

LITHOLOGIC DESCRIPTION

DIATOM-BEARING CLAYEY MUD

Major lithology: Diatom-bearing clayey mud, dark gray (N 4/0); scattered sand grains throughout, too disturbed for preservation of primary structures.

SMEAR SLIDE SUMMARY (%):

	1, 50 D
TEXTURE:	
Sand	2
Silt	41
Clay	57
COMPOSITION:	
Quartz	12
Feldspar	1
Mica	5
Clay	57
Volcanic glass	2
Accessory minerals:	
Glauconite	Tr
Heavy minerals	2
Amphibole	1
Opaque minerals	2
Diatoms	18
Radiolarians	Tr

SITE 696 HOLE B CORE 13R CORED INTERVAL 823.1-832.8 mbsl; 173.2-182.9 mbsf

TIME-ROCK UNIT	FORAMINIFERS	NANNOFOSSILS	RADIOLARIANS	DIATOMS	PALYNOMORPHS	PALEOMAGNETICS	PHYS. PROPERTIES	CHEMISTRY	SECTION	METERS	GRAPHIC LITHOLOGY	DRILLING DISTURB.	SED. STRUCTURES	SAMPLES
LOWER PLIOCENE / UPPER MIOCENE ?	B	B	F,P ?	R,P ?	B		γ=2.03 ϕ=45 ●		1	0.5			◆ ◇ ◇ ◆	* *

LITHOLOGIC DESCRIPTION

CLAYEY MUD

Major lithology: Clayey mud, dark greenish gray (5G 4/1); color change below Section 1, 60 cm, to dark gray (N 4/0); contact is moderately disturbed.

Scattered sand grains throughout; 6 cm rounded dropstone, sandstone, at Section 1, 10 cm.

SMEAR SLIDE SUMMARY (%):

	1, 47 D	1, 62 D
TEXTURE:		
Sand	2	5
Silt	35	22
Clay	61	73
COMPOSITION:		
Quartz	25	20
Feldspar	1	—
Mica	2	2
Clay	61	73
Accessory minerals:		
Opaque minerals	1	1
Amphibole	1	—
Heavy minerals	1	1
Micronodules	Tr	—
Diatoms	7	3
Radiolarians	1	—
Sponge spicules	Tr	—

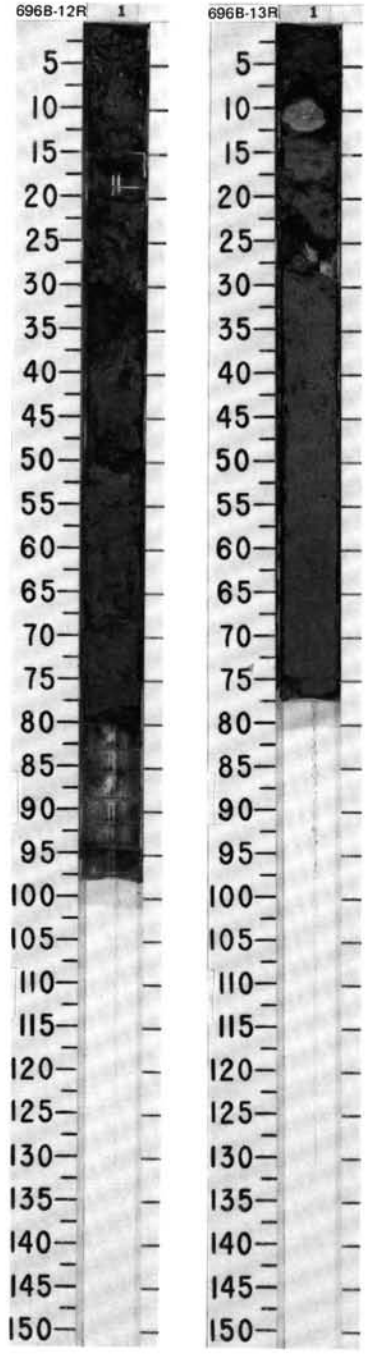

CORE 113-696B-14R NO RECOVERY

CORE 113-696B-15R NO RECOVERY

CORE 113-696B-16R NO RECOVERY

SITE 696 HOLE B CORE 17R CORED INTERVAL 861.7-871.3 mbsl; 211.8-221.5 mbsf

TIME-ROCK UNIT	BIOSTRAT. ZONE/ FOSSIL CHARACTER: FORAMINIFERS	NANNOFOSSILS	RADIOLARIANS	DIATOMS	PALYNOMORPHS	PALEOMAGNETICS	PHYS. PROPERTIES	CHEMISTRY	SECTION	METERS	GRAPHIC LITHOLOGY	DRILLING DISTURB.	SED. STRUCTURES	SAMPLES
UPPER MIOCENE	B	B	F, P/M UPPER *C. spongothorax*	C, G *D. hustedtii*	B		V=1580 ●γ=1.90 ϕ=50		1, 2, CC	0.5, 1.0			◇◇	*

LITHOLOGIC DESCRIPTION

DIATOM-BEARING CLAYEY MUD

Major lithology: Diatom-bearing clayey mud, dark gray (N 4/0), Section 1, top, gradual transition to dark greenish gray (5GY 4/1) which occurs at about Section 1, 70 cm, through Section 2.

Minor lithologies: Diatom clayey mud in Section 1, 18–23 cm, dark gray (5Y 4/1), sharp color contacts with surrounding sediment. Patches of sandy mud in Section 1, 53–55, 72–75, 79–81, 121–123, and 130–134 cm; Section 2, 10–13 cm; and CC 9–11 cm; dark gray (5Y 4/1). Dark greenish gray (5GY 4/1) ashy layers(?), Section 2, 16–17 and 28–29 cm.

Dropstones in Section 1, 2–5 cm (2 cm), rounded siltstone; Section 1, 11–14 cm (2 cm), angular slate; Section 1, 73–75 cm (2 cm), angular mudstone; Section 1, 81–82 cm (0.7 cm), angular mudstone; Section 2, 4–5 cm (1 cm), subrounded mudstone; and Section 2, 5–6 cm, angular slate.

SMEAR SLIDE SUMMARY (%):

	1, 90 D	1, 20 M
TEXTURE:		
Sand	7	10
Silt	36	42
Clay	57	48
COMPOSITION:		
Quartz	10	15
Feldspar	Tr	1
Mica	2	1
Clay	57	48
Accessory minerals:		
Micronodules	—	Tr
Opaque minerals	2	2
Heavy minerals	1	1
Garnet	1	Tr
Amphibole	—	Tr
Diatoms	25	30
Radiolarians	2	2
Sponge spicules	Tr	—

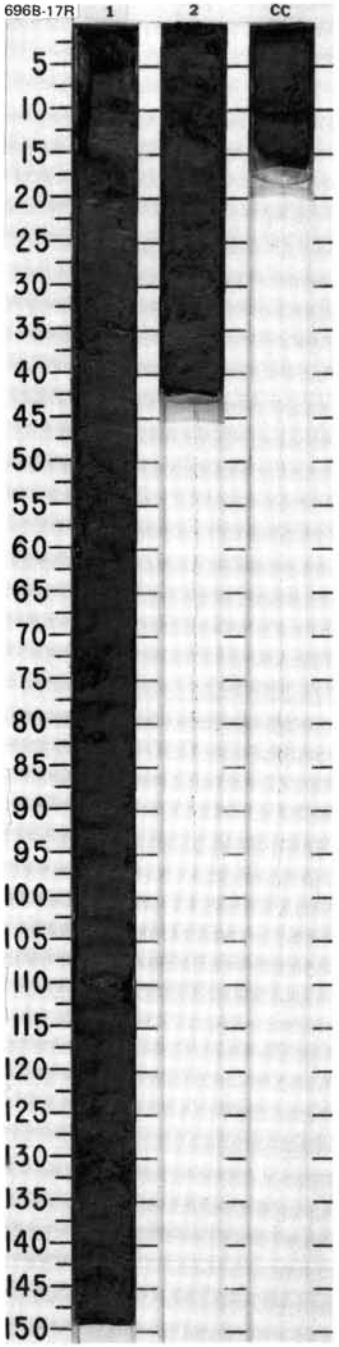

CORE 113-696B-18 NO RECOVERY

SITE 696 HOLE B CORE 19R CORED INTERVAL 871.3-880.9 mbsl; 221.5-231.1 mbsf

TIME-ROCK UNIT	BIOSTRAT. ZONE/ FOSSIL CHARACTER: FORAMINIFERS	NANNOFOSSILS	RADIOLARIANS	DIATOMS	PALYNOMORPHS	PALEOMAGNETICS	PHYS. PROPERTIES	CHEMISTRY	SECTION	METERS	GRAPHIC LITHOLOGY	DRILLING DISTURB.	SED. STRUCTURES	SAMPLES
UPPER MIOCENE	B	B	F/C,P	C,M	B				1				◇	*

LITHOLOGIC DESCRIPTION

DIATOM OOZE

Major lithology: Diatom ooze, olive gray (5Y 4/2), minor bioturbation.

Minor lithology: Muddy diatom ooze, dark gray (5Y 4/1), Section 1, 0–6 cm (silty) and 25–27 cm (clayey).

Dropstone at Section 1, 7 cm (6 mm in size), black siltstone, rounded.

SMEAR SLIDE SUMMARY (%):

	1, 5 M	1, 23 D	1, 27 M
COMPOSITION:			
Quartz	17	6	13
Feldspar	3	1	2
Clay	10	5	20
Volcanic glass	—	—	1
Accessory minerals	2	1	1
Micronodules	1	—	Tr
Diatoms	67	86	63
Radiolarians	—	Tr	—
Sponge spicules	—	1	—
Silicoflagellates	Tr	—	—

SITE 696 HOLE B CORE 20R CORED INTERVAL 881.0-890.7 mbsl; 231.1-240.8 mbsf

TIME-ROCK UNIT	BIOSTRAT. ZONE/ FOSSIL CHARACTER: FORAMINIFERS	NANNOFOSSILS	RADIOLARIANS	DIATOMS	PALYNOMORPHS	PALEOMAGNETICS	PHYS. PROPERTIES	CHEMISTRY	SECTION	METERS	GRAPHIC LITHOLOGY	DRILLING DISTURB.	SED. STRUCTURES	SAMPLES
UPPER MIOCENE	B	B	C,M	C,M	B				1	0.5			◇	*
										1.0			◇	
			C. spongothorax	D. hustedtii					2				◇	*
									3				◇	*
									4					*

LITHOLOGIC DESCRIPTION

MUDDY DIATOM OOZE and DIATOM OOZE

Major lithology: Muddy diatom ooze, olive gray (5Y 5/2), sponge-textured sediment showing some darker patches with diffuse edges, possibly due to drilling disturbance (which is moderate). Diatom ooze, olive gray (5Y 5/2), 'spongy' sediment containing some dropstones. Sharp contacts (probably caused by drilling) to minor lithology (see below).

Minor lithology: Diatom-bearing clayey mud, dark bluish gray (5B 4/1) layer at base of Section 3 and top of Section 4. Very sharp contacts to surrounding lithology.

Several dropstones <1 cm in size throughout. Dropstones >1 cm are also abundant and present in Section 1, well rounded igneous and metasediments; Section 2, rounded to subangular, metamorphics and metasediments; and Section 3, igneous and metasediments. About 10% sand-sized quartz observed in the smear slides.

SMEAR SLIDE SUMMARY (%):

	1, 50 D	2, 50 D	3, 50 D	3, 148 M
COMPOSITION:				
Quartz	25	22	10	28
Feldspar	4	—	—	Tr
Rock fragments	2	—	—	Tr
Mica	2	4	2	2
Clay	10	14	7	41
Volcanic glass	3	2	—	2
Accessory minerals	2	—	—	6
Opaque minerals	1	3	1	2
Amphibole	—	Tr	—	—
Diatoms	50	55	80	20

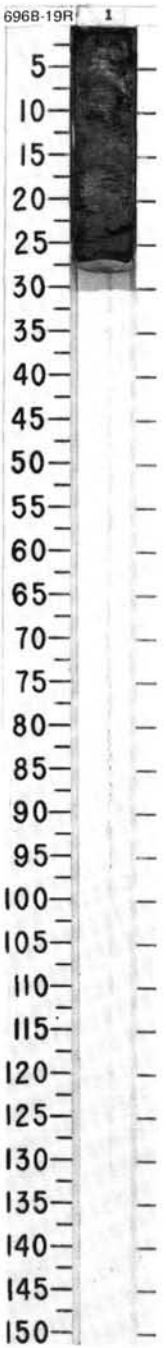

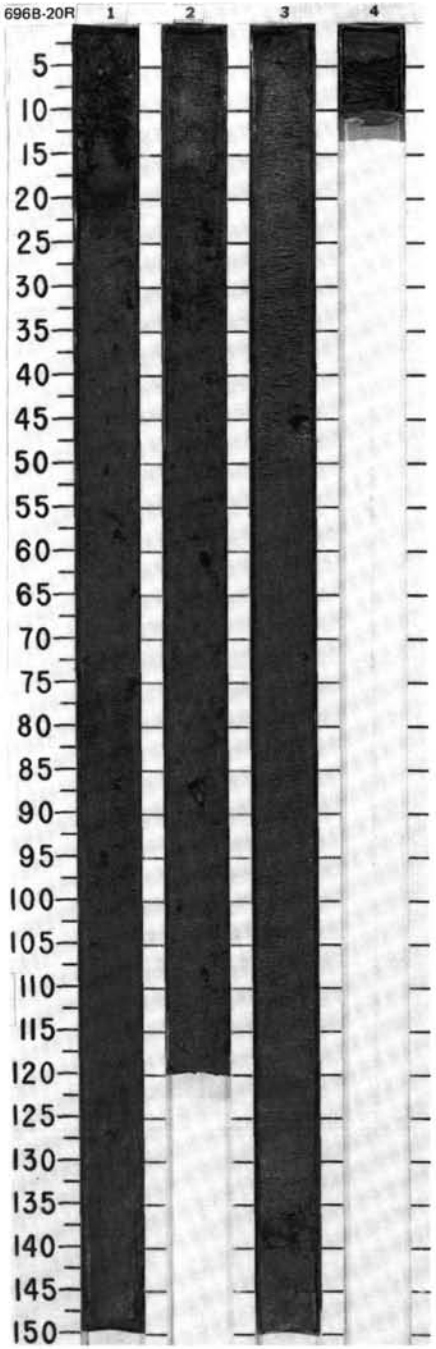

SITE 696 HOLE B CORE 21R CORED INTERVAL 890.7-900.3 mbsl; 240.8-250.4 mbsf

TIME-ROCK UNIT	BIOSTRAT. ZONE/ FOSSIL CHARACTER: FORAMINIFERS	NANNOFOSSILS	RADIOLARIANS	DIATOMS	PALYNOMORPHS	PALEOMAGNETICS	PHYS. PROPERTIES	CHEMISTRY	SECTION	METERS	GRAPHIC LITHOLOGY	DRILLING DISTURB.	SED. STRUCTURES	SAMPLES
UPPER MIOCENE	B	B	R/F,P *C. spongothorax*	C,M *D. hustedtii*	B				1, 2, 3	0.5, 1.0			◇	*

LITHOLOGIC DESCRIPTION

DIATOM OOZE and MUD-BEARING DIATOM OOZE

Major lithologies: Diatom ooze, olive (5Y 5/4 and 5Y 5/3) with olive gray in Section 1, 0–9 and 25–35 cm, and dark olive gray patches (5Y 3/2) in Section 1, 120–150 cm. Mud-bearing diatom ooze, gray (5Y 5/1). Minor color changes are present, but are too subtle to be detected with the Munsell Color Chart.

Dropstones (>0.3 cm) are present in Section 1, 55 cm (0.6 cm), subrounded sandstone; Section 2, 10 cm (1 cm), subrounded carbonate-cemented sandstone; Section 2, 100 cm (1 cm), subrounded sandstone; Section 2, 114 cm (1 cm), angular micaceous metasediment; and Section 2, 140 cm (1.5 cm), angular shale. Section 3, 18–30 cm (four 1 cm), black subrounded metasediments. No CC.

SMEAR SLIDE SUMMARY (%):

	1, 50 D	2, 50 D	3, 50 D
COMPOSITON:			
Quartz	4	10	9
Feldspar	—	—	2
Rock fragments	—	—	Tr
Mica	2	—	4
Clay	—	10	10
Volcanic glass	—	—	1
Accessory minerals	2	5	6
Opaque minerals	—	Tr	3
Diatoms	92	75	65

SITE 696 HOLE B CORE 22R CORED INTERVAL 900.3-910.0 mbsl; 250.4-260.1 mbsf

TIME-ROCK UNIT	BIOSTRAT. ZONE/ FOSSIL CHARACTER: FORAMINIFERS	NANNOFOSSILS	RADIOLARIANS	DIATOMS	PALYNOMORPHS	PALEOMAGNETICS	PHYS. PROPERTIES	CHEMISTRY	SECTION	METERS	GRAPHIC LITHOLOGY	DRILLING DISTURB.	SED. STRUCTURES	SAMPLES
UPPER MIOCENE	R,M	F,G	F/C,M *C. spongothorax*	C,M *D. hustedtii*	B				1				◇	*

LITHOLOGIC DESCRIPTION

MUDDY DIATOM OOZE

Major lithology: Muddy diatom ooze, olive gray (5Y 5/2), very disturbed spongy sediment containing two large (6–7 cm) dropstones. Bioturbation not evident.

SMEAR SLIDE SUMMARY (%):

	1, 22 D
COMPOSITION:	
Quartz	15
Mica	2
Clay	9
Accessory minerals	3
Opaque minerals	1
Diatoms	70

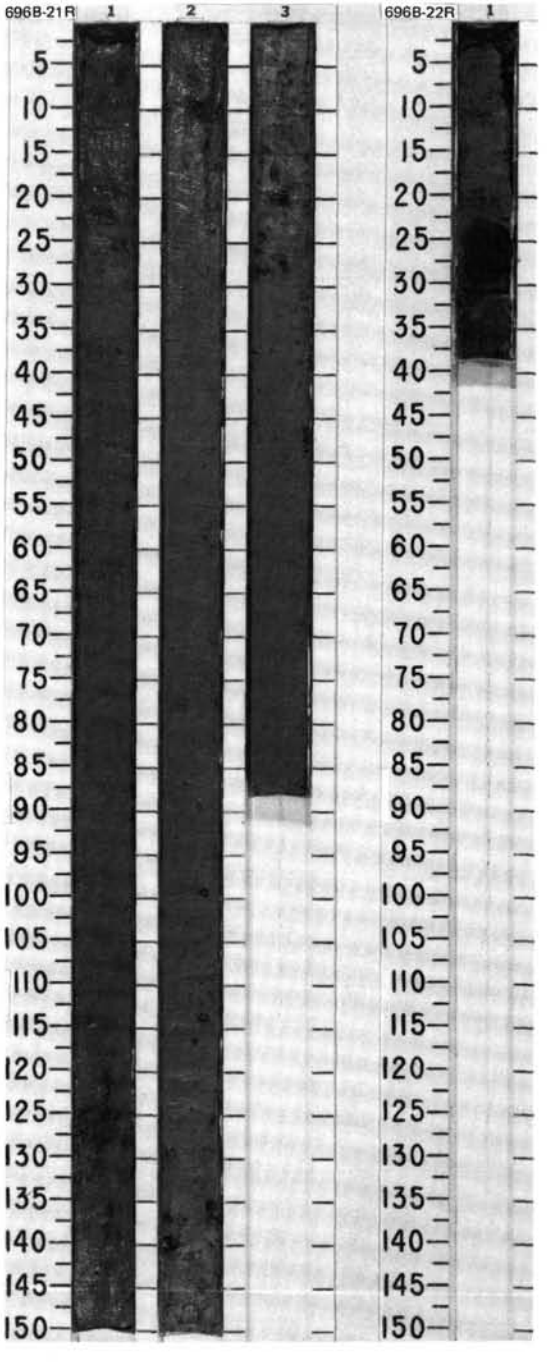

SITE 696 HOLE B CORE 23R CORED INTERVAL 910.0-919.6 mbsl; 260.1-269.7 mbsf

TIME-ROCK UNIT	FORAMINIFERS	NANNOFOSSILS	RADIOLARIANS	DIATOMS	PALYNOMORPHS	PALEOMAGNETICS	PHYS. PROPERTIES	CHEMISTRY	SECTION	METERS	GRAPHIC LITHOLOGY	DRILLING DISTURB.	SED. STRUCTURES	SAMPLES
UPPER MIOCENE	B	B	*C. spongothorax* F/C,M	*D. hustedtii* F,P	B				1, 2, 3, 4, 5, 6	0.5, 1.0				IW 10 THS; *

BIOSTRAT. ZONE/ FOSSIL CHARACTER

LITHOLOGIC DESCRIPTION

COARSE SAND

Major lithology: Coarse angular sand, dark gray (N 4/0), completely homogenized by drilling.

Minor lithology: Diatom silty mud, dark greenish gray (5G 4/1), occurring in lower 2 cm of Section 6.

SMEAR SLIDE SUMMARY (%):

	6, 42 M
TEXTURE:	
Sand	10
Silt	70
Clay	20
COMPOSITION:	
Quartz	25
Feldspar	6
Rock fragments	7
Mica	2
Clay	20
Accessory minerals	6
Opaque minerals	4
Diatoms	30

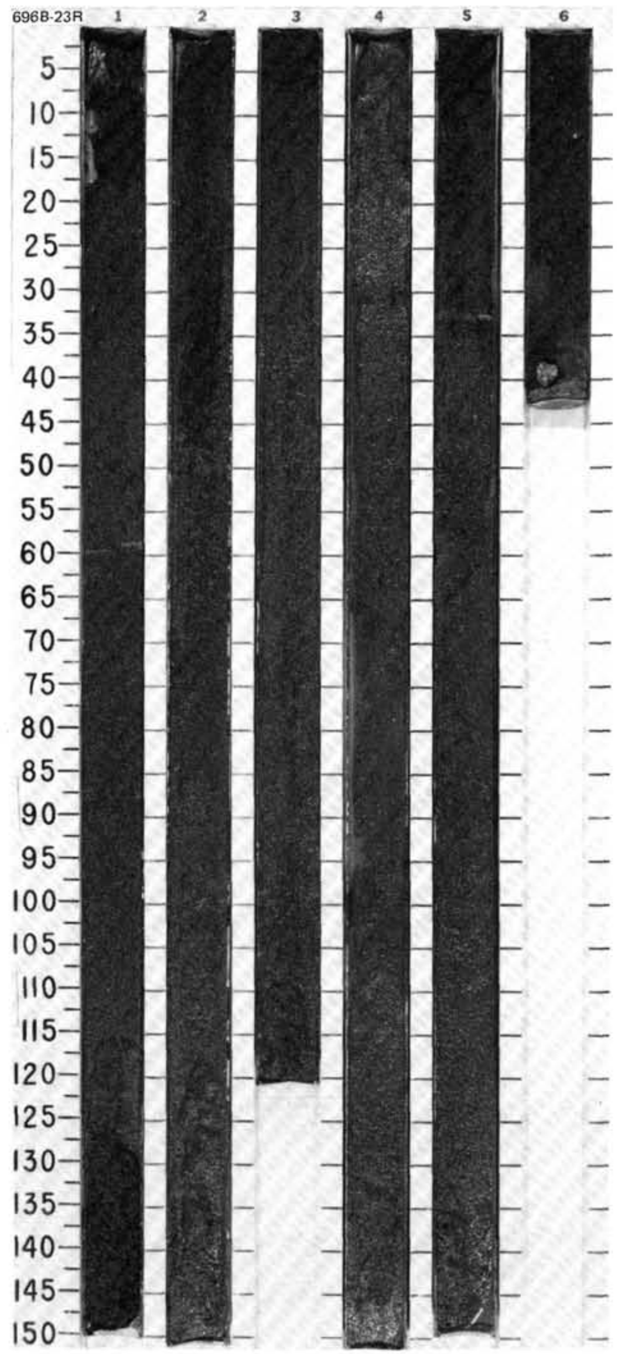

SITE 696 HOLE B CORE 24R CORED INTERVAL 919.6-929.3 mbsl; 269.7-279.4 mbsf

TIME-ROCK UNIT	FORAMINIFERS	NANNOFOSSILS	RADIOLARIANS	DIATOMS	PALYNOMORPHS	PALEOMAGNETICS	PHYS. PROPERTIES	CHEMISTRY	SECTION	METERS	GRAPHIC LITHOLOGY	DRILLING DISTURB.	SED. STRUCTURES	SAMPLES
UPPER MIOCENE	B	B	R/F, P/M *C. spongothorax*	C, M *D. hustedtii*	B		γ=1.617 ●γ=1.79 ϕ=58		1, 2, CC	0.5, 1.0			◇	*, PP, *

LITHOLOGIC DESCRIPTION

MUDDY DIATOM OOZE and DIATOM CLAYEY MUD

Major lithologies: Muddy diatom ooze, olive gray (5Y 5/2) changing to dark greenish gray (5GY 4/1) in Section 2, getting firmer downcore. In Section 2, partly indurated layers are observed every 10 to 15 cm. Diatom clayey mud, dark greenish gray (5GY 4/1). Altered volcanic ash, grayish green (5G 5/2), thin bed in CC.

Sand-sized particles (ice-rafted debris?) common throughout. Dropstones (>0.3 cm) in Section 1, 14, 23, 33, 44, and 138 cm, are subrounded to subangular and vary in size from 1 to 8 cm in size; and in Section 2, 96 cm, are subrounded, 1.5 cm in size. Drilling disturbance varies from strong to moderate. No evidence of bioturbation.

SMEAR SLIDE SUMMARY (%):

	1, 50 D	2, 50 D	CC, 5 M
TEXTURE:			
Sand	—	—	6
Silt	—	—	54
Clay	—	—	40
COMPOSITION:			
Quartz	13	15	16
Feldspar	Tr	1	3
Rock fragments	2	3	4
Mica	4	2	3
Clay	20	20	40
Volcanic glass	—	4	Tr
Accessory minerals	—	—	2
Opaque minerals	1	—	—
Zeolites	—	Tr	2
Diatoms	60	55	30

SITE 696 HOLE B CORE 25R CORED INTERVAL 929.3-938.9 mbsl; 279.4-289.0 mbsf

TIME-ROCK UNIT	FORAMINIFERS	NANNOFOSSILS	RADIOLARIANS	DIATOMS	PALYNOMORPHS	PALEOMAGNETICS	PHYS. PROPERTIES	CHEMISTRY	SECTION	METERS	GRAPHIC LITHOLOGY	DRILLING DISTURB.	SED. STRUCTURES	SAMPLES
UPPER MIOCENE	B	B	F, M MIOCENE	C, M *D. hustedtii*	B		γ=1.4 ϕ=77 ●γ=1561		1, 2	0.5, 1.0	VOID		◇	*

LITHOLOGIC DESCRIPTION

DIATOM OOZE/DIATOMITE and DIATOM CLAYEY MUD/STONE

Major lithologies: Diatom ooze/diatomite, light olive gray (5Y 5/2), moderately fractured, containing traces of bioturbation (less than 20%). Some sand-sized material in increasing abundance downward as the lithology gradually changes to a diatom clayey mud. Diatom clayey mud/stone, dark greenish gray (5GY 4/1), firm, moderately fractured sediment, slightly bioturbated, darkening toward the base of Section 1. A few cm-sized sedimentary dropstones and numerous sand-sized black particles are present.

SMEAR SLIDE SUMMARY (%):

	1, 15 D	1, 140 D
TEXTURE:		
Sand	—	Tr
Silt	—	66
Clay	—	34
COMPOSITION:		
Quartz	4	14
Feldspar	—	2
Rock fragments	Tr	2
Mica	10	34
Clay	—	6
Accessory minerals	4	—
Zeolites	—	2
Diatoms	82	40

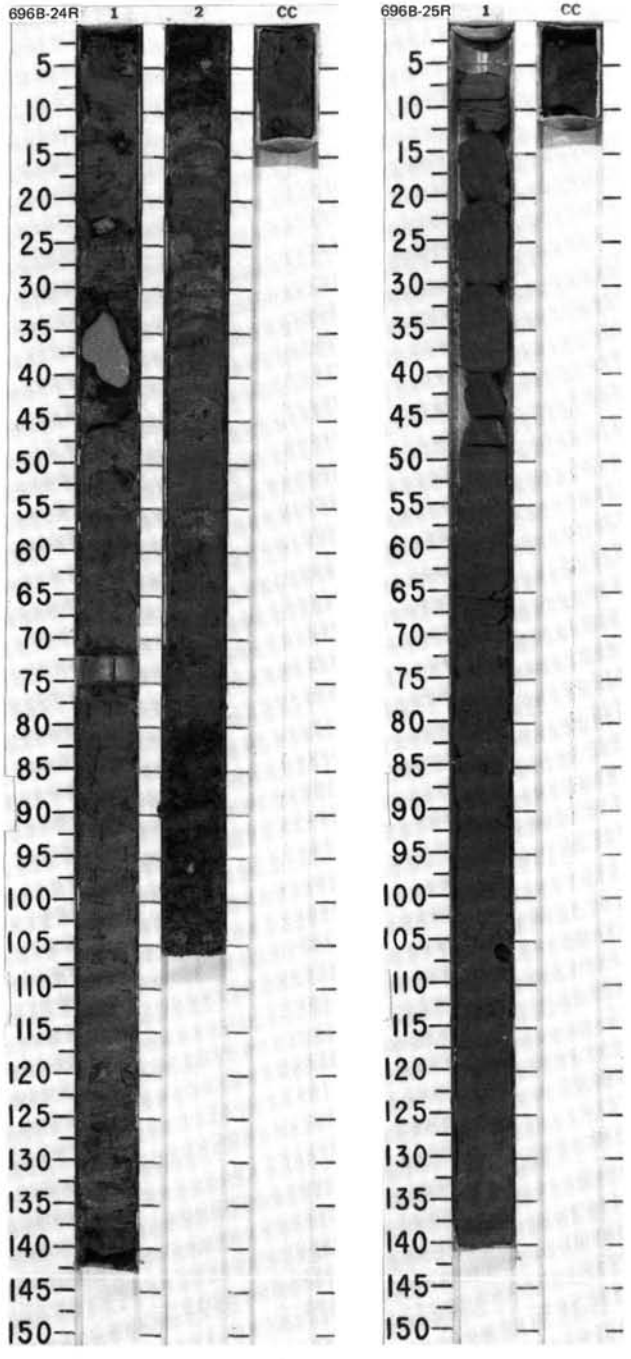

SITE 696 HOLE B CORE 26R CORED INTERVAL 938.9-948.6 mbsl; 289.0-298.7 mbsf

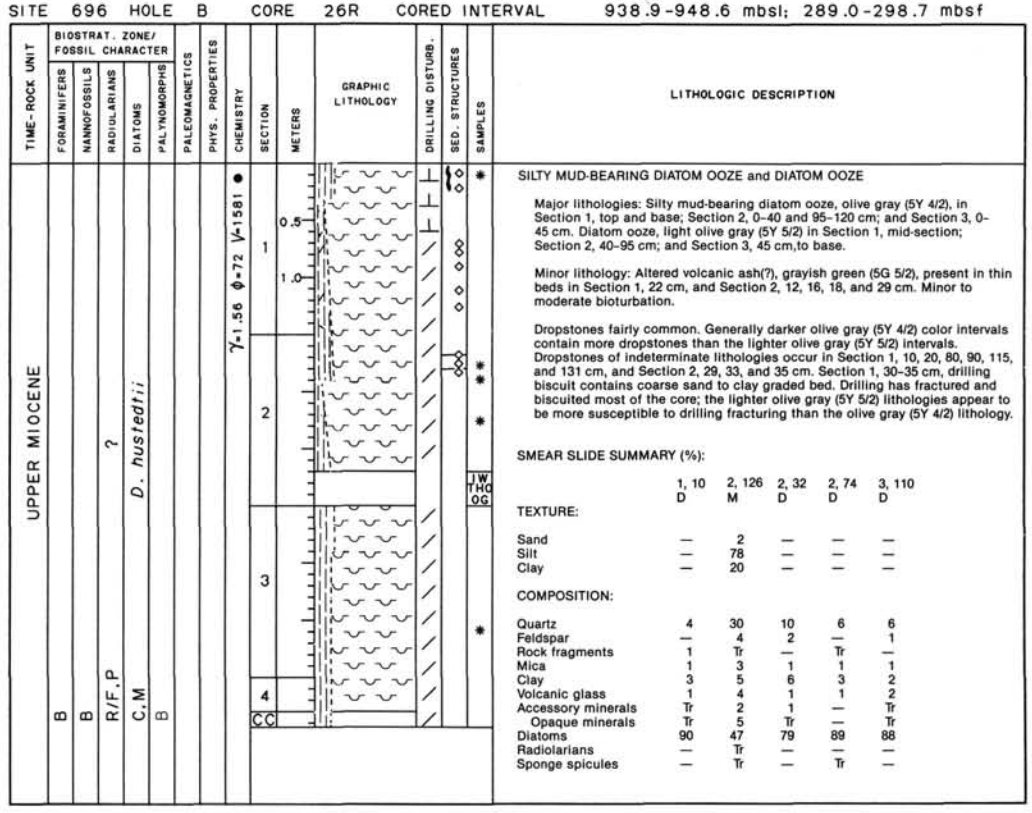

LITHOLOGIC DESCRIPTION

SILTY MUD-BEARING DIATOM OOZE and DIATOM OOZE

Major lithologies: Silty mud-bearing diatom ooze, olive gray (5Y 4/2), in Section 1, top and base; Section 2, 0-40 and 95-120 cm; and Section 3, 0-45 cm. Diatom ooze, light olive gray (5Y 5/2) in Section 1, mid-section; Section 2, 40-95 cm; and Section 3, 45 cm,to base.

Minor lithology: Altered volcanic ash(?), grayish green (5G 5/2), present in thin beds in Section 1, 22 cm, and Section 2, 12, 16, 18, and 29 cm. Minor to moderate bioturbation.

Dropstones fairly common. Generally darker olive gray (5Y 4/2) color intervals contain more dropstones than the lighter olive gray (5Y 5/2) intervals. Dropstones of indeterminate lithologies occur in Section 1, 10, 20, 80, 90, 115, and 131 cm, and Section 2, 29, 33, and 35 cm. Section 1, 30-35 cm, drilling biscuit contains coarse sand to clay graded bed. Drilling has fractured and biscuited most of the core; the lighter olive gray (5Y 5/2) lithologies appear to be more susceptible to drilling fracturing than the olive gray (5Y 4/2) lithology.

SMEAR SLIDE SUMMARY (%):

	1, 10 D	2, 126 M	2, 32 D	2, 74 D	3, 110 D
TEXTURE:					
Sand	—	2	—	—	—
Silt	—	78	—	—	—
Clay	—	20	—	—	—
COMPOSITION:					
Quartz	4	30	10	6	6
Feldspar	—	4	2	—	1
Rock fragments	1	Tr	—	Tr	—
Mica	1	3	1	1	1
Clay	3	5	6	3	2
Volcanic glass	1	4	1	1	2
Accessory minerals	Tr	2	1	—	Tr
Opaque minerals	Tr	5	Tr	—	Tr
Diatoms	90	47	79	89	88
Radiolarians	—	Tr	—	—	—
Sponge spicules	—	Tr	—	Tr	—

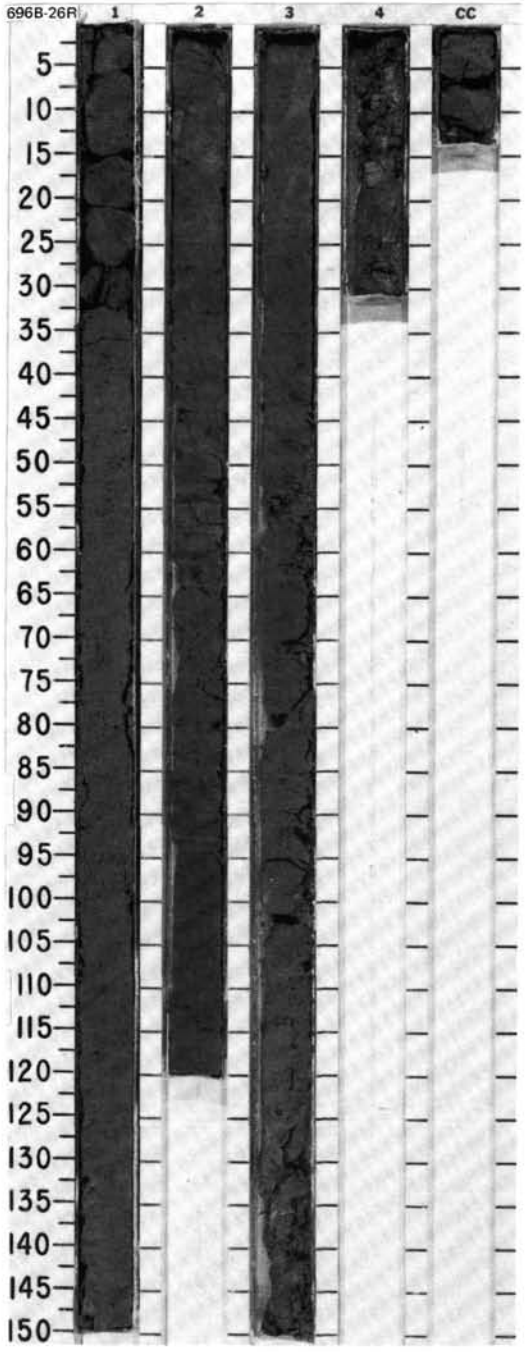

SITE 696 HOLE B CORE 27R CORED INTERVAL 948.6-958.2 mbsl; 298.7-308.3 mbsf

TIME-ROCK UNIT	BIOSTRAT. ZONE/ FOSSIL CHARACTER: FORAMINIFERS	NANNOFOSSILS	RADIOLARIANS	DIATOMS	PALYNOMORPHS	PALEOMAGNETICS	PHYS. PROPERTIES	CHEMISTRY	SECTION	METERS	GRAPHIC LITHOLOGY	DRILLING DISTURB.	SED. STRUCTURES	SAMPLES
UPPER MIOCENE	B	B	R,P	C,M	B		●7-1.40 ϕ-72 ●7-1.47 ϕ-72		1, 2	0.5, 1.0				

LITHOLOGIC DESCRIPTION

MUD-BEARING DIATOMITE

Major lithology: Mud-bearing diatomite, olive gray (5Y 4.5/2). Dropstones, subangular to rounded, up to 2 cm in size, throughout the core. Sand grains scattered throughout Section 1 and Section 2, 75 and 110 cm. Minor bioturbation in Section 1, 100–150 cm, and Section 2, 95–110 cm. Gray laminae in Section 2, 97–95 cm.

SMEAR SLIDE SUMMARY (%):

	1, 70 D	2, 50 D	2, 51 M
COMPOSITION:			
Quartz	5	3	5
Feldspar	—	—	1
Mica	2	Tr	—
Clay	10	7	11
Volcanic glass	Tr	5	—
Accessory minerals:			
Amphibole	—	Tr	Tr
Glauconite	—	—	Tr
Heavy minerals	Tr	—	1
Micronodules	1	—	—
Opaque minerals	—	1	2
Diatoms	76	80	76
Radiolarians	3	1	Tr
Sponge spicules	Tr	Tr	1
Silicoflagellates	3	3	3

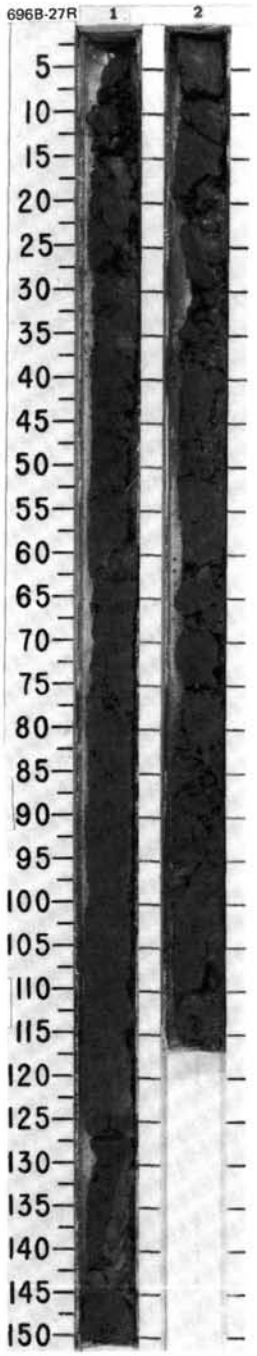

SITE 696 HOLE B CORE 28R CORED INTERVAL 958.2-967.9 mbsl; 308.0-318 mbsf

TIME-ROCK UNIT	BIOSTRAT. ZONE/ FOSSIL CHARACTER: FORAMINIFERS	NANNOFOSSILS	RADIOLARIANS	DIATOMS	PALYNOMORPHS	PALEOMAGNETICS	PHYS. PROPERTIES	CHEMISTRY	SECTION	METERS	GRAPHIC LITHOLOGY	DRILLING DISTURB.	SED. STRUCTURES	SAMPLES
UPPER MIOCENE	B	B		A, M *D. hustedtii* → *D. hustedtii* / *D. lauta* – *N. denticuloides*	B		γ=1.51 ϕ=67 V=1544 ● γ=1.6 ϕ=68 V=1551 ●		1 2 3 4	0.5 1.0				* * * *

LITHOLOGIC DESCRIPTION

SILTY MUD-BEARING DIATOMITE and SILTY MUD DIATOMITE

Major lithologies: Silty mud-bearing diatomite and silty mud diatomite, color grading through apparent color cycles from olive gray (5Y 5/2) at the top of Section 1, to dark gray (5Y 4/1) at the base of Section 1 and the top of Section 2, to olive gray (5Y 5/2) at the base of Section 2, to olive gray (5Y 4/2) at the base of Section 4.

Minor lithology: Altered volcanic ash(?), grayish green (5G 5/2), thin beds are present in Section 1, 120–122 cm, and Section 2, 4–7 and 13 cm.

Coarse sand-sized and lithified dropstones, much more common in dark gray (5Y 4/1) color zone, although unlike Core 113-696B-26R dropstones occur in both color zones. Dropstones >mm size are of indeterminate lithology and occur in Section 1, 70, 82, 100, 110, 118, 130, and 141 cm; Section 2, 4, 31, 33, 86, 93, 105, 115, 129, 131, and 143 cm; Section 3, 7, 41, 52, 70, 87, and 119 cm; and Section 4, 10, 95, 97, and 128 cm. Bioturbation minor and includes *Chondrites*. Core slight to moderately fractured and biscuited. Section 4 is the most disturbed.

SMEAR SLIDE SUMMARY (%):

	1, 50 D	1, 121 M	2, 50 D	3, 50 D	4, 50 D
COMPOSITION:					
Quartz	5	8	10	8	10
Feldspar	1	1	1	2	1
Mica	Tr	1	2	1	—
Clay	5	7	7	5	5
Volcanic glass	1	4	3	2	4
Accessory minerals:					
Micronodules	—	—	Tr	—	—
Opaque minerals	1	2	2	—	3
Heavy minerals	Tr	1	—	1	2
Amphibole	Tr	Tr	1	—	—
Glauconite	—	—	Tr	1	Tr
Diatoms	86	73	74	80	75
Radiolarians	1	—	—	Tr	Tr
Sponge spicules	Tr	1	Tr	Tr	Tr
Silicoflagellates	—	2	Tr	—	—

CORE 113-696B-29R NO RECOVERY

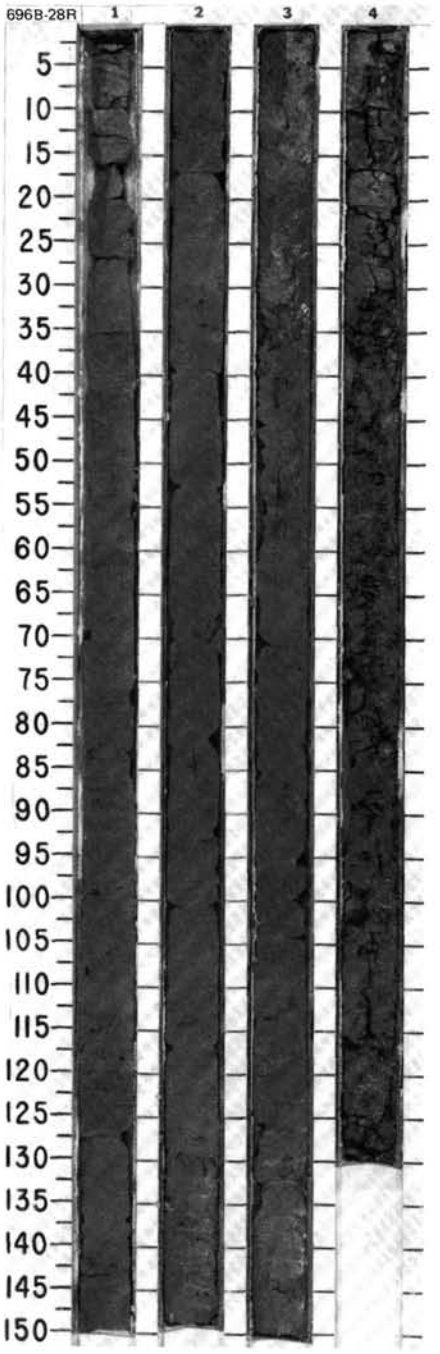

SITE 696 HOLE B CORE 30R CORED INTERVAL 977.5-987.5 mbsl; 327.6-337.3 mbsf

TIME-ROCK UNIT	BIOSTRAT. ZONE/ FOSSIL CHARACTER: FORAMINIFERS	NANNOFOSSILS	RADIOLARIANS	DIATOMS	PALYNOMORPHS	PALEOMAGNETICS	PHYS. PROPERTIES	CHEMISTRY	SECTION	METERS	GRAPHIC LITHOLOGY	DRILLING DISTURB.	SED. STRUCTURES	SAMPLES
UPPER MIOCENE	B	B	F,P	C,M					1, 2, CC	0.5, 1.0	VOID			*

D. hustedtii / D. lauta - N. denticuloides

MIOCENE

LITHOLOGIC DESCRIPTION

SILTY MUD-BEARING DIATOM OOZE and SILTY MUD DIATOM OOZE

Major lithologies: Silty mud-bearing diatom ooze in Section 1, grading down to silty mud diatom ooze in Section 2, color is between olive gray (5Y4/2) and dark greenish gray (5GY 4/1). Very disturbed to soupy in Section 1 because sediment was cut with a saw rather than split with the wire; and sediment is much softer than in overlying cores. Dropstones in Section 1 are all small (<0.8 cm), fine-grained sedimentary rocks, subangular. Dropstone in CC is gabbro, 7 cm, subangular.

SMEAR SLIDE SUMMARY (%):

	1, 129 D	2, 50 D
COMPOSITION:		
Quartz	7	14
Feldspar	2	2
Clay	4	6
Volcanic glass	2	4
Accessory minerals:		
Heavy minerals	3	1
Opaque minerals	—	2
Glauconite	—	1
Diatoms	81	70
Radiolarians	—	Tr
Sponge spicules	1	Tr
Silicoflagellates	Tr	—

SITE 696 HOLE B CORE 31R CORED INTERVAL 987.2-996.9 mbsl; 337.3-347.0 mbsf

TIME-ROCK UNIT	BIOSTRAT. ZONE/ FOSSIL CHARACTER: FORAMINIFERS	NANNOFOSSILS	RADIOLARIANS	DIATOMS	PALYNOMORPHS	PALEOMAGNETICS	PHYS. PROPERTIES	CHEMISTRY	SECTION	METERS	GRAPHIC LITHOLOGY	DRILLING DISTURB.	SED. STRUCTURES	SAMPLES
UPPER MIOCENE	B	B	?	C,M	B				1	0.5				*

D. hustedtii / D. lauta - N. denticuloides

LITHOLOGIC DESCRIPTION

SILTY MUD-BEARING DIATOM OOZE

Major lithology: Silty mud-bearing diatom ooze, olive gray (5Y 4/2), moderately disturbed, no primary structures.

A few small (< 1 cm) subangular dropstones, fine-grained sedimentary rocks.

SMEAR SLIDE SUMMARY (%):

	1, 50 D
COMPOSITION:	
Quartz	5
Clay	4
Accessory minerals	2
Diatoms	88
Sponge spicules	1
Volcanic glass	4

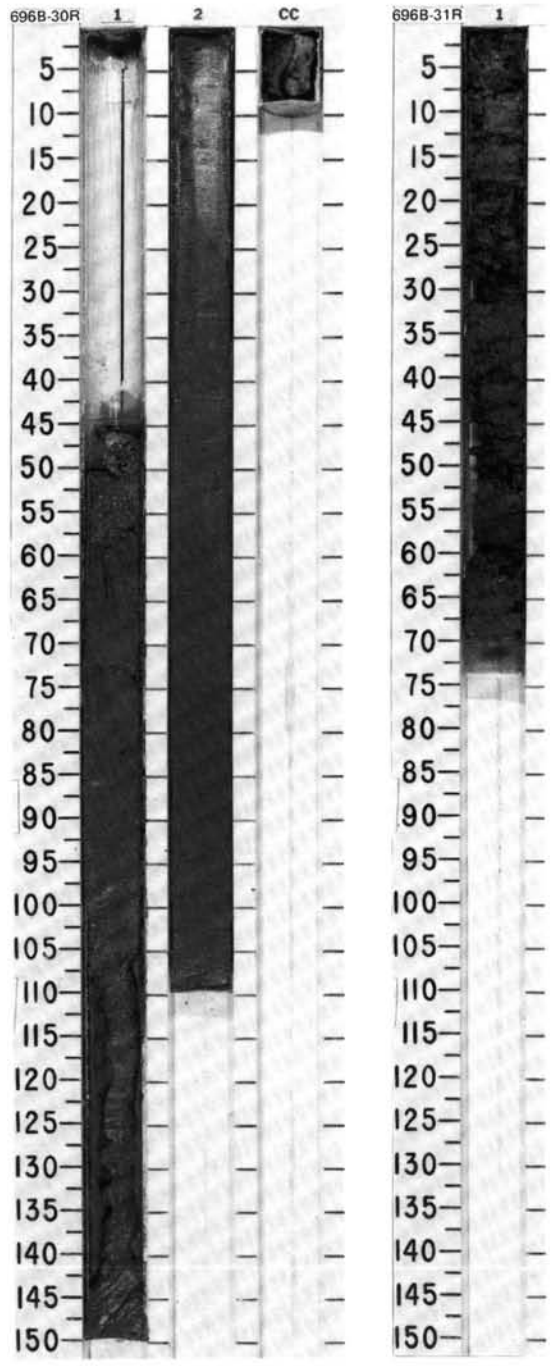

SITE 696 HOLE B CORE 32R CORED INTERVAL 996.9-1006.5 mbsl; 347.0-356.6 mbsf

TIME-ROCK UNIT	BIOSTRAT. ZONE/ FOSSIL CHARACTER: FORAMINIFERS	NANNOFOSSILS	RADIOLARIANS	DIATOMS	PALYNOMORPHS	PALEOMAGNETICS	PHYS. PROPERTIES	CHEMISTRY	SECTION	METERS	GRAPHIC LITHOLOGY	DRILLING DISTURB.	SED. STRUCTURES	SAMPLES	LITHOLOGIC DESCRIPTION
UPPER MIOCENE	B	B	? F/C,P	C,M *D. hustedtii* / *D. lauta* - *N. denticuloides*	B		●γ=1.29 ϕ=81		1, 2, 3	0.5, 1.0			◇, *	*	DIATOM OOZE and MUD-BEARING DIATOMITE

Major lithologies: Diatom ooze, olive (5Y 4/3), some minor bioturbation. Mud-bearing diatomite, olive (5Y 5/3), forms firmer layers in Section 1, 85–90, 109–111, and 130–133 cm; Section 2, 10–11, 60–86, 96–100, 115–124, 134–140, 147, and 150 cm; and Section 3, 13–17 cm.

Dropstones present in Section 1, 3 cm (4 cm in size), granite, angular; and Section 2, 32 cm (3 cm), granodiorite, rounded. A few scattered sand grains occur in Section 1, 52–70 cm.

SMEAR SLIDE SUMMARY (%):

	1, 50 D	2, 68 D	3, 14 D
COMPOSITION:			
Quartz	3	3	3
Feldspar	Tr	—	—
Mica	—	1	—
Clay	5	10	10
Accessory minerals	Tr	Tr	Tr
Micronodules	—	1	1
Zeolites	—	—	2
Diatoms	92	82	82
Radiolarians	—	2	2
Sponge spicules	—	1	Tr

SITE 696 HOLE B CORE 33R CORED INTERVAL 1006.8-1016.2 mbsl; 356.6-366.3 mbsf

TIME-ROCK UNIT	BIOSTRAT. ZONE/ FOSSIL CHARACTER: FORAMINIFERS	NANNOFOSSILS	RADIOLARIANS	DIATOMS	PALYNOMORPHS	PALEOMAGNETICS	PHYS. PROPERTIES	CHEMISTRY	SECTION	METERS	GRAPHIC LITHOLOGY	DRILLING DISTURB.	SED. STRUCTURES	SAMPLES	LITHOLOGIC DESCRIPTION
UPPER MIOCENE	B	B	MIOCENE F,M	B	B				CC						CHERT

Major lithology: Chert, dark olive gray (5Y 3/2), 3-cm-thick piece in CC. Contains *Zoophycos* burrow about 0.8 cm thick, filled with olive chert (5Y 4/3). Rest of chert is faintly laminated.

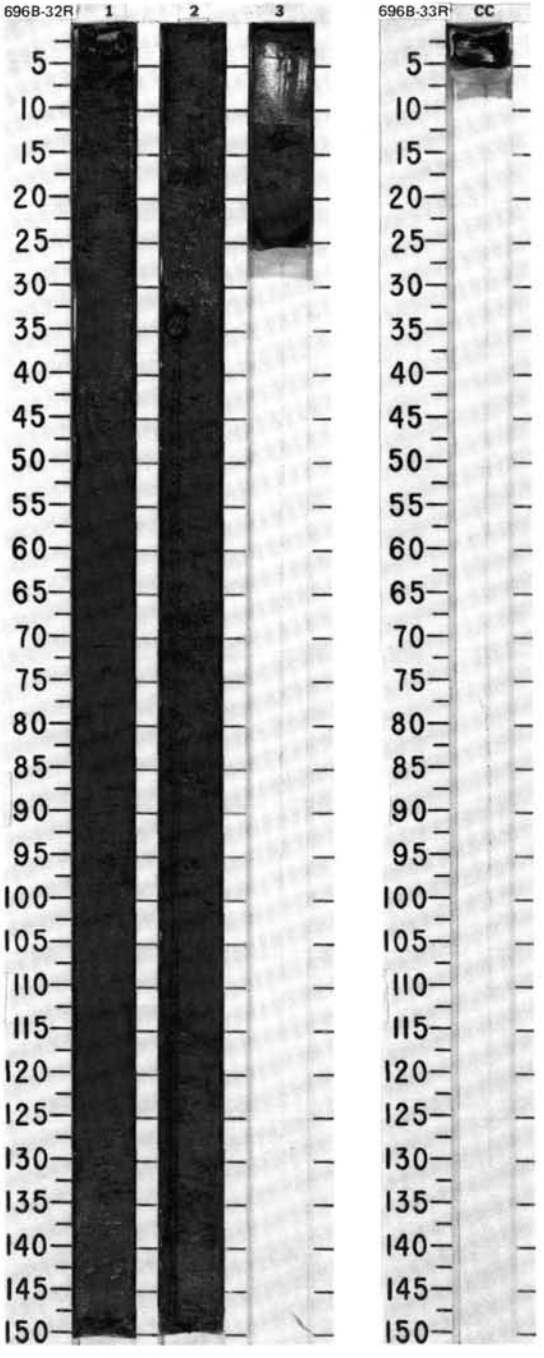

SITE 696 HOLE B CORE 34R CORED INTERVAL 1016.2-1025.9 mbsl; 366.3-376.0 mbsf

TIME-ROCK UNIT	FORAMINIFERS	NANNOFOSSILS	RADIOLARIANS	DIATOMS	PALYNOMORPHS	PALEOMAGNETICS	PHYS. PROPERTIES	CHEMISTRY	SECTION	METERS	GRAPHIC LITHOLOGY	DRILLING DISTURB.	SED. STRUCTURES	SAMPLES
UPPER MIOCENE	B	B	R, ? MIOCENE	C, M ?	B		●γ=1.38 ϕ=78		1, 2, 3	0.5, 1.0				* IW THC OG * *

LITHOLOGIC DESCRIPTION

DIATOM OOZE/DIATOMITE

Major lithology: Diatom ooze/diatomite, transitional degree of induration, olive (5Y 4/3, 4/4). Surface broken during splitting with wire. No primary structures.

Minor lithology: Muddy diatom ooze/diatomite, olive gray (5Y 4/2), containing about 10% manganese micronodules and Mn-coated grains; Section 2, 56–73 and 119–136 cm. Few small dropstones (0.2–0.3 cm) in Section 1.

SMEAR SLIDE SUMMARY (%):

	1, 50 D	2, 121 M	3, 50 D
COMPOSITION:			
Quartz	3	9	3
Feldspar	—	1	—
Clay	3	5	3
Accessory minerals	Tr	1	Tr
Micronodules	1	10	1
Zeolites	—	—	Tr
Diatoms	93	74	93
Sponge spicules	Tr	—	—

CORES 113-696B-35R to -39R NO RECOVERY

SITE 696 HOLE B CORE 40R CORED INTERVAL 1074.1-1083.8 mbsl; 424.2-433.9 mbsf

TIME-ROCK UNIT	FORAMINIFERS	NANNOFOSSILS	RADIOLARIANS	DIATOMS	PALYNOMORPHS	PALEOMAGNETICS	PHYS. PROPERTIES	CHEMISTRY	SECTION	METERS	GRAPHIC LITHOLOGY	DRILLING DISTURB.	SED. STRUCTURES	SAMPLES
LOWER UPPER-UPPER MIDDLE MIOCENE	B	B	R, P MIOCENE	C, M *D. hustedtii* / B *D. lauta - N. denticuloides*			γ=1.36 ϕ=74 ●		1					*

LITHOLOGIC DESCRIPTION

DIATOMITE

Major lithology: Diatomite, olive (5Y 4/4), homogeneous and highly fractured by drilling.

SMEAR SLIDE SUMMARY (%):

	1, 10 D
COMPOSITION:	
Quartz	4
Feldspar	1
Clay	2
Accessory minerals:	
Opaque minerals	Tr
Diatoms	93
Radiolarians	Tr

CORES 113-696B-41R to -43R NO RECOVERY

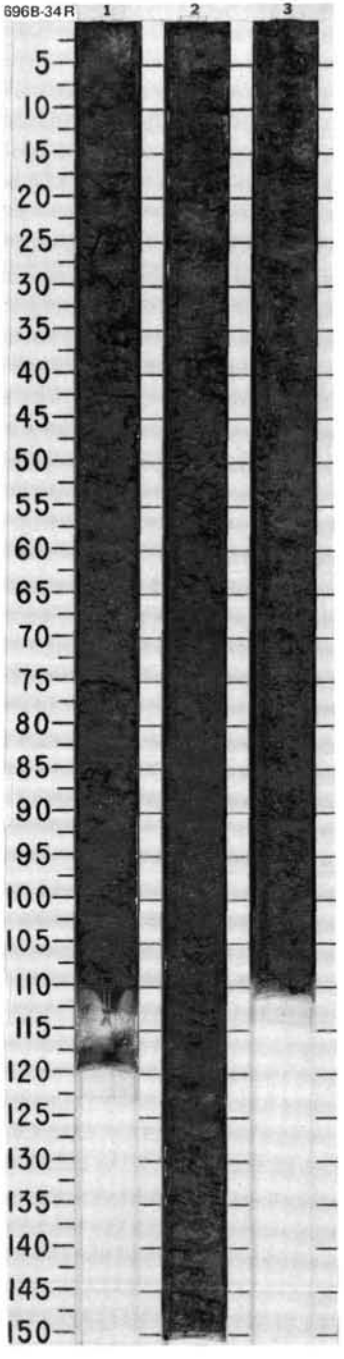

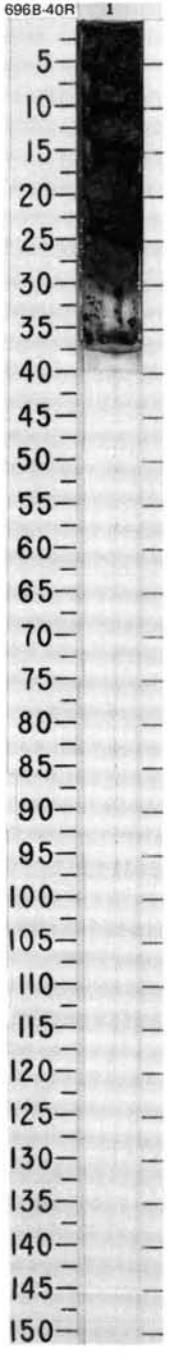

SITE 696 HOLE B CORE 44R CORED INTERVAL 1112.7-1122.4 mbsl; 462.8-472.5 mbsf

TIME-ROCK UNIT	BIOSTRAT. ZONE/ FOSSIL CHARACTER: FORAMINIFERS	NANNOFOSSILS	RADIOLARIANS	DIATOMS	PALYNOMORPHS	PALEOMAGNETICS	PHYS. PROPERTIES	CHEMISTRY	SECTION	METERS	GRAPHIC LITHOLOGY	DRILLING DISTURB.	SED. STRUCTURES	SAMPLES	LITHOLOGIC DESCRIPTION
LOWER UPPER-UPPER MIDDLE MIOCENE	B	B	C, M	C, M	B				1						CHERT Major lithology: Chert, black (5Y 2.5/1), very light, conchoidal fractures, fragmented.
			MIOCENE	*D. hustedtii*	*D. lauta - N. denticuloides*										

SITE 696 HOLE B CORE 45R CORED INTERVAL 1122.4-1131.9 mbsl; 472.5-482.0 mbsf

TIME-ROCK UNIT	BIOSTRAT. ZONE/ FOSSIL CHARACTER: FORAMINIFERS	NANNOFOSSILS	RADIOLARIANS	DIATOMS	PALYNOMORPHS	PALEOMAGNETICS	PHYS. PROPERTIES	CHEMISTRY	SECTION	METERS	GRAPHIC LITHOLOGY	DRILLING DISTURB.	SED. STRUCTURES	SAMPLES	LITHOLOGIC DESCRIPTION
MIDDLE MIOCENE	B	B	C, M	A, G	B		χ=1.36 Φ=79 χ=1562 ● χ=1.56 Φ=85 χ=1550 ●		1 2	0.5 1.0				* * *	DIATOMITE and SILTY MUD-BEARING DIATOMITE Major lithologies: Diatomite, olive (5Y 4/4), grading into silty mud-bearing diatomite, olive gray (5Y 4/2). Indurated sediments, slightly fractured and moderately bioturbated. Bioturbation is dominated by *Planolites* and *Chondrites*. Some of the larger burrow areas are white (2.5Y 8/0), but with the same composition.
			MIDDLE - EARLY MIOCENE	*D. hustedtii*	*D. lauta - N. denticuloides*										

SMEAR SLIDE SUMMARY (%):

	1, 56 D	1, 68 D	2, 10 D
COMPOSITION:			
Quartz	4	3	8
Feldspar	—	—	1
Mica	—	—	1
Clay	2	2	5
Volcanic glass	1	—	2
Accessory minerals	Tr	1	Tr
Opaque minerals	Tr	Tr	Tr
Glauconite	Tr	—	Tr
Amphiboles	Tr	Tr	Tr
Diatoms	93	94	83
Radiolarians	Tr	—	—
Sponge spicules	Tr	—	Tr

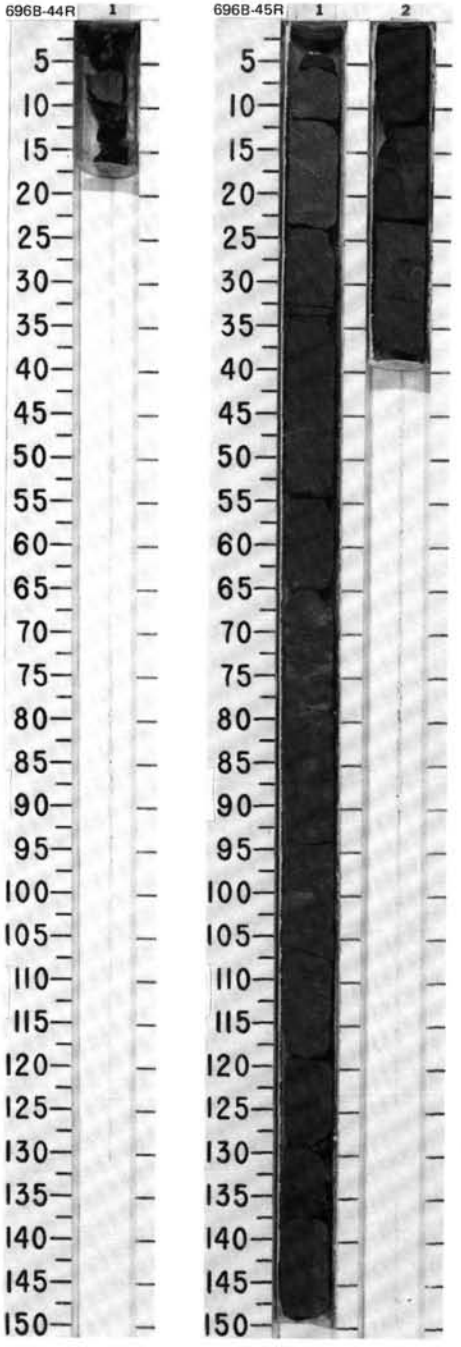

SITE 696 HOLE B CORE 46R CORED INTERVAL 1131.9-1141.5 mbsl; 482.0-491.6 mbsf

TIME-ROCK UNIT	FORAMINIFERS	NANNOFOSSILS	RADIOLARIANS	DIATOMS	PALYNOMORPHS	PALEOMAGNETICS	PHYS. PROPERTIES	CHEMISTRY	SECTION	METERS	GRAPHIC LITHOLOGY	DRILLING DISTURB.	SED. STRUCTURES	SAMPLES
MIDDLE MIOCENE	B	B	C, M	A, G	B		γ=1.40 V=1783 ● 0-65		1	0.5				*

D. hustedtii / D. lauta - N. denticuloides

LITHOLOGIC DESCRIPTION

MUDDY DIATOMITE and DIATOMITE

Major lithologies: Muddy diatomite, olive (5Y 4/3), with burrow fills of olive gray (5Y 4/2) and dark gray (5Y 4/1); moderately to strongly bioturbated, mainly *Planolites*, some *Chondrites*. *Teichichnus* at Section 1, 47 cm; vertical burrow at 62 cm. Glauconite seen on core surface but is only a trace constituent of smear slides. Diatomite, olive gray (5Y 4/2), minor to moderate bioturbation, at Section 1, 30 to 45 cm.

SMEAR SLIDE SUMMARY (%):

	1, 22 D
COMPOSITION:	
Quartz	7
Mica	2
Clay	20
Accessory minerals:	
Micronodules	1
Diatoms	66
Radiolarians	3
Sponge spicules	1

SITE 696 HOLE B CORE 47R CORED INTERVAL 1141.5-1151.1 mbsl; 491.6-501.2 mbsf

TIME-ROCK UNIT	FORAMINIFERS	NANNOFOSSILS	RADIOLARIANS	DIATOMS	PALYNOMORPHS	PALEOMAGNETICS	PHYS. PROPERTIES	CHEMISTRY	SECTION	METERS	GRAPHIC LITHOLOGY	DRILLING DISTURB.	SED. STRUCTURES	SAMPLES
MIDDLE MIOCENE	B	B	F, M	C, M			γ=1.63 V=1627 ● 0-72		1	0.5 1.0				* *

MIDDLE-EARLY MIOCENE

D. hustedtii

D. lauta - N. denticuloides

LITHOLOGIC DESCRIPTION

MUDDY DIATOMITE

Major lithology: Muddy diatomite, olive gray (5Y 4/2), moderately to strongly bioturbated, burrow fills are generally darker than the surrounding sediment. Burrows are *Planolites* and *Teichichnus*. Sand, quartz(?) and glauconite, on core surface.

Minor lithologies: Muddy diatomite in Section 1, 125-143 cm, olive gray (5Y 5/2), minor bioturbation, differs from major lithology above by having more mud. Chert in Section 1, 0-16 cm, black (5Y 2.5/1), light brownish gray (2.5Y 6/2), and dark olive gray (5Y 3/2). Some lamination and minor bioturbation, fragmented.

SMEAR SLIDE SUMMARY (%):

	1, 60 D	1, 136 M
COMPOSITION:		
Quartz	5	10
Feldspar	Tr	—
Mica	3	2
Clay	20	25
Volcanic glass	Tr	Tr
Accessory minerals:		
Heavy minerals	1	1
Glauconite	2	2
Micronodules	3	1
Amphibole	Tr	1
Diatoms	61	54
Radiolarians	3	3
Sponge spicules	2	1

SITE 696 HOLE B CORE 48R CORED INTERVAL 1151.1-1160.6 mbsl; 501.2-510.7 mbsf

TIME-ROCK UNIT: LOWER MIDDLE or UPPER LOWER MIOCENE to LOWER MIDDLE or LOWER MIOCENE

BIOSTRAT. ZONE/FOSSIL CHARACTER: FORAMINIFERS B; NANNOFOSSILS B; RADIOLARIANS F,P; DIATOMS C,M *N. grossepunctata* (?); PALYNOMORPHS B

PALEOMAGNETICS

PHYS. PROPERTIES: γ-1.41 ϕ-1.78 V_p-1623 ●; γ-1.42 ϕ-.75 V_p-1729 ●

CHEMISTRY

SECTION 1, 2, 3; METERS 0.5, 1.0

GRAPHIC LITHOLOGY: VOID

DRILLING DISTURB.

SED. STRUCTURES

SAMPLES

LITHOLOGIC DESCRIPTION

SILTY MUD-BEARING DIATOMITE

Major lithology: Silty mud-bearing diatomite, primarily olive gray (5Y 4/2) in Section 1, olive gray (5Y 5/2) and olive (5Y 4/3) in Section 2, and olive (5Y 5/3) in Section 3.

Minor lithologies: Pumice/glass fragments 1–2 mm in size are scattered throughout, except for Section 1, 122 cm, to Section 2, 65 cm; 1-cm angular pumice clast in Section 2, 76 cm. Diatom dolomite, light olive gray (5Y 6/2), hard, moderate to strong bioturbation, in Section 1, 96–106 cm. Fine-grained dolomite forms about 45% of sediment.

Moderate to strong bioturbation, including *Planolites* with *Chondrites* and *Zoophycos*. Pelleted *Zoophycos* occurs in Section 2, 17 cm, and large *Teichichnus* in Section 3, 17–25 cm. Intervals with abundant burrow fills of dark gray (5Y 4/1) in Section 1, 19–26, 38–45, and 74–80 cm. Parallel lamination in Sections 1 and 3, wavy laminations in Section 2, 42–44 cm.

SMEAR SLIDE SUMMARY (%):

	1, 44 D	1, 70 D	1, 103 M	2, 50 D
COMPOSITION:				
Quartz	4	5	1	2
Feldspar	1	1	—	Tr
Clay	5	4	—	1
Volcanic glass	5	4	7	4
Calcite/dolomite	Tr	11	45	2
Accessory minerals	3	Tr	3	3
Glauconite	—	1	1	—
Diatoms	81	72	40	86
Radiolarians	1	2	3	2
Sponge spicules	Tr	Tr	Tr	—

SITE 696 HOLE B CORE 49R CORED INTERVAL 1160.6-1170.1 mbsl; 510.7-520.2 mbsf

TIME-ROCK UNIT: MIDDLE MIOCENE to LOWER MIDDLE MIOCENE

BIOSTRAT. ZONE/FOSSIL CHARACTER: FORAMINIFERS B; NANNOFOSSILS B; RADIOLARIANS C,M; DIATOMS *N. grossepunctata*; PALYNOMORPHS B

PALEOMAGNETICS

PHYS. PROPERTIES: γ-1.5 ϕ-.76 V_p-1584 ●

CHEMISTRY: ● 0.1%

SECTION 1, CC; METERS 0.5, 1.0

GRAPHIC LITHOLOGY

DRILLING DISTURB.

SED. STRUCTURES

SAMPLES

LITHOLOGIC DESCRIPTION

SILTY MUD-BEARING DIATOMITE

Major lithology: Silty mud-bearing diatomite, olive gray (5Y 4/2, 5/2), moderately to highly fractured; some moderate bioturbation preserved in drilling biscuits. Few pumice grains up to 3 mm throughout.

Minor lithologies: Volcanic ash-bearing diatomite, very dark gray (5Y 3/1), in Section 1, 62–63 cm. Chert, very dark gray (5Y 3/1); fragments near top of Section 1 and in CC, laminated and dark olive gray (5Y 3/2) and very dark gray (5Y 3/1). Dropstone, gabbro, rounded, 5 cm long, in Section 1, 0–3 cm (may not be in place).

SMEAR SLIDE SUMMARY (%):

	1, 62 M	1, 75 D
COMPOSITION:		
Quartz	5	4
Feldspar	1	Tr
Clay	Tr	2
Volcanic glass	8	3
Calcite/dolomite	—	Tr
Accessory minerals:		
Heavy minerals	2	2
Opaque minerals	1	1
Micronodules	11	—
Diatoms	70	85
Radiolarians	2	2
Sponge spicules	Tr	1

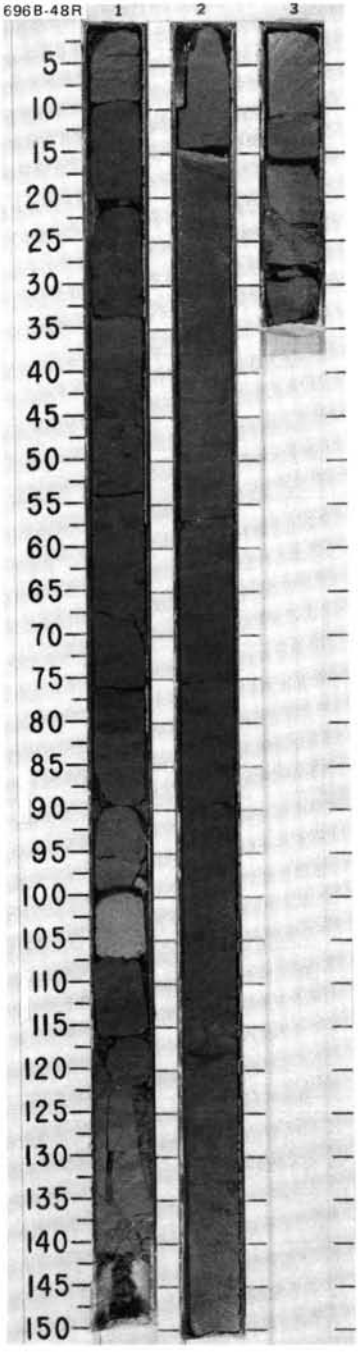

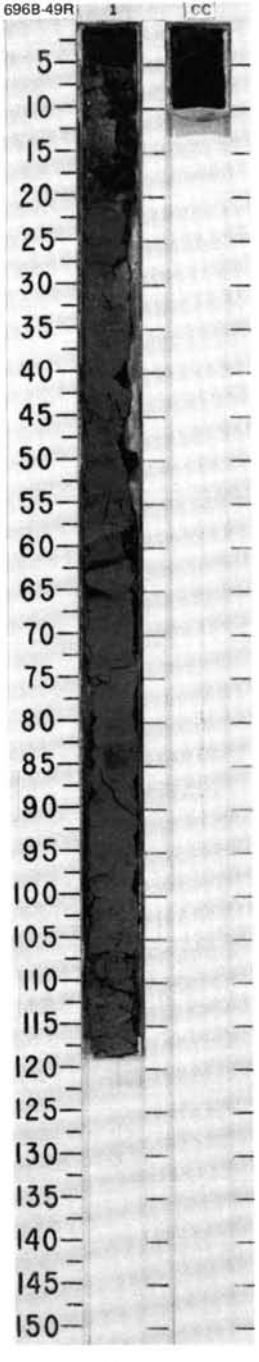

SITE 696 HOLE B CORE 50R CORED INTERVAL 1170.1-1179.7 mbsl; 520.2-529.8 mbsf

TIME-ROCK UNIT	BIOSTRAT. ZONE/ FOSSIL CHARACTER: FORAMINIFERS	NANNOFOSSILS	RADIOLARIANS	DIATOMS	PALYNOMORPHS	PALEOMAGNETICS	PHYS. PROPERTIES	CHEMISTRY	SECTION	METERS	GRAPHIC LITHOLOGY	DRILLING DISTURB.	SED. STRUCTURES	SAMPLES
MIDDLE MIOCENE	B	B	LOWER MIDDLE-LOWER MIOCENE F, P	*N. grossepunctata* C, M	B		χ 2.29 Φ 27.46 χ 1.58 Φ 69	0.1%	1	0.5 1.0				*
									2					*

LITHOLOGIC DESCRIPTION

CHERT, MUDDY DIATOMITE, and RADIOLARIAN-BEARING SILTY MUD DIATOMITE

Major lithologies: Chert, black (5Y 2.5/2) and dark gray (5Y 4/1); many pieces are laminated, some are moderately bioturbated, in Section 1,0–67 cm. Muddy diatomite, olive gray (5Y 4/2); moderate to strong bioturbation, including *Teichichnus*, *Planolites*, *Zoophycos*, and *Chondrites*. *Teichichnus* is filled with darker, glauconite-rich sediment and Mn micronodules, in Section 1,67–119 cm. Radiolarian-bearing silty mud diatomite, olive gray (5Y 4/2) and dark olive gray (5Y 3/2); minor to moderate bioturbation, including *Teichichnus* and *Planolites*. Many of the radiolarians and all of the rock fragments are coated with Fe/Mn *oxides and/or glauconite*.

SMEAR SLIDE SUMMARY (%):

	1, 90 D	2, 22 D
COMPOSITION:		
Quartz	5	5
Feldspar	Tr	10
Rock fragments	—	8
Mica	2	2
Clay	20	10
Accessory minerals:		
Amphibole	Tr	1
Glauconite	Tr	2
Opaque minerals	1	—
Heavy minerals	Tr	—
Micronodules	1	1
Diatoms	66	40
Radiolarians	3	20
Sponge spicules	2	2

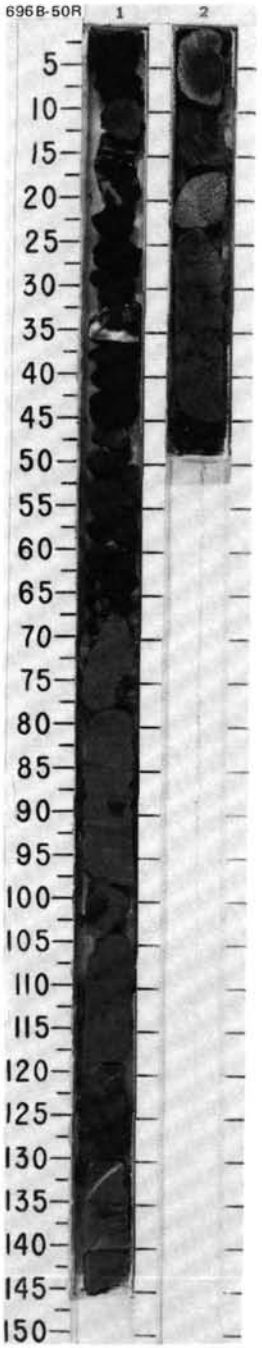

SITE 696 HOLE B CORE 51R CORED INTERVAL 1179.7-1189.3 mbsl: 529.8-539.4 mbsf

TIME-ROCK UNIT	BIOSTRAT. ZONE/ FOSSIL CHARACTER: FORAMINIFERS	NANNOFOSSILS	RADIOLARIANS	DIATOMS	PALYNOMORPHS	PALEOMAGNETICS	PHYS. PROPERTIES	CHEMISTRY	SECTION	METERS	GRAPHIC LITHOLOGY	DRILLING DISTURB.	SED. STRUCTURES	SAMPLES
?	B	B	C,P	B	B		γ=2.27 0-19 V=3746 ● ● 23.5%		1 2	0.5 1.0			THC	* *

LITHOLOGIC DESCRIPTION

DIATOM- AND GLAUCONITE-BEARING SANDY MUDSTONE

Major lithology: Diatom- and glauconite-bearing sandy mudstone, very dark gray (5Y 3/1), some lamination; minor to moderate bioturbation, including *Teichichnus*. Glauconite about 25%. The quartz-glauconite component is well-sorted fine sand. Local carbonate cement at base of Section 1.

Minor lithologies: Chert, black (5Y 2.5/1), some pieces laminated, in Section 1, 4–18 cm. Claystone, very dark gray (5Y 3/1), occurs as rip-up clasts and patches in Section 1, 53–80 cm, and Section 2, 30–40 and 72–73 cm.

SMEAR SLIDE SUMMARY (%):

	1, 55 D	2, 37 M
TEXTURE:		
Sand	51	10
Silt	15	10
Clay	34	80
COMPOSITION:		
Quartz	15	5
Feldspar	5	2
Rock fragments	—	7
Mica	3	—
Clay	34	80
Calcite/dolomite	—	Tr
Accessory minerals:		
Amphibole	3	—
Glauconite	25	2
Opaque minerals	1	2
Heavy minerals	3	2
Diatoms	10	—
Sponge spicules	1	Tr

SITE 696 HOLE B CORE 52R CORED INTERVAL 1189.3-1198.8 mbsl: 539.4-548.9 mbsf

TIME-ROCK UNIT	BIOSTRAT. ZONE/ FOSSIL CHARACTER: FORAMINIFERS	NANNOFOSSILS	RADIOLARIANS	DIATOMS	PALYNOMORPHS	PALEOMAGNETICS	PHYS. PROPERTIES	CHEMISTRY	SECTION	METERS	GRAPHIC LITHOLOGY	DRILLING DISTURB.	SED. STRUCTURES	SAMPLES
?	B	B	F/C,P ?	B	B				1 CC					*

LITHOLOGIC DESCRIPTION

GLAUCONITIC SANDY MUDSTONE

Major lithology: Glauconitic sandy mudstone, very dark gray (5Y 3/1); minor to moderate bioturbation. Section highly fragmented by drilling.

SMEAR SLIDE SUMMARY (%):

	1, 5 D
TEXTURE:	
Sand	55
Silt	30
Clay	15
COMPOSITION:	
Quartz	10
Feldspar	7
Rock fragments	30
Clay	15
Accessory minerals:	
Amphibole	2
Glauconite	30
Opaque minerals	3
Heavy minerals	3
Diatoms	Tr
Radiolarians	Tr

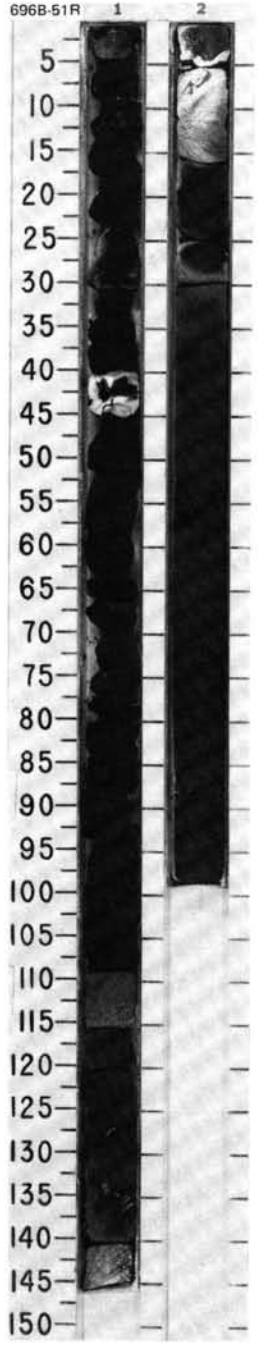

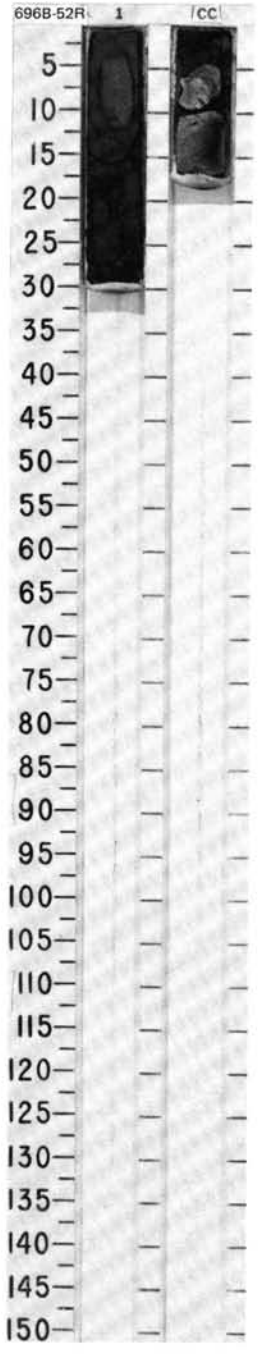

SITE 696 HOLE B CORE 53R CORED INTERVAL 1198.8-1208.4 mbsl; 548.9-558.5 mbsf

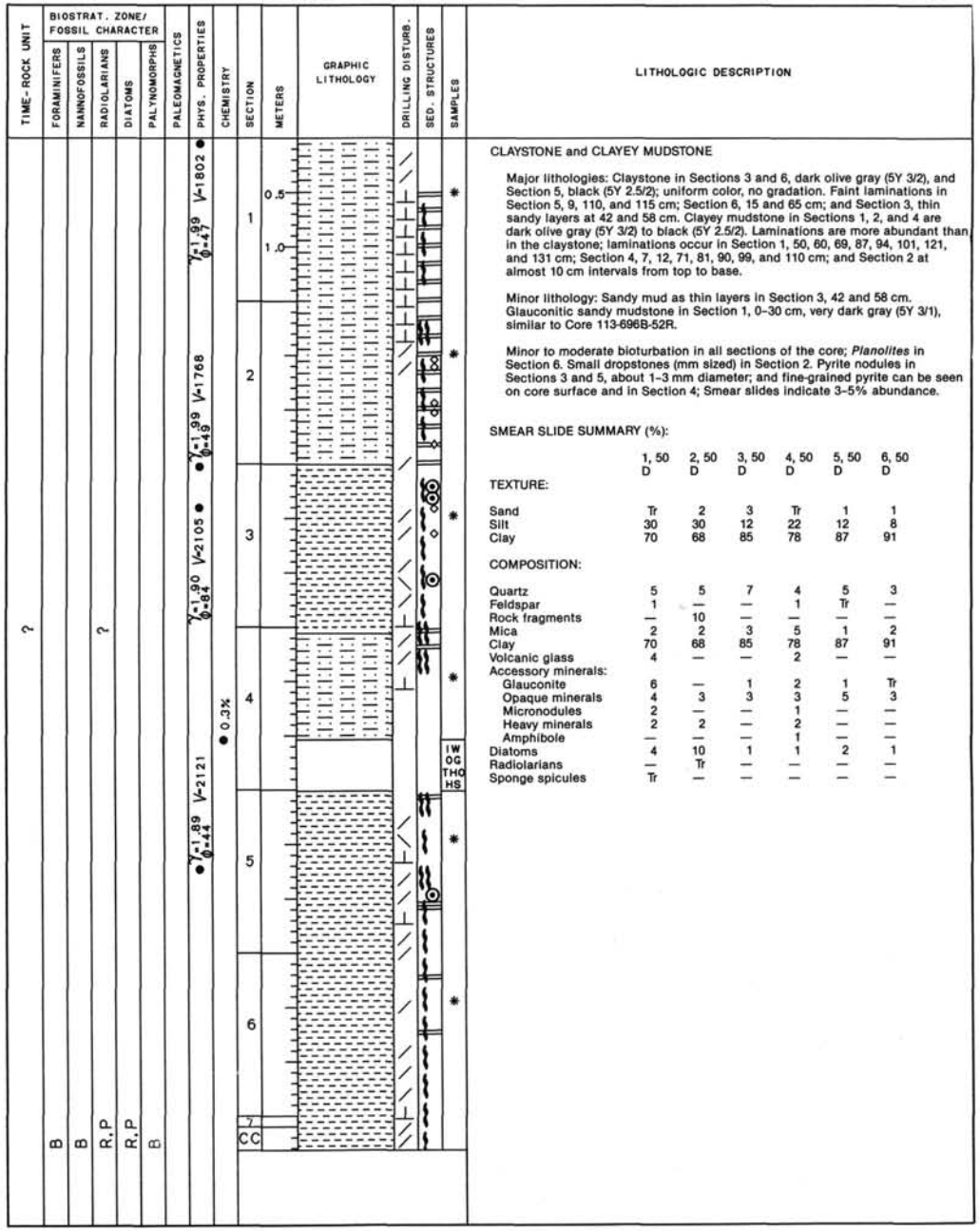

CLAYSTONE and CLAYEY MUDSTONE

Major lithologies: Claystone in Sections 3 and 6, dark olive gray (5Y 3/2), and Section 5, black (5Y 2.5/2); uniform color, no gradation. Faint laminations in Section 5, 9, 110, and 115 cm; Section 6, 15 and 65 cm; and Section 3, thin sandy layers at 42 and 58 cm. Clayey mudstone in Sections 1, 2, and 4 are dark olive gray (5Y 3/2) to black (5Y 2.5/2). Laminations are more abundant than in the claystone; laminations occur in Section 1, 50, 60, 69, 87, 94, 101, 121, and 131 cm; Section 4, 7, 12, 71, 81, 90, 99, and 110 cm; and Section 2 at almost 10 cm intervals from top to base.

Minor lithology: Sandy mud as thin layers in Section 3, 42 and 58 cm. Glauconitic sandy mudstone in Section 1, 0–30 cm, very dark gray (5Y 3/1), similar to Core 113-696B-52R.

Minor to moderate bioturbation in all sections of the core; *Planolites* in Section 6. Small dropstones (mm sized) in Section 2. Pyrite nodules in Sections 3 and 5, about 1–3 mm diameter; and fine-grained pyrite can be seen on core surface and in Section 4; Smear slides indicate 3–5% abundance.

SMEAR SLIDE SUMMARY (%):

	1, 50 D	2, 50 D	3, 50 D	4, 50 D	5, 50 D	6, 50 D
TEXTURE:						
Sand	Tr	2	3	Tr	1	1
Silt	30	30	12	22	12	8
Clay	70	68	85	78	87	91
COMPOSITION:						
Quartz	5	5	7	4	5	3
Feldspar	1	—	—	1	Tr	—
Rock fragments	—	10	—	—	—	—
Mica	2	2	3	5	1	2
Clay	70	68	85	78	87	91
Volcanic glass	4	—	—	2	—	—
Accessory minerals:						
Glauconite	6	—	1	2	1	Tr
Opaque minerals	4	3	3	3	5	3
Micronodules	2	—	—	1	—	—
Heavy minerals	2	2	—	2	—	—
Amphibole	—	—	—	1	—	—
Diatoms	4	10	1	1	2	1
Radiolarians	—	Tr	—	—	—	—
Sponge spicules	Tr	—	—	—	—	—

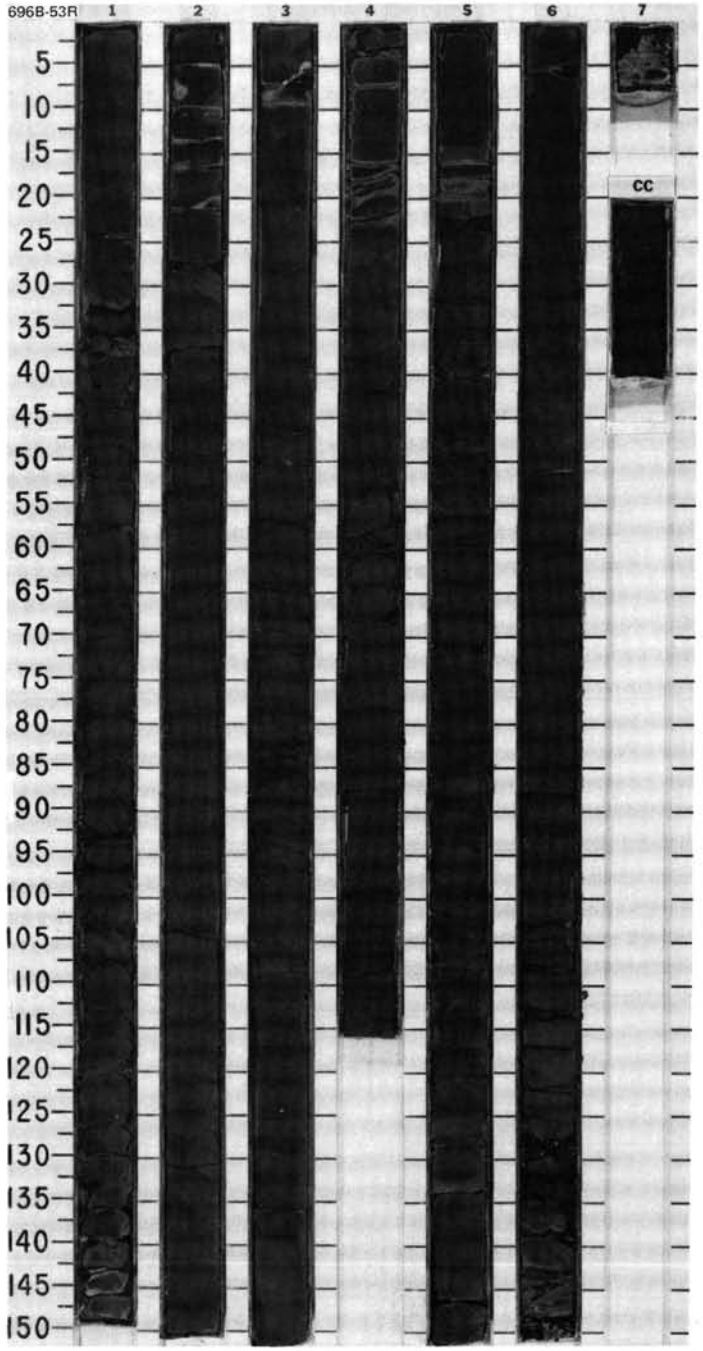

SITE 696 HOLE B CORE 54R CORED INTERVAL 1208.4-1218.1 mbsl; 558.5-568.2 mbsf

TIME-ROCK UNIT	BIOSTRAT. ZONE/FOSSIL CHARACTER: FORAMINIFERS	NANNOFOSSILS	RADIOLARIANS	DIATOMS	PALYNOMORPHS	PALEOMAGNETICS	PHYS. PROPERTIES	CHEMISTRY	SECTION	METERS	GRAPHIC LITHOLOGY	DRILLING DISTURB.	SED. STRUCTURES	SAMPLES
?	B	B	R,P	B	B	● γ=1.95 V=1777 Φ=47	● γ=1.92 Φ=47	● 0.2%	1 2 3 4 CC	0.5 1.0				* * * *

LITHOLOGIC DESCRIPTION

CLAYSTONE, CLAYEY MUDSTONE, and SILTY MUDSTONE (Grading from sandy mudstone to claystone)

Major lithologies: Claystone to silty mudstone, dark olive gray (5Y 3/2). Cyclic grading from coarse to fine; grading takes place on the scale of 40 to > 150 cm. Claystone in CC is black (5Y 2.5/1), with faint laminations and moderate bioturbation, including *Planolites*. Coarsest bed occurs in Section 4, 0-5 cm.

A few cm-sized rounded sedimentary dropstones(?) are present, sandstone in Section 2 and shale in Section 4; and smaller sized ice-rafted detritus is also present. Small pyrite "concretions" are present and more common in Section 1, 80-120 cm. Silicified benthic foraminifers are present on the surface.

SMEAR SLIDE SUMMARY (%):

	1, 60 D	2, 60 D	3, 10 D	4, 2 M
TEXTURE:				
Sand	—	2	4	15
Silt	12	44	56	65
Clay	88	54	40	20
COMPOSITION:				
Quartz	3	18	30	58
Feldspar	—	6	6	6
Rock fragments	—	4	2	4
Mica	4	8	4	1
Clay	88	54	40	20
Volcanic glass	—	—	Tr	2
Accessory minerals	—	6	10	—
Glauconite	Tr	Tr	2	1
Zeolites	1	Tr	Tr	2
Opaque minerals	4	4	6	6

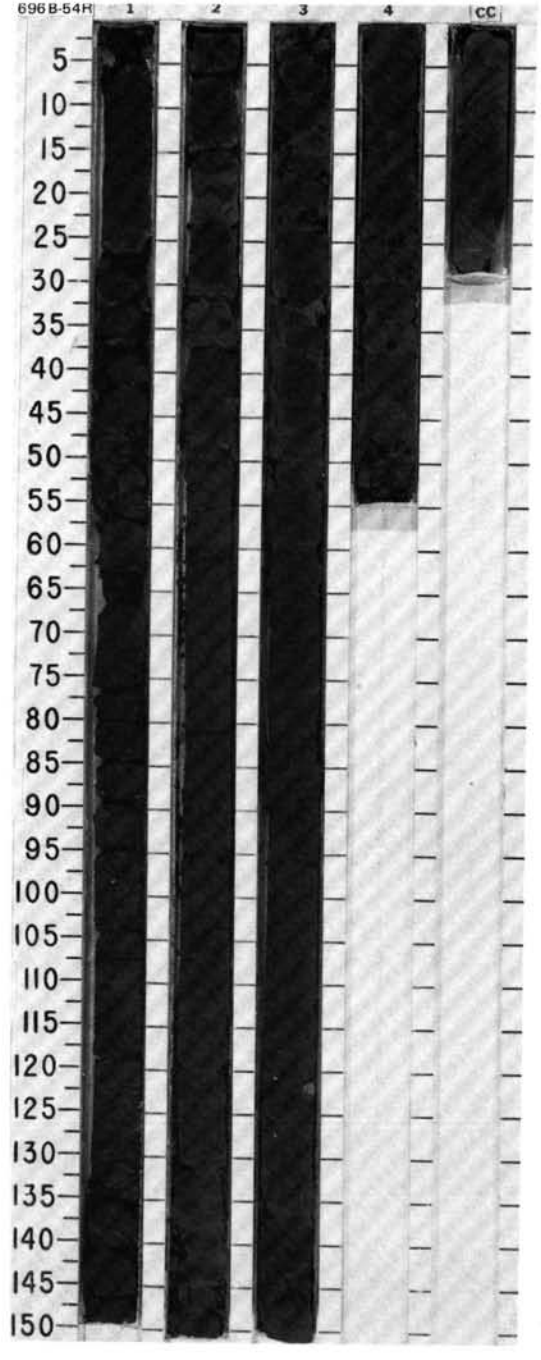

SITE 696 HOLE B CORE 55R CORED INTERVAL 1218.1-1227.8 mbsl; 568.2-577.9 mbsf

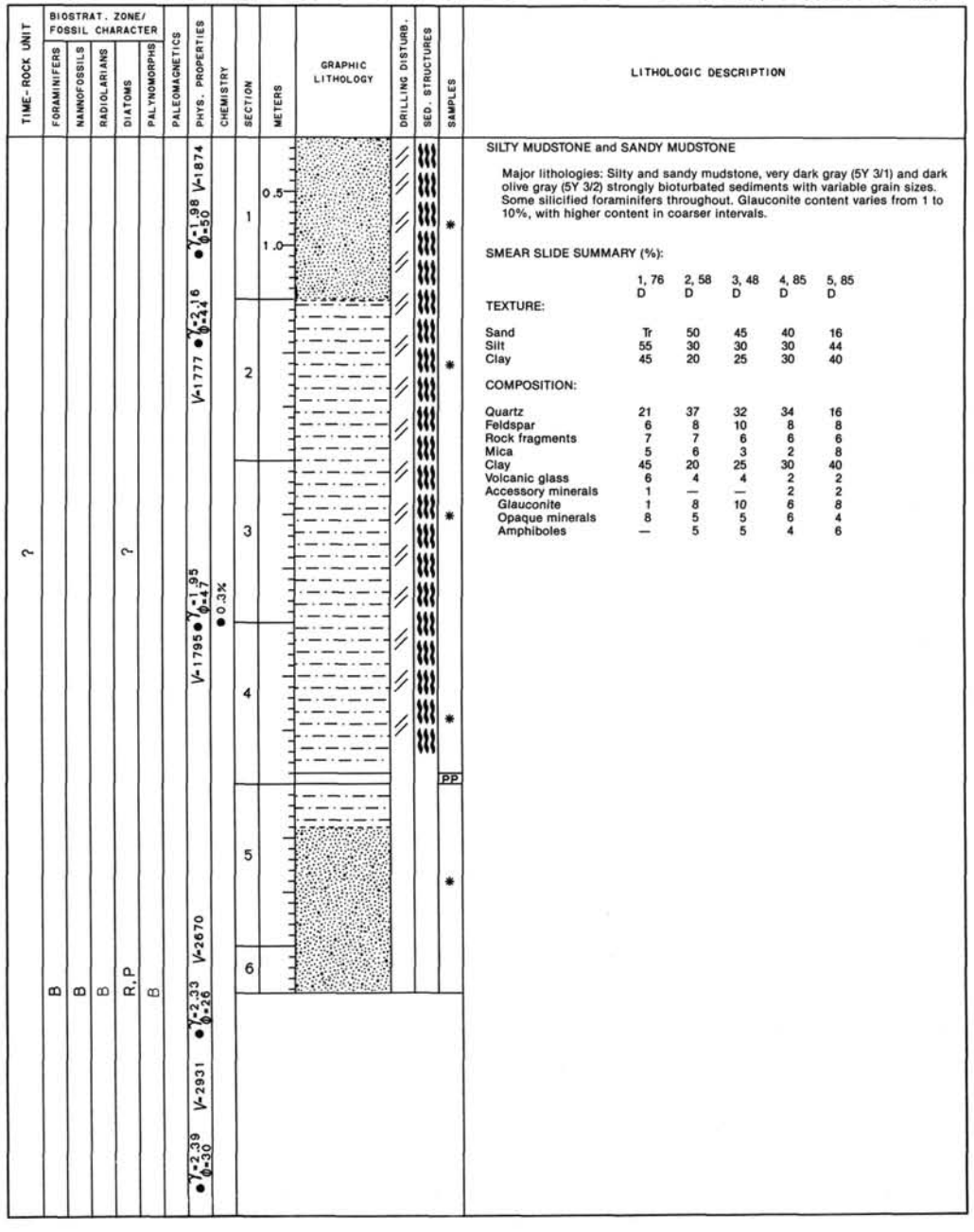

SILTY MUDSTONE and SANDY MUDSTONE

Major lithologies: Silty and sandy mudstone, very dark gray (5Y 3/1) and dark olive gray (5Y 3/2) strongly bioturbated sediments with variable grain sizes. Some silicified foraminifers throughout. Glauconite content varies from 1 to 10%, with higher content in coarser intervals.

SMEAR SLIDE SUMMARY (%):

	1, 76 D	2, 58 D	3, 48 D	4, 85 D	5, 85 D
TEXTURE:					
Sand	Tr	50	45	40	16
Silt	55	30	30	30	44
Clay	45	20	25	30	40
COMPOSITION:					
Quartz	21	37	32	34	16
Feldspar	6	8	10	8	8
Rock fragments	7	7	6	6	6
Mica	5	6	3	2	8
Clay	45	20	25	30	40
Volcanic glass	6	4	4	2	2
Accessory minerals	1	—	—	2	2
Glauconite	1	8	10	6	8
Opaque minerals	8	5	5	6	4
Amphiboles	—	5	5	4	6

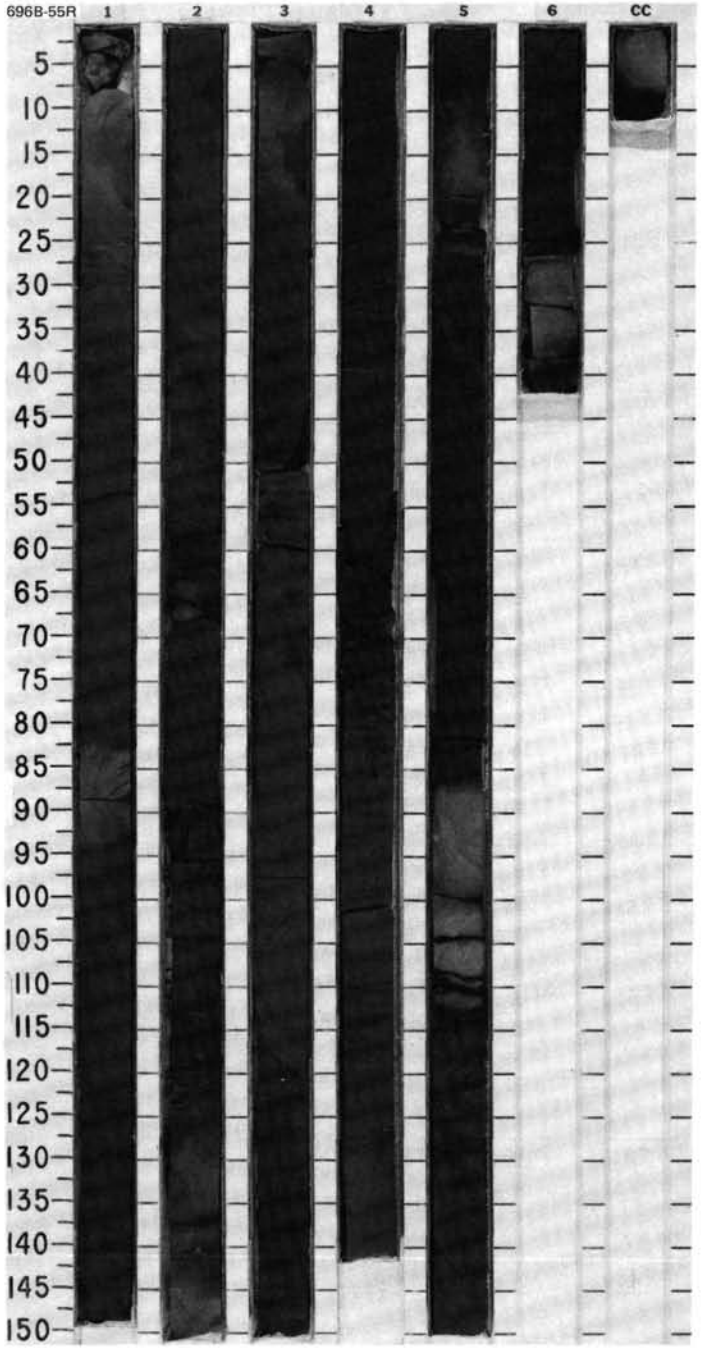

SITE 696 HOLE B CORE 56R CORED INTERVAL 1227.8-1237.5 mbsl; 577.9-587.6 mbsf

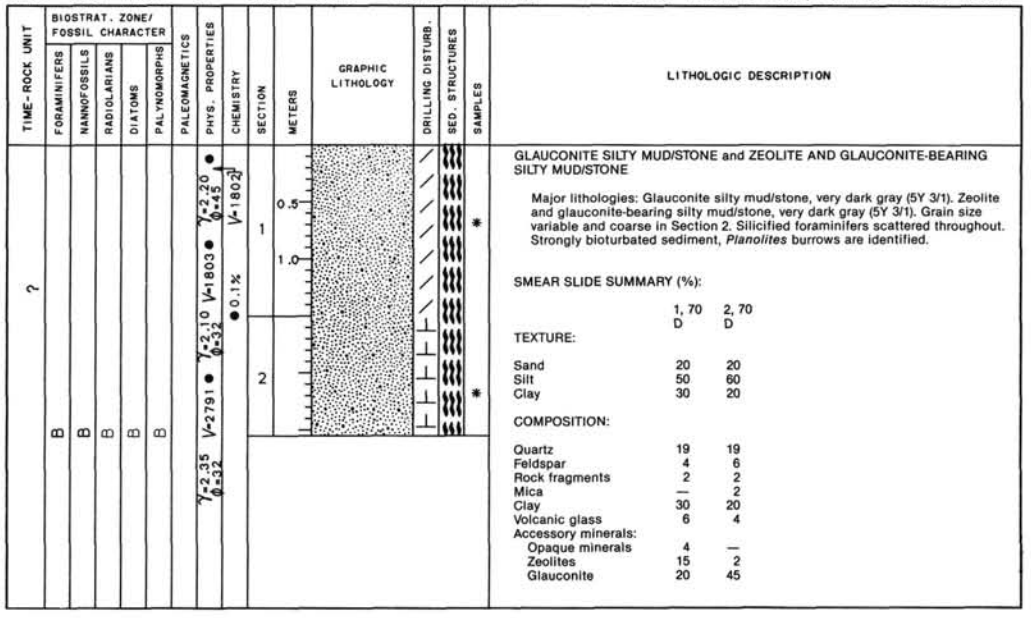

LITHOLOGIC DESCRIPTION

GLAUCONITE SILTY MUD/STONE and ZEOLITE AND GLAUCONITE-BEARING SILTY MUD/STONE

Major lithologies: Glauconite silty mud/stone, very dark gray (5Y 3/1). Zeolite and glauconite-bearing silty mud/stone, very dark gray (5Y 3/1). Grain size variable and coarse in Section 2. Silicified foraminifers scattered throughout. Strongly bioturbated sediment, *Planolites* burrows are identified.

SMEAR SLIDE SUMMARY (%):

	1, 70 D	2, 70 D
TEXTURE:		
Sand	20	20
Silt	50	60
Clay	30	20
COMPOSITION:		
Quartz	19	19
Feldspar	4	6
Rock fragments	2	2
Mica	—	2
Clay	30	20
Volcanic glass	6	4
Accessory minerals:		
Opaque minerals	4	—
Zeolites	15	2
Glauconite	20	45

SITE 696 HOLE B CORE 57R CORED INTERVAL 1237.5-1247.1 mbsl; 587.6-597.2 mbsf

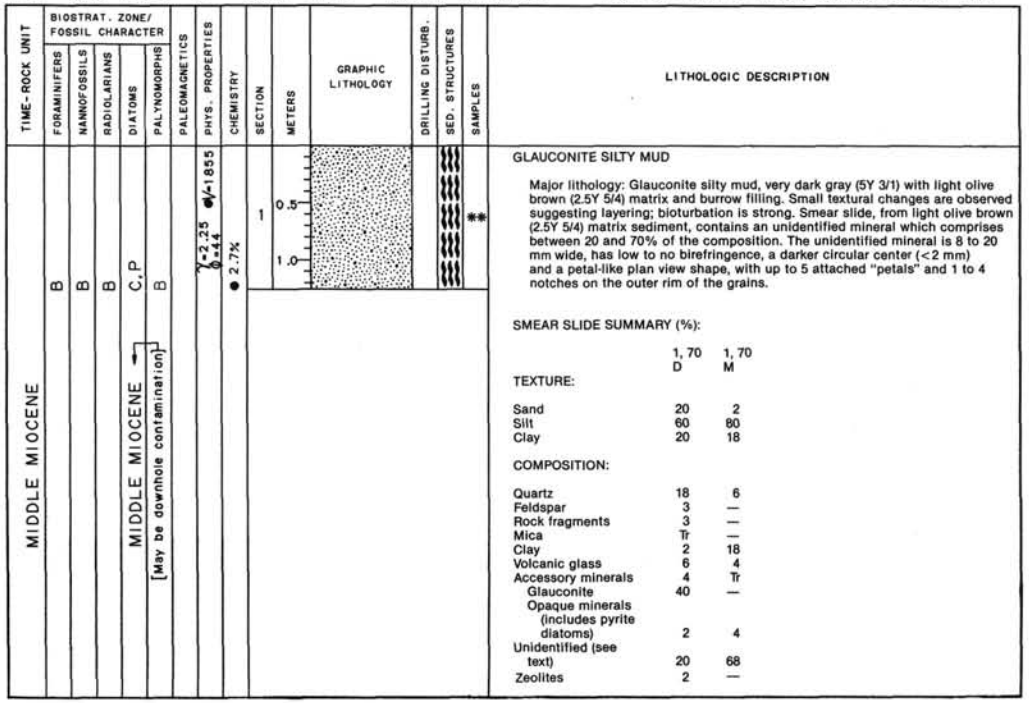

LITHOLOGIC DESCRIPTION

GLAUCONITE SILTY MUD

Major lithology: Glauconite silty mud, very dark gray (5Y 3/1) with light olive brown (2.5Y 5/4) matrix and burrow filling. Small textural changes are observed suggesting layering; bioturbation is strong. Smear slide, from light olive brown (2.5Y 5/4) matrix sediment, contains an unidentified mineral which comprises between 20 and 70% of the composition. The unidentified mineral is 8 to 20 mm wide, has low to no birefringence, a darker circular center (<2 mm) and a petal-like plan view shape, with up to 5 attached "petals" and 1 to 4 notches on the outer rim of the grains.

SMEAR SLIDE SUMMARY (%):

	1, 70 D	1, 70 M
TEXTURE:		
Sand	20	2
Silt	60	80
Clay	20	18
COMPOSITION:		
Quartz	18	6
Feldspar	3	—
Rock fragments	3	—
Mica	Tr	—
Clay	2	18
Volcanic glass	6	4
Accessory minerals	4	Tr
Glauconite	40	—
Opaque minerals (includes pyrite diatoms)	2	4
Unidentified (see text)	20	68
Zeolites	2	—

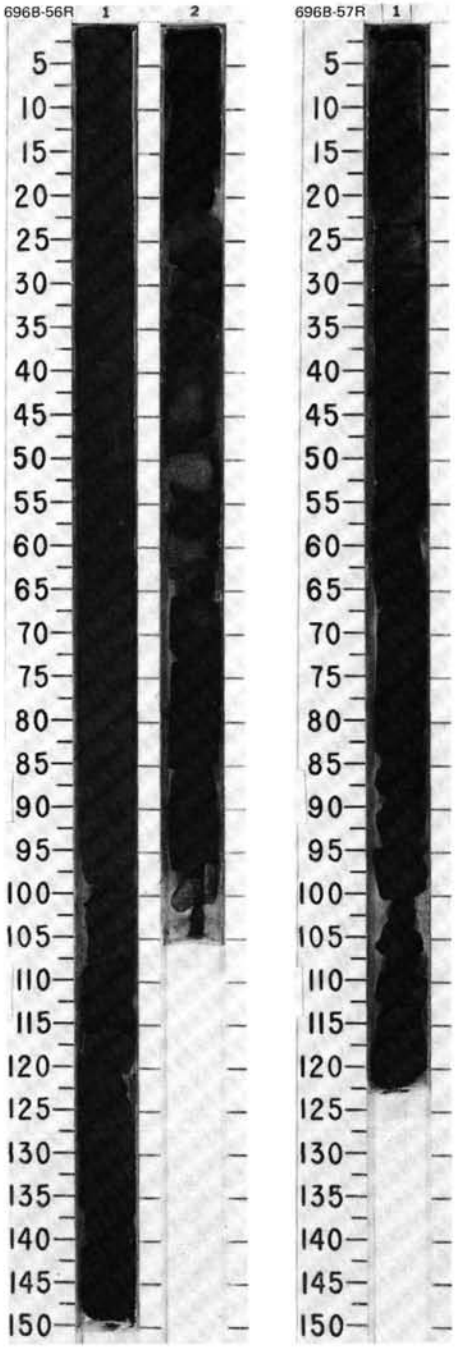

SITE 696 HOLE B CORE 58R CORED INTERVAL 1247.1-1256.8 mbsl; 597.2-606.9 mbsf

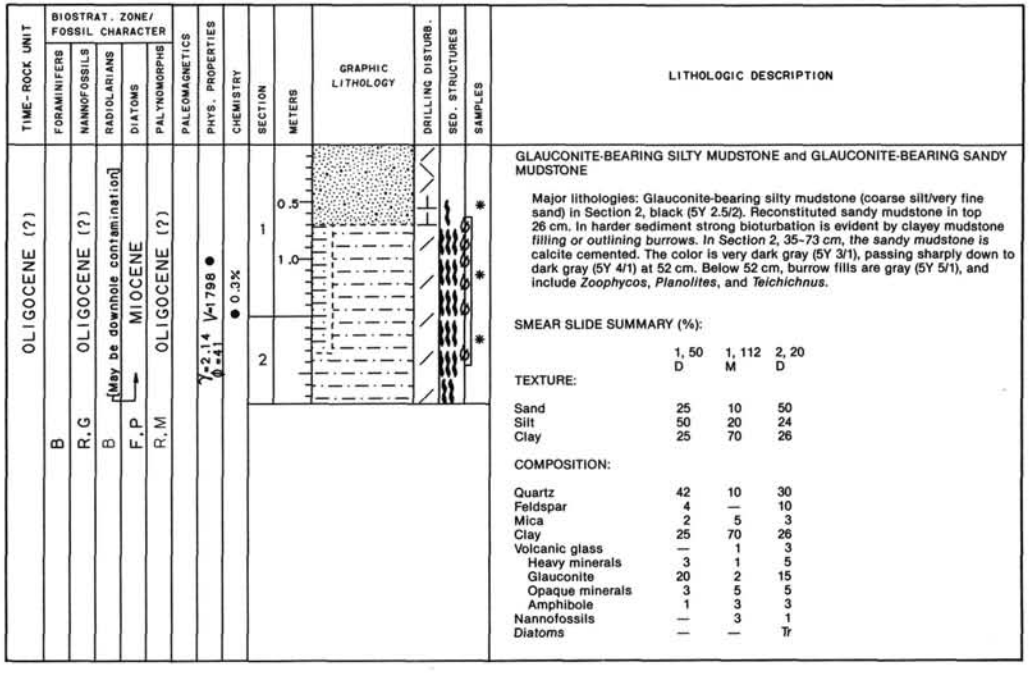

GLAUCONITE-BEARING SILTY MUDSTONE and GLAUCONITE-BEARING SANDY MUDSTONE

Major lithologies: Glauconite-bearing silty mudstone (coarse silt/very fine sand) in Section 2, black (5Y 2.5/2). Reconstituted sandy mudstone in top 26 cm. In harder sediment strong bioturbation is evident by clayey mudstone *filling or outlining burrows. In Section 2, 35-73 cm, the sandy mudstone is* calcite cemented. The color is very dark gray (5Y 3/1), passing sharply down to dark gray (5Y 4/1) at 52 cm. Below 52 cm, burrow fills are gray (5Y 5/1), and include *Zoophycos*, *Planolites*, and *Teichichnus*.

SMEAR SLIDE SUMMARY (%):

	1, 50 D	1, 112 M	2, 20 D
TEXTURE:			
Sand	25	10	50
Silt	50	20	24
Clay	25	70	26
COMPOSITION:			
Quartz	42	10	30
Feldspar	4	—	10
Mica	2	5	3
Clay	25	70	26
Volcanic glass	—	1	3
Heavy minerals	3	1	5
Glauconite	20	2	15
Opaque minerals	3	5	5
Amphibole	1	3	3
Nannofossils	—	3	1
Diatoms	—	—	Tr

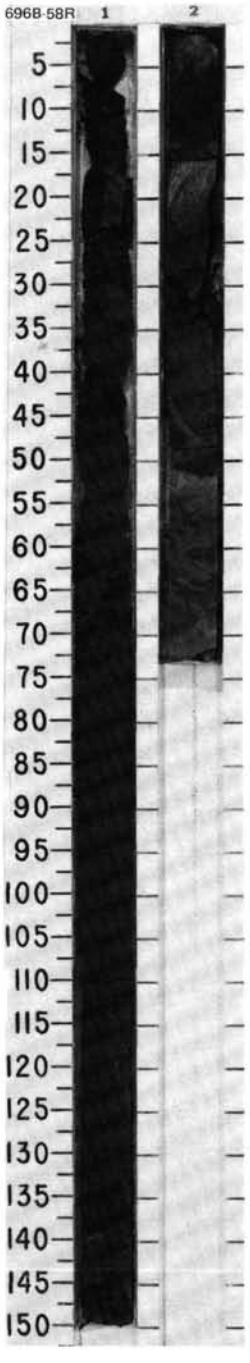

SITE 696 HOLE B CORE 59R CORED INTERVAL 1256.8-1266.5 mbsl; 606.9-616.6 mbsf

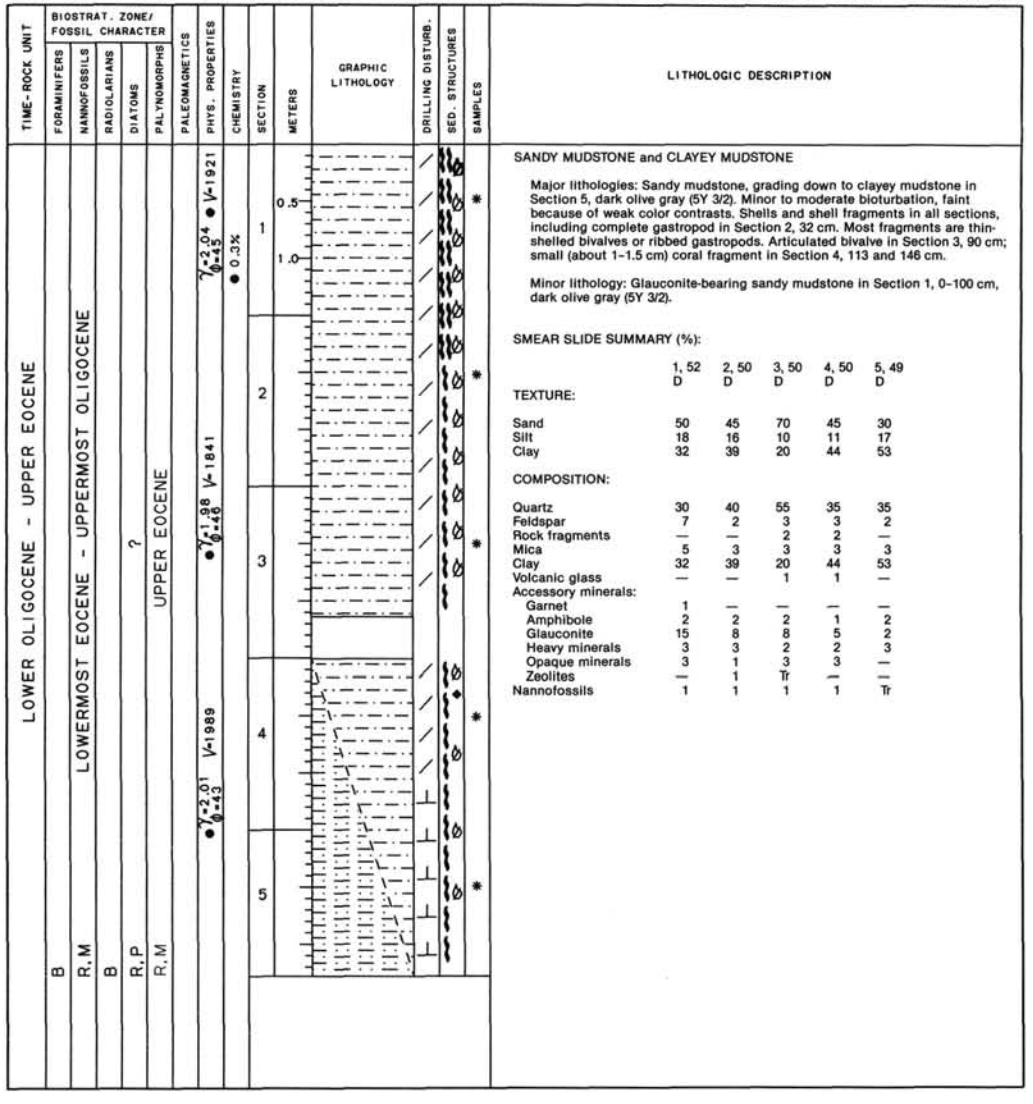

LITHOLOGIC DESCRIPTION

SANDY MUDSTONE and CLAYEY MUDSTONE

Major lithologies: Sandy mudstone, grading down to clayey mudstone in Section 5, dark olive gray (5Y 3/2). Minor to moderate bioturbation, faint because of weak color contrasts. Shells and shell fragments in all sections, including complete gastropod in Section 2, 32 cm. Most fragments are thin-shelled bivalves or ribbed gastropods. Articulated bivalve in Section 3, 90 cm; small (about 1–1.5 cm) coral fragment in Section 4, 113 and 146 cm.

Minor lithology: Glauconite-bearing sandy mudstone in Section 1, 0–100 cm, dark olive gray (5Y 3/2).

SMEAR SLIDE SUMMARY (%):

	1, 52 D	2, 50 D	3, 50 D	4, 50 D	5, 49 D
TEXTURE:					
Sand	50	45	70	45	30
Silt	18	16	10	11	17
Clay	32	39	20	44	53
COMPOSITION:					
Quartz	30	40	55	35	35
Feldspar	7	2	3	3	2
Rock fragments	—	—	2	2	—
Mica	5	3	3	3	3
Clay	32	39	20	44	53
Volcanic glass	—	—	1	1	—
Accessory minerals:					
Garnet	1	—	—	—	—
Amphibole	2	2	2	1	2
Glauconite	15	8	8	5	2
Heavy minerals	3	3	2	2	3
Opaque minerals	3	1	3	3	—
Zeolites	—	1	Tr	—	—
Nannofossils	1	1	1	1	Tr

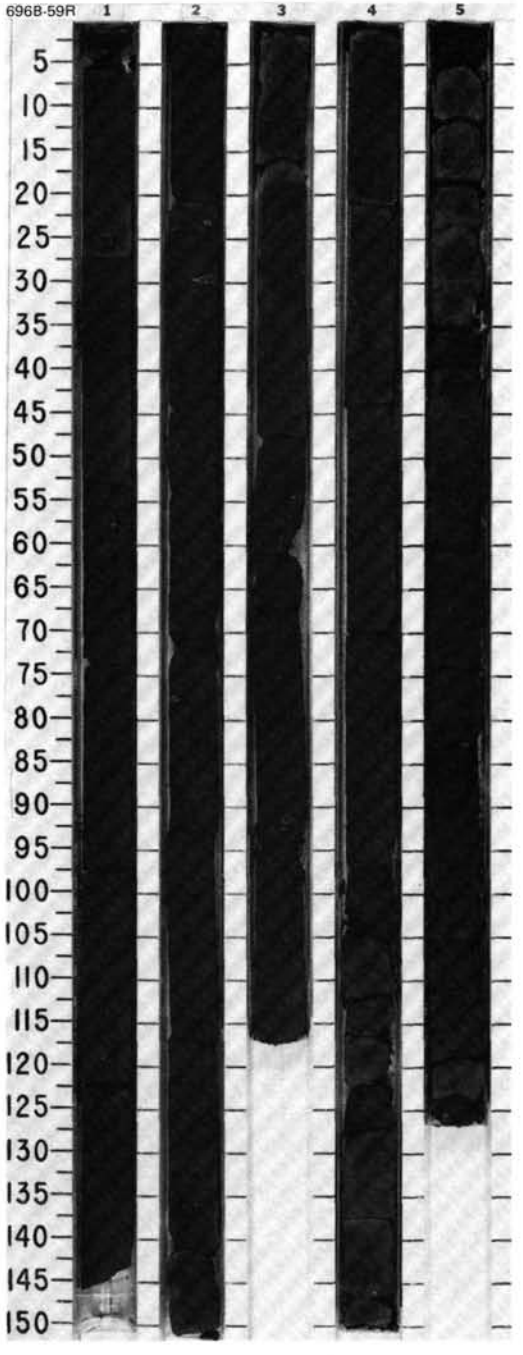

SITE 696 HOLE B CORE 60R CORED INTERVAL 1266.5-1276.1 mbsl; 616.6-626.2 mbsf

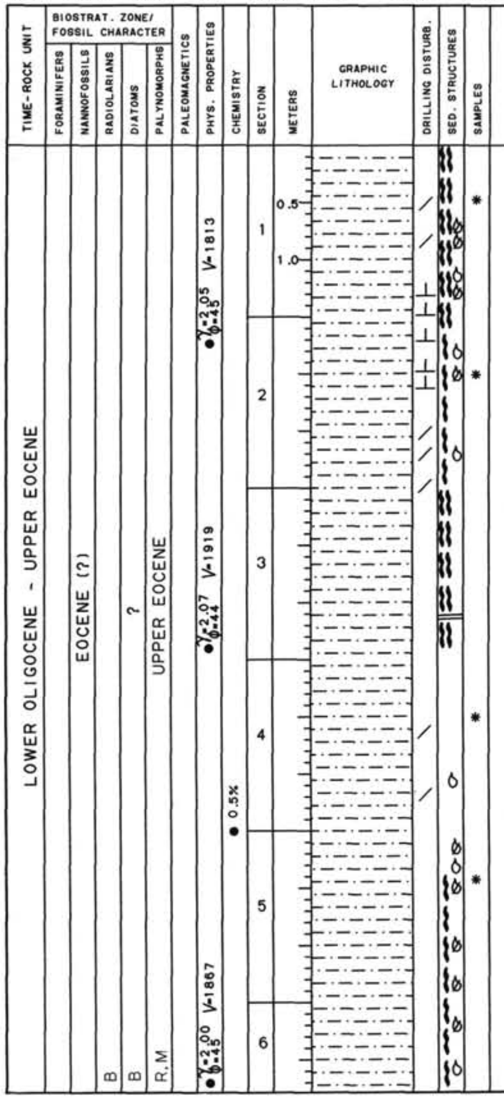

LITHOLOGIC DESCRIPTION

SANDY MUDSTONE

Major lithology: Sandy mudstone, uniform dark olive gray, Sections 2 through 6. Few benthic foraminifers on core surface, Section 2. A few shell fragments and a complete and ribbed bivalve are present in Section 1, 109 cm. Gastropod and bivalve shells found in all Sections, except Section 3. Whole specimens found in Section 2, 140 cm, and Section 5, 67 cm.

Minor lithologies: Glauconite-bearing sandy mudstone, Section 1, 0–110 cm, dark olive gray (5Y 3/2), faint moderate bioturbation. Glauconite sandy mudstone, dark olive gray (5Y 3/2), found as layers in Section 3, 124–129, Section 4, 0–10 cm, in large burrow fill at Section 4, 35 cm, and Section 5, 50–80 cm.

Minor to moderate faint bioturbation in Sections 1 through 3 only. Bioturbation in Section 1 includes *Planolites* at 28 cm and a vertical burrow at 86 cm.

SMEAR SLIDE SUMMARY (%):

	1, 50 D	2, 50 D	3, 50 D	4, 50 D	5, 50 D
TEXTURE:					
Sand	50	55	50	65	60
Silt	30	20	25	15	20
Clay	20	25	25	20	20
COMPOSITION:					
Quartz	51	48	30	55	40
Feldspar	5	3	5	10	10
Rock fragments	—	—	—	—	10
Mica	3	5	7	2	1
Clay	20	25	25	20	20
Accessory minerals:					
Micronodules	—	—	—	3	3
Weathered minerals	—	7	7	—	—
Glauconite	10	3	10	5	12
Amphibole	3	2	3	3	2
Garnet	1	1	—	—	—
Opaque minerals	2	3	5	1	—
Heavy minerals	5	2	7	—	1
Zeolites	Tr	—	—	—	—
Nannofossils	—	1	1	1	1
Diatoms	—	Tr	—	—	Tr
Sponge spicules	—	Tr	—	—	—

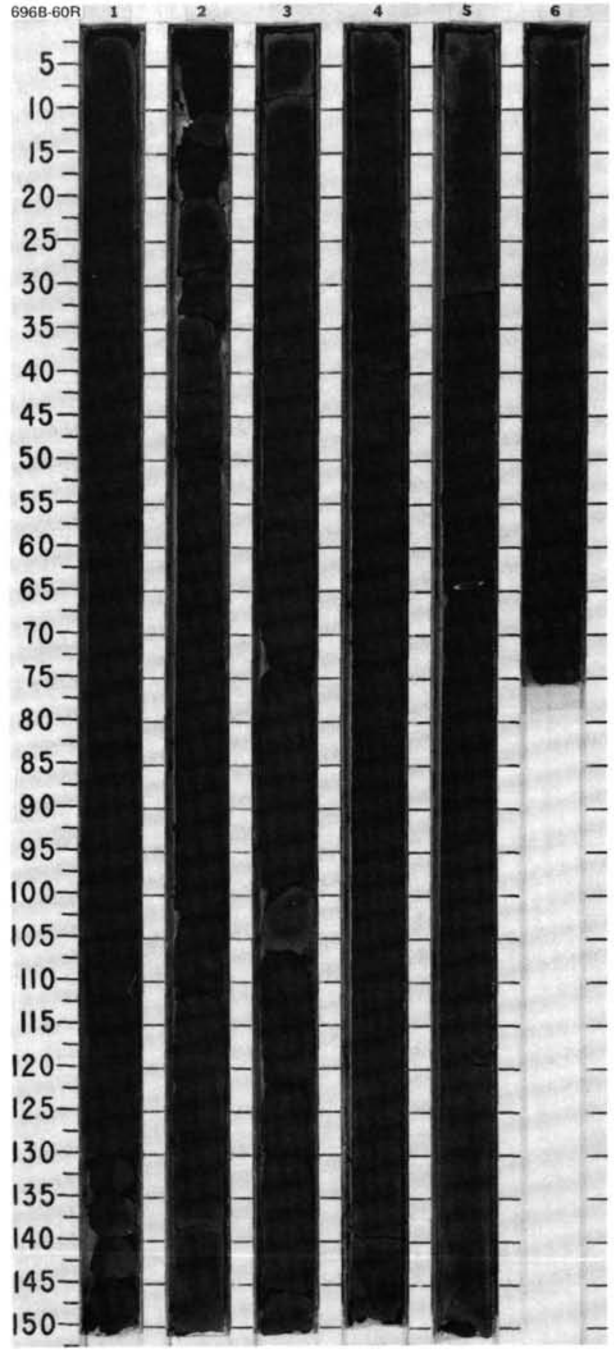

SITE 696 HOLE B CORE 61R CORED INTERVAL 1276.1-1285.8 mbsl; 626.2-635.9 mbsf

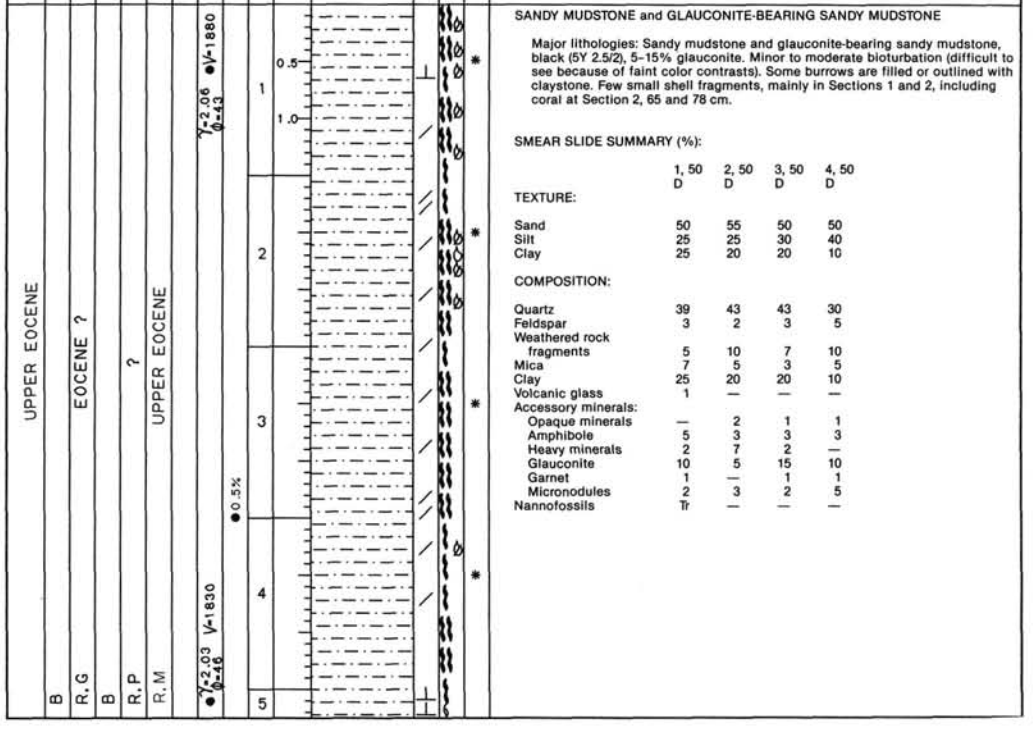

LITHOLOGIC DESCRIPTION

SANDY MUDSTONE and GLAUCONITE-BEARING SANDY MUDSTONE

Major lithologies: Sandy mudstone and glauconite-bearing sandy mudstone, black (5Y 2.5/2), 5–15% glauconite. Minor to moderate bioturbation (difficult to see because of faint color contrasts). Some burrows are filled or outlined with claystone. Few small shell fragments, mainly in Sections 1 and 2, including coral at Section 2, 65 and 78 cm.

SMEAR SLIDE SUMMARY (%):

	1, 50 D	2, 50 D	3, 50 D	4, 50 D
TEXTURE:				
Sand	50	55	50	50
Silt	25	25	30	40
Clay	25	20	20	10
COMPOSITION:				
Quartz	39	43	43	30
Feldspar	3	2	3	5
Weathered rock fragments	5	10	7	10
Mica	7	5	3	5
Clay	25	20	20	10
Volcanic glass	1	—	—	—
Accessory minerals:				
Opaque minerals	—	2	1	1
Amphibole	5	3	3	3
Heavy minerals	2	7	2	—
Glauconite	10	5	15	10
Garnet	1	—	1	1
Micronodules	2	3	2	5
Nannofossils	Tr	—	—	—

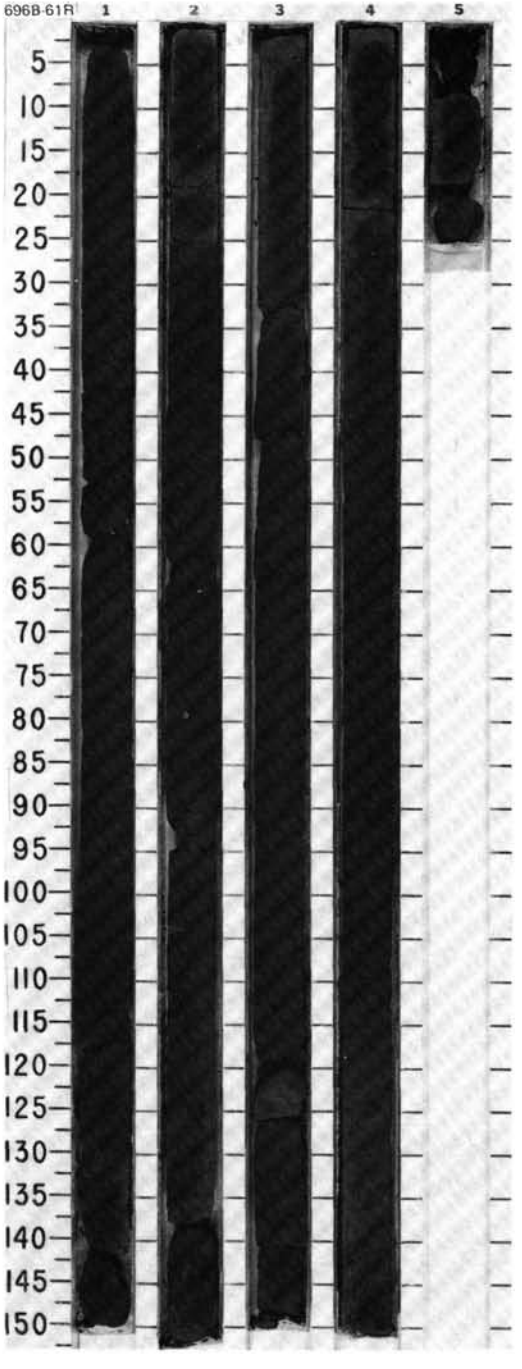

SITE 696 HOLE B CORE 62R CORED INTERVAL 1285.8-1295.5 mbsl; 635.9-645.6 mbsf

TIME-ROCK UNIT: LOWER OLIGOCENE / UPPER EOCENE

BIOSTRAT. ZONE/FOSSIL CHARACTER: MIDDLE (?) - UPPER EOCENE; ? ; OLIGOCENE ?

PALEOMAGNETICS

PHYS. PROPERTIES: ●V-4246; ●0.9%; ●γ=1.85 V-1982 Φ=41

CHEMISTRY

SECTION: 1, 2, 3, 4, 5, 6

METERS: 0.5; 1.0

GRAPHIC LITHOLOGY: VOID

DRILLING DISTURB.

SED. STRUCTURES

SAMPLES: IW; OG

LITHOLOGIC DESCRIPTION

SANDY MUDSTONE

Major lithology: Sandy mudstone, black (5Y 2.5/2) grading to dark olive gray (5Y 3/2), with calcareous levels, in Section 2, 52-76 cm, Section 4, 105-125 cm, and Section 5, 55-63 cm. Slight to moderate bioturbation. Small shell fragments throughout the core; coral in Section 6, 52 cm.

SMEAR SLIDE SUMMARY (%):

	1, 20 D	2, 100 D	3, 100 D	4, 100 D	5, 100 D	6, 100 D	7, 100 D
TEXTURE:							
Sand	50	55	60	60	55	50	60
Silt	30	25	20	20	25	30	25
Clay	20	20	20	20	20	20	15
COMPOSITION:							
Quartz	38	37	42	43	31	38	32
Feldspar	3	3	3	3	1	1	3
Rock fragments	10	10	15	15	20	20	25
Mica	5	3	3	3	3	3	2
Clay	20	20	20	20	20	20	15
Volcanic glass	—	—	—	Tr	—	—	—
Accessory minerals:							
Zeolites	—	—	—	—	1	—	2
Amphibole	5	3	3	3	3	5	3
Glauconite	10	10	5	5	7	3	7
Garnet	1	1	2	1	2	2	2
Heavy minerals	3	5	3	3	5	3	2
Micronodules	3	5	3	2	2	3	5
Opaque minerals	1	—	—	—	3	2	2
Nannofossils	1	1	1	2	2	Tr	Tr

Cont.

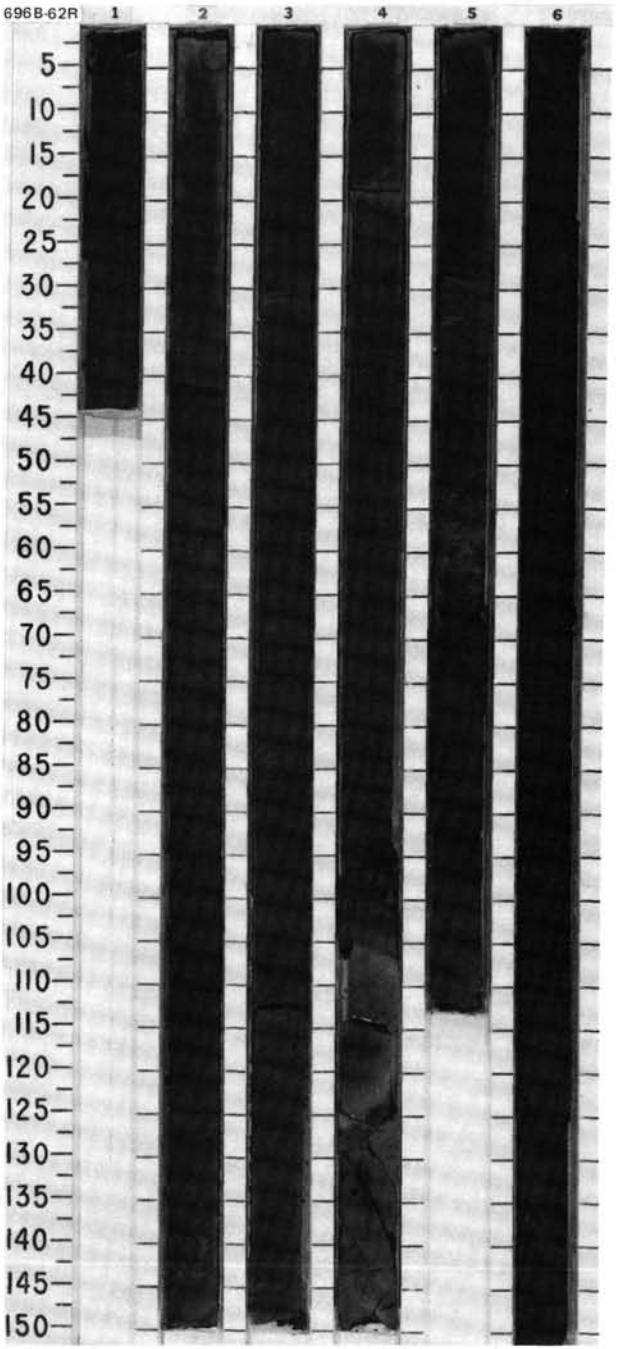

SITE 696 HOLE B CORE 62R CORED INTERVAL 1285.8-1295.5 mbsl; 635.9-645.6 mbsf

TIME-ROCK UNIT	BIOSTRAT. ZONE/ FOSSIL CHARACTER: FORAMINIFERS	NANNOFOSSILS	RADIOLARIANS	DIATOMS	PALYNOMORPHS	PALEOMAGNETICS	PHYS. PROPERTIES	CHEMISTRY	SECTION	METERS	GRAPHIC LITHOLOGY	DRILLING DISTURB.	SED. STRUCTURES	SAMPLES	LITHOLOGIC DESCRIPTION
	B	R,G	B	R,P	R,M		●γ=1.99 ϕ=35 V=1847		7 8 CC	0.5 1.0				*	Cont.